Reconstructing Climate Variability in the North Atlantic during the Late Holocene: an Integrated Biomarker Approach

Gemma Rueda Ferrer

PhD Thesis

March 2013

Institut de Ciència i Tecnologia Ambientals

Universitat Autònoma de Barcelona

Advisor: Dr. Antoni Rosell-Melé

icta Institut de Ciència i Tecnologia Ambientals • UAB

UAB Universitat Autònoma de Barcelona

Reconstructing climate variability in the North Atlantic during the late Holocene: an integrated biomarker approach.

Tesi Doctoral realitzada per:

GEMMA RUEDA FERRER

Sota la direcció del Dr. Antoni Rosell Melé a l'Institut de Ciència i Tecnologia Ambientals (ICTA), d'acord amb els requeriments del programa de Doctorat en Ciència i Tecnologia Ambientals de la Universitat Autònoma de Barcelona (UAB) per a l'obtenció del títol de Doctora en Ciència i Tecnologia Ambientals.

Bellaterra (Barcelona), 22 de març de 2013.

La Doctoranda	El Director de la Tesi
Gemma Rueda Ferrer	Antoni Rosell Melé

Universitat Autònoma de Barcelona

Com diu el refrany,

"La constància tot ho venç"

INDEX

Agraïments / Acknowledgements

Al llarg d'aquests quatre anys i mig sou moltes les persones que heu contribuït d'una manera o altra al desenvolupament i finalització d'aquesta tesi doctoral. A tots vosaltres us estic profundament agraïda. Molt especialment, vull donar les gràcies a:

Al Dr. Antoni Rosell-Melé per haver-me donat l'oportunitat d'introduir-me al món de la recerca, iniciant un projecte de final de carrera de Ciències Ambientals que ha acabat en la present tesi doctoral. Gràcies per les hores de discussions científiques i pel suport rebut durant aquests anys. També agraeixo haver tingut l'oportunitat de participar en una campanya de mostreig a l'Oceà Antàrtic i de viatjar a conferències internacionals per a presentar els resultats obtinguts.

A la Dra. Susanne Fietz, por su interés en mi trabajo, por las discusiones científicas y por todo lo que me ha enseñado durante estos años. A la Dra. Carme Huguet, per transmetre la seva passió investigadora, per les crítiques constructives i per estar sempre a punt per a donar un cop de mà. A la Núria Moraleda, excel.lent tècnic de laboratori amb qui he tingut la sort de compartir els problemes i les solucions del dia a dia al laboratori. Al Dr. Pau Comes, per ajudar-me en varis aspectes, sempre amb un toc de bon humor.

A tots els companys del Laboratori de l'Esfera Ambiental i de la Sala de Becaris de l'ICTA, passats i presents. Tots vosaltres heu estat el suport del dia a dia: Marina, Alfredo, Migue, Nata, Núria M., Bastian, Anna, Núria V., Pau, Sergio, Susanne, Carme, Laura, Pati, Gema, Saioa, Sònia, Claudio, Eva, Pedro, Min, Francyne, Josep, Carles... i tots aquells que en un moment o altre heu passat pel laboratori o la sala.

Als companys del Departament de Proteòmica del CSIC-UAB. Especialment al Dr. Joan Villanueva per aconseguir que l'espectròmetre de masses funcionés correctament durant els períodes d'anàlisi de GDGTs.

In 2011, I spent three months in LOCEAN (UPMC, Paris) working at Dr. Guillaume Massé's laboratory. Many thanks to Guillaume, Vincent, Marie Helene, Anne, Irina, Loïc, Ivia, Johan, Kaarina, Aurelie, Lyacine, David, Lewis… and to all of you who made my daily work possible there. Thanks for making me feel at home abroad.

I would like to thank the people who gave me samples or contributed to obtain the samples used in this thesis: Dr. Richard Gyllencreutz, Dr. Leonid Polyak, Dr. Robert Spielhagen, Dr. Mona Henriksen. Special thanks to Mona who undertook soil and water sampling in Norway each month during one year. Moltes gràcies als meus intrèpids companys de mostreig a Ulldeter: Guillem i Roger, i puntualment l'Edu i la Tonis.

Als meus pares. El vostre suport incondicional ha estat la base per arribar fins aquí. Gràcies per les ganes incansables d'entendre a què m'he estat dedicant durant aquests quatre anys, i per transmetre'm que amb esforç, perseverança i una bona dosi d'il·lusió, un pot fer el que es proposi.

A la meva iaia Antònia. Sens dubte, li hauria encantat tenir aquest llibre entre les mans. Que t'acaronin els estels.

A en Jep i la Tonis. Per preocupar-vos del meu benestar i fer-me sentir com a casa.

Als meus amics: a tota la colla esponja, a les ambientòlogues i a les lokifriends. Per tots els bons moments que passem junts/es. Estar amb vosaltres em carrega les piles. I ara tindré més temps!

A en Guillem. Per caminar dia rera dia al meu costat i ajudar-me a assolir el cim, tant si plou com si fa sol. Gràcies per ser-hi sempre.

Esta tesis doctoral se ha realizado con el soporte económico del Ministerio de Educación y Ciencia (MEC/MICINN) a través de una beca de Formación del Profesorado Universitario (FPU AP2008-00801), los proyectos ICECARB (POL2006-0299/CGL) y TETRACLIM (CGL2010-15000).

Bellaterra, 22 de març de 2013

Gemma

Abstract

The North Atlantic and Arctic Oceans play an important role in modulating European climate variability. Oceanic records of sea surface temperature (SST) variability covering the last 2000 years at high resolution in this region are scarce. Obtaining new high resolution reconstructions in this area is necessary to increase the level of understanding on how the climate system has varied during the last millennia, to put the recent warming into a wide context and to investigate if the natural modes of climate variability observed from instrumental records can be projected to the past. This PhD thesis focuses on generating new records of multidecadal climate variability in the North Atlantic Ocean, analyzing organic proxies (biomarkers) in marine sedimentary cores that cover the last 2000 – 4400 years. We generated new climate reconstructions in the two main paths where the northward flowing North Atlantic current meet the Arctic Ocean - the eastern Fram Strait and the Barents Sea - and also in a highly sensitive area to changes in the internal modes of climate variability and the interaction between the North Atlantic Ocean and European climate - the Skagerrak -. We used well established organic proxies (i.e. alkenones) but also recently developed ones (IP25, GDGT based proxies) to produce reconstructions based on SST but also on additional climate parameters such as sea ice cover variability, mean air temperature and export productivity. In addition, we tested the applicability of the relatively new proxies based on GDGTs in a marine sedimentary core from the Skagerrak and in soils from southern Norway and the Pyrenees. The TEX_{86} gave SST estimates that were similar to regional annual means in the Skagerrak but the MBT/CBT air temperature estimates were closer to summer temperatures. This bias towards a specific season was not due to changes in the synthesis of GDGTs in soils through an entire annual cycle or to an enhanced transport of the lipids to the Skagerrak with the Glomma River during this period. We suggest that the GDGTs in the Skagerrak might be a result of a mixture between lipids transported from southernmost locations and *in situ* production. The origin of these lipids in the Skagerrak should be addressed before applying these proxies in this area with reliability. From the records located in the eastern Fram Strait and the Barents Sea, positioned in the two main paths where the northward flowing North Atlantic Current meet the Arctic, we interpret there was a progressive increase in temperature probably due to a warming in or an enhancement of the North Atlantic Current. This trend started at ~1000 – 1300 AD but was accentuated from ~1500 - 1600 AD until the most recent part of the records. In the Skagerrak, an area influenced by 90% North Atlantic water, a long term cooling that lasted until AD 1300 was reversed by a progressive warming since AD 1600 until present even though insolation continued to decrease. We suggest that the warming trends observed in the three records during the last ~400 years were caused by changes in internal modes of climate variability such as more frequent predominantly positive phases of the Arctic Multidecadal Variability, the North Atlantic Oscillation or the Atlantic Multidecadal Oscillation. The impact of human activity on climate might be superimposed on a longer term warming trend caused by changes in natural modes of climate variability that progressively affected the study areas during the last ~400 years.

Resum

L'Oceà Atlàntic Nord i l'Oceà Àrtic són components essencials per la regulació de la variabilitat climàtica a Europa. En aquesta regió, les reconstruccions climàtiques de temperatura superficial del mar (SST) que cobreixen els darrers 2000 anys a alta resolució són escasses. Obtenir noves reconstruccions climàtiques a l'Atlàntic Nord a alta resolució és rellevant per tal d'entendre millor com funciona el sistema climàtic. En base a aquestes reconstruccions, es pot conèixer com ha variat el clima durant els darrers mil·lenis, encabir l'actual escalfament global en un context més ampli i investigar si els modes de variabilitat climàtica natural que s'han definit a través d'observacions instrumentals recents també afectaren el clima en el passat. Aquesta Tesi Doctoral té per objectiu generar noves reconstruccions de variabilitat climàtica a escala multidecadal a la regió de l'Oceà Atlàntic Nord pels darrers 2000 – 4400 anys, analitzant *proxies* geoquímiques orgàniques (biomarcadors) en registres sedimentaris marins. S'ha reconstruït la variabilitat climàtica en les dues entrades principals de la corrent de l'Atlàntic Nord a l'Oceà Àrtic – l'est de l'Estret de Fram i el mar de Barents – i també en una regió especialment sensible als canvis en els modes de variabilitat climàtica natural i a la interacció entre l'Oceà Atlàntic Nord i el clima continental Europeu – el Skagerrak -. S'han utilitzat tant *proxies* orgàniques ben establertes (i.e. alquenones) com *proxies* climàtiques desenvolupades recentment (IP25 i *proxies* basades en GDGTs), per tal de produïr reconstruccions basades no només en SST però també en paràmetres climàtics adicionals tals com la variabilitat en la coberta de gel marí, la temperatura de l'aire i la productivitat marina exportada. A més, s'ha estudiat l'aplicabilitat de les noves *proxies* basades en GDGTs en el registre marí del Skagerrak i en sòls localitzats al sud de Noruega i als Pirineus. Les SST estimades amb el *proxy* TEX_{86} mostren valors similars a la temperatura mitjana anual de la zona mentre que les temperatures de l'aire reconstruïdes amb el MBT/CBT s'apropen als valors instrumentals de l'estiu per a aquesta regió. Aquest esbiaixament no és degut a canvis en la síntesi dels GDGTs en els sòls durant un cicle annual, ni a un transport preferent dels lípids amb el Riu Glomma durant aquest període. Probablement, al Skagerrak, els GDGTs són una mescla entre lípids transportats des de latituds més baixes i producció *in situ* en aquesta zona. Suggerim que per a obtenir reconstruccions acurades utilitzant aquestes *proxies* al Skagerrak, caldria primer investigar-ne el seu origen. Dels registres climàtics generats a l'est de l'Estret de Fram i al mar de Barents, interpretem que hi va haver un increment progressiu en la temperatura o en el transport de calor de la Corrent de l'Atlàntic Nord cap a l'Àrtic. Aquesta tendència va començar als anys ~1000 – 1300 AD però s'accentuà des de ~1500 - 1600 AD fins al present. Al Skagerrak, una zona influenciada per un 90% de massa d'aigua procedent de l'Atlàntic Nord, hi va haver un refredament de la SST fins a 1300 AD que es va veure revertit per un escalfament des de 1600 AD tot i que la insolació va continuar decreixent. Suggerim que les tendències d'escalfament observades en els tres registres durant els últims ~400 anys podrien estar causades per canvis en modes de variabilitat climàtica tals com un increment en la freqüència mitjana de fases positives de la Variabilitat Multidecadal de l'Àrtic, la Oscil·lació de l'Atàntic Nord o la Oscil·lació Multidecadal de l'Atlàntic. L'impacte antropogènic sobre el clima estaria sobreposat a una tendència climàtica d'escalfament que hauria afectat de forma progressiva les zones d'estudi durant els darrers ~400 anys.

CHAPTER 1

Introduction

1. Introduction

Climate change has become an issue of growing concern in the last decades. Global average temperatures have increased ~0.9 ^{o}C during the last century and more than half of this warming has taken place since the 1970s (Figure 1.1A; IPCC, 2007). Warming of the oceans, rising sea levels, glaciers melting, sea ice retreating in the Arctic and reduced snow cover in the Northern Hemisphere are noticeable effects of this warming trend (IPCC, 2007). Part of the observed increase in global average temperatures is very likely (>90% probability of occurrence) due to the observed increase in anthropogenic greenhouse gas concentrations (IPCC, 2007). However, it is not the only factor affecting climate variability.

Climate on Earth varies from interannual to geological time scales as a result from both internal and external factors (Bradley, 1999; Ruddiman, 2001). For instance, during the Holocene – the geological epoch covering the last 11500 years - a variety of natural processes have modulated climate variability including intrinsic modes of variability in the atmosphere – ice - ocean system (internal forcings) as well as changes in solar radiation and volcanic aerosols, and to a lower degree changes in Earth orbital parameters (external forcings) (Bradley, 1999; Ruddiman, 2001).

To understand the impact of human activity on climate, it is essential to describe and understand the natural trends of long term climate variability. It is therefore imperative to know how the complex atmosphere – ice - ocean system that shapes climate variability on Earth works at decadal to multidecadal time scales and even longer. During the Late Holocene (the last 2000 – 4000 years) external factors modulating the Earth's climate at millennial time scales such as the continental arrangement, orography, Earth orbital parameters and the spatial extent of continental ice sheets have not changed significantly (Mann, 2007). Therefore reconstruction of natural climate variability over the last 2000 – 4000 years provides a context for estimating the range of natural climate variability in which to interpret the modern warming (Mann, 2007).

Instrumental measurements of climate parameters based on extensive and high quality data exist for the last 150 - 200 years only. To evaluate long term climate changes at decadal to multicentennial time scales we need to reconstruct past environmental change using indirect or proxy methods. A proxy is a measurable parameter that gives indirect information of an unobservable environmental factor such as temperature, salinity, productivity or sea ice (Wefer et al., 1999). Several geochemical proxies are currently used to reconstruct past environmental parameters and they can be subdivided into proxies based on inorganic or organic fossil remains.

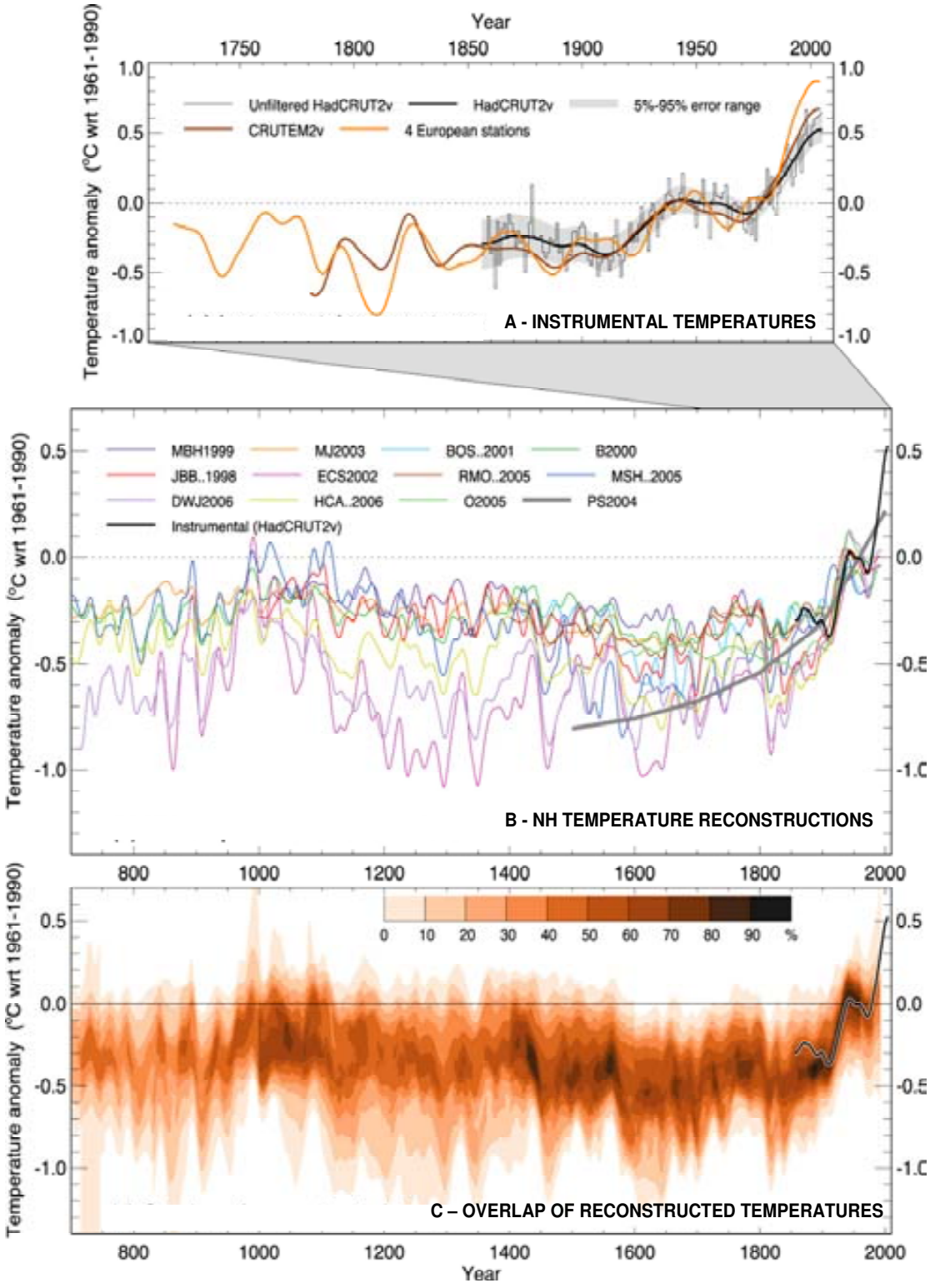

Figure 1.1. Records of Northern Hemisphere temperature variation published in the Fourth Assessment Report of the Intergovernmental Panel on Climate Change (IPCC, 2007). (A) Annual mean instrumental temperature records from land and marine temperatures covering the period 1856-2005 (HadCrut2V), land only temperatures for the period 1781 – 2004 AD (CRUTEM2v) and only four European stations going back to 1721 until 2004 AD. (B) Various multiproxy reconstructions for the last 1300 years and the Instrumental record HadCrut2V. (C) Overlap of all temperature reconstructions and their uncertainty range. The figure is from IPCC, 2007.

Examples of geochemical inorganic proxies include $\delta^{18}O$ (Erez and Luz, 1983) and Mg/Ca ratios of foraminifera assemblages (Lea, 2003). Geochemical organic proxies, or biomarkers, for reconstructing past temperatures are based on the relative distributions of algal and archaeal lipids remains (Brassell et al., 1986a,b; Schouten et al., 2002; Weijers et al., 2007a).

1.1. Northern Hemisphere climate variability during the last 2000 years

The first high resolution multiproxy reconstruction of climate variability in the Northern Hemisphere that covered the last 1800 years showing statistical error bars was based on a statistical synthesis of various proxies derived from tree rings, corals, ice cores and historical records (Figure 1.1B, MBH1999 and MJ2003; Mann et al., 1998; Mann et al., 1999; Mann and Jones, 2003). Due to the statistical techniques used, the reconstruction showed little low frequency variability in the data. The authors concluded that Northern Hemisphere surface temperatures decreased gradually from AD 1000 to 1850 and then increased sharply towards present. The graph that showed this trend was called thereafter the *hockey stick* and it has been subject of further study and debate thereafter. Several additional reconstructions have been generated since then, using different statistical methods and proxy datasets and are shown in figure 1.1B (Rutherford et al., 2005; Moberg et al., 2005; D'Arrigo et al., 2006; Hegerl et al., 2006; Pollack and Smerdon, 2004; Oerlemans, 2005). When the compilation of all these datasets is viewed together, the result is a picture with greater low frequency variability at centennial time scales than the variability observed in the original *hockey stick* graph (IPCC, 2007). Taking into account the individual statistical uncertainties associated to each reconstruction (Figure 1.1C) the compilation shows relatively warm conditions in the 11th and early 15th centuries and cool conditions in the 17th and early 19th centuries (IPCC, 2007). However, in agreement with the original *hockey stick* dataset, the 20th century shows the warmest conditions of the last 1300 years (IPCC, 2007). Despite showing much higher multidecadal to centennial scale variability than the *hockey stick* dataset, all the reconstructions are within the envelope of uncertainty range indicated in the original reconstruction (IPCC, 2007). There are a few well dated climate reconstructions spanning back to the last 2000 years in the Northern Hemisphere, and the existing ones are from extratropical terrestrial locations (Jones et al., 2003).

The North Atlantic and Arctic Oceans are critical constituents of the climate system (Bjerknes, 1964). The North Atlantic Current transports warm and tropical waters northward, releasing heat to the atmosphere in the North Atlantic region

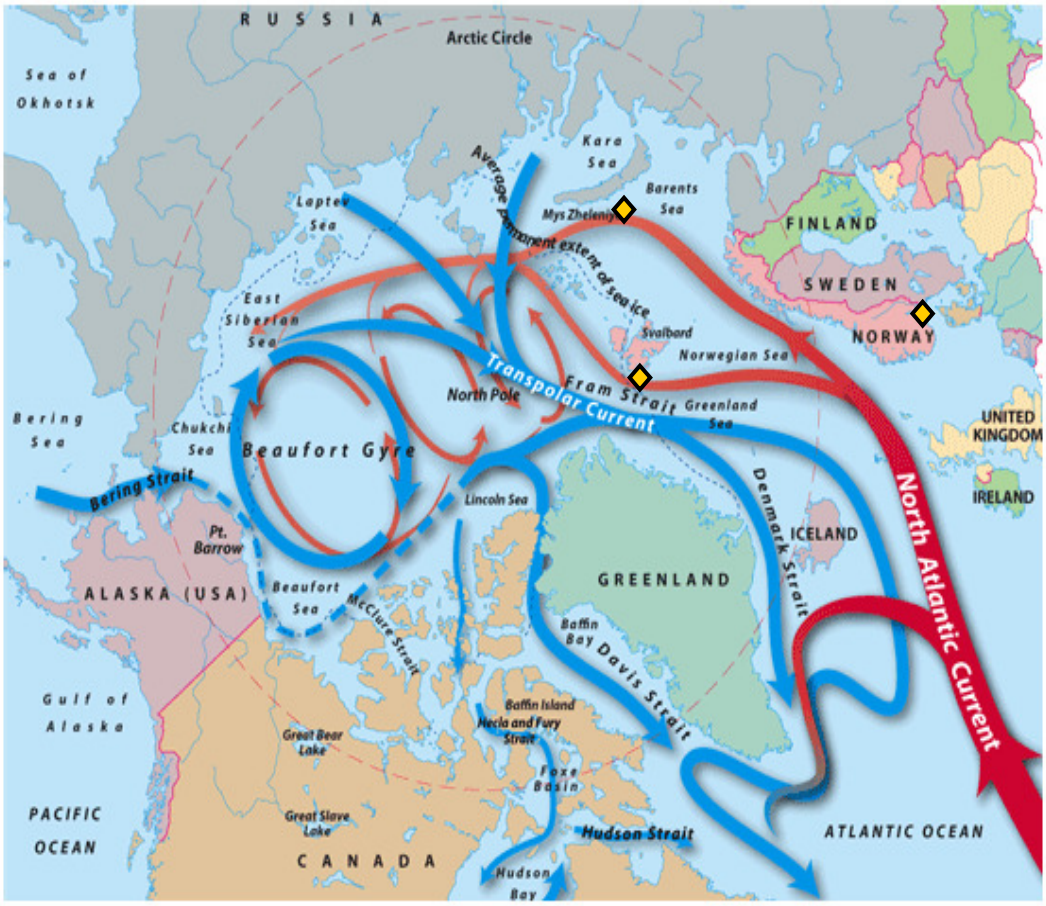

Figure 1.2. Surface ocean circulation in the North Atlantic and Arctic Oceans. Warm tropical waters flow northward (red arrows) releasing heat to the North Atlantic region and flowing into depths of the Arctic Ocean. Cold waters (blue arrows) sink in the North Atlantic and flow southward to drive the Ocean Conveyor. The orange diamonds indicate the location of the three marine sedimentary cores studied in this thesis. Figure from the Woods Hole Oceanographic Institution (www.whoi.edu, visited on 1st March 2013).

(Figure 1.2). When this ocean current reaches the cold atmosphere and water of the Arctic Ocean it sinks, forming the North Atlantic Deep Water that flow southwards driving the Ocean Conveyor. Therefore this current is a surface expression of the Atlantic Meridional Overturning Circulation (AMOC), an essential component of the global climate system (Vellinga and Wood, 2002).

Sea surface temperature (SST) variability in the North Atlantic has a profound influence on climate in Europe on decadal time scales (Sutton and Hodson, 2005; Knight et al., 2006; Folland et al., 2009) and the patterns of temperature variability in the Atlantic Ocean influence the patterns of European climate change (Sutton and Dong, 2012). During the Late Holocene, multidecadal climate variability in the North Atlantic has been controlled by a number of external and internal climate forcings.

1.2. Mechanisms of decadal to multidecadal climate variability in the North Atlantic and the Arctic

1.2.1. External forcings

Insolation is defined as periodic changes in parameters of the orbit of the Earth around the Sun that modify the seasonal and latitudinal distribution of incoming solar radiation at the top of the atmosphere (Berger, 1978). Changes in the distribution of insolation dominate climate variability on multimillennial timescales (Ruddiman, 2001) but they also played a central role in shaping global scale changes in climate during the Holocene (Mayewski et al., 2004). Summer insolation at 65 ^{o}N has decreased continuously by 10% after 11 Kyr BP towards present (Berger and Loutre 1991) and it has been proposed as a possible forcing related to a long term sea surface temperature cooling reconstructed across the North Atlantic region during this time period (Marchal et al, 2002). For the last 2000 years it is likely that a combination of external factors including solar (superimposed on long term variability in insolation) and volcanic forcings but also anthropogenic emissions of greenhouse gasses and sulphate aerosols represented the principal external forcings of climate variability (Jones and Mann, 2004).

1.2.2. Internal forcings

Internal forcings are the factors that affect long term internal variability in the coupled atmosphere – ice – ocean system. In the North Atlantic and Arctic Oceans the following factors have been proposed by several authors to control climate variability during the Late Holocene, although there is ongoing debate on which of them should be considered causes or effects (Miettinen et al., 2012 and references therein):

- Internal variability of the AMOC.
- Variations of the North Atlantic Current inflow controlled by subpolar gyre dynamics.
- Oscillations and input of cold freshwater from the Labrador Sea area and the East Greenland Current.
- Close coupling between surface and deep waters.
- Variability in the pressure gradient at sea level over North Atlantic and the Arctic areas.

A few climate indices have been established for defining natural modes of climate variability in the North Atlantic – Arctic region at interannual to multidecadal time scales. These modes of variability are large scale climate patterns characterized by a particular set of atmospheric and oceanic conditions (Grossmann and Krotzbach, 2009). Despite the awareness of their importance for climate variability, many issues remain open about the specific climate processes governing these modes of natural climate variability, on how did they vary in the past and will vary in the future (Hurrell, 2003). These modes of climate variability are described below.

1.2.2.1. The North Atlantic Oscillation / the Arctic Oscillation (NAO/AO)

The North Atlantic Oscillation (NAO) (Van Loon and Rogers, 1978) and the Arctic Oscillation (AO) (Thompson and Wallace, 1998) refer to an atmospheric mass redistribution between the subtropical Atlantic and the Arctic that can greatly modify the mean westerly winds speed and direction over the Atlantic and consequently affect the transport and distribution of heat and moisture between the Atlantic Ocean and the surrounding continents (Figure 1.3) (Hurrell, 2003). The NAO can be viewed as the North Atlantic regional manifestation of the AO (Marshall et al., 2001) and both indices are closely related (Thompson and Wallace, 1998). These indices influence climate on interannual to multidecadal time scales.

The NAO is described as the synchronous variation of the sea level pressure gradient between the Icelandic Low and the Azores High on timescales from daily to multidecadal (Van Loon and Rogers, 1978). When there are negative sea level pressure over the Icelandic region and the Arctic but positive sea level pressure over the Azores region, the NAO is in a positive phase. In this situation, stronger than average westerly winds dominate across the North Atlantic bringing wetter and warmer than average conditions in northerwestern Europe and Scandinavia but drier and colder weather in southwestern Europe and the Mediterranean zones. Instead, when the pressure gradient between the Azores High and the Iceland Low decreases, the NAO is in a negative phase. In this situation, the westerly winds are weaker than average and the storm track is directed to middle latitudes of the Atlantic Ocean and Western Europe, bringing warmer and wetter conditions over southwestern Europe, the Mediterranean and the northwest Atlantic but colder and drier conditions in Scandinavia and northwestern Europe. A positive (negative) phase of the NAO index is also associated with cold (warm) SST anomalies in the subpolar North Atlantic and the East Atlantic (0 – 30 ^{o}N) but warm (cold) anomalies in the West Atlantic (20 – 45 ^{o}N) (Figure 1.3; Van Loon and Rogers, 1978; Marshall et al., 2001).

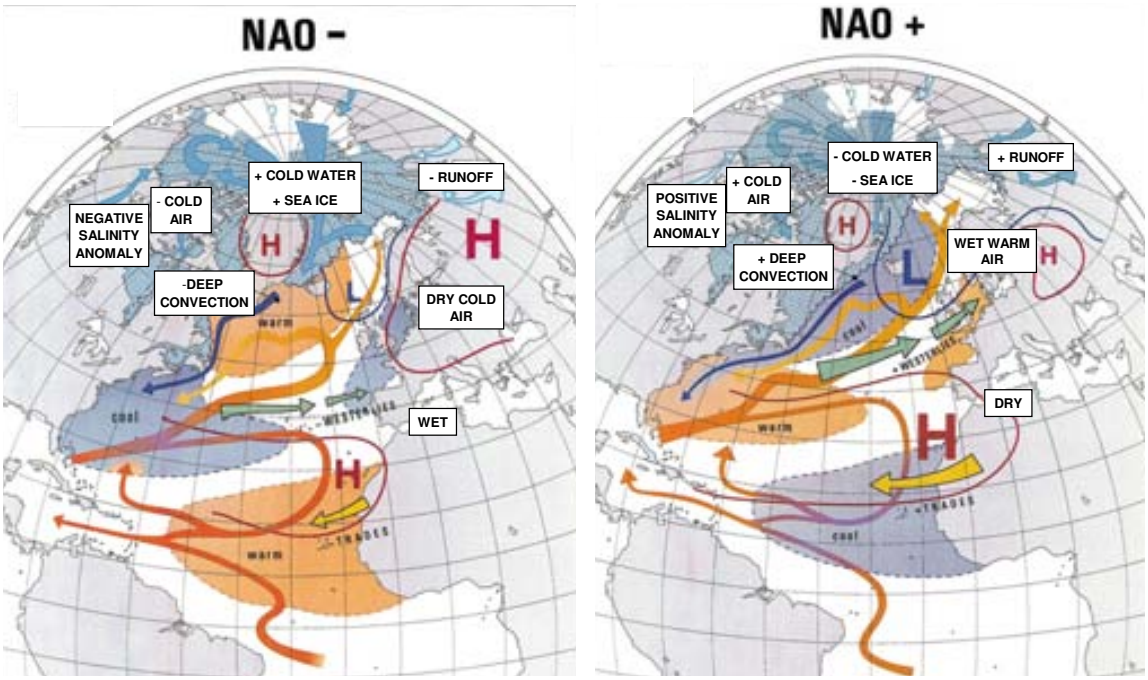

Figure 1.3. The two phases of the North Atlantic Oscillation (NAO) and the related changes in the atmosphere – ice – ocean system. Wanner et al. (2001).

1.2.2.2. Atlantic Multidecadal Oscillation (AMO)

Schlesinger and Ramankutty (1994) identified a low frequency variability pattern in North Atlantic SSTs with an oscillation period of 60-90 years. This pattern of multidecadal variability over the North Atlantic region has become known as the Atlantic Multidecadal Oscillation (AMO; Kerr, 2000). The AMO is calculated as the relative variability in SST over the North Atlantic region compared to relative average temperature variability in the rest of the world's oceans. Temperature in the North Atlantic Ocean has oscillated between anomalously warm and cold phases (positive and negative AMO phases) that lasted several decades at a time (Figure 1.4; Knudsen et al., 2011; Sutton and Dong, 2012). Paleoclimate reconstructions suggest a quasi persistent mode of variability with a quasi persistent 55 to 70 year AMO existed during long periods of the last 8000 years (Knudsen et al., 2011). This oscillatory variability in climate over the North Atlantic is attributed to internal variability of the ocean circulation associated to the AMOC (Schlesinger and Ramankutty, 1994; Vellinga et al., 2004) and this view is supported by climate simulations (Delworth and Mann, 2000; Knight et al., 2006). Currently research efforts are focused on understanding the climate forcings and mechanisms that influence the AMO (Dima and Lohmann, 2006; Ottera et al., 2010; Booth et al., 2012).

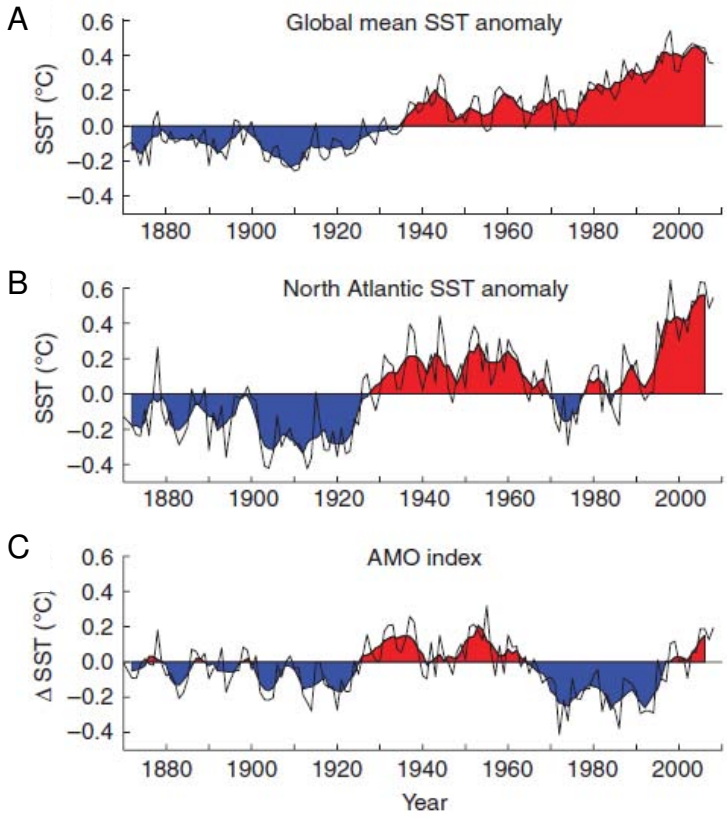

Figure 1.4. Global and North Atlantic climate trends over the period 1870 – 2008 (Knudsen et al., 2011). (A) Global annual mean SST anomalies. (B) North Atlantic SST anomalies. (C) The AMO index calculated after subtracting the global mean SST anomalies from the North Atlantic SST anomalies. Thick black lines indicate five year running means. (Figure from Knudsen et al., 2011).

1.2.2.3. Arctic Multidecadal Variability (Arctic MDV)

Low frequency oscillations with a similar period of those decribed for the AMO (50 – 80 years) have also been observed in the Arctic (Polyakov and Johnsson, 2000) and have been referred to as the Arctic Multidecadal Variability (MDV) pattern (Polyakov et al., 2004). Two phases of the Arctic MDV were described after observation of interactions between the different components of the ocean – ice – atmosphere system and related long term climate variability (Figure 1.5; Polyakov et al, 2004). Briefly, a period characterized by low pressures over the Arctic leads to increased transport of warm air and water from the North Atlantic into the Arctic, excess ice and freshwater transport through the Fram Strait from the Arctic. In this situation it is said that the Arctic MDV is in positive phase. On the contrary, when high sea level pressure dominate over the Arctic, the transport of warm air and water from the North Atlantic to the Arctic as well as the ice and freshwater export from the Arctic to the North Atlantic via the Fram Strait are reduced. This scenario is a negative phase of the Arctic

MDV (Polyakov et al., 2004). The analysis of data obtained from recent observations show that Atlantic surface and deep water temperature, Arctic surface air temperature, ice extent and fast ice thickness in the marginal Seas of Siberia exhibit long term MDV (Polyakov et al, 2004). The decadal climate variability patterns described in the AO index and the multidecadal climate variability defined in the two phases of Arctic MDV drive large amplitude long term natural climate variability in the Arctic (Polyakov and Johnsson, 2000).

Two phases of the Arctic Multidecadal Variability (MDV)

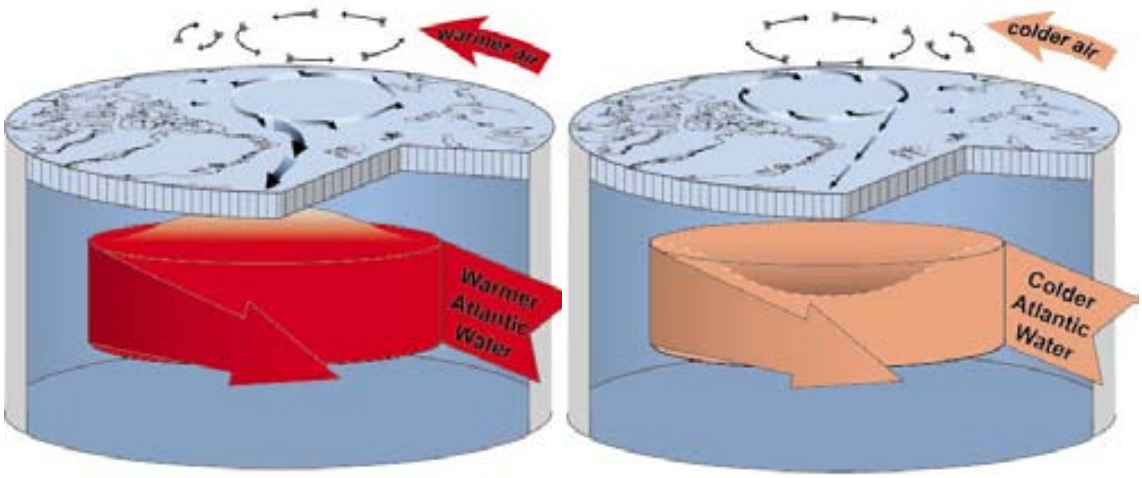

Positive phase

- Increase of transport of warmer air and water from the North Atlantic into the Arctic.
- Anticyclonic Beaufort Gyre is weakened;
- Cyclonic circulation in the eastern Arctic is intensified;
- Excess ice and fresh water transport through Fram Strait from the Arctic, suppressing deep-water convection in the Greenland Sea;
- Increased cyclonicity causing divergence of ice drift and surface circulation, leading to doming of the Atlantic Water.
- Suppressed Arctic High resulting in weaker anticyclonic ice drift and surface circulation, divergence of surface currents

Negative phase

- Decrease of transport of warmer air and water from the North Atlantic into the Arctic.
- Anticyclonic Beaufort Gyre is strengthened;
- Cyclonic circulation in the eastern Arctic is suppressed;
- Less ice and fresh water transport through Fram Strait from the Arctic, enhancing deep-water convection in the Greenland Sea;
- Decreased cyclonicity causing convergence of ice drift and surface circulation, leading to depression of the Atlantic Water.
- Well-developed Arctic High resulting in intensified anticyclonic ice drift and surface circulation, convergence of surface currents

Figure 1.5. Positive and negative phases of the Arctic Multidecadal Variability (MDV) are shown in this scheme (Polyakov et al., 2004). The particular changes in the atmosphere – ice – ocean system are described for each phase. Figure from http://research.iarc.uaf.edu/multidecadal_variability/ (Visited on 1st March 2013).

1.3. Biomarkers for paleoclimate reconstruction

Organic proxies, or biomarkers, are organic molecules that can be preserved in marine, lacustrine sediments and soils for thousands or even millions of years. The analysis of biomarkers gives an indirect observation of past climate variability and other environmental parameters. Distinct organisms synthesize organic molecules that can give information on past environments (Figure 1.6). A detailed description of the biomarkers used in this PhD thesis is given below.

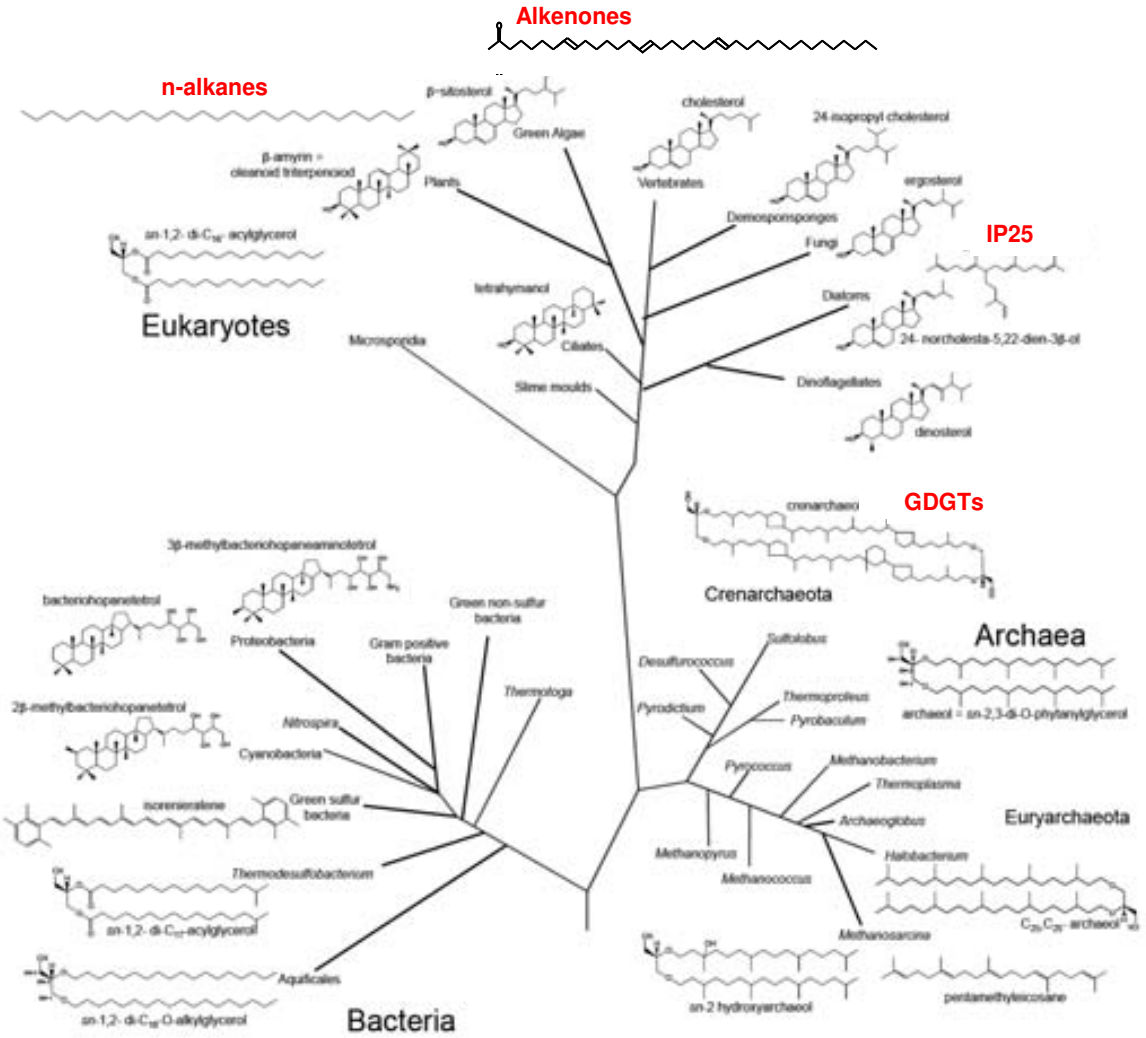

Figure 1.6. A "Tree of Life" illustrating the diverse lipid structures characteristic from various organisms at the domain level. Many of these structures are preserved in organic matter and can be extracted from marine sediments and soils. The biomarkers that were used in this thesis are highlighted in red. The figure is adapted after Johnson et al. (2013).

1.3.1. Alkenones

Alkenones are long chain ketones with 37 to 40 carbon atoms (C_{37}, C_{38}, C_{39}, C_{40}) and 2 to 4 double bonds or unsaturations (i.e. $C_{37:2}$, $C_{37:3}$, $C_{37:4}$) (Figure 1.7). They are ubiquitous compounds in the oceans worldwide and they are usually found in marine sediments together with alkyl alkenoates (Figure 1.7). Alkenones are biosynthesized by some algae of the class *Prymnesiophyceae* (Marlowe et al., 1984a, Marlowe et al., 1984b). The main producers of alkenones in the oceans are the widespread species of coccolithophorids *Emiliana huxleyi* and *Gephyrocapsae oceanica* (Volkman et al., 1980, Volkman et al., 1995, Conte et al., 1995). The number of double bonds contained in the hydrocarbon chain is directly related to the water temperature where the algae synthesizing alkenones live. In colder waters, more of the $C_{37:3}$ alkenone and less of the $C_{37:2}$ are synthesized, whereas in warmer waters it is the opposite (Brassell et al., 1986a,b).

1.3.1.1. U^{K}_{37} and $U^{K'}_{37}$ indices for sea surface temperature reconstruction

The alkenone unsaturation index U^{K}_{37} is a measure of the relative distribution of the di, tri and tetraunsaturated ketones (Brassell et al., 1986a,b) expressed as:

$$U^{K}_{37} = \frac{C_{37:2} - C_{37:4}}{C_{37:2} + C_{37:3} + C_{37:4}}$$

As the tetraunsaturated ketone is only found at high latitudes, a simplified index excluding $C_{37:4}$ alkenone was proposed, the $U^{K'}_{37}$ (Prahl and Wakeham, 1987):

$$U^{K'}_{37} = \frac{C_{37:2}}{C_{37:2} + C_{37:3}}$$

Prahl and Wakeham (1987) cultivated a single strain of *Emiliana huxleyi* and incubated it at a range of temperatures. They analyzed the relative distribution of Alkenones in samples from this culture experiment, and found a linear relationship between $U^{K'}_{37}$ and water temperature:

$$U^{K'}_{37} = 0.040 \cdot SST(^{o}C) - 0.110 \quad (R^2 = 0.989)$$

This relationship was further validated comparing the laboratory results with the $U^{K'}_{37}$ analyses in water column particulate samples retrieved from the eastern Pacific Ocean, with measured *in situ* water temperature (Prahl et al., 1988). The authors obtained a slightly modified linear relationship to temperature:

$$U^{K'}_{37} = 0.034 \cdot SST + 0.039(^{o}C) \quad (R^2 = 0.994)$$

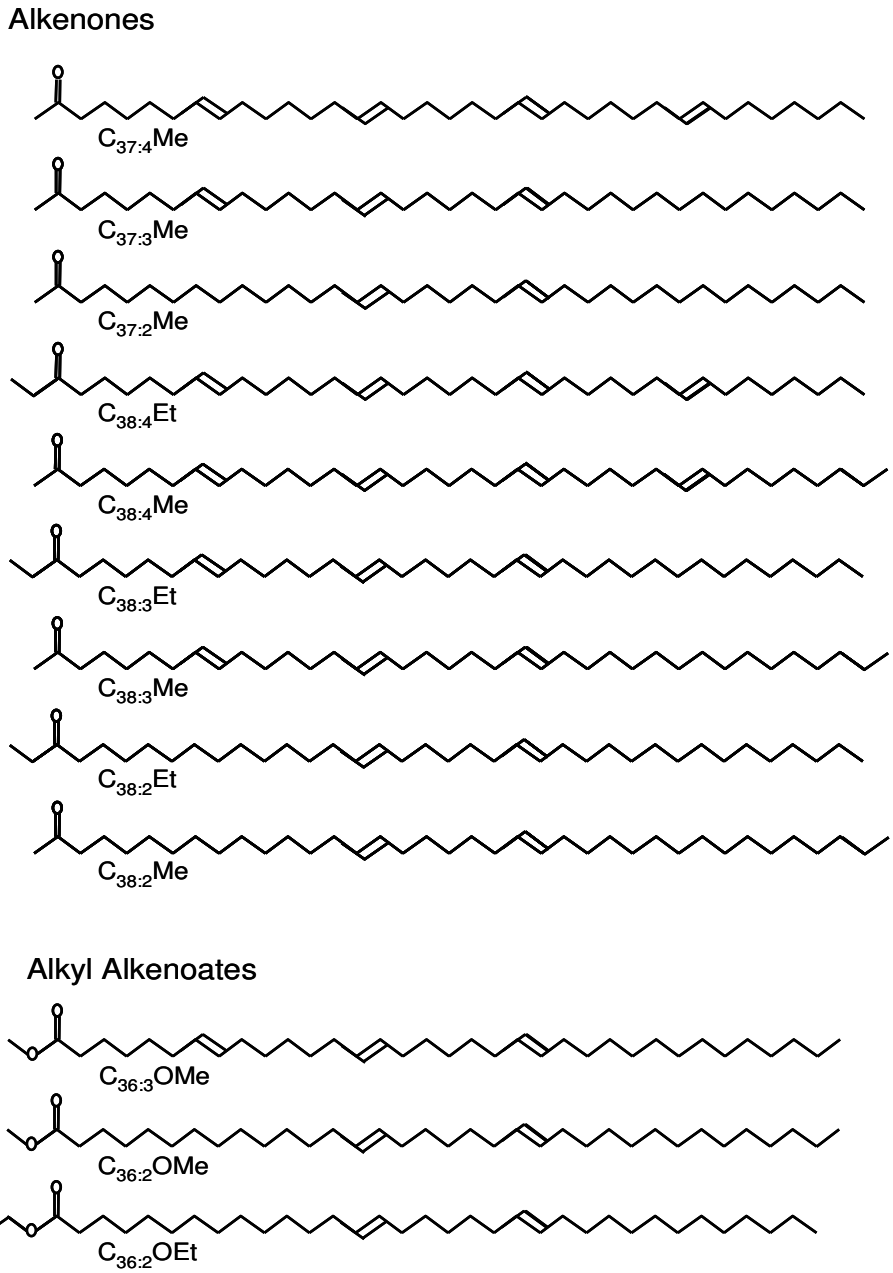

Figure 1.7. Molecular structures of alkenones and alkyl alkenoates (Bendle et al., 2009).

Müller et al. (1998) established a global core top calibration from the analysis of the $U^{K'}_{37}$ index in 370 surface sediments that encompassed the Atlantic, Indian and Pacific Oceans from 60 °N to 60 °S (Figure 1.8). They calibrated the $U^{K'}_{37}$ index towards annual mean atlas SST at 0 m water depth, covering a temperature range from 0 to 29 °C. The resulting relationship was:

$$U^{K'}_{37} = 0.033 \cdot SST(^{o}C) + 0.044 \quad (R^2 = 0.958)$$

This calibration is, within error limits, identical to the previous calibration by Prahl et al. (1988) based on culture studies. In addition, the calibration from Müller et al. (1988) covers the entire range of temperature and biogeographic zones of alkenone synthesizers. However, it is biased toward continental margin sediments (Herbert, 2003).

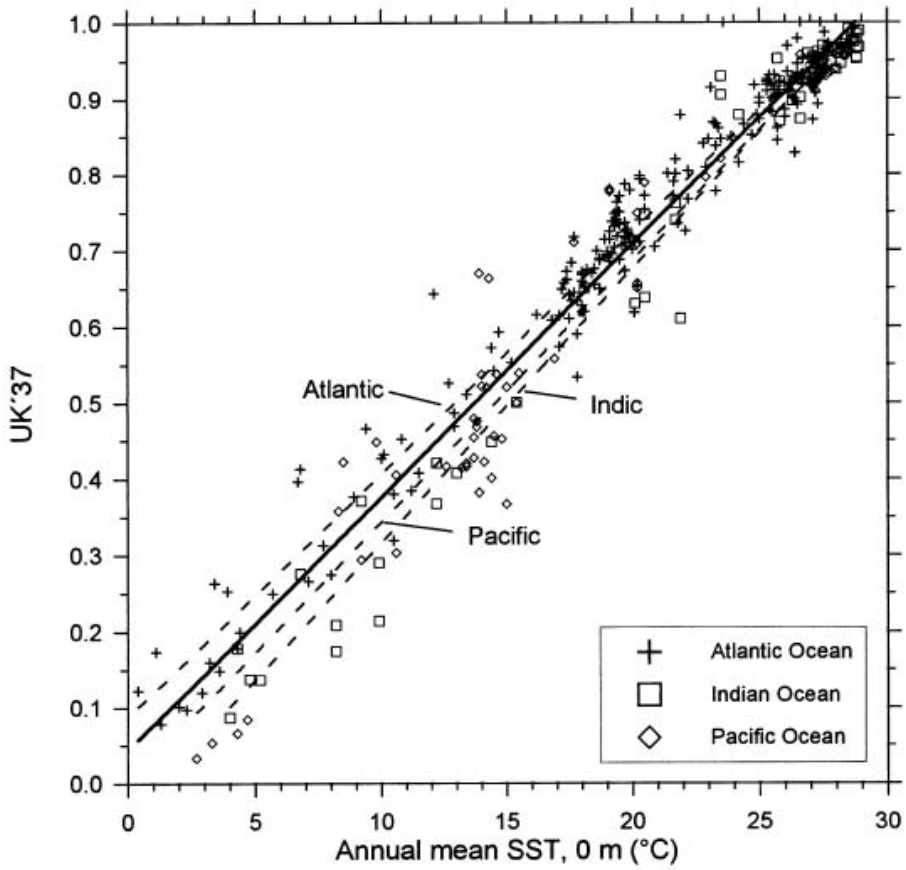

Figure 1.8. Müller et al. (1998) correlation between $U^{K'}_{37}$ and annual mean SST (0 m) for surface sediments from the global Ocean between 60 °S and 60 °N. The obtained global core top calibration ($U^{K'}_{37}$ = 0.033 · SST + 0.044) is absolutely identical to the equation obtained from culture experiments ($U^{K'}_{37}$ = 0.033 · SST + 0.043) of the coccolithophorid *Emiliana huxleyi* by Prahl and Wakeham (1987) corroborating its general applicability (Müller et al., 1998).

Increasing error in SST estimates from regions in the Nordic seas where SST is lower than 6 °C were reported, and more accurate SST estimates are usually obtained using the original index U^{K}_{37} that incorporates the $C_{37:4}$ alkenone (Rosell-Melé et al., 1994; Rosell-Melé, 1998; Bendle and Rosell-Melé, 2004). Rosell-Melé et al. (1995) conducted a field calibration of the U^{K}_{37} index that included 109 surface sediments from the northeastern Atlantic (2 °S – 75 °N). They obtained high correlation coefficients

using surface temperatures (0 m) calibrated towards U^{K}_{37} values and the calibration equation yielded valid reconstructions over a wide range of SST (0 – 28 °C) (Rosell-Melé et al., 1995). The resulting calibration using annual temperatures at 0 m water depth is:

$$U^{K}_{37} = 0.162 \pm 0.02 + 0.029 \pm 0.001 \cdot SST \ (R^2 = 0.981)$$

Furthermore Bendle and Rosell-Melé (2004) collected surface waters across the Nordic Seas and analyzed the alkenone content in filtered particulate organic matter. They found that the estimates of $U^{K'}_{37}$ in the Nordic Seas are regionally constrained. In the northern Atlantic, the Norwegian basin and the Icelandic Shelf the $U^{K'}_{37}$ estimates fell within the linear range of the global core top calibration by Müller et al. (1998). Reliable $U^{K'}_{37}$ estimates can therefore be obtained in these areas if the circulation and sedimentary regimes are similar to present conditions, i.e. in recent sediments from the Late Holocene (Bendle and Rosell-Melé, 2004).

1.3.1.2. $\%C_{37:4}$ as a qualitative indicator of polar water mass extent

In the subpolar and polar regions of the Nordic Seas, there is an increased proportion of the alkenone $C_{37:4}$ relative to $C_{37:3}$ and $C_{37:2}$ alkenones (Rosell-Melé et al., 1994, Rosell-Melé 1998). This can be expressed with the index $\%C_{37:4}$ as suggested by Rosell-Melé et al., (1998):

$$\%C_{37:4} = \frac{C_{37:4}}{C_{37:2} + C_{37:3} + C_{37:4}} \times 100$$

The percent of $C_{37:4}$ is related to salinity in the Nordic Seas and the North Atlantic, and higher $\%C_{37:4}$ is found in water masses with decreased salinity and viceversa (Rosell-Melé, 1998, Rosell-Melé et al., 2002). Further research showed that although the $\%C_{37:4}$ index can not be used to quantitatively reconstruct past variations in salinity, it has potential as a qualitative indicator of polar water mass extent (Bendle et al., 2005). For instance, the analysis of alkenones in surface water column particulates revealed that high $\%C_{37:4}$ values formed a cluster associated with polar waters whereas low values were related to Atlantic waters. The intermediate water masses showed in between $\%C_{37:4}$ values (Bendle et al., 2005). This proxy has been used in a variety of environments and time spans to reconstruct past variability in water mass type (Bard et al., 2000; Martrat et al., 2004; McClymont et al., 2008; Rosell-Melé et al., 1998; Rosell-Melé et al., 2002; Martínez-Garcia et al., 2010).

The value of $\%C_{37:4}$ has also been used as an indicator for the reliability of the $U^{K'}_{37}$ SST based estimates. Rosell-Melé (1998) recommended caution when considering

absolute SST values in the Nordic Seas and proposed a threshold value of 5% in the percent of $C_{37:4}$ from which the relationship between $U^{K'}_{37}$ and SST was subject to increasing errors. However, as mentioned above, further research found that the estimates of $U^{K'}_{37}$ in the Nordic Seas are regionally constrained (Bendle and Rosell-Melé 2004).

1.3.2. Glycerol dialkyl glycerol tetraethers (GDGTs)

Isoprenoid and branched Glycerol dialkyl glycerol tetraethers (GDGTs; Figure 1.9) are cell membrane lipids of high molecular weight synthesized by Archaea (DeRosa and Gambacorta, 1988) and Bacteria (Weijers et al., 2006a). Some features distinguish the molecular structures of archaeal from the bacterial lipids (Koga et al., 1993). Archaea biosynthesize different types of isoprenoid GDGTs with a basic molecular structure consisting of two isoprenoid chains with 40 carbons that are linked to two polar head groups by ether bonds and two terminal glycerols (Koga and Morii, 2005). In addition, isoprenoid GDGTs can contain from none to eight cyclopentane moieties and even a cyclohexane ring with four cyclopentane moieties (crenarchaeol and crenarchaeol regioisomer) (Figure 1.9; Schouten et al, 2000; Sinninghe Damsté et al., 2002).

Incubation experiments showed that there was a positive relationship between the number of cyclopentane rings in isoprenoid GDGTs with increasing culture temperature. This is considered to be an adaptation mechanism to maintain cell membrane fluidity at increasing temperatures (De Rosa and Gambacorta, 1988; Gliozzi et al., 1983; Uda et al., 2001). These lipids are synthesized by marine Thaumarchaeota, formerly known as Group I Crenarchaoeta (Brochier-Armanet et al., 2008), which are widespread in the marine water column and dominate the populations of prokaryotes in the Oceans (Karner et al., 2001), and are also ubiquitous in terrestrial environments (Leininger et al., 2006).

Branched GDGTs have both archaeal and bacterial molecular structure traits but are hypothesized to be of bacterial origin on the basis of the stereochemistry of their glycerol moieties (Weijers et al., 2006a). Their lipid structure consist of branched instead of isoprenoid alkyl chains, with four to six methyl branches and can contain up to two cyclopentane moieties (Figure 1.9; Sinninghe Damsté et al., 2000; Weijers et al., 2006a). It is likely that the microbes synthesizing these lipids are heterotrophs (Pancost and Sinninghe Damsté, 2003; Weijers et al., 2009). The group of bacteria that synthesize branched GDGTs has not been identified yet, but recently GDGT I (Figure 1.9) was found in two species of *Acidobacteria* (Sininghé-Damsté et al., 2011). However,

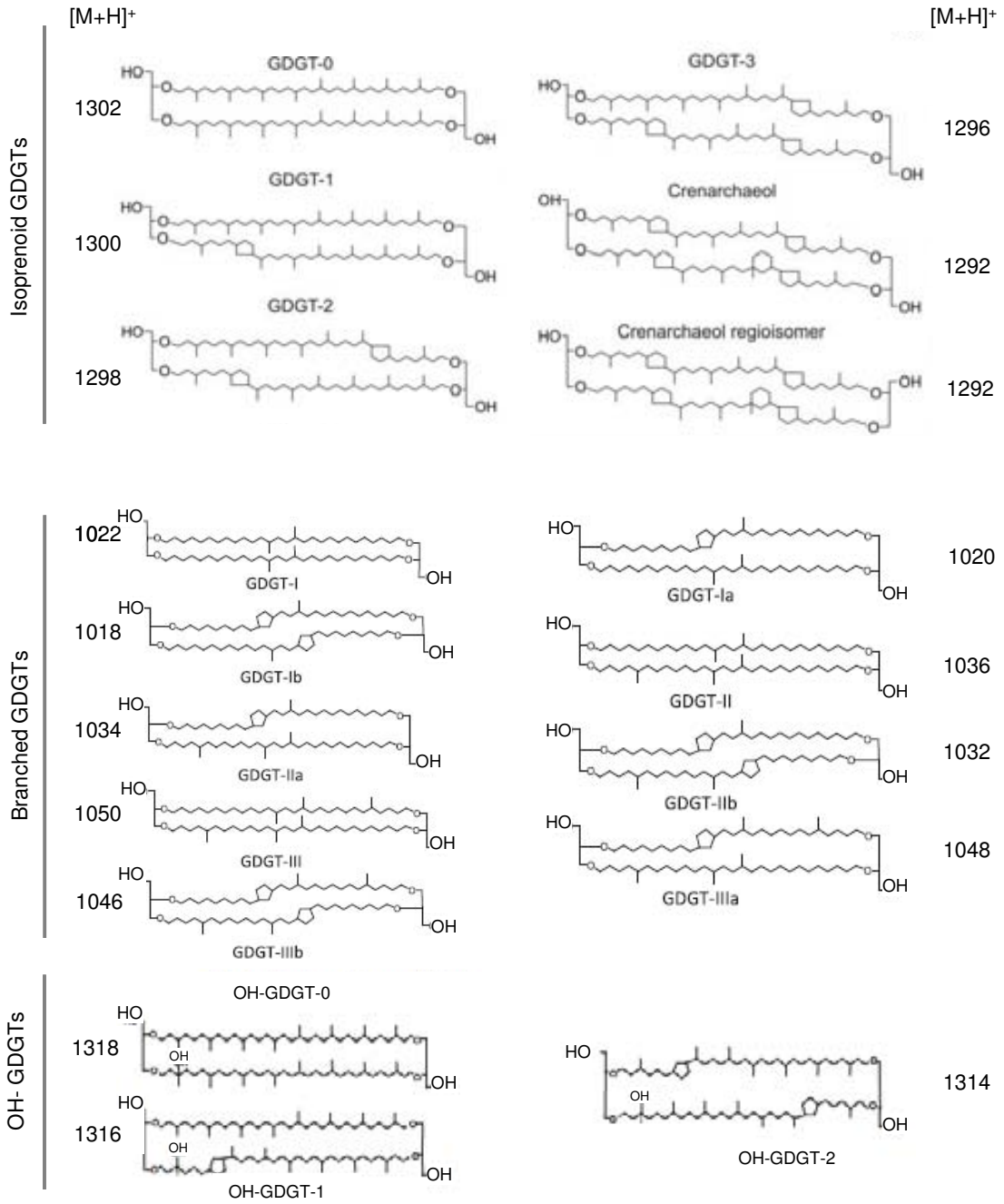

Figure 1.9. Structures and *m/z* values of GDGT protonated molecules [M+H]+. The figure illustrates isoprenoid (GDGTs 0 to VI; Schouten et al., 2000), branched (GDGT-I,a,b to III,a,b; Sinninghe-Damsté et al., 2000) and recently discovered hydroxy-GDGT or OH-GDGT (Liu et al., 2012).

Acidobacteria have an aerobic metabolism and branched GDGTs occur in higher proportions in low oxygen environments, suggesting that other groups of bacteria also synthesize branched GDGTs (Sininghé-Damsté et al., 2011). Branched GDGTs were initially identified as exclusive of terrestrial environments as they occur ubiquitously in peat bogs (Sinninghe Damsté et al., 2000) and soils (Weijers et al., 2006b, 2007a) but also in sedimentary settings that receive significant terrestrial input such as coastal marine

sediments (Hopmans et al., 2004). Moreover, *in situ* production of branched GDGTs in lacustrine sediments (Tierney and Russsell, 2009; Tierney et al., 2010, Sinninghe – Damsté et al., 2009; Bechtel et al., 2010, Blaga et al., 2010; Zink et al., 2010; Sun et al., 2011) and in coastal marine sites (Peterse et al, 2009a; Zhu et al., 2011) has been recently suggested. Furthermore, Fietz et al. (2012) found that crenarchaeol and branched GDGTs were correlated on a regional basis in globally distributed records. This finding was unexpected, as crenarchaeol was understood as a marker for mesophilic Thaumarchaeota mostly of aquatic origin (Sinninghe Damsté et al., 2002), whereas branched GDGTs were proposed as markers for soil bacteria (Weijers et al., 2010). They suggested that a mixed source origin for both GDGT types in lacustrine and marine settings could explain the positive correlation found between both markers in worldwide distributed sites (Fietz et al., 2012).

In living cells, the GDGTs that constitute the membrane lipid bilayer have polar head groups attached to the carbon chains. This structure is referred to as intact polar lipid (Figure 1.10). However, the polar head groups of both isoprenoid and branched GDGTs were found to be detached and easily degraded within weeks after the cell lysis (White et al., 1979; Harvey et al., 1986). In the aquatic environment, the process can happen already in the water column and only the remaining structure of cell material sinks to the seafloor. The structure remaining after polar head group separation is named core GDGT (Figure 1.9).

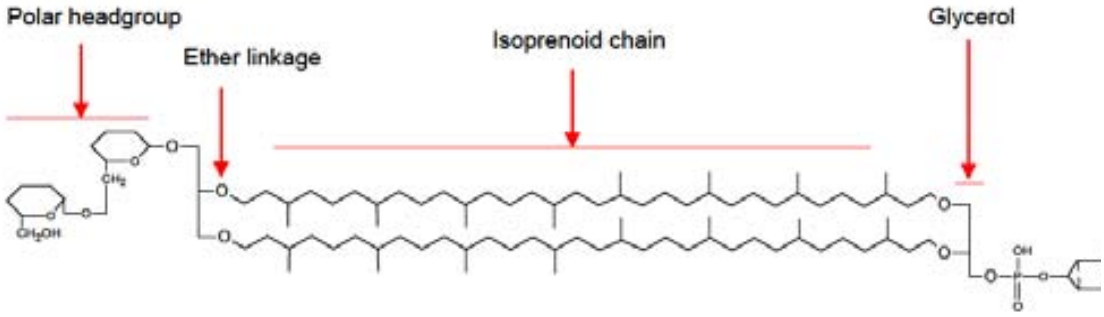

Figure 1.10. Example of an intact polar lipid molecular structure. In living cells, the polar head groups are attached to glycerol moieties, which are in turn linked with ether bonds to the double C_{40} isoprenoid chains (Escala, 2009).

In the last decade, proxies for estimating past variations in air (MBT/CBT) and water temperatures (TEX_{86}), as well as variability in terrestrial organic matter input to the aquatic environment (BIT) have been developed based on core GDGTs and are described below. Part of the GDGT data generated within this PhD thesis were used in

parallel studies in which we aimed to expand the understanding and limits of applicability of these recently developed proxies (Escala et al., 2009; Fietz et al., 2011a,b; Fietz et al., 2012, Fietz et al., 2013, Ho et al., in review). Another part of the GDGT data has been used in chapters 3, 4 and 5.

1.3.2.1. TEX_{86} index for SST reconstruction

The index of tetraethers with 86 carbons (TEX_{86}) was proposed in 2002 as a new molecular proxy for estimating past SSTs (Schouten et al., 2002). It is based on the relative distribution of isoprenoid GDGTs (Figure 1.9). The index is defined as follows (the numbers refer to the *m/z* values of GDGT protonated molecules shown in figure 1.9):

$$TEX_{86} = \frac{[1298]+[1296]+[1292\ \text{regioisomer}]}{[1300]+[1298]+[1296]+[1292\ \text{regioisomer}]}$$

The TEX_{86} index correlated with annual mean SST in a small set of surface sediment samples (n = 44; Figure 1.11A; Schouten et al., 2002). An extensive global core top calibration (n = 284) correlated the TEX_{86} with annual mean temperatures of the upper mixed layer of the water column, establishing a linear correlation with SST for the temperature range between 5 and 30 °C (Figure 1.11A; Kim et al., 2008):

$$SST\ (^{o}C) = 56.2 \cdot TEX_{86} - 10.8\ (R^2 = 0.935)$$

They found that from -2 °C to 5 °C the relationship between TEX_{86} and SST was no longer linear, suggesting that the TEX_{86} was not applicable in the polar oceans (Kim et al., 2008). Further research extended the calibration with the addition of surface sediments mainly from the polar oceans further confirming that other factors than SST influenced TEX_{86} variability in these regions (Kim et al., 2010). However they found that at temperatures below 15 °C, a modified GDGT index that excluded the crenarchaeol regioisomer, the TEX_{86}^{L}, correlated better than the TEX_{86} with SST:

$$TEX_{86}^{L} = -LOG\frac{[1298]}{[1300]+[1298]+[1296]}$$

$$SST\ (^{o}C) = 67.5 \cdot TEX_{86}^{L} + 46.9\ (R^2 = 0.86)$$

The calibration error of the TEX_{86}^{L} with temperature has a value of 4 °C (Figure 1.11B; Kim et al., 2010), which is larger than the error of other SST proxies such as the $U^{K'}_{37}$ index that has an error of 1.5 °C (Müller et al., 1998). The TEX_{86} proxies are less accurate in reconstructing absolute temperatures (Schouten et al., 2013).

A calibration of the TEX_{86} and TEX_{86}^{L} indices in subpolar and Polar regions using core top samples from 160 sites distributed across the Arctic, Southern Ocean and the North Pacific is in progress (Ho et al., in review). The main implication regarding the area of study within this thesis is that the relationship of the TEX_{86} proxies to water temperature varies depending on the region where it is applied. In fact, the data from the Fram Strait forms a separate cluster compared to the rest of the dataset and in the Barents Sea region, the indices based on isoprenoid GDGTs do not covary with water temperature (Ho et al., in review). Therefore caution is necessary with the application of TEX_{86}^{L} in the Arctic region of the Atlantic Ocean.

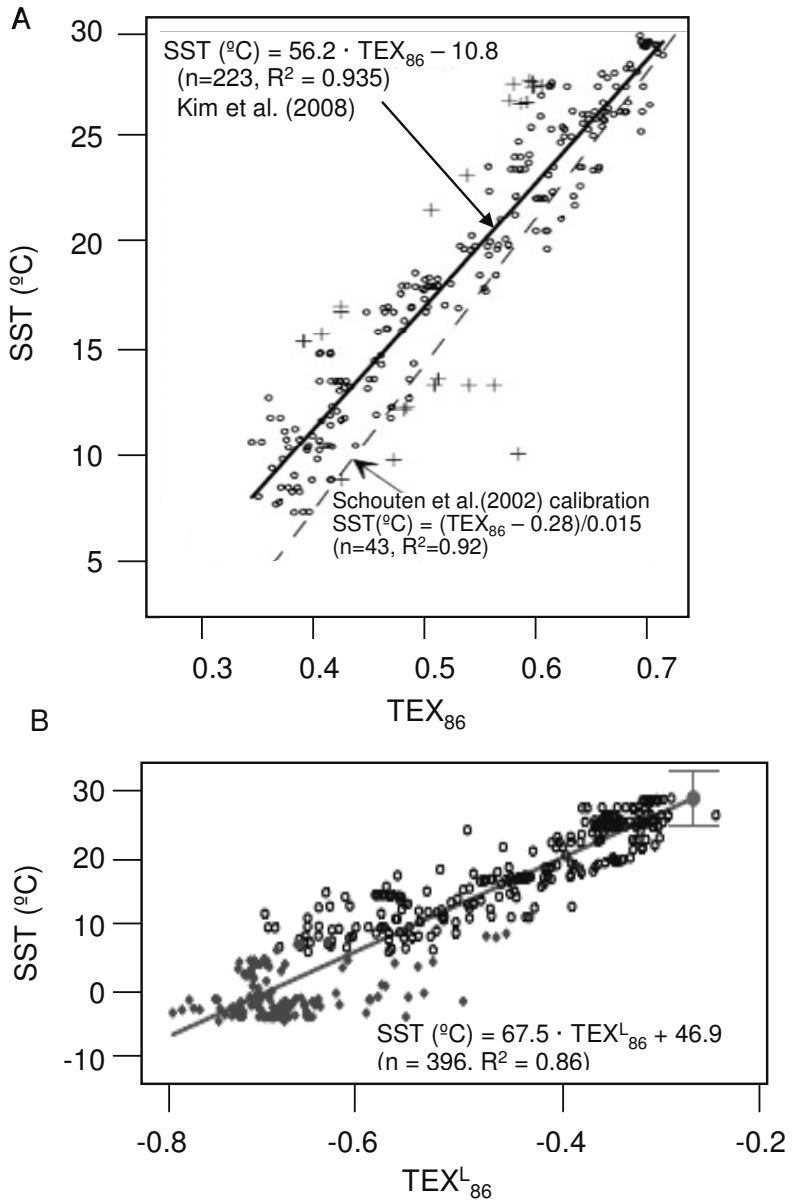

Figure 1.11. Relationship between annual mean SST and the TEX_{86} (A: Kim et al., 2008, Schouten et al., 2002) and TEX^{L}_{86} (B: Kim et al., 2010) from global core top studies.

Very recently, a new class of GDGTs with a hydroxylation in one of the alkyl chains has been identified in marine sediments (Figure 1.9; Liu et al., 2012). Huguet et al. (2013) have recently reported that these hydroxy-GDGTs (OH-GDGTs) are widespread and abundant in marine and lacustrine environments and found increasing contributions of these compounds towards higher latitudes and lower water temperatures. There is a significant correlation between the relative abundance of OH-GDGTs and SST in surface sediments, suggesting that these newly identified lipids have potential to become new proxies for reconstructing past SST in the lower range of water temperatures that are found at high latitudes (Huguet et al., 2013). Moreover, at a regional scale in the Nordic Seas the OH-GDGTs are ubiquitous, their relative abundance to the total pool of GDGTs increases in polar water masses and the number of cyclopentane rings in OH-GDGTs has been found to increase with water temperature (Fietz et al., 2013). Although being based on a limited number of samples, these studies shed light on the development of new GDGT based proxies that could be used as complementary paleothermometers in the polar regions (Fietz et al., 2013).

1.3.2.2. MBT/CBT index as a continental paleothermometer

After measuring the branched GDGT content in 134 globally distributed soil samples Weijers et al. (2007a) found that the number of methyl alkyl chains in branched GDGTs, expressed as the methylation index of branched tetraethers (MBT), correlated with air temperature ($R^2 = 0.62$) and with the pH of the soil ($R^2 = 0.37$) (Figure 1.12). In addition, they found that the number of cyclopentane moieties expressed with the cyclization index of branched tetraethers (CBT) correlated with the pH of the soil ($R^2 = 0.70$) (Weijers et al., 2007a). The MBT and CBT indices were defined as follows:

$$CBT = -LOG\left(\frac{([1020]+[1034])}{([1022]+[1036])}\right)$$

$$MBT = \frac{[1022]+[1020]+[1018]}{[1050]+[1048]+[1046]+[1036]+[1034]+[1032]+[1022]+[1020]+[1018]}$$

The numbers in the above equations refer to the *m/z* values of GDGT protonated molecules shown in figure 1.9. The correlation between mean annual air temperature (MAT) and the MBT/CBT indices was defined as (Figure 1.12; Weijers et al., 2007a):

$$MBT = 0.122 + 0.187 \cdot CBT + 0.020 \cdot MAT \ (R^2 = 0.77)$$

Recently this calibration was expanded with the analysis of 278 globally distributed soils (Peterse et al., 2012). The authors simplified the MBT index to the MBT' index, which excludes the GDGTs with mass 1048 and 1046 since they are generally below the detection limit or occur in low abundance in the environment:

$$MBT' = \frac{[1022]+[1020]+[1018]}{[1050]+[1036]+[1034]+[1032]+[1022]+[1020]+[1018]}$$

The following new equation was obtained (Peterse et al., 2012):

$$MAT = 0.81 - 5.67 \cdot CBT + 31.0 \cdot MBT' \ (R^2 = 0.59).$$

The error of the calibration is 5 °C and therefore gives large uncertainties in absolute MAT estimates (Peterse et al., 2012). However, the error in the calibration is considered a systematic one and the error in using MAT estimates within a single downcore to reconstruct past relative variations in temperature should be lower (Schouten et al., 2013).

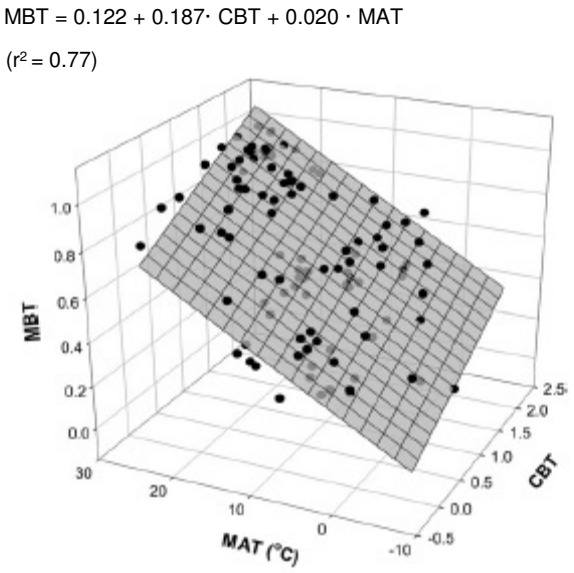

Figure 1.12. Calibration plot of the MBT and CBT indices measured in soils vs. annual mean air temperature (MAT) (Weijers et al., 2007a).

The relationship between the relative distribution of branched GDGT and soil temperature and pH was further studied. For example, a measure of the relative abundance of branched GDGTs in an altitudinal soil transect yielded a good correlation of MBT/CBT with MAT, but absolute estimates were higher than measured temperatures (Sinninghe-Damsté et al., 2008). Another study conducted in geothermally heated soils over a large temperature range (12 – 41 °C) further confirmed the dependence of the MBT/CBT index on soil temperature and pH (Peterse

et al. 2009b). Different regional studies gave small but significant different correlations of the MBT/CBT index with MAT and soil pH, suggesting that regional soil calibrations might give more precise air temperature estimates rather than the global ones (Schouten et al., 2013).

To date the MBT/CBT proxy has been used to reconstruct past changes in air temperature at different temporal scales and in a wide range of geographical settings, for instance the Congo deep sea fan (Weijers et al., 2007b), North America (Fawcett et al., 2011), East Greenland (Schouten et al., 2008), the Arctic (Weijers et al., 2007c), marine sediments near Svalbard (Peterse et al., 2009a), and the East China sea (Zhu et al., 2011).

1.3.2.3. BIT index as indicative of terrigenous input

Hopmans et al. (2004) defined the branched isoprenoid tetraether (BIT) index as the relative abundance between crenarchaeol and three branched GDGTs, which are the most frequently and abundantly found in soils (Hopmans et al., 2004):

$$\mathrm{BIT} = \frac{[1300] + [1298] + [1296]}{[1300] + [1298] + [1296] + [\mathrm{crenarchaeol}]}$$

The ratio was intended as a proxy of terrestrial organic inputs on the basis that crenarchaeol was a dominant GDGT in the aquatic environment, whereas branched GDGTs seemed to be predominant in the terrestrial environment. The ratio would be expected to have values close to 0 when measured in open marine sediments and close to 1 when analyzed in soil and peat samples. Values in between would be indicative of the relative contribution of terrestrial organic matter to the aquatic environment (Hopmans et al., 2004). The BIT index has been also used as an indicator for assessing the applicability of the TEX_{86} index in marine coastal areas because soil derived organic matter transported to the marine environment can contain isoprenoid GDGTs that can potentially bias the TEX_{86} temperature estimates (Weijers et al., 2006b). It was reported that BIT values above 0.3 (Weijers et al., 2006b) or above 0.2 (Zhu et al., 2011) biased the TEX_{86} water temperature estimates.

However, recent studies reassessed the BIT index applicability by Fietz et al. (2011b) showed that at different time spans and settings - Alboran Sea, Fram Strait, North East Atlantic, Southern Ocean and Lake Baikal – the BIT index does not only reflect changes in the input of terrestrial organic matter but it also depends on the variations in the *in situ* production of crenarchaeol sinthesized by Thaumarchaeota in the aquatic environment, and proposed that the quantification of fluxes of branched

GDGTs might be a better indicator of terrestrial inputs to the aquatic environment (Fietz et al., 2011b). Similar results were found in the Gulf of Mexico (Smith et al., 2012).

1.3.3. Highly branched isoprenoid (HBI) alkenes

A small number of marine and freshwater diatoms that belong to the genera *Haslea, Rhizosolenia, Navicula* and *Pleurosigma* biosynthesize highly branched isoprenoid alkenes (HBI) (Volkman et al., 1994; Massé et al., 2004; Sinninghe-Damsté et al., 2004). These secondary metabolites have uncommon molecular structures and can contain 20, 25 or 30 carbons (C_{20}, C_{25} and C_{30} alkenes), although the C_{25} alkenes are the most commonly reported and found to be widely distributed in marine sediments worldwide (Rowland and Robson, 1990; Belt et al., 2000). Most of the C_{25} HBI that have been found in marine sediments contain from 2 to 5 double bonds, but unsaturated isomers have been reported as well (Rowland and Robson, 1990; Wraige et al., 1997; Belt et al., 2000). Although the mechanisms involved in HBI biosynthesis in diatoms have been described, their metabolic function in diatom cells is still unknown (Massé et al., 2004).

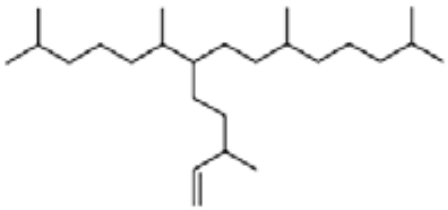

Figure 1.13. Molecular structure of IP25 (Belt et al., 2007).

1.3.3.1. Ice proxy with 25 carbon atoms (IP25)

Belt et al. (2007) collected sea ice samples across the Canadian Arctic Archipelago and the Hudson Bay during the spring algal bloom and identified C_{25} HBI mono-unsaturated alkenes in the sample extracts (Figure 1.13). They found that this compound was selectively synthesized by some Arctic sea ice diatoms, probably of the genera *Haslea*, but they did not detect the C_{25} HBI in open water phytoplankton samples collected from an East-West transect across the Canadian Arctic Archipelago (Belt et al., 2007). Based on these facts, they renamed this specific C_{25} HBI monoene as Ice Proxy with 25 Carbon Atoms (IP25), establishing the basis for a new tool for reconstructing past sea ice cover variability (Belt et al., 2007).

After identification of IP25 as a specific compound in Arctic sea ice (Belt et al., 2007), the accumulation of this molecule in Arctic sea ice cores was analyzed by Brown et al. (2011). Most of the IP25 (ca. 90%) was found to be synthesized within the lower 5 cm inside the interstitial channels formed after brine release and maximum accumulation of IP25 was found between 1 to 3 cm from the ice-water interface (Brown et al., 2011). This study provided further evidence for a selective sea ice diatom origin for IP25. They found a strong seasonal influence in IP25 production. It was not detected during winter, its abundance started increasing in spring and reached maximum concentrations (more than 90% of total) when the algal bloom took place at the end of spring (Brown et al., 2011). The dependence of IP25 on the seasonality of the sea ice cover was further confirmed by Fahl and Stein (2012) after studying the material collected in sediment traps deployed in a region of the Arctic Ocean with seasonal ice cover conditions (Figure 1.14). During winter permanent ice cover conditions, IP25 did not reach the sediment traps whereas a maximum in IP25 was detected at the end of spring when sea ice cover started melting (Fahl and Stein 2012).

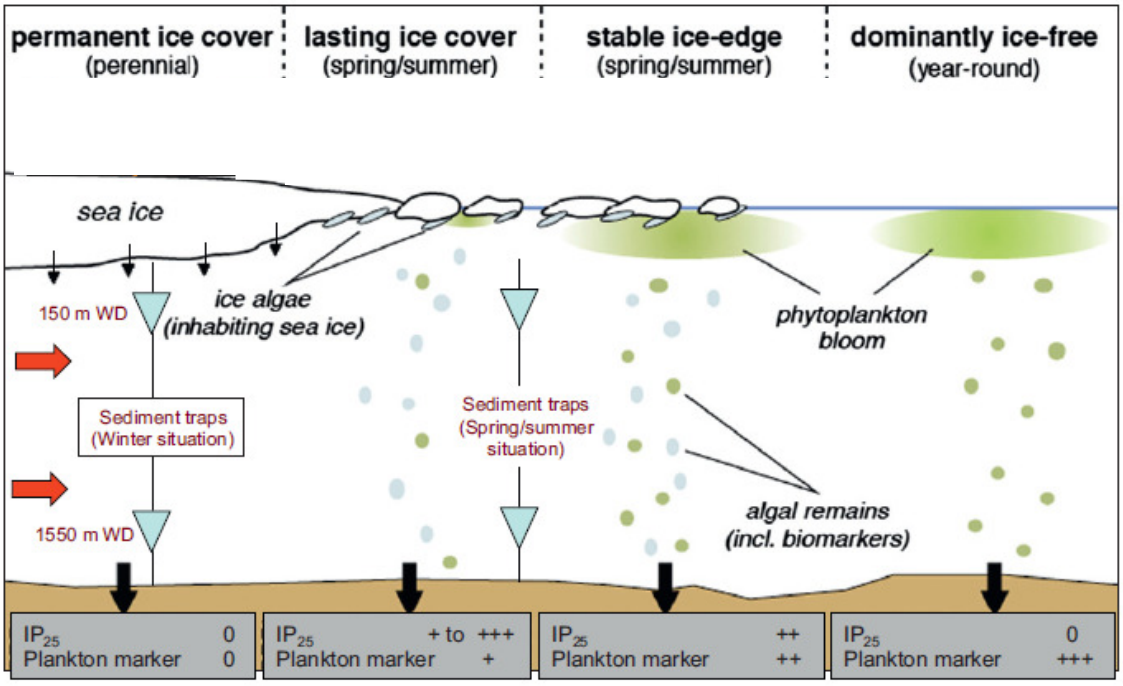

Figure 1.14. Illustration of different sea surface conditions over an annual cycle in an area characterized with seasonal sea ice cover conditions. The blue and green particles in the illustrated water column indicate IP25 and phytoplankton fluxes from the surface to the seafloor, which vary depending on the sea ice cover conditions in the study area. The grey boxes at the bottom of the figure indicate the relative amount of IP25 and of the plankton marker that would be expected to be found in the marine sedimentary record in each surface sea ice cover condition. The sediment traps locations refer to sediment trap study in the Lomonosov Ridge from Fahl and Stein (2012) discussed in the text. The figure is from Fahl and Stein (2012).

The growth of sea ice diatoms is controlled by various factors such as the availability of nutrients in the underlying water column, sea ice thickness and snow cover, rapid bottom ice melt and it is also subject to light availability (Belt and Müller, 2013 and references therein). As light availability is limited under thick and dense ice cover, under perennial ice cover conditions the accumulation of diatoms synthesizing IP25 and its subsequent release to the seafloor is significantly reduced (Belt et al., 2007). Therefore when IP25 is not detected in the marine sediments, it can indicate open sea water conditions but also permanent sea ice cover conditions year round (Figure 1.14) (Belt et al., 2007). One way of resolving such ambiguity in the sea ice biomarker could be comparing the relative downcore abundances of IP25 to a phytoplankton marker indicative of open water conditions (Müller et al., 2009). This approach was applied in a sediment core from the Yermak Plateau, using brassicasterol abundance as an indicator of ice free sea surface conditions (Müller et al. 2009). The absence (or low abundance) of both brassicasterol and IP25 was related to past permanent sea ice cover conditions whereas the presence of brassicasterol and absence of IP25 was associated to periods of ice free conditions (Müller et al., 2009). Müller et al. (2011) combined both IP25 and phytoplankton markers into the PIP25 index, defined as follows:

$$PIP25 = IP25 / (IP25 + (\text{phytoplankton marker} * C))$$

Where "IP25" and "phytoplankton marker" are given in their respective concentrations. Accounting for a possible significant concentration difference between IP25 and the phytoplankton marker, a concentration balance factor between the two markers is taken into account as follows:

$$C = \text{mean IP25 concentration} / \text{mean phytoplankton marker concentration}$$

Furthermore IP25 and phytoplankton markers were analyzed in a set of surface sediments from the Fram Strait (Müller et al., 2011) and the Barents Sea (Navarro-Rodriguez, 2012) and the data was combined to satellite derived sea ice cover concentrations. They found a correlation between the PIP25 and the sea ice cover satellite data, which is different for the two regions. High PIP25 values were associated to areas with a dense spring ice cover, moderate values in sites close to the ice edge, low values in regions characterized by seasonal ice cover and finally very low or zero values in ice free areas year round (Müller et al., 2011). Although recent studies have used brassicasterol as a phytoplankton indicator of open water conditions, it could also be feasible to determine PIP25 indices using other marine biomarkers synthesized by organisms living in the surface oceans under ice free conditions (Müller et al., 2011).

As mentioned earlier, Fahl and Stein (2012) also found a correlation between sea ice cover conditions throughout the annual cycle and the amount of IP25, but also with

the brassicasterol and the PIP25 index. In addition, they found that both IP25 and brassicasterol values decreased systematically from 150 m to 1550 m of the water column, possibly due to biogeochemical degradation with increasing water depth or incorporation of organic carbon to the food web (Brown and Belt, 2012). Therefore IP25 concentrations in the sedimentary record should be interpreted as exported productivity from the surface of the water column to the seafloor (Figure 1.15).

In the recent years, IP25 has been used in paleoclimate studies to reconstruct past sea ice cover variability in different settings across the Arctic Ocean and encompassing different time spans (Massé et al., 2008, Andrews et al., 2009; Müller et al., 2009, 2012; Belt et al., 2010; Vare et al., 2009, 2010).

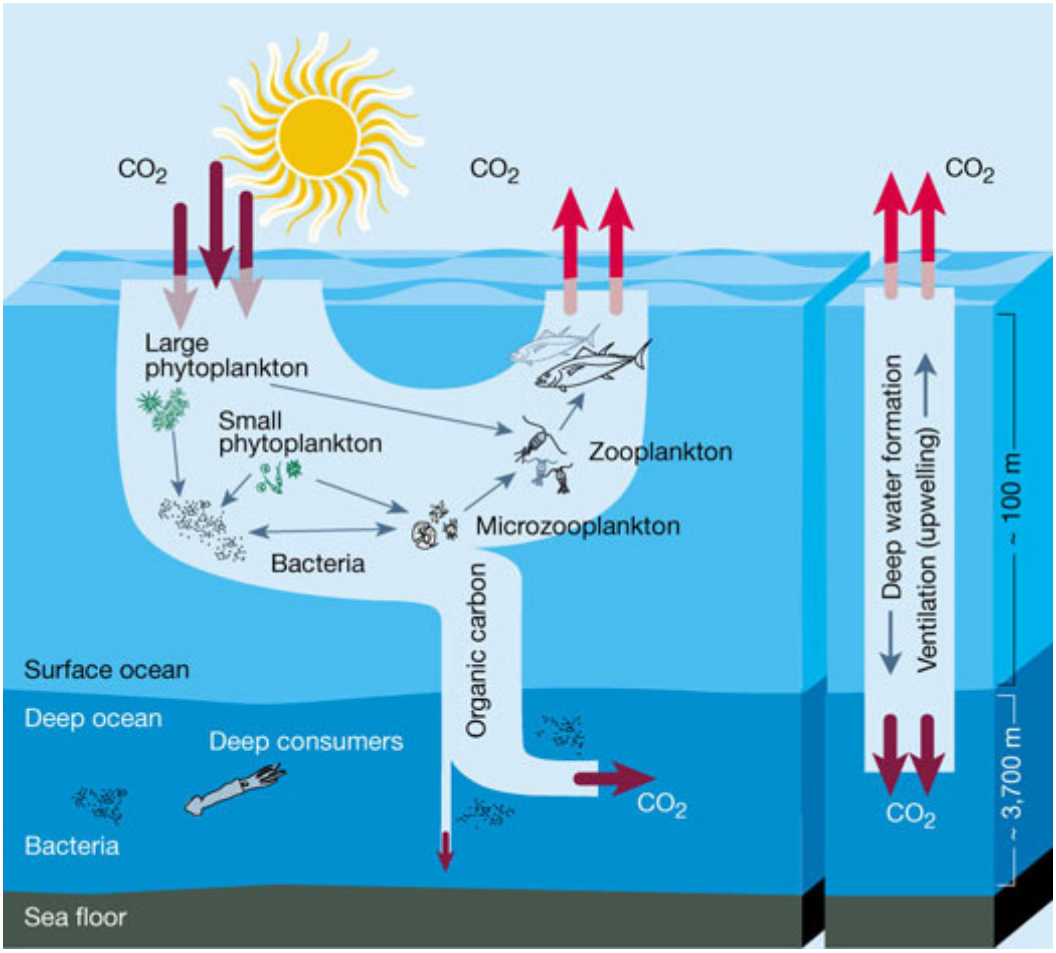

Figure 1.15. Illustration representative of the biological pump. Various biologically mediated processes are responsible for transporting carbon from the ocean surface to the ocean depths. The amount of organic carbon that sinks to the seafloor without being recycled into CO_2 is the export production. The illustration is from Chisholm (2000).

1.3.4. Chlorins

Algae and higher plants biosynthesize pigments necessary for photosynthesis, the most common being Chlorophyll *a*. This pigment has a ring shaped molecular structure with a tetrapyrrole ring in the center (Figure 1.16). Chlorophyll *a* is quickly degraded within the water column or at the sediment-water interface but a significant portion is preserved in diagenetic transformation products known as chlorins (Figure 1.16; Spooner et al., 1994; Louda et al., 2002). Diagenesis of organic compounds can be influenced by various factors such as the amount of oxygen in the water column, the residence time of the molecule before deposition, molecular reactivity and bioturbation in the sediments. The amount of chlorins preserved in sedimentary records relies on the initial amount of pigments synthesized in the upper water column, the subsequent diagenesis and finally the transfer efficiency from the water column towards the seafloor (Figure 1.15). This is a common consideration when using biomarker compounds concentration or fluxes and therefore it is more accurate to consider that changes in biomarker concentration reflect variability in export production rather than surface productivity (Rosell-Melé and McClymont, 2007). Chlorins are considered potential proxies for total primary export production reconstruction (Harris et al., 1996) and downcore variations of chlorins have been used to study variability in marine export production in several sedimentary settings for instance in the North Atlantic and Nordic Seas (Rosell-Melé et al., 1997; Rosell-Melé and Koç, 1997).

1.3.5. n-alkanes

n-alkanes are organic compouds synthesized by algae, bacteria and terrestrial higher plants, with a molecular structure based on a straight chain of carbon and hydrogen linked by single bonds (Eglington and Hamilton, 1963). Their distribution in marine sediments varies according to their main biological source. For instance, all plants predominantly synthesize n-alkanes with odd carbon chain lengths but in addition land plants synthesize mostly long chain protective cuticular waxes (C_{25}-C_{35}) to preserve the water content in their leaves (Eglington and Hamilton, 1967). Instead, aquatic algae synthesize short chain alkanes (C_{15}-C_{21}) and bacteria synthesize low abundances of n-alkanes in the range from C_{10} to C_{29} (Clark and Blumer, 1967; Goutx and Saliot, 1980). As the characteristic n-alkane distribution differs considerably from algae to terrestrial higher plants, their range of chain length ant the predominance of odd over even carbon numbers is indicative of the source origin. The relative predominance of odd over even carbon atoms in n-alkanes can be quantified with the carbon preference index (CPI) (Bray and Evans, 1961):

$$CPI_{n-m} = \frac{(\sum_{i=n}^{m} C_{i+1})}{(\sum_{i=n}^{m} C_i) + (\sum_{i=n+1}^{m+1} C_i)}$$

Where *n* is the starting and *m* the ending n-alkane used for calculating CPI. It is usually calculated over the entire range of long chain n-alkanes present in the sediment sample. The concentration of n-alkanes has been used to assess the variability in the input of terrestrial or land derived organic matter to the ocean in a wide variety of settings and time scales (Villanueva et al., 1997; Schefuss et al., 2003; Lopez-Martinez et al., 2006; Martínez-Garcia et al., 2009).

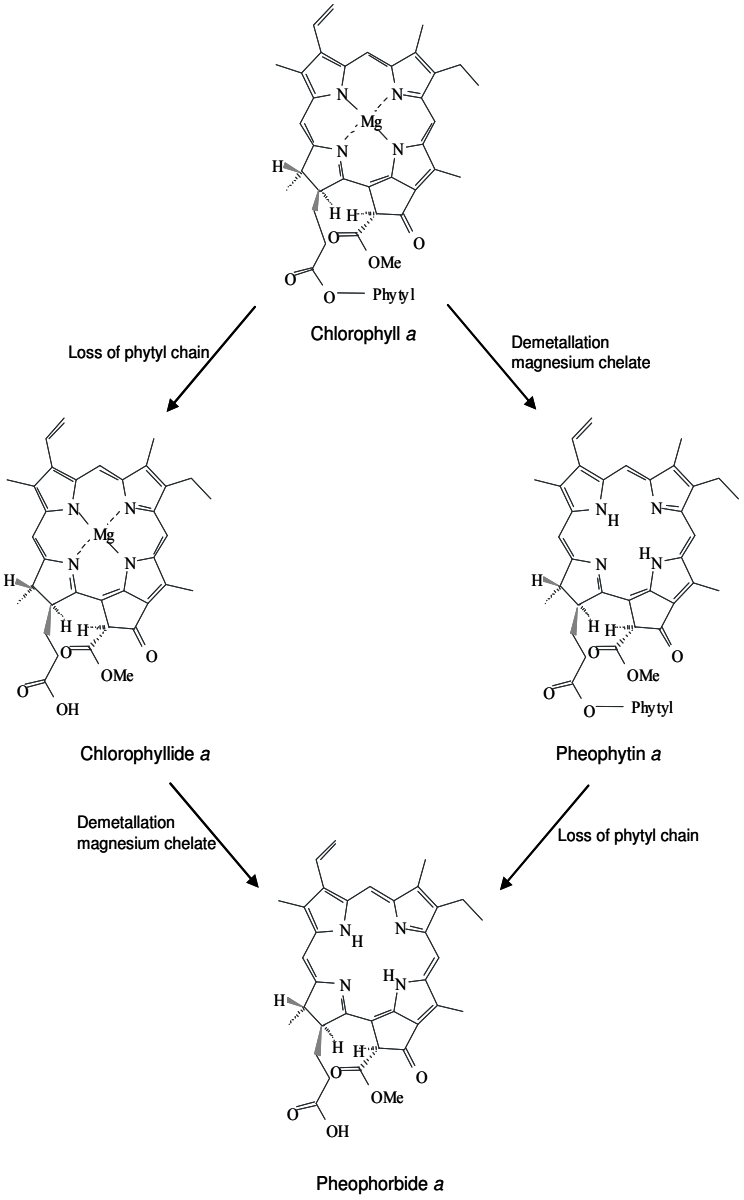

Figure 1.16. Molecular structures of chlorophyll *a* and their common derivatives (chlorins). The arrows indicate the diagenetic pathways. From Bendle (2003).

1.3.6. Bulk organic matter properties: carbon and nitrogen abundances and isotopic ratios

Marine sediments and soils contain an accumulation of organic matter derived from both autochthonous and allochthonous sources. Organic carbon contained in marine sediments can vary with the amount of primary productivity in the water column, the export rate to the seafloor, decomposition and preservation of organic matter in the study site. In soils, the organic carbon content can vary with the region's climate, the dominant types of vegetation, the texture of the soil and the land use. The ratio between carbon and nitrogen (C/N ratio) differs between marine or terrestrial sources of organic matter, because terrestrial organisms have lower amounts of non-protein materials compared to marine organisms. The analysis of the C/N ratio in marine sediments can give a qualitative indication of the source origin of the organic matter. For instance, high C/N values (~20) are indicative of organic matter synthesized by higher plants, therefore indicating a terrestrial input in the marine environment (Meyers and Ishiwatari, 1993). Low C/N ratios (~6-9) are indicative of organic matter derived from marine organisms (Müller, 1977). Finally, soil derived organic matter present C/N ratios in between (~8 – 20) (Hedges and Oades, 1997).

The stable isotopic composition of organic carbon δ^{13}Corg in marine sediments has been used to assess the origin of the organic matter. It is a quantitative measure that allows determining if there was a significant input of terrestrial organic matter in a marine environment or if the organic matter was mainly derived from marine algae (Winkelmann and Knies, 2005). The stable isotopic composition of nitrogen δ^{15}N measured in bulk marine sediments reflect marine organic matter, terrestrial organic matter and also inorganic nitrogen. It has been used to determine changes in the source of nutrients or the relative nutrient utilization in the overlaying surface waters (Schubert and Calvert, 2001).

1.4. Objectives and outline of this thesis

The North Atlantic and Arctic Oceans play an important role in modulating European climate variability. Oceanic records of SST variability covering the last 2000 years at high resolution in this region are scarce. There is a need therefore to obtain new high resolution reconstructions of variability in SST in this region for the Late Holocene and contribute to (I) increase the level of understanding on how the climate system varied in the recent millennia; (II) put the recent warming into a wider context and (III) investigate if the mechanisms of multidecadal climate variability observed from instrumental records could be also observed in the past. The main objective of

this thesis is to generate new records of multidecadal climate variability in the North Atlantic Ocean, analyzing organic proxies (biomarkers) in marine sedimentary cores that cover the last 2000 – 4400 years. The specific objectives are to:

- Generate new climate reconstructions using well established proxies (i.e. alkenones) but also recently developed ones (IP25, GDGT based proxies) to produce reconstructions based on SST but also on additional climate parameters such as sea ice cover variability, mean air temperature and export productivity.
- Provide further knowledge on the relationship between temperature estimates based on GDGT proxies and instrumental temperature observations in marine sediments from the Skagerrak (Chapter 3) and in soils from southern Norway and the Pyrenees (Chapter 4).
- Generate new records of multidecadal climate variability in the eastern Fram Strait and the Barents Sea, the two main paths where the northward flowing North Atlantic current meet the Arctic Ocean (Chapters 5 and 6).
- Reconstruct multidecadal SST variability in the Skagerrak, southern Scandinavia, a highly sensitive area to changes in the internal modes of climate variability and the interaction between the North Atlantic Ocean and European climate (Chapter 7).
- Investigate the linkage between the newly generated climate reconstructions and the mechanisms of decadal to multidecadal climate variability in the North Atlantic and the Arctic (Chapters 5 to 7).

1.5. References

Andrews JT, Belt ST, Olafsdottir S, Massé G and Vare LL (2009) Sea ice and marine climate variability for NW Iceland/Denmark Strait over the last 2000 cal. yr BP. The Holocene 19(5): 775–784: doi:10.1177/0959683609105302.

Bard E, Rostek F, Turon J-L and Gendreau S (2000) Hydrological Impact of Heinrich Events in the Subtropical Northeast Atlantic. Science 289(5483): 1321–1324: doi:10.1126/science.289.5483.1321.

Bechtel A, Smittenberg RH, Bernasconi SM and Schubert CJ (2010) Distribution of branched and isoprenoid tetraether lipids in an oligotrophic and a eutrophic Swiss lake: Insights into sources and GDGT-based proxies. Organic Geochemistry 41(8): 822–832: doi:10.1016/j.orggeochem.2010.04.022.

Belt ST and Müller J (2013) The Arctic sea ice biomarker IP25: a review of current understanding, recommendations for future research and applications in palaeo sea ice reconstructions. Quaternary Science Reviews: doi:10.1016/j.quascirev.2012.12.001.

Belt ST, Allard WG, Massé G, Robert J-M and Rowland SJ (2000) Highly branched isoprenoids (HBIs): identification of the most common and abundant sedimentary isomers. Geochimica et Cosmochimica Acta 64(22): 3839–3851: doi:10.1016/S0016-7037(00)00464-6.

Belt ST, Massé G, Rowland SJ, Poulin M, Michel C and LeBlanc B (2007) A novel chemical fossil of palaeo sea ice: IP25. Organic Geochemistry 38(1): 16–27: doi:10.1016/j.orggeochem.2006.09.013.

Belt ST, Vare LL, Massé G, Manners HR, Price JC, MacLachlan SE, Andrews JT and Schmidt S (2010) Striking similarities in temporal changes to spring sea ice occurrence across the central Canadian Arctic Archipelago over the last 7000 years. Quaternary Science Reviews 29(25–26): 3489–3504: doi:10.1016/j.quascirev.2010.06.041.

Bendle J and Rosell-Melé A (2004) Distributions of UK37 and UK37′ in the surface waters and sediments of the Nordic Seas: Implications for paleoceanography. Geochemistry, Geophysics, Geosystems 5(11): doi:10.1029/2004GC000741.

Bendle J, (2003). Palaeoceanography of the Holocene and Late-Glacial N.E. Atlantic: Development and application of biomarker proxies of environmental change. PhD Thesis. University of Durham

Bendle J, Rosell-Melé A and Ziveri P (2005) Variability of unusual distributions of alkenones in the surface waters of the Nordic seas. Paleoceanography 20(2): doi:10.1029/2004PA001025.

Bendle JAP, Rosell-Melé A, Cox NJ and Shennan I (2009) Alkenones, alkenoates, and organic matter in coastal environments of NW Scotland: Assessment of potential application for sea level reconstruction. Geochemistry, Geophysics, Geosystems 10(12): doi:10.1029/2009GC002603.

Berger A (1978) Long-term variations of caloric insolation resulting from the earth's orbital elements. Quaternary Research 9(2): 139–167: doi:10.1016/0033-5894(78)90064-9.

Berger A and Loutre MF (1991) Insolation values for the climate of the last 10 million years. Quaternary Science Reviews 10(4): 297–317: doi:10.1016/0277-3791(91)90033-Q.

Bjerknes J (1964) Atlantic Air-Sea Interaction. Advances in Geophysics 10: 1.

Blaga CI, Reichart G-J, Schouten S, Lotter AF, Werne JP, Kosten S, Mazzeo N, Lacerot G and Sinninghe Damsté JS (2010) Branched glycerol dialkyl glycerol tetraethers in lake sediments: Can they be used as temperature and pH proxies? Organic Geochemistry 41(11): 1225–1234: doi:10.1016/j.orggeochem.2010.07.002.

Booth BBB, Dunstone NJ, Halloran PR, Andrews T and Bellouin N (2012) Aerosols implicated as a prime driver of twentieth-century North Atlantic climate variability. Nature 484(7393): 228–232: doi:10.1038/nature10946.

Bradley RS, (1999) Paleoclimatology: Reconstructing Climates of the Quaternary. Academic: San Diego, 1-610.

Brassell SC, Brereton RG, Eglinton G, Grimalt J, Liebezeit G, Marlowe IT, Pflaumann U and Sarnthein M (1986b) Palaeoclimatic signals recognized by chemometric treatment of molecular stratigraphic data. Organic Geochemistry 10(4–6): 649–660: doi:10.1016/S0146-6380(86)80001-8.

Brassell SC, Eglinton G, Marlowe IT, Pflaumann U and Sarnthein M (1986a) Molecular stratigraphy: a new tool for climatic assessment. Nature 320(6058): 129–133: doi:10.1038/320129a0.

Bray E. and Evans E. (1961) Distribution of n-paraffins as a clue to recognition of source beds. Geochimica et Cosmochimica Acta 22(1): 2–15: doi:10.1016/0016-7037(61)90069-2.

Brochier-Armanet C, Boussau B, Gribaldo S and Forterre P (2008) Mesophilic Crenarchaeota: proposal for a third archaeal phylum, the Thaumarchaeota. Nature reviews. Microbiology 6(3): 245–252: doi:10.1038/nrmicro1852.

Brown TA and Belt ST (2012) Identification of the sea ice diatom biomarker IP25 in Arctic benthic macrofauna: direct evidence for a sea ice diatom diet in Arctic heterotrophs. Polar Biology 35(1): 131–137: doi:10.1007/s00300-011-1045-7.

Brown TA, Belt ST, Philippe B, Mundy CJ, Massé G, Poulin M and Gosselin M (2011) Temporal and vertical variations of lipid biomarkers during a bottom ice diatom bloom in the Canadian Beaufort Sea: further evidence for the use of the IP25 biomarker as a proxy for spring Arctic sea ice. Polar Biology 34(12): 1857–1868: doi:10.1007/s00300-010-0942-5.

Chisholm SW (2000) Oceanography: Stirring times in the Southern Ocean. Nature 407(6805): 685–687: doi:10.1038/35037696.

Clark RC and Blumer M, (1967) Distribution of n-paraffins in marine organisms and sediment. Limnology and Oceanography, 79-87.

Conte MH, Thompson A, Eglinton G and Green JC (1995) Lipid Biomarker Diversity in the Coccolithophorid Emiliania Huxleyi (prymnesiophyceae) and the Related Species Gephyrocapsa Oceanica1. Journal of Phycology 31(2): 272–282: doi:10.1111/j.0022-3646.1995.00272.x.

D'Arrigo R, Wilson R and Jacoby G (2006) On the long-term context for late twentieth century warming. Journal of Geophysical Research: Atmospheres 111(D3): doi:10.1029/2005JD006352.

De Rosa M and Gambacorta A (1988) The lipids of archaebacteria. Progress in lipid research 27(3): 153–175.

Delworth TL and Mann ME (2000) Observed and simulated multidecadal variability in the Northern Hemisphere. Climate Dynamics 16(9): 661–676: doi:10.1007/s003820000075.

Dima M and Lohmann G (2007) A Hemispheric Mechanism for the Atlantic Multidecadal Oscillation. Journal of Climate 20(11): 2706–2719: doi:10.1175/JCLI4174.1.

Eglinton G and Hamilton RJ (1967) Leaf epicuticular waxes. Science 156(3780): 1322–1335.

Eglinton G, Hamilton RJ, (1963) The distribution of alkanes. In: Swain T (ed.) Chemical Plant Taxonomy. Academic Press, 187–217.

Erez J, Luz B (1983) Experimental paleotemperature equation for planktonic foraminifera. Geochimica et Cosmochimca Acta 47, 1025–1031.

Escala M, (2009) Application of tetraether membrane lipids as proxies for continental climate reconstruction in Iberian and Siberian lakes. PhD Tesis. Universitat Autònoma de Barcelona.

Fahl K and Stein R (2012) Modern seasonal variability and deglacial/Holocene change of central Arctic Ocean sea-ice cover: New insights from biomarker proxy records. Earth and Planetary Science Letters 351–352: 123–133: doi:10.1016/j.epsl.2012.07.009.

Fawcett PJ, Werne JP, Anderson RS, Heikoop JM, Brown ET, Berke MA, Smith SJ, Goff F, Donohoo-Hurley L, Cisneros-Dozal LM, Schouten S, Sinninghe Damsté JS, Huang Y,

Toney J, Fessenden J, WoldeGabriel G, Atudorei V, Geissman JW and Allen CD (2011) Extended megadroughts in the southwestern United States during Pleistocene interglacials. Nature 470(7335): 518–521: doi:10.1038/nature09839.

Fietz S, Huguet C, Bendle J, Escala M, Gallacher C, Herfort L, Jamieson R, Martínez-Garcia A, McClymont EL, Peck VL, Prahl FG, Rossi S, Rueda G, Sanson-Barrera A and Rosell-Melé A (2012) Co-variation of crenarchaeol and branched GDGTs in globally-distributed marine and freshwater sedimentary archives. Global and Planetary Change 92–93: 275–285: doi:10.1016/j.gloplacha.2012.05.020.

Fietz S, Huguet C, Hambach B, Rueda G, Rosell-Melé A, (2013) Hydroxylated isoprenoidal GDGTs in the Nordic Seas. Marine Chemistry doi 10.1016/j.marchem.2013.02.007.

Fietz S, Martínez-Garcia A, Huguet C, Rueda G and Rosell-Melé A (2011b) Constraints in the application of the Branched and Isoprenoid Tetraether index as a terrestrial input proxy. Journal of Geophysical Research: Oceans 116(C10): doi:10.1029/2011JC007062.

Fietz S, Martínez-Garcia A, Rueda G, Peck VL, Huguet C, Escala M and Rosell-Melé A (2011a) Crenarchaea and phytoplankton coupling in sedimentary archives: Common trigger or metabolic dependence? Limnology and Oceanography 56(5): 1907–1916: doi:10.4319/lo.2011.56.5.1907.

Folland CK, Knight J, Linderholm HW, Fereday D, Ineson S and Hurrell JW (2009) The Summer North Atlantic Oscillation: Past, Present, and Future. Journal of Climate 22(5): 1082–1103: doi:10.1175/2008JCLI2459.1.

Gliozzi A, Paoli G, De Rosa M and Gambacorta A (1983) Effect of isoprenoid cyclization on the transition temperature of lipids in thermophilic archaebacteria. Biochimica et Biophysica Acta (BBA) - Biomembranes 735(2): 234–242: doi:10.1016/0005-2736(83)90298-5.

Goutx M and Saliot A (1980) Relationship between dissolved and particulate fatty acids and hydrocarbons, chlorophyll a and zooplankton biomass in Villefranche Bay, Mediterranean Sea. Marine Chemistry 8(4): 299–318: doi:10.1016/0304-4203(80)90019-5.

Grossmann I and Klotzbach PJ (2009) A review of North Atlantic modes of natural variability and their driving mechanisms. Journal of Geophysical Research: Atmospheres 114(D24): doi:10.1029/2009JD012728.

Harris PG, Zhao M, Rosell-Melé A, Tiedemann R, Sarnthein M and Maxwell JR (1996) Chlorin accumulation rate as a proxy for Quaternary marine primary productivity. Nature 383(6595): 63–65: doi:10.1038/383063a0.

Harvey HR, Fallon RD and Patton JS (1986) The effect of organic matter and oxygen on the degradation of bacterial membrane lipids in marine sediments. Geochimica et Cosmochimica Acta 50(5): 795–804: doi:10.1016/0016-7037(86)90355-8.

Hedges J. and Oades J. (1997) Comparative organic geochemistries of soils and marine sediments. Organic Geochemistry 27(7–8): 319–361: doi:10.1016/S0146-6380(97)00056-9.

Hegerl GC, Crowley TJ, Hyde WT and Frame DJ (2006) Climate sensitivity constrained by temperature reconstructions over the past seven centuries. Nature 440(7087): 1029–1032: doi:10.1038/nature04679.

Herbert TD (2003) Alkenone Paleotemperature Determinations. Treatise on Geochemistry. Elsevier, 391–432.

Ho SL, Mollenhauer G, Fietz S, Martínez-Garcia A, Lamy F, Rueda G, Schipper K, Méheust M, Rosell-Melé A, Stein R, Tiedemann R, (2013) Appraisal of the TEX86 and TEX86L thermometries in the subpolar and polar regions. Earth and Planetary Science Letters in review.

Hopmans EC, Weijers JWH, Schefuß E, Herfort L, Sinninghe-Damste JS and Schouten S (2004) A novel proxy for terrestrial organic matter in sediments based on branched and isoprenoid tetraether lipids. Earth and Planetary Science Letters 224(1-2): 107–116: doi:j.epsl.2004.05.012.

Huguet C, Fietz S and Rosell-Melé A (2013) Global distribution patterns of hydroxy glycerol dialkyl glycerol tetraethers. Organic Geochemistry: doi:10.1016/j.orggeochem.2013.01.010.

Hurrell JW, Kushnir Y, Ottersen G and Visbeck M (2003) An overview of the North Atlantic Oscillation. In: Hurrell JW, Kushnir Y, Ottersen G and Visbeck M (eds) Geophysical Monograph Series. Washington, D. C.: American Geophysical Union, 1–35.

IPCC (2007) Climate change 2007: The physical science basis. In: Solomon S, Qin D, Manning M, Chen Z, Marquis M, Averyt KB, Tignor M and Miller HL (ed.) Contribution of working group I to the Fourth Assessment Report of the Intergovernmental Panel on Climate Change, 1-966.

Johnson CM, McLennan SM, McSween HY and Summons RE (2013) Smaller, better, more: Five decades of advances in geochemistry. In, Bickford, ME, ed, The Web of Geological Sciences: Advances, Impacts, and Interactions: Geological Society of America Special Paper 500, in press.

Jones PD and Mann ME (2004) Climate over past millennia. Reviews of Geophysics 42(2): doi:10.1029/2003RG000143.

Jones PD, Briffa KR and Osborn TJ (2003) Changes in the Northern Hemisphere annual cycle: Implications for paleoclimatology? Journal of Geophysical Research: Atmospheres 108(D18): doi:10.1029/2003JD003695.

Karner MB, DeLong EF and Karl DM (2001) Archaeal dominance in the mesopelagic zone of the Pacific Ocean. Nature 409(6819): 507–510: doi:10.1038/35054051.

Kerr RA (2000) A North Atlantic Climate Pacemaker for the Centuries. Science 288(5473): 1984–1985: doi:10.1126/science.288.5473.1984.

Kim J-H, Schouten S, Hopmans EC, Donner B and Sinninghe Damsté JS (2008) Global sediment core-top calibration of the TEX86 paleothermometer in the ocean. Geochimica et Cosmochimica Acta 72(4): 1154–1173: doi:10.1016/j.gca.2007.12.010.

Kim J-H, Van der Meer J, Schouten S, Helmke P, Willmott V, Sangiorgi F, Koç N, Hopmans EC and Damsté JSS (2010) New indices and calibrations derived from the distribution of crenarchaeal isoprenoid tetraether lipids: Implications for past sea surface temperature reconstructions. Geochimica et Cosmochimica Acta 74(16): 4639–4654: doi:10.1016/j.gca.2010.05.027.

Knight JR, Folland CK and Scaife AA (2006) Climate impacts of the Atlantic Multidecadal Oscillation. Geophysical Research Letters 33(17): doi:10.1029/2006GL026242.

Knudsen MF, Seidenkrantz M-S, Jacobsen BH and Kuijpers A (2011) Tracking the Atlantic Multidecadal Oscillation through the last 8,000 years. Nature Communications 2: 178: doi:10.1038/ncomms1186.

Koga Y and Morii H (2005) Recent advances in structural research on ether lipids from archaea including comparative and physiological aspects. Bioscience, biotechnology, and biochemistry 69(11): 2019–2034.

Koga Y, Nishihara M, Morii H and Akagawa-Matsushita M (1993) Ether polar lipids of methanogenic bacteria: structures, comparative aspects, and biosyntheses. Microbiological Reviews 57(1): 164–182.

Lea DW (2003) Elemental and isotopic proxies of past ocean temperatures, in: Holland, H.D., Turekian, K., (Eds.), The Ocean and Marine Geochemistry. Treatise on Geochemistry, vol. 6 Elsevier-Pergamon, Oxford, pp. 365–390.

Leininger S, Urich T, Schloter M, Schwark L, Qi J, Nicol GW, Prosser JI, Schuster SC and Schleper C (2006) Archaea predominate among ammonia-oxidizing prokaryotes in soils. Nature 442(7104): 806–809: doi:10.1038/nature04983.

Liu X-L, Lipp JS, Simpson JH, Lin Y-S, Summons RE and Hinrichs K-U (2012) Mono- and dihydroxyl glycerol dibiphytanyl glycerol tetraethers in marine sediments: Identification of both core and intact polar lipid forms. Geochimica et Cosmochimica Acta 89: 102–115: doi:10.1016/j.gca.2012.04.053.

López-Martínez C, Grimalt JO, Hoogakker B, Gruetzner J, Vautravers MJ and McCave IN (2006) Abrupt wind regime changes in the North Atlantic Ocean during the past 30,000–60,000 years. Paleoceanography 21(4): doi:10.1029/2006PA001275.

Louda W, Liu L and Baker EW (2002) Senescence- and death-related alteration of chlorophylls and carotenoids in marine phytoplankton. Organic Geochemistry 33(12): 1635–1653: doi:10.1016/S0146-6380(02)00106-7.

Mann ME (2007) Climate Over the Past Two Millennia. Annual Review of Earth and Planetary Sciences 35(1): 111–136: doi:10.1146/annurev.earth.35.031306.140042.

Mann ME and Jones PD (2003) Global surface temperatures over the past two millennia. Geophysical Research Letters 30(15): doi:10.1029/2003GL017814.

Mann ME, Bradley RS and Hughes MK (1998) Global-scale temperature patterns and climate forcing over the past six centuries. Nature 392(6678): 779–787: doi:10.1038/33859.

Mann ME, Bradley RS and Hughes MK (1999) Northern hemisphere temperatures during the past millennium: Inferences, uncertainties, and limitations. Geophysical Research Letters 26(6): 759–762: doi:10.1029/1999GL900070.

Marchal O, Cacho I, Stocker TF, Grimalt JO, Calvo E, Martrat B, Shackleton N, Vautravers M, Cortijo E, Van Kreveld S, Andersson C, Koç N, Chapman M, Sbaffi L, Duplessy J-C, Sarnthein M, Turon J-L, Duprat J and Jansen E (2002) Apparent long-term cooling of the sea surface in the northeast Atlantic and Mediterranean during the Holocene. Quaternary Science Reviews 21(4–6): 455–483: doi:10.1016/S0277-3791(01)00105-6.

Marlowe IT, Brassell SC, Eglinton G and Green JC (1984a) Long chain unsaturated ketones and esters in living algae and marine sediments. Organic Geochemistry 6: 135–141: doi:10.1016/0146-6380(84)90034-2.

Marlowe IT, Green JC, Neal AC, Brassell SC, Eglinton G and Course PA (1984b) Long chain (n-C37–C39) alkenones in the Prymnesiophyceae. Distribution of alkenones and other lipids and their taxonomic significance. British Phycological Journal 19(3): 203–216: doi:10.1080/00071618400650221.

Marshall J, Kushnir Y, Battisti D, Chang P, Czaja A, Dickson R, Hurrell J, McCartney M, Saravanan R and Visbeck M (2001) North Atlantic climate variability: phenomena, impacts and mechanisms. International Journal of Climatology 21(15): 1863–1898: doi:10.1002/joc.693.

Martínez-Garcia A, Rosell-Melé A, Geibert W, Gersonde R, Masqué P, Gaspari V and Barbante C (2009) Links between iron supply, marine productivity, sea surface temperature, and CO2 over the last 1.1 Ma. Paleoceanography 24(1): doi:10.1029/2008PA001657.

Martínez-Garcia A, Rosell-Melé A, McClymont EL, Gersonde R and Haug GH (2010) Subpolar Link to the Emergence of the Modern Equatorial Pacific Cold Tongue. Science 328(5985): 1550–1553: doi:10.1126/science.1184480.

Martrat B, Grimalt JO, Lopez-Martinez C, Cacho I, Sierro FJ, Flores JA, Zahn R, Canals M, Curtis JH and Hodell DA (2004) Abrupt Temperature Changes in the Western Mediterranean over the Past 250,000 Years. Science 306(5702): 1762–1765: doi:10.1126/science.1101706.

Massé G, Belt ST, Rowland SJ and Rohmer M (2004) Isoprenoid biosynthesis in the diatoms Rhizosolenia setigera (Brightwell) and Haslea ostrearia (Simonsen). Proceedings of the National Academy of Sciences of the United States of America 101(13): 4413–4418: doi:10.1073/pnas.0400902101.

Massé G, Rowland SJ, Sicre M-A, Jacob J, Jansen E and Belt ST (2008) Abrupt climate changes for Iceland during the last millennium: Evidence from high resolution sea ice reconstructions. Earth and Planetary Science Letters 269(3–4): 565–569: doi:10.1016/j.epsl.2008.03.017.

Mayewski PA, Rohling EE, Curt Stager J, Karlén W, Maasch KA, David Meeker L, Meyerson EA, Gasse F, Van Kreveld S, Holmgren K, Lee-Thorp J, Rosqvist G, Rack F, Staubwasser M, Schneider RR and Steig EJ (2004) Holocene climate variability. Quaternary Research 62(3): 243–255: doi:10.1016/j.yqres.2004.07.001.

McClymont EL, Rosell-Melé A, Haug GH and Lloyd JM (2008) Expansion of subarctic water masses in the North Atlantic and Pacific oceans and implications for mid-Pleistocene ice sheet growth. Paleoceanography 23(4): doi:10.1029/2008PA001622.

Meyers PA and Ishiwatari R (1993) Lacustrine organic geochemistry—an overview of indicators of organic matter sources and diagenesis in lake sediments. Organic Geochemistry 20(7): 867–900: doi:10.1016/0146-6380(93)90100-P.

Miettinen A, Divine D, Koç N, Godtliebsen F and Hall IR (2012) Multicentennial Variability of the Sea Surface Temperature Gradient across the Subpolar North Atlantic over the Last 2.8 kyr. Journal of Climate 25(12): 4205–4219: doi:10.1175/JCLI-D-11-00581.1.

Moberg A, Sonechkin DM, Holmgren K, Datsenko NM and Karlén W (2005) Highly variable Northern Hemisphere temperatures reconstructed from low- and high-resolution proxy data. Nature 433(7026): 613–617: doi:10.1038/nature03265.

Müller J, Massé G, Stein R and Belt ST (2009) Variability of sea-ice conditions in the Fram Strait over the past 30,000 years. Nature Geoscience 2(11): 772–776: doi:10.1038/ngeo665.

Müller J, Wagner A, Fahl K, Stein R, Prange M and Lohmann G (2011) Towards quantitative sea ice reconstructions in the northern North Atlantic: A combined biomarker and numerical modelling approach. Earth and Planetary Science Letters 306(3–4): 137–148: doi:10.1016/j.epsl.2011.04.011.

Müller P. (1977) C/N ratios in Pacific deep-sea sediments: Effect of inorganic ammonium and organic nitrogen compounds sorbed by clays. Geochimica et Cosmochimica Acta 41(6): 765–776: doi:10.1016/0016-7037(77)90047-3.

Müller PJ, Kirst G, Ruhland G, Von Storch I and Rosell-Melé A (1998) Calibration of the alkenone paleotemperature index UK37′ based on core-tops from the eastern South Atlantic and the global ocean (60°N-60°S). Geochimica et Cosmochimica Acta 62(10): 1757–1772: doi:10.1016/S0016-7037(98)00097-0.

Navarro-Rodriguez A, Belt ST, Knies J and Brown TA (2013) Mapping recent sea ice conditions in the Barents Sea using the proxy biomarker IP25: implications for palaeo sea ice reconstructions. Quaternary Science Reviews: doi:10.1016/j.quascirev.2012.11.025.

Oerlemans J (2005) Extracting a Climate Signal from 169 Glacier Records. Science 308(5722): 675–677: doi:10.1126/science.1107046.

Otterå OH, Bentsen M, Drange H and Suo L (2010) External forcing as a metronome for Atlantic multidecadal variability. Nature Geoscience 3(10): 688–694: doi:10.1038/ngeo955.

Pancost RD and Sinninghe Damsté J (2003) Carbon isotopic compositions of prokaryotic lipids as tracers of carbon cycling in diverse settings. Chemical Geology 195(1-4): 29–58.

Peterse F, Kim J-H, Schouten S, Kristensen DK, Koç N and Sinninghe Damsté JS (2009a) Constraints on the application of the MBT/CBT palaeothermometer at high latitude environments (Svalbard, Norway). Organic Geochemistry 40(6): 692–699: doi:10.1016/j.orggeochem.2009.03.004.

Peterse F, Schouten S, Van der Meer J, Van der Meer MTJ and Sinninghe Damsté JS (2009b) Distribution of branched tetraether lipids in geothermally heated soils: Implications for the MBT/CBT temperature proxy. Organic Geochemistry 40(2): 201–205: doi:10.1016/j.orggeochem.2008.10.010.

Peterse F, Van der Meer J, Schouten S, Weijers JWH, Fierer N, Jackson RB, Kim J-H and Sinninghe Damsté JS (2012) Revised calibration of the MBT–CBT paleotemperature proxy based on branched tetraether membrane lipids in surface soils. Geochimica et Cosmochimica Acta 96: 215–229: doi:10.1016/j.gca.2012.08.011.

Pollack HN and Smerdon JE (2004) Borehole climate reconstructions: Spatial structure and hemispheric averages. Journal of Geophysical Research: Atmospheres 109(D11): doi:10.1029/2003JD004163.

Polyakov IV and Johnson MA (2000) Arctic decadal and interdecadal variability. Geophysical Research Letters 27(24): 4097: doi:10.1029/2000GL011909.

Polyakov IV, Alekseev GV, Timokhov LA, Bhatt US, Colony RL, Simmons HL, Walsh D, Walsh JE and Zakharov VF (2004) Variability of the Intermediate Atlantic Water of the Arctic Ocean over the Last 100 Years. Journal of Climate 17(23): 4485–4497: doi:10.1175/JCLI-3224.1.

Prahl FG and Wakeham SG (1987) Calibration of unsaturation patterns in long-chain ketone compositions for palaeotemperature assessment. Nature 330(6146): 367–369: doi:10.1038/330367a0.

Prahl FG, Muehlhausen LA and Zahnle DL (1988) Further evaluation of long-chain alkenones as indicators of paleoceanographic conditions. Geochimica et Cosmochimica Acta 52(9): 2303–2310: doi:10.1016/0016-7037(88)90132-9.

Rosell-Melé A (1998) Interhemispheric appraisal of the value of alkenone indices as temperature and salinity proxies in high-latitude locations. Paleoceanography 13(6): 694–703: doi:10.1029/98PA02355.

Rosell-Melé A and Koç N (1997) Paleoclimatic significance of the stratigraphic occurrence of photosynthetic biomarker pigments in the Nordic seas. Geology 25(1): 49–52: doi:10.1130/0091-7613(1997)025<0049:PSOTSO>2.3.CO;2.

Rosell-Melé A and McClymont EL, (2007) Biomarkers as palaeoceanographic proxies, In: Hillaire-Marcel C and de Vernal A (ed.) Proxies in late Cenozoic paleoceanography. Elsevier: Amsterdam, 441-490.

Rosell-Melé A, Carter J and Eglinton G (1994) Distributions of long-chain alkenones and alkyl alkenoates in marine surface sediments from the North East Atlantic. Organic Geochemistry 22(3–5): 501–509: doi:10.1016/0146-6380(94)90122-8.

Rosell-Melé A, Jansen E and Weinelt M (2002) Appraisal of a molecular approach to infer variations in surface ocean freshwater inputs into the North Atlantic during the last glacial. Global and Planetary Change 34(3–4): 143–152: doi:10.1016/S0921-8181(02)00111-X.

Rosell-Melé A, Maslin MA, Maxwell JR and Schaeffer P (1997) Biomarker evidence for "Heinrich" events. Geochimica et Cosmochimica Acta 61(8): 1671–1678: doi:10.1016/S0016-7037(97)00046-X.

Rosell-Mele A., Eglinton G., Pflaumann U. and Sarnthein M. (1995) Atlantic core-top calibration of the UK37 index as a sea-surface palaeotemperature indicator. Geochimica et Cosmochimica Acta 59(15): 3099–3107: doi:10.1016/0016-7037(95)00199-A.

Rosell-Melé; A, Weinelt M, Sarnthein M, Koç N and Jansen E (1998) Variability of the Arctic front during the last climatic cycle: application of a novel molecular proxy. Terra Nova 10(2): 86–89.

Rowland SJ and Robson JN (1990) The widespread occurrence of highly branched acyclic C20, C25 and C30 hydrocarbons in recent sediments and biota—A review. Marine Environmental Research 30(3): 191–216: doi:10.1016/0141-1136(90)90019-K.

Ruddiman WF, (2001) Earth's Climate, Past and Future. Freeman: New York, 1- 465.

Rutherford S, Mann ME, Osborn TJ, Briffa KR, Jones PD, Bradley RS and Hughes MK (2005) Proxy-Based Northern Hemisphere Surface Temperature Reconstructions: Sensitivity to Method, Predictor Network, Target Season, and Target Domain. Journal of Climate 18(13): 2308–2329: doi:10.1175/JCLI3351.1.

Schefuß E, Schouten S, Jansen JHF and Sinninghe Damsté JS (2003) African vegetation controlled by tropical sea surface temperatures in the mid-Pleistocene period. Nature 422(6930): 418–421: doi:10.1038/nature01500.

Schlesinger ME and Ramankutty N (1994) An oscillation in the global climate system of period 65–70 years. Nature 367(6465): 723–726: doi:10.1038/367723a0.

Schouten S, Eldrett J, Greenwood DR, Harding I, Baas M and Sinninghe Damsté J (2008) Onset of long-term cooling of Greenland near the Eocene-Oligocene boundary as revealed by branched tetraether lipids. Geology 36(2): 147–150: doi:10.1130/G24332A.1.

Schouten S, Hopmans EC and Sinninghe Damsté JS (2013) The organic geochemistry of glycerol dialkyl glycerol tetraether lipids: A review. Organic Geochemistry 54: 19–61: doi:10.1016/j.orggeochem.2012.09.006.

Schouten S, Hopmans EC, Pancost RD and Damsté JSS (2000) Widespread occurrence of structurally diverse tetraether membrane lipids: Evidence for the ubiquitous presence of low-temperature relatives of hyperthermophiles. Proceedings of the National Academy of Sciences 97(26): 14421–14426: doi:10.1073/pnas.97.26.14421.

Schouten S, Hopmans EC, Schefuß E and Sinninghe Damsté JS (2002) Distributional variations in marine crenarchaeotal membrane lipids: a new tool for reconstructing ancient sea water temperatures? Earth and Planetary Science Letters 204(1–2): 265–274: doi:10.1016/S0012-821X(02)00979-2.

Schubert CJ and Calvert SE (2001) Nitrogen and carbon isotopic composition of marine and terrestrial organic matter in Arctic Ocean sediments: implications for nutrient utilization and organic matter composition. Deep-sea research. Part 1. Oceanographic research papers 48(3): 789–810.

Sinninghe Damsté JS, Hopmans EC, Pancost RD, Schouten S and Geenevasen JAJ (2000) Newly discovered non-isoprenoid glycerol dialkylglycerol tetraether lipids in sediments. Chemical Communications (17): 1683–1684: doi:10.1039/B004517I.

Sinninghe Damsté JS, Muyzer G, Abbas B, Rampen SW, Massé G, Allard WG, Belt ST, Robert J-M, Rowland SJ, Moldowan JM, Barbanti SM, Fago FJ, Denisevich P, Dahl J, Trindade LAF and Schouten S (2004) The Rise of the Rhizosolenid Diatoms. Science 304(5670): 584–587: doi:10.1126/science.1096806.

Sinninghe Damsté JS, Ossebaar J, Abbas B, Schouten S and Verschuren D (2009) Fluxes and distribution of tetraether lipids in an equatorial African lake: Constraints on the application of the TEX86 palaeothermometer and BIT index in lacustrine settings. Geochimica et Cosmochimica Acta 73(14): 4232–4249: doi:10.1016/j.gca.2009.04.022.

Sinninghe Damsté JS, Ossebaar J, Schouten S and Verschuren D (2008) Altitudinal shifts in the branched tetraether lipid distribution in soil from Mt. Kilimanjaro (Tanzania): Implications for the MBT/CBT continental palaeothermometer. Organic Geochemistry 39(8): 1072–1076: doi:10.1016/j.orggeochem.2007.11.011.

Sinninghe Damsté JS, Rijpstra WIC, Hopmans EC, Weijers JWH, Foesel BU, Overmann J and Dedysh SN (2011) 13,16-Dimethyl Octacosanedioic Acid (iso-Diabolic Acid), a Common Membrane-Spanning Lipid of Acidobacteria Subdivisions 1 and 3. Applied and Environmental Microbiology 77(12): 4147–4154: doi:10.1128/AEM.00466-11.

Sinninghe Damsté JS, Schouten S, Hopmans EC, Van Duin ACT and Geenevasen JAJ (2002) Crenarchaeol: the characteristic core glycerol dibiphytanyl glycerol tetraether membrane lipid of cosmopolitan pelagic crenarchaeota. Journal of lipid research 43(10): 1641–1651.

Smith RW, Bianchi TS and Li X (2012) A re-evaluation of the use of branched GDGTs as terrestrial biomarkers: Implications for the BIT Index. Geochimica et Cosmochimica Acta 80: 14–29: doi:10.1016/j.gca.2011.11.025.

Spooner N, Rodger Harvey H, Pearce GES, Eckardt CB and Maxwell JR (1994) Biological defunctionalisation of chlorophyll in the aquatic environment II: action of endogenous algal enzymes and aerobic bacteria. Organic Geochemistry 22(3–5): 773–780: doi:10.1016/0146-6380(94)90138-4.

Sun Q, Chu G, Liu M, Xie M, Li S, Ling Y, Wang X, Shi L, Jia G and Lü H (2011) Distributions and temperature dependence of branched glycerol dialkyl glycerol tetraethers in recent lacustrine sediments from China and Nepal. Journal of Geophysical Research: Biogeosciences 116(G1): doi:10.1029/2010JG001365.

Sutton RT and Dong B (2012) Atlantic Ocean influence on a shift in European climate in the 1990s. Nature Geoscience 5(11): 788–792: doi:10.1038/ngeo1595.

Sutton RT and Hodson DLR (2005) Atlantic Ocean Forcing of North American and European Summer Climate. Science 309(5731): 115–118: doi:10.1126/science.1109496.

Thompson DWJ and Wallace JM (1998) The Arctic oscillation signature in the wintertime geopotential height and temperature fields. Geophysical Research Letters 25(9): 1297–1300: doi:10.1029/98GL00950.

Tierney JE (2009) Distributions of branched GDGTs in a tropical lake system: Implications for lacustrine application of the MBT/CBT paleoproxy. Organic Geochemistry 40(9): 1032–1036.

Tierney JE, Russell JM, Eggermont H, Hopmans EC, Verschuren D and Sinninghe Damsté JS (2010) Environmental controls on branched tetraether lipid distributions in tropical East African lake sediments. Geochimica et Cosmochimica Acta 74(17): 4902–4918: doi:10.1016/j.gca.2010.06.002.

Uda I, Sugai A, Itoh YH and Itoh T (2001) Variation in molecular species of polar lipids from Thermoplasma acidophilum depends on growth temperature. Lipids 36(1): 103–105: doi:10.1007/s11745-001-0914-2.

Van Loon H and Rogers JC (1978) The Seesaw in Winter Temperatures between Greenland and Northern Europe. Part I: General Description. Monthly Weather Review 106(3): 296–310: doi:10.1175/1520-0493(1978)106<0296:TSIWTB>2.0.CO;2.

Vare LL, Massé G and Belt ST (2010) A biomarker-based reconstruction of sea ice conditions for the Barents Sea in recent centuries. The Holocene 20(4): 637–643: doi:10.1177/0959683609355179.

Vare LL, Massé G, Gregory TR, Smart CW and Belt ST (2009) Sea ice variations in the central Canadian Arctic Archipelago during the Holocene. Quaternary Science Reviews 28(13–14): 1354–1366: doi:10.1016/j.quascirev.2009.01.013.

Vellinga M and Wood RA (2002) Global Climatic Impacts of a Collapse of the Atlantic Thermohaline Circulation. Climatic Change 54(3): 251–267: doi:10.1023/A:1016168827653.

Vellinga M and Wu P (2004) Low-Latitude Freshwater Influence on Centennial Variability of the Atlantic Thermohaline Circulation. Journal of Climate 17(23): 4498–4511: doi:10.1175/3219.1.

Villanueva J, Grimalt JO, Cortijo E, Vidal L and Labeyriez L (1997) A biomarker approach to the organic matter deposited in the North Atlantic during the last climatic cycle. Geochimica et Cosmochimica Acta 61(21): 4633–4646: doi:10.1016/S0016-7037(97)83123-7.

Volkman JK, Barrerr SM, Blackburn SI and Sikes EL (1995) Alkenones in Gephyrocapsa oceanica: Implications for studies of paleoclimate. Geochimica et Cosmochimica Acta 59(3): 513–520: doi:10.1016/0016-7037(95)00325-T.

Volkman JK, Barrett SM and Dunstan GA (1994) C25 and C30 highly branched isoprenoid alkenes in laboratory cultures of two marine diatoms. Organic Geochemistry 21(3–4): 407–414: doi:10.1016/0146-6380(94)90202-X.

Volkman JK, Eglinton G, Corner EDS and Forsberg TEV (1980) Long-chain alkenes and alkenones in the marine coccolithophorid Emiliania huxleyi. Phytochemistry 19(12): 2619–2622: doi:10.1016/S0031-9422(00)83930-8.

Wanner H, Brönnimann S, Casty C, Gyalistras D, Luterbacher J, Schmutz C, Stephenson DB and Xoplaki E (2001) North Atlantic Oscillation – Concepts And Studies. Surveys in Geophysics 22(4): 321–381: doi:10.1023/A:1014217317898.

Wefer G, Berger WH, Bijma J and Fischer G, (1999) Clues to ocean history: a brief overview of proxies. In: Fischer G and Wefer G (ed.) Use of proxies in paleoceanography: examples from the South Atlantic. Springer: New York, 1-734.

Weijers JWH, Panoto E, Van Bleijswijk J, Schouten S, Rijpstra WIC, Balk M, Stams AJM and Sinninghe Damsté JS (2009) Constraints on the Biological Source(s) of the Orphan Branched Tetraether Membrane Lipids. Geomicrobiology Journal 26(6): 402–414: doi:10.1080/01490450902937293.

Weijers JWH, Schefuß E, Schouten S and Sinninghe Damsté J (2007b) Coupled Thermal and Hydrological Evolution of Tropical Africa over the Last Deglaciation. Science 315(5819): 1701–1704: doi:10.1126/science.1138131.

Weijers JWH, Schouten S, Hopmans EC, Geenevasen JAJ, David ORP, Coleman JM, Pancost RD and Sinninghe Damsté JS (2006a) Membrane lipids of mesophilic anaerobic bacteria thriving in peats have typical archaeal traits. Environmental microbiology 8(4): 648–657: doi:10.1111/j.1462-2920.2005.00941.x.

Weijers JWH, Schouten S, Sluijs A, Brinkhuis H and Sinninghe Damsté JS (2007c) Warm arctic continents during the Palaeocene–Eocene thermal maximum. Earth and Planetary Science Letters 261(1–2): 230–238: doi:10.1016/j.epsl.2007.06.033.

Weijers JWH, Schouten S, Spaargaren OC and Sinninghe Damsté JS (2006b) Occurrence and distribution of tetraether membrane lipids in soils: Implications for the use of the TEX86

proxy and the BIT index. Organic Geochemistry 37(12): 1680–1693: doi:10.1016/j.orggeochem.2006.07.018.

Weijers JWH, Schouten S, Van den Donker JC, Hopmans EC and Sinninghe Damsté JS (2007a) Environmental controls on bacterial tetraether membrane lipid distribution in soils. Geochimica et Cosmochimica Acta 71(3): 703–713: doi:10.1016/j.gca.2006.10.003.

White DC, Davis WM, Nickels JS, King JD and Bobbie RJ (1979) Determination of the sedimentary microbial biomass by extractible lipid phosphate. Oecologia 40(1): 51–62: doi:10.1007/BF00388810.

Winkelmann D and Knies J (2005) Recent distribution and accumulation of organic carbon on the continental margin west off Spitsbergen. Geochemistry, Geophysics, Geosystems 6(9): doi:10.1029/2005GC000916.

Wraige EJ, Belt ST, Lewis CA, Cooke DA, Robert J-M, Massé G and Rowland SJ (1997) Variations in structures and distributions of C25 highly branched isoprenoid (HBI) alkenes in cultures of the diatom, Haslea ostrearia (Simonsen). Organic Geochemistry 27(7–8): 497–505: doi:10.1016/S0146-6380(97)00086-7.

Zhu C, Weijers JWH, Wagner T, Pan J-M, Chen J-F and Pancost RD (2011) Sources and distributions of tetraether lipids in surface sediments across a large river-dominated continental margin. Organic Geochemistry 42(4): 376–386: doi:10.1016/j.orggeochem.2011.02.002.

Zink K-G, Vandergoes MJ, Mangelsdorf K, Dieffenbacher-Krall AC and Schwark L (2010) Application of bacterial glycerol dialkyl glycerol tetraethers (GDGTs) to develop modern and past temperature estimates from New Zealand lakes. Organic Geochemistry 41(9): 1060–1066: doi:10.1016/j.orggeoch

CHAPTER 2

Methods

2. Methods

This chapter contains a description of the analytical procedures used to obtain the results presented in this thesis. A general overview is given in Figure 2.1. The majority of the samples was prepared and analyzed at Laboratori de l'Esfera Ambiental, Institut de Ciència i Tecnologia Ambientals, Universitat Autònoma de Barcelona (LERA, ICTA, UAB) facilities. The instrumental analysis of GDGTs was conducted at the Laboratori de Proteòmica from Consejo Superior de Investigaciones Científicas (CSIC) and the UAB. The marine sediment samples from the Barents Sea record were prepared for IP25 analysis at Laboratoire d'Oceanographie et du Climat Exprimentations et Approaches Numériques located at Université Pierre et Marie Curie (LOCEAN, UPMC, Paris, France) in collaboration with Dr. Guillaume Massé. Barents Sea samples were further treated and analyzed for the rest of the biomarkers at ICTA facilities.

2.1. Glassware and other utensils

The materials used during the laboratory procedures were thoroughly cleaned prior to use. This practice prevented contamination of the samples with compounds that could interfere with the instrumental analysis of biomarkers. Furthermore, utensils that could interact with the samples at any point of the laboratory procedure, such as syringes or recipients, were also cleaned by rinsing with solvent prior to use.

Glassware was combusted at 450 ^{o}C for 4 hours prior to use. Reusable glassware with solid residues was rinsed and soaked in a 1% HNO_3 solution during 24h. Afterwards the glassware was rinsed with tap water, dionized water and then soaked in a 2% BioSel solution (a phosphate-free alkaline detergent) during 24h. The glassware was rinsed with tap and dionized water. Subsequently, the volumetric material was rinsed with acetone, wrapped in aluminium foil and stored until use. The non volumetric, reusable glass material was dried in the oven at 105 ^{o}C, afterwards it was wrapped in aluminium foil and combusted at 450 ^{o}C for 4 hours.

2.2. Organic biomarker analysis

2.2.1. Freeze drying and homogenization

Samples were stored frozen at -20 ^{o}C, and freeze-dried prior to extraction using a Telstar Cryodos device with temperature of the cryogenic trap set at -42 ^{o}C and vacuum at 0.2 mbar. The process lasted 24 to 48 h depending on the amount of water

retained in the sediment samples. Dry samples were manually homogenized using a mortar and a pestle. Between samples, the mortar and pestle were sequentially rinsed with tap and dionized water, acetone and dichloromethane:methanol (2:1, v/v).

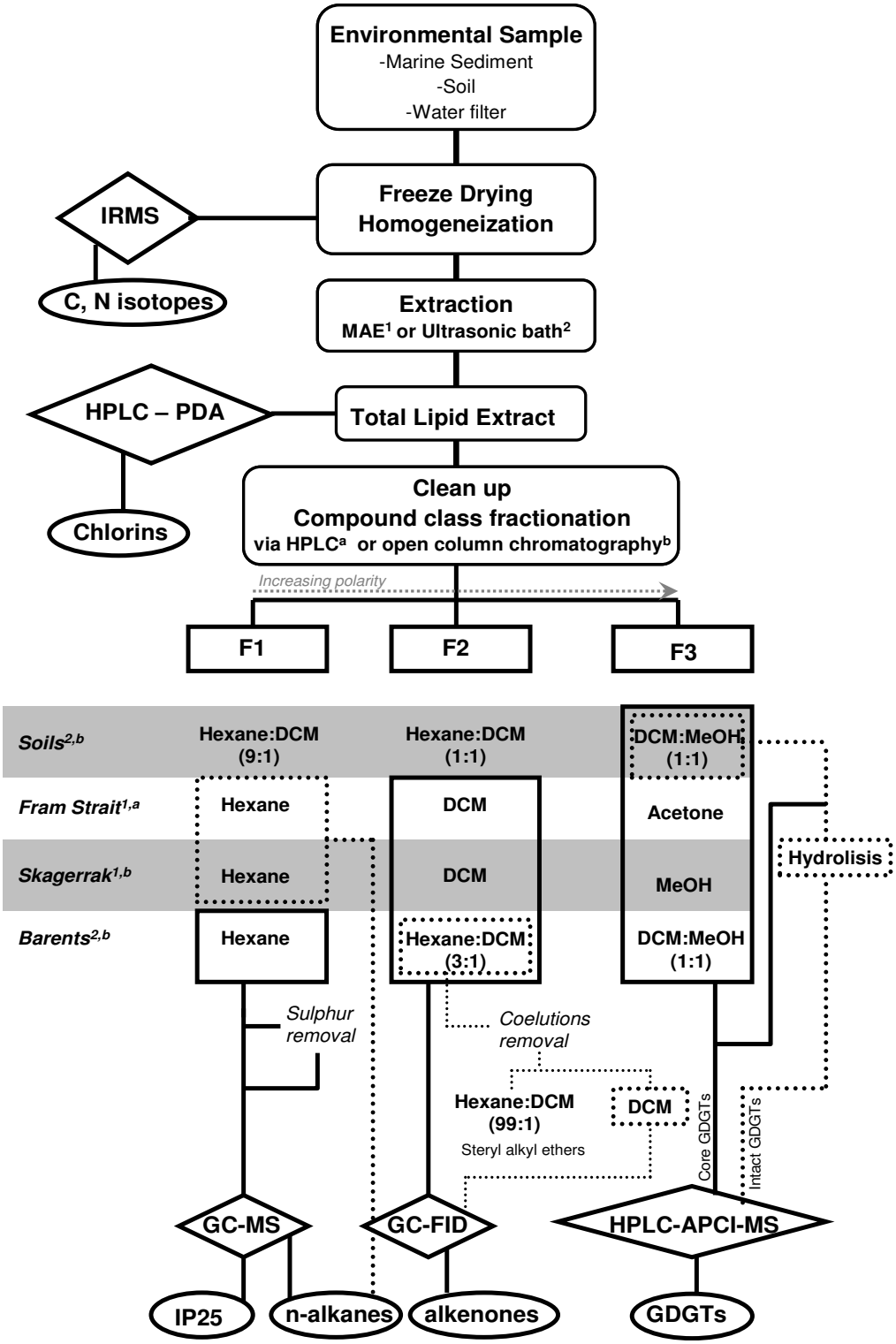

Figure 2.1. Scheme of the analytical methodology used in this thesis.

2.2.2. Lipid extraction

Internal standards (Table 2.1) were added to the samples prior to extraction of the biomarkers. The lipid content was extracted using microwave assisted extraction (MAE) or an ultrasonic bath depending on the nature of the samples and on the facilities of the laboratory in which they were prepared. Depending on the sample origin, 1 or 2 g of sediment were weighted in a GX-2000 precision balance.

Table 2.1. Summary of the internal standards used.

Internal Standard	Chemical Class	Analytical Device	Monitored at m/z	Compound Quantification
2-Nonadecanone▲	Ketone	GC-FID	-	Alkenones
18-Pentatriacontanone ▪	Ketone	GC-FID	-	Alkenones
Hexatriacontane ▲	Alkane	GC-FID	-	n-alkanes
7-Hexylnonadecane ▪	Alkane	GC-MS	266	IP25, n-alkanes
GR ▲	Tetraether	HPLC-MS	1208	GDGTs

▲Added at ICTA; ▪ Added at LOCEAN

2.2.2.1 Microwave assisted extraction

Sediment samples from the Fram Strait (chapter 5) and the Skagerrak (chapters 3 and 7) were extracted via MAE (Kornilova and Rosell-Melé, 2003) using a CEM-MARS 5 microwave accelerated reaction system that was equipped with 14 Greenchem pressure vessels with Teflon containers of 100 mL capacity. The weighted sediment, a magnetic stirrer, the internal standards and 10 mL of dichloromethane:methanol 3:1 (v/v) were inserted into each vessel. As the microwave carrousel had a capacity for 14 vessels, we proceeded in batches of 12 samples, 1 reference sample and 1 solvent blank. The microwave increased the vessel contents temperature to 70 ^{o}C in 2.5 min and held it at this temperature for 5 min. The vessels cooled down to room temperature after 30 min. The extracts were decanted into Pyrex glass vials and centrifuged at 1200 rpm for 6 min using a Rotofix 32 centrifuge (Hettich Zentrifugen). The extracts were transferred to new Pyrex glass vials. Afterwards, the organic extract was taken to dryness by means of a miVac Duo concentrator coupled to a cold trap (Genevac) and a Thermo Savant vacuum pump unit, hereafter referred to as Centrivap.

2.2.2.2 Ultrasonic bath extraction

Sediment samples (2 g) from core PL96-126 retrieved in the Barents Sea (chapter 6) were ultrasonically extracted with 3 mL of dichloromethane:methanol (2:1, v/v). The vials containing the extracted sediment samples were centrifuged at 2500 rpm during 2 minutes and the supernatant was transferred to a new vial. The samples were extracted two more times using the same procedure. The extracts were combined and dried under a N_2 stream with a hot plate at 35 ^{o}C. Once dry, the extracts were removed immediately to prevent possible compound loss.

Soil and river water samples (chapter 4) were prepared following the procedure described by Huguet et al. (2010) as it yields the most accurate quantification of total intact lipids. The samples were extracted with methanol and sonicated in an ultrasonic bath for 5 minutes (x3), dichloromethane:methanol (1:1, v/v; x3) and finally dichloromethane (x3). After each sonication, samples were centrifuged to separate the sediment from the extract, all the supernatants were combined and the solvent mixture was evaporated in the centrivap.

2.2.3. Total extract clean up

2.2.3.1 Hydrolysis

The organic extracts of the Skagerrak samples selected for the analysis of GDGTs in chapter 3 were hydrolyzed overnight with 8% potassium hydroxide in methanol. The neutral fraction was recovered with hexane by liquid-liquid extraction. The extract was washed with dionized water to remove residual potassium hydroxide and taken to near dryness by vacuum rotary evaporation. The remaining extract was transferred to a smaller vial and dried under a gentle N_2 stream. Afterwards the samples were dissolved in 200 µl hexane:n-propanol (99:1, v/v) and filtered through a 0.45 µm Millipore PVDF filter prior to instrumental analysis.

2.2.3.2 Clean up chromatography

High performance liquid chromatography

The Fram Strait downcore extracts were purified with a silica column using a Thermo Surveyor high performance liquid chromatographic system (HPLC). Extracts were eluted through a glass pipette filled with glass wool and sodium sulphate, dried and re-dissolved in 100 µL of hexane:dichloromethane (50:50, v/v). The sample was manually injected in the HPLC, that was equipped with a stainless steal inline filter (2

μm pore size) and a Lichrospher Silicon dioxide column (4.6 x 250 mm, 5μm; Teknokroma). Compound class fractionation was achieved running consecutively n-hexane (0-2.75 minutes; n-alkane containing fraction), dichloromethane (2.76-5.75 minutes; alkenone containing fraction), acetone (5.76-9.25 minutes; GDGTs containing fraction) and n-hexane (9.26-13.5 minutes; column stabilization and cleaning) with a 2 mL min^{-1} flow. Fractions were manually collected into glass vials, and dried using the centrivap. The HPLC column was flushed between batches of samples using acetone and methanol.

Open glass column chromatography

The rest of the samples analyzed in this thesis were cleaned up with open column chromatography. A Pasteur pipette was filled with 0.5 g of silica (bottom) of 230-400 mesh particle size and 0.5 g of sodium sulphate (top). Silica and cotton were previously cleaned with dichloromethane:methanol at 2:1 (v:v) during 12 hours using a Soxhlet. Silica was dried at 105 ^{o}C and deactivated with 5% dionized water. Sodium sulphate was cleaned via combustion at the oven at 450 ^{o}C during 4 hours. The mobile phases used to elute the compounds differed slightly in each set of samples and are described below. Upon compound elution, each fraction was recovered in a different vial and afterwards the solvent was evaporated in the centrivap. The dry extracts of each fraction were then transferred to 1.5 mL vials and stored dry and frozen until instrumental analysis.

The total lipid extracts of the Skagerrak (chapter 7) and the Fram Strait marine water column filters (chapter 5) were eluted with hexane (3 mL; Fraction 1: n-alkanes), dichloromethane (3 mL; Fraction 2: alkenones) and methanol (3 mL; Fraction 3: GDGTs).

The soil and river water samples from southern Norway and the Pyrenees (chapter 4) were purified according to the method developed by Huguet et al. (2010) to analyze core and intact GDGTs. The lipid extracts were transferred to a column filled with 0.5 g of activated silica and the fractions eluted with hexane:dichloromethane (9:1, v/v; 3mL; Fraction 1), hexane:dichloromethane (1:1, v/v; 3 mL; Fraction 2) and dichloromethane:methanol (1:1, v/v; 3 mL; Fraction 3; GDGTs). The last fraction containing both core and intact GDGTs was split into two samples. One part was filtered through a 0.45 μm PTFE filter (Advantec) and stored frozen until instrumental analysis. The other half was hydrolyzed to break the polar head groups and allow quantification of both core and intact polar lipids (Huguet et al., 2010). For performing the hydrolysis, sample vials were flushed with N_2 , then 2 mL of 5% HCl in methanol

(v/v) were added and the vials were sealed with Teflon lined caps. The vials were placed in a heating block at 70 ºC for 4 h. GDGTs were recovered with a liquid-liquid extraction using dichloromethane and dionized water (1:1, v/v). After mixing vigorously, the dichloromethane fraction was recovered and transferred to a new vial. This procedure was repeated three more times. All the recovered dichloromethane extracts were combined in a single vial and rinsed six times with dionized water, to remove any traces of HCl. The extracts were dried and filtered prior to instrumental analysis (Huguet et al., 2010).

The Barents Sea extracts (chapter 6) were eluted through 0.5 g activated silica with a consecutive addition of hexane (6 mL; Fraction 1: IP25, n-alkanes), hexane:dichloromethane (3:1, v/v; 8 mL; Fraction 2: alkenones) and dichloromethane:methanol (1:1, v/v; 7 mL; Fraction 3: GDGTs). Each fraction was collected in a different vial and taken to dryness under a gentle N_2 stream and using a hot plate at 35 ºC.

The second fraction of the Barents Sea samples was further fractionated to remove steryl alkyl ethers that coeluted with alkenones. The fraction was further cleaned using 0.5 g of 5 % deactivated silica and a consecutive addition of hexane:dichloromethane (99:1, v/v; 8mL; steryl alkyl ethers) and dichloromethane (3 mL; alkenones).

2.2.3.3 Sulphur removal

The procedure for removing sulphur was applied to the first fraction of Barents Sea samples and consisted of a liquid-liquid extraction using tetrabutylammonium sulfite reagent, hereafter TBA sulfite reagent. The TBA sulfite reagent was prepared by mixing a solution of 3.39% tetrabutylammonium hydrogen sulphate in dionized water with three 20 mL portions of hexane, and 25 g of sodium sulphite. Then, 1 mL of hexane, 1 mL of TBA sulphite reagent and 2 mL of 2-propanol were added to the vial containing fraction 1 and the mixture was shaken for 1 min. Next, 3 mL of dionized water were added to the vial and it was shaken again for 1 min. The vials were centrifuged at 2500 rpm during 2 min and hexane - the supernatant - was transferred to a new vial. The liquid-liquid extraction was repeated three times in total. The three hexane extracts were combined in a single vial. The extract was dried in a gentle N_2 stream using a hot plate at 35 ºC. Once dry the samples were removed immediately to prevent HBI loss.

2.2.4. Instrumental analysis

2.2.4.1. Visible spectrophotometry

Chlorins were analyzed following the methods described by Nuñez (2005). The total extract was completely dried and then it was dissolved in acetone. Samples were analyzed with automatic or manual injection in a Thermo Surveyor HPLC coupled to a photodiode array detector (HPLC-PDA). The HPLC ran in off-column mode using a flow restrictor from Pickering Laboratories Inc. Acetone was used as mobile phase at 1ml min^{-1} flow. Visible spectrophotometry was monitored for a wavelength range similar to the visible spectrum (λ = 300-800nm) and a continuous absorbance spectrum was obtained (Figure 2.2). Total abundance of chlorins was determined integrating the peak response area at 662 nm wavelength. We used an external standard curve for quantification of chlorins. Successive dilutions of the pigment *phyrophaeophorbide a methyl ester* in acetone were injected successively in the HPLC-PDA, and the relative response of the peak area was measured (Figure 2.3). A linear equation was used to convert areas to concentration (Figure 2.3).

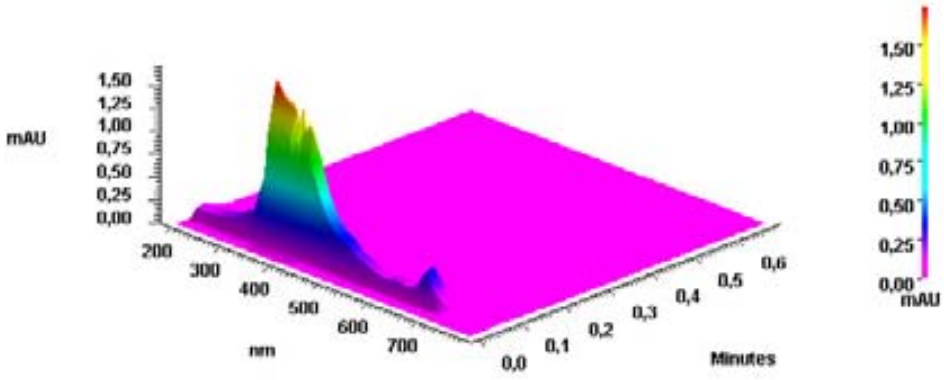

Figure 2.2. Chromatogram of chlorin analysis with an HPLC-PDA system. The x-axis shows wavelengths from 300 to 800 nm, the y axis shows the duration of the analysis in minutes and the z-axis shows the absorbance in mili-arbitrary units (mAU).

The concentration of chlorins per gram sediment was calculated using the external standard calibration curve and also considering the dilution factor, defined as the amount of sample injected in the HPLC compared to the total volume of the dilution. The remaining extracts were dried under a gentle nitrogen stream. They were stored sealed and frozen at -20ºC until further sample purification (described in section 2.2.3).

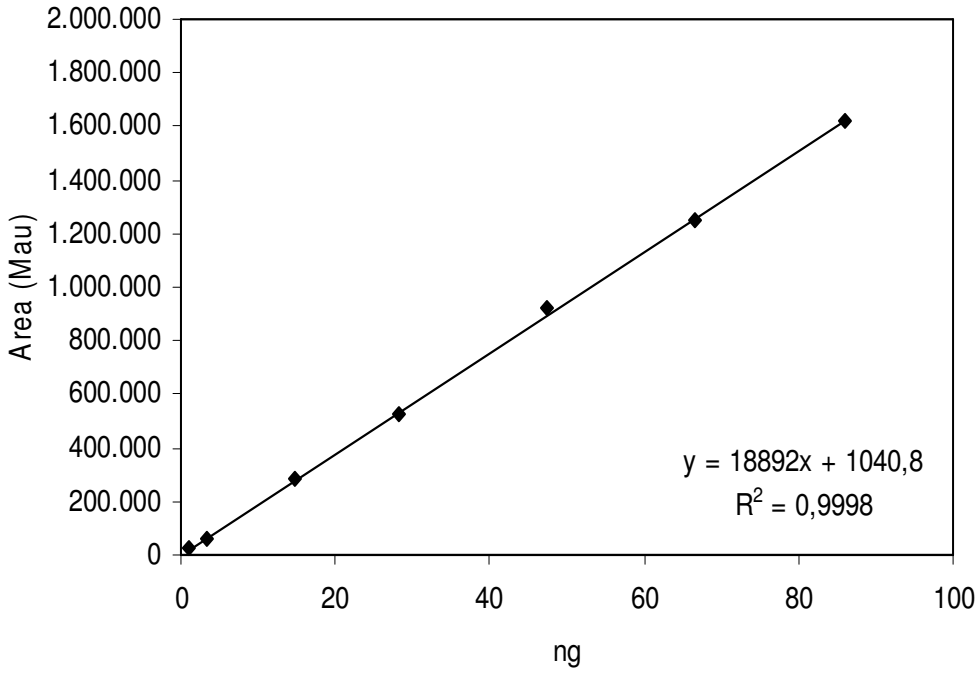

Figure 2.3. External calibration curve for chlorin quantification via HPLC-PDA

2.2.4.2. Gas Chromatography Flame Ionization Detector (GC-FID)

The n-alkanes (fraction 1) and the alkenones (fraction 2) were analyzed using a Thermo Trace Ultra gas chromatograph fitted with a flame ionization detector (GC-FID). Dry extracts were re-dissolved in isooctane and injected in the GC-FID using a Thermo TriPlus autosampler. Automatic injection of the sample was performed in splitless injection mode. The injector and the detector temperatures were set at 310 ^{o}C and at 320 ^{o}C, respectively. Helium was used as carrier gas with a constant flux of 1.5 mL min^{-1}. Compounds were separated through an Agilent HP-1 capillary column of 60 m length, 0.25 mm internal diameter and 0.25 μm film thickness connected to a 5 m guard column using a press-fit. For n-alkane fraction analysis, oven temperature was held at 80 ^{o}C during 1 min, increased to 120 ^{o}C at a rate of 20 ^{o}C min^{-1}, then increased to 320 ^{o}C at 6 ^{o}C min^{-1} and remained at 320 ^{o}C during 20 min. For alkenone fraction analysis, the oven temperature was held at 80 ^{o}C during 1 min, it increased to 120 ^{o}C at a rate of 30 ^{o}C min^{-1}, then it increased to 320 ^{o}C at 50 ^{o}C min^{-1} and it was finally held at this temperature for 30 min.

External standards were used for identification of alkenones and n-alkanes in the GC-FID based on their retention time. A sample of fractionated fuel that contained a range of n-alkanes from C_{40} to C_{15} was used as an external standard for n-alkane

identification based on comparison of their retention times (Elordui-Zapatarietxe et al., 2008) (Figure 2.4). Likewise, a standard sample containing only a mixture of $C_{37:3}$ and $C_{37:2}$ ketones was used for alkenone identification (Figure 2.5). Quantification of alkenones and n-alkanes was assessed using known concentrations of internal standards added prior to extraction (Table 2.1).

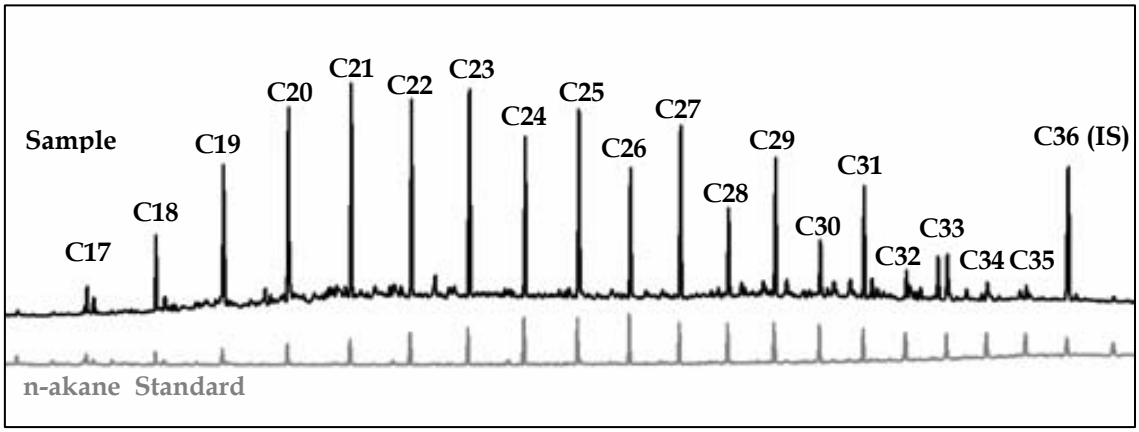

Figure 2.4. Identification of n-alkanes in Fram Strait samples (black chromatogram) via retention time comparison to a fractionated fuel sample (grey). The internal standard is also noted (C36 IS).

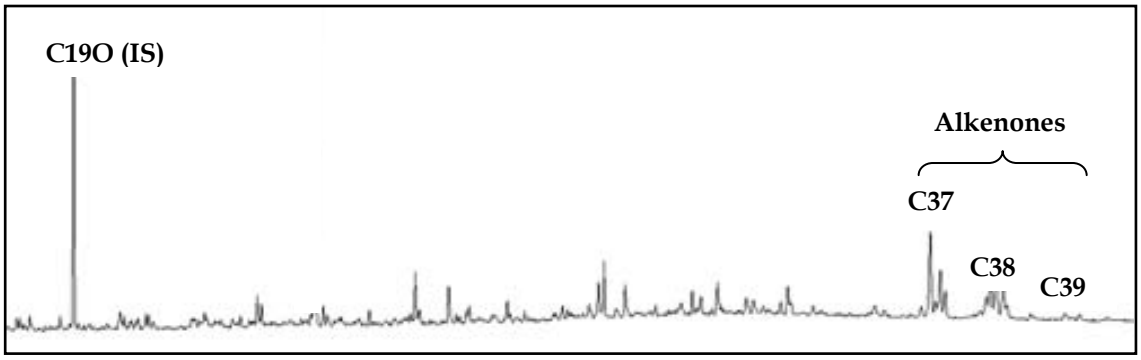

Figure 2.5. Chromatogram representative of the analysis of alkenones in the GC-FID. The internal standard (C19O IS) and three groups of alkenones (C_{37}, C_{38} and C_{39}) can be observed.

It was observed that the $U^{K'}_{37}$ temperature estimates could present significant errors (> 0.5 ^{o}C) when the amount of alkenones injected in the GC-FID system was close to the limit of detection (Rosell-Melé, 1994; Rosell-Melé et al., 1995; Grimalt et al., 2001). We injected successive dilutions of an alkenone standard for establishing the limit for reliable $U^{K'}_{37}$ measurements in our system (Figure 2.6). The threshold for reliable analysis of $U^{K'}_{37}$ with a temperature estimation error < 0.5 ^{o}C was determined for our system at an amount of 15 ng for each alkenone injected in the GC-FID equipment. In addition, an alkenone standard, and a standard sediment sample were

injected when the system was at its optimum conditions and their $U^{K'}_{37}$ values were determined. These standard samples were injected routinely between environmental samples analysis. If there was a bias higher than 0.5 ºC in the $U^{K'}_{37}$ temperature estimates the GC-FID system was thoroughly checked to get the system back to optimum conditions for example by replacing or cutting a part of the guard column or replacing the injection liner.

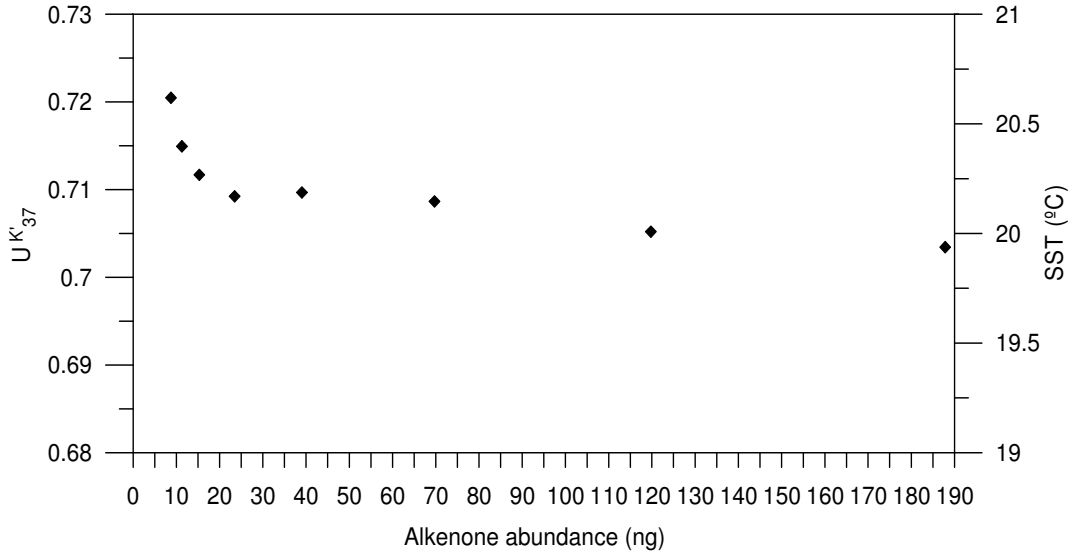

Figure 2.6. Change of the $U^{K'}_{37}$ index with decreasing amount of alkenone injected in the GC-FID. The right axis shows the magnitude of SST change calculated with the calibration from Müller et al. (1998)

2.2.4.3. Gas Chromatography coupled to Mass Spectrometry (GC-MS)

For IP25 analysis, fraction 1 dry extracts were re-dissolved in hexane and an aliquot of the sample was automatically injected into an Agilent 7890A Gas Chromatography Mass Spectrometry system (GC-MS). The extracts eluted through an Agilent HP5-MS fused silica column, that had 30 m length, an internal diameter of 0.25 mm and a film thickness of 0.25 µm. Helium was used as carrier gas with a flow of 1.1 mL min^{-1}. The initial oven temperature was 40 ºC, it increased gradually to 300 ºC at a rate of 10 ºC min^{-1} and the final temperature was held during 10 min. The injector temperature was set at 250 ºC and the transfer line temperature at 280 ºC. The mass spectrometer ion source and quadrupole temperatures were set at 230 ºC and 150 ºC respectively. The analysis was performed at single ion monitoring (SIM) mode of the following target ion masses *m/z* 99, 191, 266, 346, 348 and 350. Figure 2.7 shows a chromatogram and the mass spectra at full scan for the IP25 peak identified in samples form the Barents Sea.

For quantifying IP25, 200 ng of a mixture of 7-Hexylnonadecane (*m/z* = 266) and 9-Octyl-8-heptadecene (*m/z* = 350) were added prior to extraction and used as internal standards. The abundance of IP25 was calculated comparing the relative response of its molecular ion (*m/z* = 350) to the relative response of the abundant fragment ion of the internal standard 7-hexylnonadecane (*m/z* = 266). An external calibration curve considering the GC-MS response of the internal standard at different concentrations yielded a linear relationship with $R^2 = 0.99$.

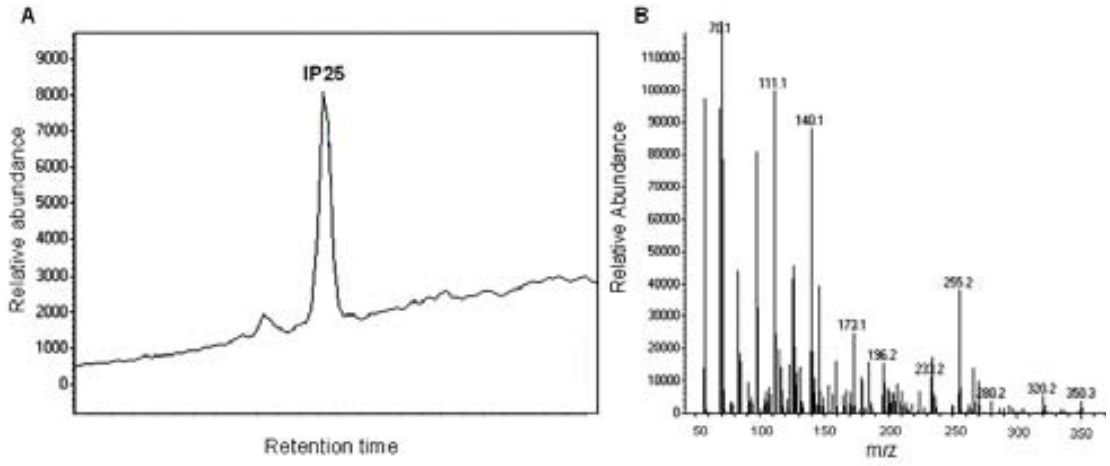

Figure 2.7. IP25 chromatogram (A) and its corresponding mass spectra (B) in full scan for a sample from the Barents Sea.

A set of alkenone samples previously analyzed in the GC-FID, were also injected in the GC-MS to check if there were other compounds interfering with the alkenones The mass spectra characteristic for alkenones in samples from the Barents Sea are shown in figure 2.8. For instance, in samples from core PL96-126 some compounds were found to coelute with alkenones. As described in section 2.2.3.2 further sample purification was needed to isolate the alkenones. After the purification step, two fractions were obtained and the first one contained the steryl alkyl ethers whereas the second contained the alkenones (Figure 2.9, black chromatogram: alkenones; red chromatogram: steryl alkyl ethers). After GC-MS analysis of these samples and comparison of their mass spectra with the existing literature, we concluded that the interfering compounds were steryl alkyl ethers (Figure 2.10, A: C27:1 sterol - C10 alkyl ether, B: C28:1 sterol – C10 alkyl ether; Schouten et al., 2005).

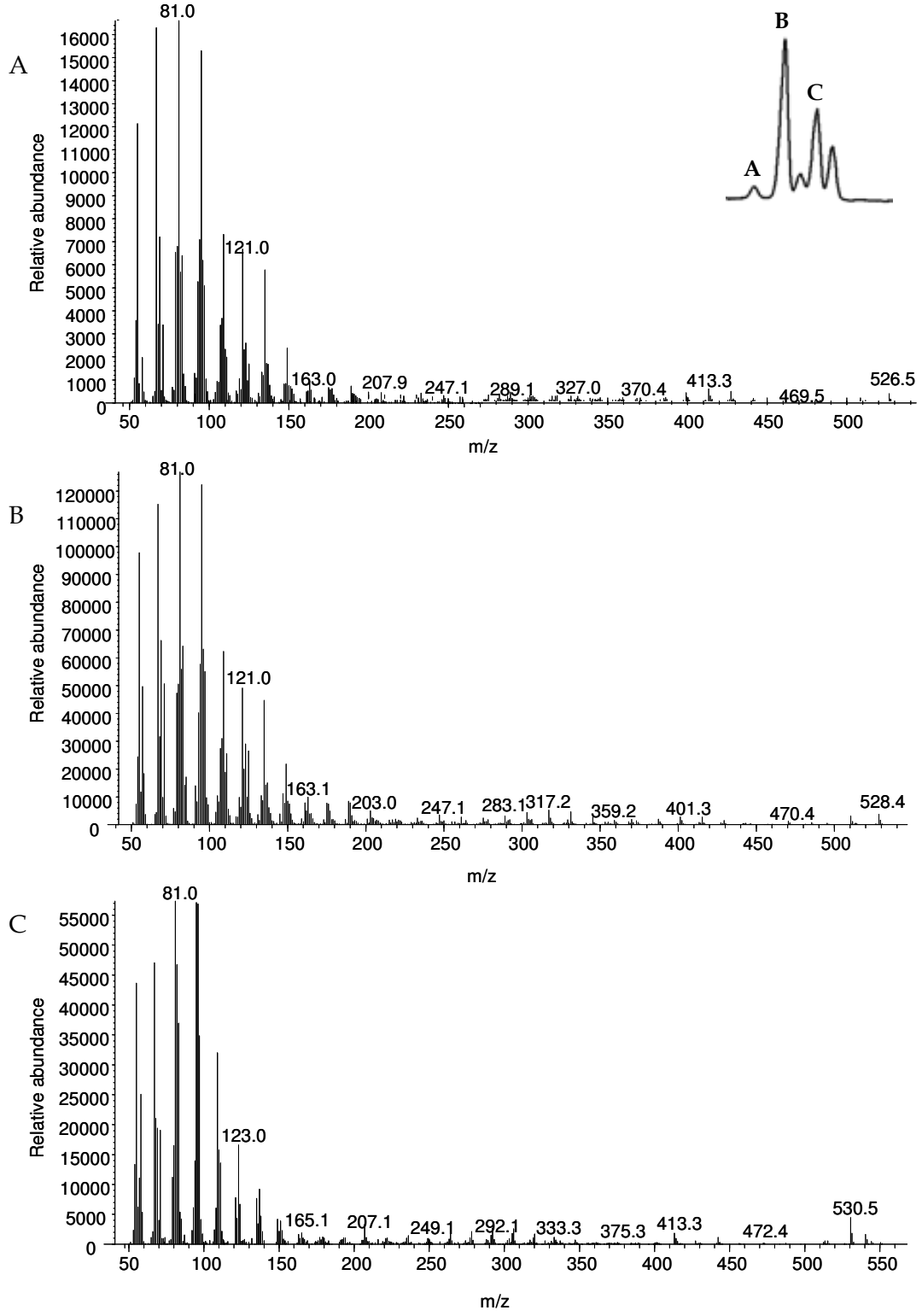

Figure 2.8. Analysis and identification of alkenones with GC-MS. The letters in the chromatogram indicate the corresponding mass spectra for the following alkenones analyzed in this thesis: $C_{37:4}$ (A), $C_{37:3}$ (B), $C_{37:2}$ (C).

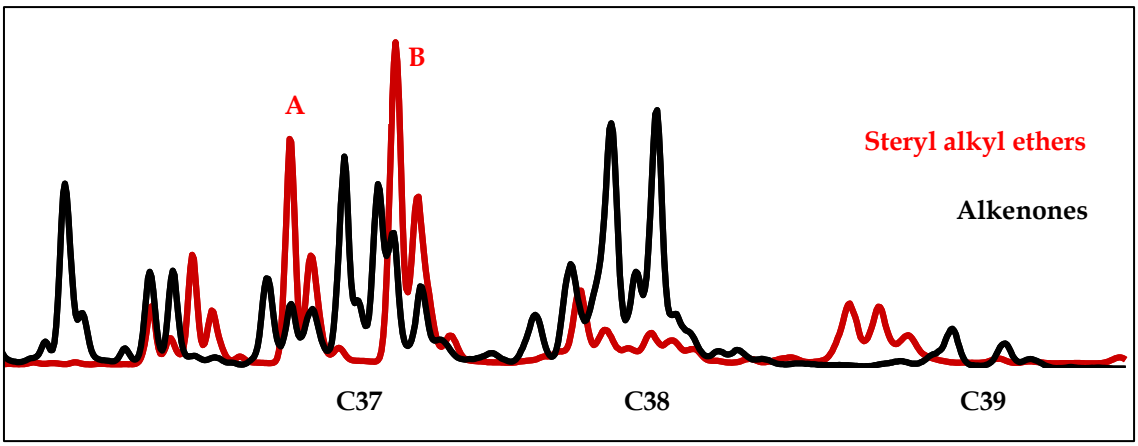

Figure 2.9. Superposition of the chromatograms obtained after GC-FID analysis of the two fractions obtained after a second step purification of fraction 2 samples from core PL96-126. The red chromatogram shows the steryl alkyl ethers, the compounds coeluting with the alkenones (fraction 1 obtained after a second step purification of fraction 2). The black chromatogram shows the purified sample containing the alkenones after the second step cleaning of the samples (fraction 2).

2.2.4.4. High Performance Liquid Chromatography Atmospheric Pressure Chemical Ionization Mass Spectrometry (HPLC-APCI-MS)

For GDGT analysis, the third fraction was dried and dissolved in 200 µL hexane:n-propanol (98.5:1.5, v/v) and filtered through a 0.5 µm PTFE filter (Advantec). An aliquot of sample was automatically injected in a Dionex P680 HPLC coupled to a Thermo Finnigan TSQ Quantum Discovery Max quadrupole mass spectrometer with an atmospheric pressure chemical ionization (APCI) interface set in positive mode. Following the methods described in Escala et al. (2009) the extracts eluted through a Tracer Excel CN column (Teknokroma) with a length of 20 cm, a diameter of 0.4 cm and a particle size of 3 µm. A pre-column filter and a guard column were fitted to the column. The mobile phase was initially hexane:n-propanol (98.5:1.5) at a flow of 0.6 mL min^{-1}. The proportion of n-propanol was kept constant at 1.5% for 4 minutes, after it increased gradually to 5% during 11 minutes, then it increased to 10% for 1 minute and it remained at this proportion for 4 minutes. Finally, it decreased back to 1.5% during 1 minute and was held at these conditions for 9 more minutes until the end of the run. The parameters of the APCI interface were set as follows to generate positive ion spectra: corona discharge 3 µA, vaporizer temperature 400 ^{o}C, sheath gas pressure 49 mTorr, auxiliary gas (N_2) pressure 5 mTorr and capillary temperature 200 ^{o}C. GDGTs were detected in selected ion monitoring (SIM) mode at the following mass to charge ratio (*m/z*): 1302, 1300, 1298, 1296, 1292, 1050, 1048, 1046, 1036, 1034, 1032, 1022, 1020, 1018 and the internal standard GR at 1208 *m/z*. For quantifying the total abundance of intact GDGTs we subtracted the amount of lipids quantified in the half

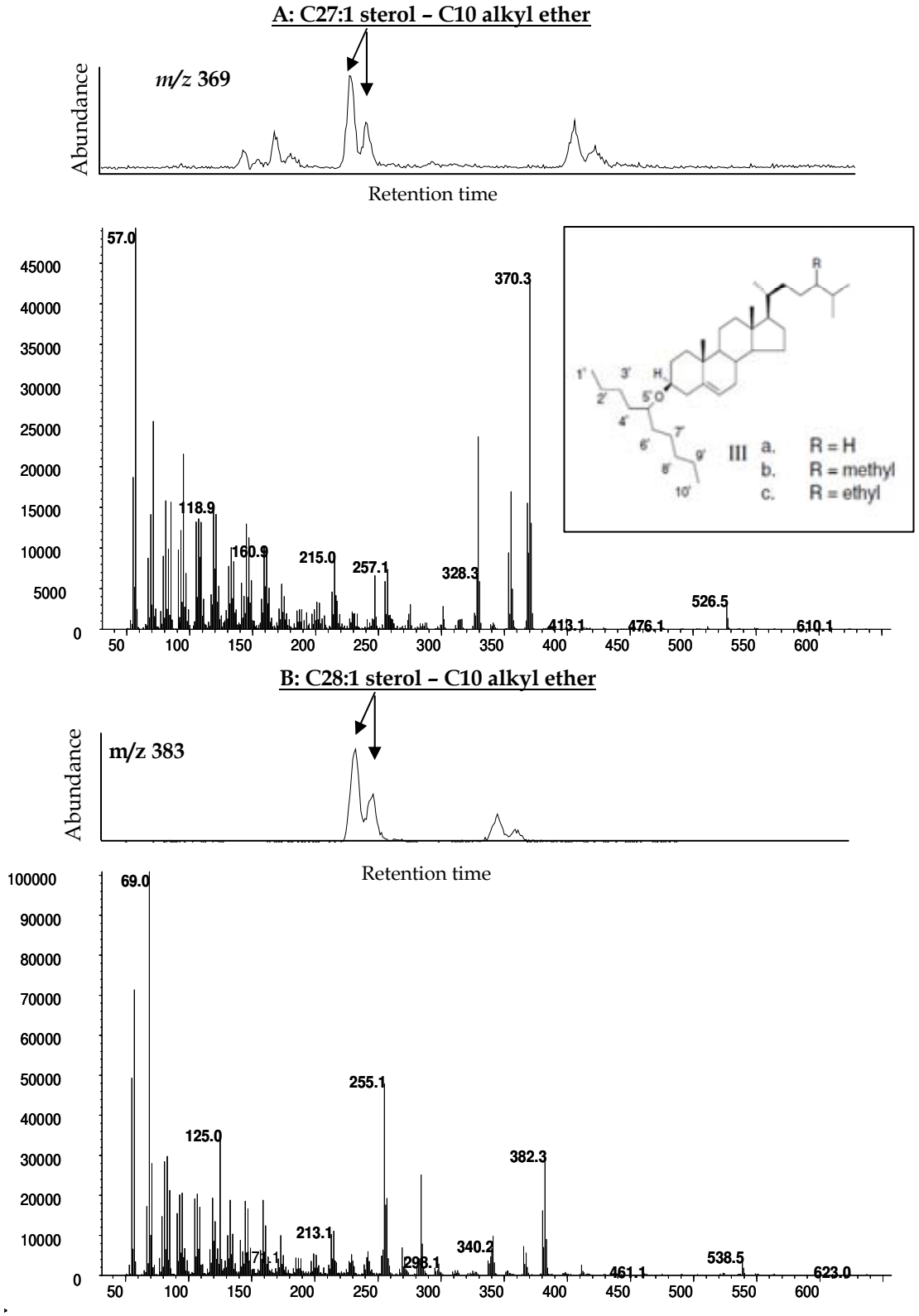

Figure 2.10. Identification of steryl alkyl ethers via GC-MS in samples from core PL96-126. Chromatogram at *m/z* 369 (A) and 383 (B) and full scan mass spectra at the retention times indicated with arrows. The compounds were identified as (A) C27:1 sterol – C10 alkyl ether and (B) C28:1 sterol – C10 alkyl ether. The molecular structure of the compounds is shown next to mass spectra (A) (from Schouten et al. (2005)).

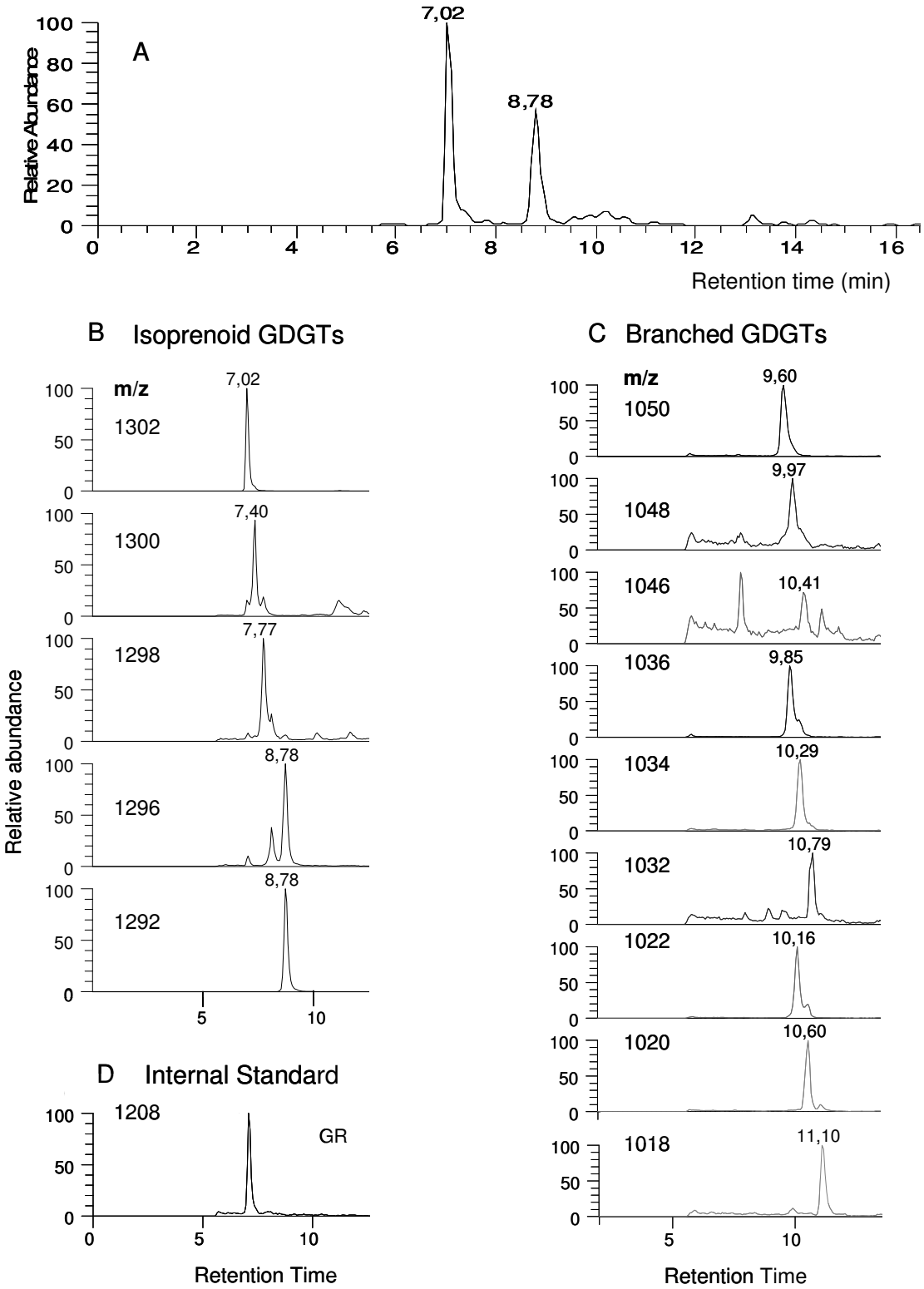

Figure 2.11. Chromatograms of the GDGT analysis in our HPLC-APCI-MS system. (A) Total ion current and Single Ion Monitoring at each GDGT *m/z* for (B) isoprenoid GDGTs (C) branched GDGTs (D) and the internal standard GR.

sample that was hydrolyzed (Huguet et al., 2010). In Figure 2.11 the chromatogram at each *m/z* for all the GDGTs and the internal standard is shown.

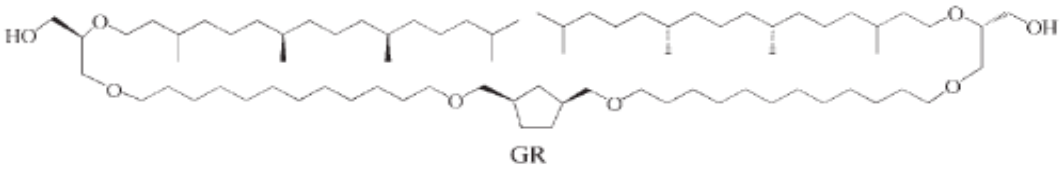

Figure 2.12. Molecular structure of the synthetic tetraether compound GR used as internal standard for GDGT analysis (Réthoré et al., 2007).

Quantification of GDGTs was achieved using the compound GR as an internal standard, a synthetic tetraether lipid with a structure typical of neutral archaeal membrane lipids (Figure 2.12) and a *m/z* of 1208 (Réthoré et al., 2007). Prior to extraction, 65 ng of GR were added to the sample. The average response factor of the standard GR versus the isolated isoprenoid GDGT-0 standard with a *m/z* of 1302 was 1.2±0.1 (Escala, 2009). The reproducibility of the quantification of GDGTs using GR as a standard is higher than 90% (Escala, 2009).

The linear range where the relationship between the concentration of the compound and the response of the detector is linear was assessed injecting consecutively increasing concentrations of the GR standard and calculating the peak area in each concentration (Figure 2.13).

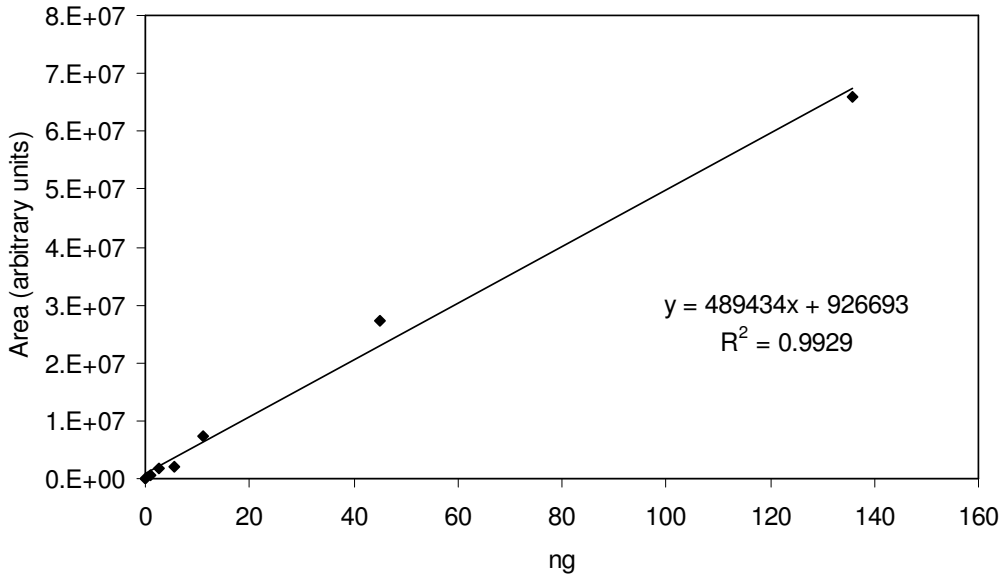

Figure 2.13. External calibration curve for determination of the linear range, using the standard GR analyzed via HPLC-APCI-MS.

In 2009, an interlaboratory comparison study for the TEX_{86} and BIT indices was performed (Schouten et al., 2009) and our laboratory was one of the 21 participants (Escala, 2009). Since then, a standard sediment sample has been injected routinely in our HPLC-APCI-MS system before the analysis of sample sets. A new tuning of the APCI-MS system was performed when the TEX_{86} values were more than 0.02 units different from the standard value.

2.2.5. Quality controls

2.2.5.1. Procedure blanks

A solvent blank was extracted every batch of samples and analyzed exactly as the rest of the samples. This routine allowed controlling any possible contamination during the preparative analysis of the samples.

2.2.5.2. Detection and quantification limits

To establish the minimum amount of analyte that could be detected and quantified with reasonable certainty, we injected solvent blanks routinely and calculated the detection and quantification limits. As defined by the the IUPAC (1997) the minimum measurement that can be detected with reasonable confidence (X_L) is given by calculating the average of all the blank analysis (X_{bi}) and their standard deviation (S_{bi}). Depending on the confidence level desired, an accordingly different numerical factor is applied (K) (IUPAC, 1997). The general equation is the following:

$$X_L = X_{bi} + K \cdot S_{bi}$$

Following the general equation described above, we calculated the limit of detection (LOD) and the limit of quantification (LOQ) applying a K factor equivalent to 3 and 10 respectively:

$$LOD = X_{bi} + 3S_{bi}$$

$$LOQ = X_{bi} + 10S_{bi}$$

The LOD and LOQ values for each GDGT *m/z* are given in Table 2.2 and are expressed in pg of injected compound. For IP25 analysis, the detection and quantification limits were calculated on the basis of the injection of 10 process blanks. For IP25 analysis, the values were established at 0.08 ng for LOD 0.1 ng for LOQ.

Table 2.2. Limit of detection (LOD) and limit of quantification (LOQ) for the GDGTs analysis (pg).

Injected pg	GDGT m/z													
	1302	1300	1298	1296	1292	1050	1048	1046	1036	1034	1032	1022	1020	1018
LOD	40.1	1.0	0.2	0.3	54.4	1.5	0.9	0.3	0.9	0.8	0.4	2.1	1.3	1.5
LOQ	101.1	2.6	0.6	0.9	134.8	3.9	2.2	0.7	2.1	2.0	1.0	5.1	3.6	3.5

2.2.5.3. Analytical reproducibility

A substantial amount of marine sediment from the Fram Strait was freeze-dried and homogenized. Afterwards it was used as standard sediment, extracted each batch of samples to assess analytical reproducibility and stability in the analysis of biomarkers and the related indices. The biomarkers quantification showed a reproducibility >90% (1σ, n = 30). The reproducibility of the $U^{K'}_{37}$ index temperature estimates was equivalent to 0.5 ^{o}C (1σ, n = 30). The reproducibility of the analysis of GDGT based temperature estimates was equivalent to 0.6 ^{o}C (1σ, n = 30). The reproducibility of the analysis of IP25 was 0.2 ng g^{-1} (1σ, n = 10).

2.3. Ancillary measurements

2.3.1. Carbon and nitrogen abundances and isotopic ratios

The total abundance of carbon and nitrogen and their isotopic ratios $\delta^{15}N$ and $\delta^{13}C$ were measured at low resolution - one sample every 10 cm – in the sediment core from the Barents Sea. The analysis was performed using an Elemental Analyzer Flash 1112 coupled to an isotope ratio mass spectrometer Thermo Delta V Advantage (EA-IRMS) with a Conflo III interface. Sediment samples were freeze dried and homogenized. For organic carbon analysis samples were prepared in Ag capsules. Samples were decarbonised with an HCl atmosphere by depositing them next to a solution of HCl (32%) in a closed desiccator. The reaction took place during 12 h at 5 ^{o}C. For nitrogen analysis, samples were prepared in Sn capsules and no acidification was performed, as acid treatment reduces de precision of the measurements of C/N and N (Brodie et al., 2011). Samples were combusted at 1020 ^{o}C and the CO_2 and N_2 generated were carried with Helium to the reactor where the isotope ratios $^{13}C/^{12}C$ and $^{15}N/^{14}N$ were measured. The results are expressed in the standard delta (δ) notation that considers the measured isotope ratios in the samples (IRsample) and in the

standards (IRstandard). The following equation was applied for obtaining both $\delta^{13}C$ and $\delta^{15}N$:

$$\delta\ (‰) = (IRsample/IRstandard - 1) \cdot 1000$$

The reference standards used for scaling the $\delta^{13}C$ and $\delta^{15}N$ measurements were Vienna Pee Dee Belemnite (VPDB) and air nitrogen respectively. The precision of the analysis for %organic carbon and for $\delta^{13}C$ was 0.4 % and 0.15 ‰. For the nitrogen analogues precision was 0.2 % and 0.07 ‰ respectively (1σ, n = 10).

2.3.2. Total organic matter

The total amount of organic matter in soil samples from Ulldeter and Øsaker was analyzed via loss on ignition (LOI). Considering that organic matter is a coarse estimate for organic carbon content, this technique gives a semi-quantitative estimate for the total organic carbon (TOC) contained in the soil or sediment sample (Schumacher, 2002).

For analyzing LOI in soil samples we followed the methodology described in Heiri et al. (2001). Aluminium trays were dried in an oven at 105 ºC for 1 hour. 1 g of dry soil sample was deposited in a dry aluminium tray and remained for 15 hours at 105 ºC in the oven. Afterwards the dry samples were weighted (DW_{105}) and the samples were heated to 550 ºC for 4 hours. Then the ash weight was noted (DW_{550}) and the LOI value was calculated using the following equation as described in Heiri et al. (2001):

$$LOI = (DW_{105} - DW_{550})/DW_{105}$$

2.4. References

Brodie CR, Casford JSL, Lloyd JM, Leng MJ, Heaton THE, Kendrick CP and Yongqiang Z (2011) Evidence for bias in C/N, δ13C and δ15N values of bulk organic matter, and on environmental interpretation, from a lake sedimentary sequence by pre-analysis acid treatment methods. Quaternary Science Reviews 30(21–22): 3076–3087: doi:10.1016/j.quascirev.2011.07.003.

Elordui-Zapatarietxe S, Albaigés J and Rosell-Melé A (2008) Fast preparation of the seawater accommodated fraction of heavy fuel oil by sonication. Chemosphere 73(11): 1811–1816: doi:10.1016/j.chemosphere.2008.08.018.

Escala M (2009) Application of tetraether membrane lipids as proxies for continental climate reconstruction in Iberian and Siberian lakes. PhD Tesis. Universitat Autònoma de Barcelona.

Escala M, Fietz S, Rueda G and Rosell-Melé A (2009) Analytical Considerations for the Use of the Paleothermometer Tetraether Index86 and the Branched vs Isoprenoid Tetraether

Index Regarding the Choice of Cleanup and Instrumental Conditions. Analytical Chemistry 81(7): 2701–2707: doi:10.1021/ac8027678.

Grimalt JO, Calvo E and Pelejero C (2001) Sea surface paleotemperature errors in UK'37 estimation due to alkenone measurements near the limit of detection. Paleoceanography 16(2): 226–232: doi:10.1029/1999PA000440.

Heiri O, Lotter AF and Lemcke G (2001) Loss on ignition as a method for estimating organic and carbonate content in sediments: reproducibility and comparability of results. Journal of Paleolimnology 25(1): 101–110: doi:10.1023/A:1008119611481.

Huguet C, Martens-Habbena W, Urakawa H, Stahl DA and Ingalls AE (2010) Comparison of extraction methods for quantitative analysis of core and intact polar glycerol dialkyl glycerol tetraethers (GDGTs) in environmental samples. Limnology and Oceanography: Methods 8: 127–145: doi:10.4319/lom.2010.8.127.

IUPAC (1997) Compendium of Chemical Terminology, 2nd ed. (the "Gold Book"). Compiled by A. D. McNaught and A. Wilkinson. Blackwell Scientific Publications, Oxford (1997). XML on-line corrected version: http://goldbook.iupac.org (2006-) created by M. Nic, J. Jirat, B. Kosata; updates compiled by A. Jenkins. ISBN 0-9678550-9-8. doi:10.1351/goldbook. .

Kornilova O and Rosell-Melé A (2003) Application of microwave-assisted extraction to the analysis of biomarker climate proxies in marine sediments. Organic Geochemistry 34(11): 1517–1523: doi:10.1016/S0146-6380(03)00155-4.

McClymont EL, Martínez-Garcia A and Rosell-Melé A (2007) Benefits of freeze-drying sediments for the analysis of total chlorins and alkenone concentrations in marine sediments. Organic Geochemistry 38(6): 1002–1007: doi:10.1016/j.orggeochem.2007.01.006.

Nuñez N (2005) Export ProductivityDuring Last Glacial Maximum. Master Thesis in Environmental Science. Institut de Ciència i Tecnologia Ambientals, Universitat Autònoma de Barcelona. 39-58 pp.

Réthoré G, Montier T, Le Gall T, Delépine P, Cammas-Marion S, Lemiègre L, Lehn P and Benvegnu T (2007) Archaeosomes based on synthetic tetraether-like lipids as novel versatile gene delivery systems. Chemical communications (20): 2054–2056.

Rosell-Melé A (1994) Long-chain alkenones, alkyl alkenoates and total pigment abundances as climatic proxy-indicators in the Northeastern Atlantic. PhD Thesis. University of Bristol.

Rosell-Melé A, Carter J, Parry A and Eglinton G (1995) Novel procedure for the determination of the UK37 in sediment samples. Analytical Chemistry 67, 1283-1289.

Schouten S, Hopmans EC, Van der Meer J, Mets A, Bard E, Bianchi TS, Diefendorf A, Escala M, Freeman KH, Furukawa Y, Huguet C, Ingalls A, Ménot-Combes G, Nederbragt AJ, Oba M, Pearson A, Pearson EJ, Rosell-Melé A, Schaeffer P, Shah SR, Shanahan TM, Smith RW, Smittenberg R, Talbot HM, Uchida M, Van Mooy BAS, Yamamoto M, Zhang Z and Sinninghe Damsté JS (2009) An interlaboratory study of TEX86 and BIT analysis using high-performance liquid chromatography–mass spectrometry. Geochemistry, Geophysics, Geosystems 10(3): doi:10.1029/2008GC002221.

Schouten S, Rampen SW, Geenevasen JAJ and Sinninghe Damsté JS (2005) Structural identification of steryl alkyl ethers in marine sediments. Organic Geochemistry 36(9): 1323–1333: doi:10.1016/j.orggeochem.2005.04.002.

Schumacher BA (2002) Methods for the determination of total organic carbon (toc) in soils and sediments. U.S. Environmental Protection Agency, Washington, DC, EPA/600/R-02/069 (NTIS PB2003-100822).

CHAPTER 3

Comparison of instrumental and GDGT based estimates of sea surface and air temperatures from the Skagerrak

This chapter is a modified version of an article published in:

Rueda G, Rosell-Melé A, Escala M, Gyllencreutz R and Backman J (2009) Comparison of instrumental and GDGT-based estimates of sea surface and air temperatures from the Skagerrak. *Organic Geochemistry* 40(2): 287–291: doi:10.1016/j.orggeochem.2008.10.012.

3.1. Abstract

Sea surface temperatures (SST) and annual mean air temperatures (MAT) were estimated for the last 200 years from glycerol dialkyl glycerol tetraethers (GDGTs) proxies in a marine sediment core from the Skagerrak, off southern Norway. The reconstructed values compared well to annual SST and summer air temperatures obtained from composite regional instrumental records. The bias of the reconstructed air temperature towards summer values could be due to site specific dynamics not accounted for in the global calibration. We suggest that the branched GDGTs may reach the Skagerrak preferentially in summer months coinciding with the highest discharge of the Glomma River. In addition, part of the lipids could be originated in the southern North Sea, thus contributing to high reconstructed temperature values. An alternative hypothesis is that the organisms synthesizing branched GDGTs are more active during summer, as southern Scandinavia soils are snow covered during several months.

Keywords Skagerrak; SST; air temperature; TEX_{86}; MBT; CBT

3.2. Introduction

One of the greatest challenges in reconstructing past temperatures is to obtain sea surface and air temperatures from the same archive, the ultimate goal being the correlation of continental and ocean temperatures and understanding issues such as the interaction between ocean circulation and land climates. This might be undertaken using glycerol dialkyl glycerol tetraethers (GDGTs), membrane lipids derived from Archaea, and bacterial membrane lipids, which occur ubiquitously in aquatic environments and soils. One of the proxies based on these lipids is the TEX_{86} (Schouten et al., 2002), applied to estimate past sea surface temperatures (SST) by quantifying the average number of cyclopentane rings in tetraethers with 86 carbon atoms in sediments (Figure 1.9). Thus, values of TEX_{86} in surface sediments from a wide range of locations worldwide strongly correlate to SST, and appear not to be dependent on salinity or nutrient concentration (Wuchter et al., 2004, 2005).

Another proxy based on branched GDGTs (Figure 1.9), produced by unknown anaerobic bacteria living in soils (Weijers et al., 2006a), has been recently proposed to estimate past mean air temperatures (MAT) (Weijers et al., 2007b). The proxy quantifies the degree of cyclisation of branched tetraethers (CBT), and the methylation extent of branched tetraethers (MBT). The CBT correlates with soil pH, whereas MBT depends

on soil pH and annual mean air temperature (Weijers et al., 2007b). These proxies have been used for instance to reconstruct large scale continental temperature changes in tropical Africa from the Last Glacial Maximum to the Holocene (Weijers et al., 2007a), although in comparison to TEX_{86} few reports exist on their application and calibration (Sinninghe Damsté et al., 2008).

Another GDGT proxy, the branched versus isoprenoid tetraether (BIT) index (Hopmans et al., 2004) has been proposed and applied to determine the relative inputs through time of fluvial soil organic matter in marine environments (e.g., Menot et al., 2006). It is estimated through the ratio of the relative amount of branched GDGTs derived from anaerobic bacteria living in soils and peat bogs (Weijers et al., 2006b) and crenarchaeol, a GDGT found to be predominant in a wide variety of aquatic marine environments (e.g. Wuchter et al., 2005, 2006).

Given that GDGT proxies are relatively new, uncertainties remain on their general applicability and interpretation. To shed some new light on this question, here we test the TEX_{86}, MBT and CBT proxies by applying them to a high resolution marine sediment core, and comparing their estimates for the last 200 years with regional instrumental records of sea surface and air temperatures.

3.3. Samples and data acquisition description

Core MD99-2286 (58º43'46.2''N, 10º12'18.6''E; 225 m water depth) was retrieved from the northeastern Skagerrak (Figure 3.1). The age model was established using 27 AMS ^{14}C dates (Gyllencreutz et al., 2005). The core spans the last glacial/interglacial cycle, but in this study we focus on the period AD 1800-1996 (3.5 to 242.5 cm below sediment core surface). This interval is dated by one ^{14}C date (Gyllencreutz et al., 2005) and four indirect ^{210}Pb dates by correlation to the ^{210}Pb-dated gravity core Sk000209-2 (58º43'50.4''N, 10º11'46.8''E 226 m water depth, 622 m away from core MD99-2286) (Senneset, 2002; Gyllencretuz, 2005). All dates discussed here are in calendar years.

Instrumental SST values were obtained from the International Comprehensive Ocean-Atmosphere Data Set (http://icoads.noaa.gov/) as an average of the data included in an area between 56ºN and 60ºN and 6ºE and 12ºE. The instrumental air temperature record was obtained from the average of seven records from meteorological stations located in Oslo, Faerder, Kristiansand, Torungen, Göteberg, Tranebjerg and Copenhaguen, reported in Rimfrost (www.rimfrost.no) (Figure 3.1). Both sea and air temperature records have been smoothed using a gaussian 3σ filter with ±1σ error (Figure 3.2).

The analytical methods followed to analyze GDGTs were described in chapter 2. TEX_{86} was converted to annual mean SST using the equation in Kim et al. (2008) where T (^{o}C) = - 10.78 +56.2 · TEX_{86} (R^2 = 0.935). CBT and MBT values were converted to annual MAT using the equations from Weijers et al. (2007b) where CBT = 3.3283 – 0.3847 * pH and MBT = 0.867 – 0.096 ·pH + 0.021 ·MAT.

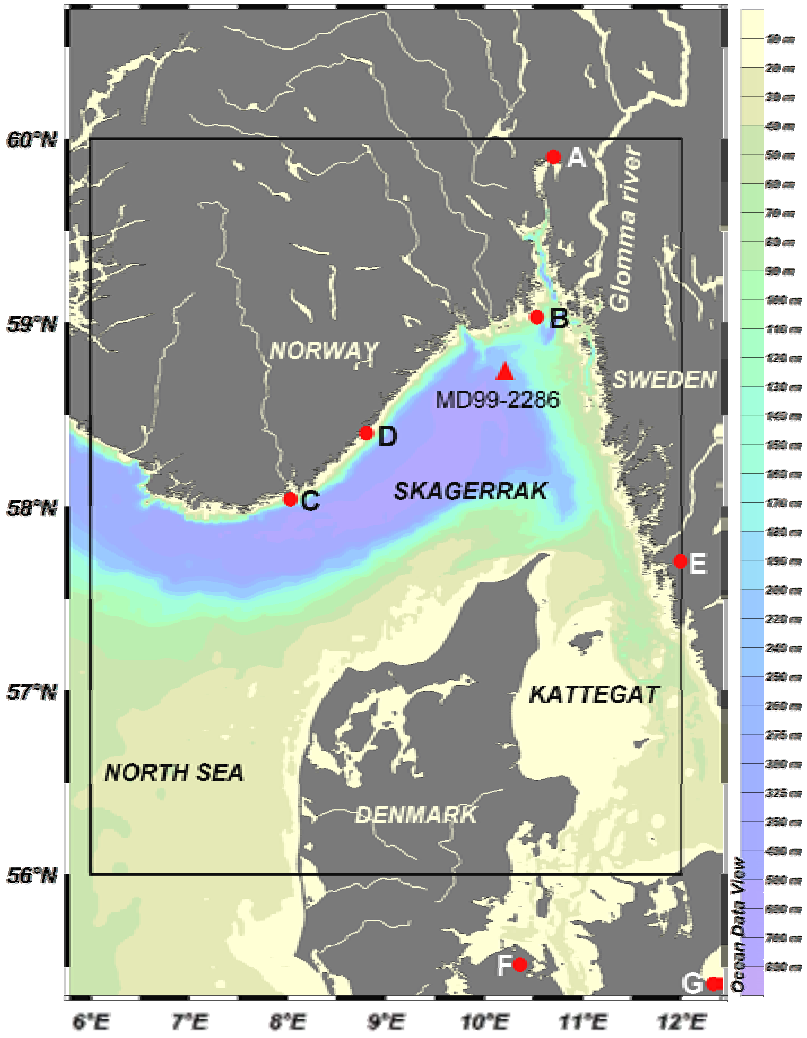

Figure 3.1. Map indicating the location of core MD99-2286 (triangle) in the Skagerrak. Circles indicate the location of the instrumental air temperature records from (A) Oslo, (B) Faerder, (C) Kristiansand, (D) Torungen, (E) Göteberg, (F) Tranebjerg, and (G) Copenhaguen. The black solid rectangle defines the area considered to derive the instrumental sea surface temperatures (56^{o}N to 60^{o}N in latitude and 6^{o}E to 12^{o}E in longitude) in http://icoads.noaa.gov/.

3.4. Results and discussion

A key point in the interpretation of the TEX_{86} and MBT/CBT estimates is the attribution of the signal to a specific geographical region, related to the origin and source of the GDGTs. The sedimentary lipids included in TEX_{86} have been proposed to originate from the upper water column, approximately above 100 m water depth (Wuchter et al., 2005). In contrast, branched GDGTs originate from land sources (Schouten et al., 2000; Hopmans et al., 2004). In the area of study, they are likely to be transported by the Glomma River (Figure 3.1), which is the largest river draining into the Skagerrak, and that enters the sea close to the coring site. It has its highest discharge in May-June-July (data from the Global Runoff Data Centre, http://grdc.bafg.de). Consequently, the highest flux of branched GDGTs from Scandinavia to the coring site could be expected to occur during summer too. In our core, BIT values range from 0.06 to 0.08, with an average value of 0.07 (Figure 3.2C), suggesting a clear dominance of marine GDGTs over those from continental origin. Given that large inputs of branched GDGTs could bias the TEX_{86} estimates (Weijers et al., 2006b), these low BIT values support the use of TEX_{86} as a SST proxy in our core. However, the low BIT values measured here differ from the relatively high BIT (0.22) that was reported in Hopmans et al. (2004) in Holocene sediments from the Skagerrak. In addition, van Dongen et al. (2000) also found relatively high amounts of fluvially transported terrestrial biomarkers in this site, suggesting a relatively substantial influx of organic matter from rivers. In fact, this is supported by the high signal to noise ratio in the mass spectrometric analysis of branched GDGTs found in our samples. Therefore the lower BIT results in our study are likely due to large amounts of crenarchaeol sedimented in our site.

The average SST for the last 200 yrs estimated from TEX_{86} in core MD99-2286 is 11.1 ^{o}C, while values range from 9.6 to 13.9 ^{o}C (figure 3.2A). This is similar to the annual mean instrumental values, which average 10.0 ^{o}C and range between 7.5 and 12.2 ^{o}C. Van Dongen et al. (2000) analyzed alkenone contents in recent sediments (not dated) from a site near to our core, which showed an average $U^{K}_{37'}$ - SST of 11-12 ^{o}C. However, TEX_{86} SST estimates for the 20th century from the Drammensfjord (southern Norway) by Huguet et al. (2007) recalculated with the calibration by Kim et al (2008) yield values which are between 12.4 ^{o}C and 16.1 ^{o}C.

The TEX_{86} estimates from core MD99-2286 correlate better to instrumental annual mean SST rather than to values from a particular season (see seasonal SST in figure 3.2A). This could be expected as TEX_{86} in sediments is calibrated against annual mean SST (Kim et al., 2008), and rather reflects an integrated annual mean SST from which

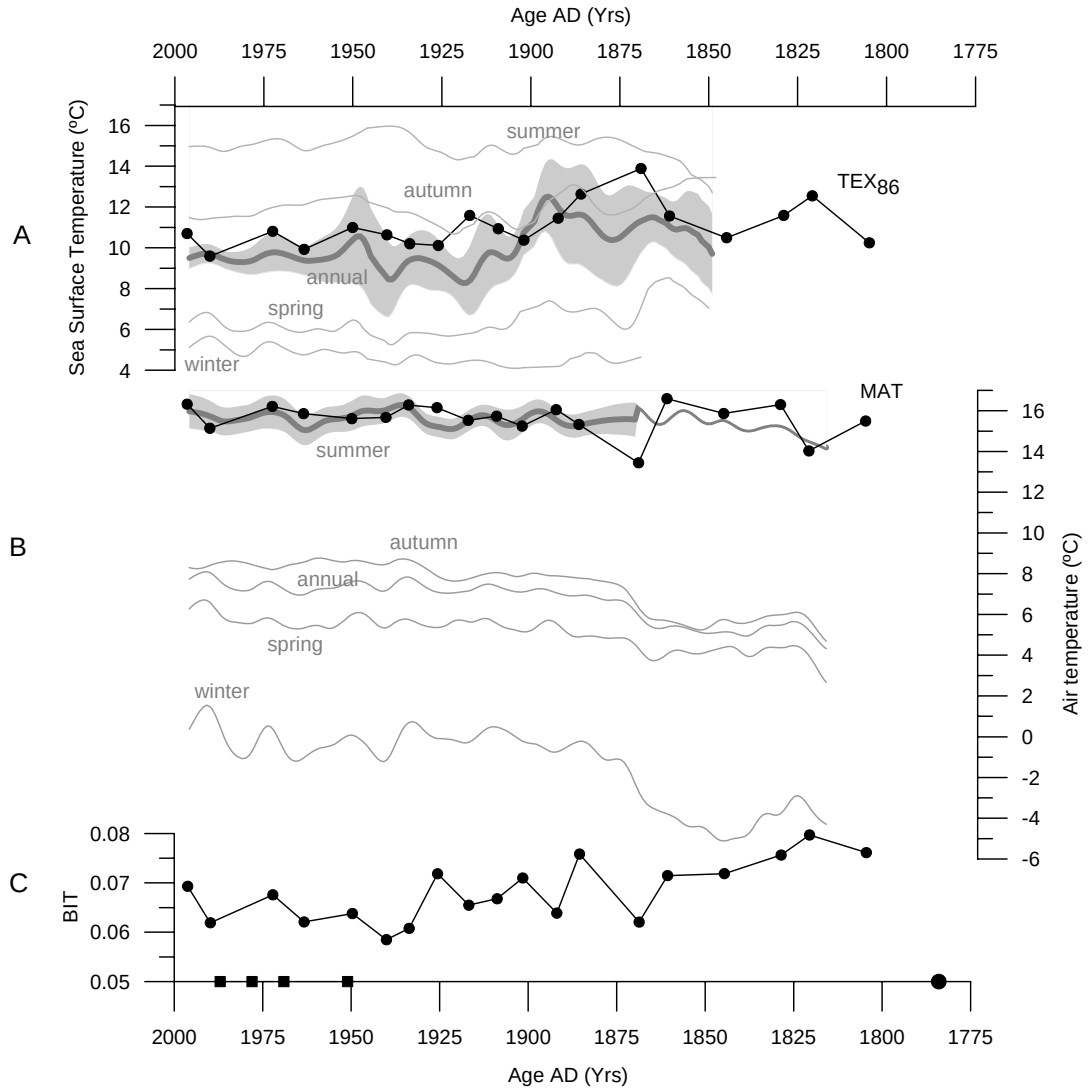

Figure 3.2. (A) Sea surface temperature (SST) estimated from TEX_{86} (black dots) and the gauss 3σ filtered regional instrumental seasonal SST records (grey line). The grey area denotes the standard deviation ±1σ for the annual mean. (B) Air temperature estimated from MAT (black dots) and the gauss 3σ filtered regional instrumental seasonal and mean annual air temperature (grey line). The grey area is the standard deviation ±1σ, for summer mean. Prior to the year AD 1870 only data from the Oslo station is available. (C) Relative inputs of terrestrial vs marine GDGTs inputs estimated from the BIT index. In the x axis, four ^{210}Pb dates (squares) and one ^{14}C date (dot) used to define the age model.

any seasonal SST signal has been lost (Wuchter et al., 2006). In contrast, Herfort et al. (2006a) found that TEX_{86} derived SST reflected winter temperatures in the southern North Sea, in accordance with 16s rDNA analysis from that region revealing that the archaeal cells were more abundant during the winter months.

Despite the overall resemblance between the TEX_{86} reconstructed and instrumental SST records there is an apparent offset between them, where the TEX_{86} record appears to lag the instrumental trend. The density of data points is different in

both records, but at this stage we think that is probably due to age model uncertainties. For instance, the maximum TEX_{86} derived SST (13.9 ^{o}C) is dated at AD 1869, where the 1σ dating error is between AD 1901 and 1817. In fact, the SST maximum observed in the instrumental record (12.2 ^{o}C, AD 1895) fits within the age model range probabilities.

The average air temperature estimated from MBT and CBT (annual MAT, figure 3.2B) is 15.6 ^{o}C, and values range between 13.4 to 16.6 ^{o}C. These values, rather than with the instrumental annual mean, are in agreement with the instrumental record of regional summer mean air temperature, which averages 15.5 ^{o}C and ranges between 14.2 and 16.3 ^{o}C (see figure 3.2B for seasonal air temperatures). The trends in MAT estimates and instrumental summer temperature record are similar, but not in phase, arguably also due to age uncertainties as discussed above for the SST record.

The close agreement between GDGT-based annual MAT estimates with summer temperatures could be partly explained by site-specific dynamics which are not accounted for in the global soil correlation (Weijers et al., 2007b) used to calculate MAT. In fact, Sinninghe Damsté et al. (2008) reconstructed higher MAT values than those based on in situ measurements, suggesting that local calibrations may result in more accurate MAT reconstructions. On the other hand, from 0.9 kyr until present the sedimentation in the Skagerrak has been dominated by southern North Sea and Atlantic Ocean sources (Gyllencreutz and Kissel, 2006). Herfort et al. (2006b) detected branched GDGTs in suspended particulate organic matter in surface seawater from the southern North Sea. Therefore the branched GDGTs found in our core for the last 200 years might have partly originated in the southern North Sea and transported and deposited into the Skagerrak. Arguably this could contribute to explaining the higher annual MAT estimates in comparison to the regional instrumental air temperature record in our site. An alternative or complementary explanation could be that the hitherto unknown group of terrestrial bacteria synthesizing branched GDGTs is more active during summer than the rest of the year, as Scandinavian soils are snow covered during several months.

3.5. Conclusions

Using GDGT-based proxies we have reconstructed sea surface and air temperatures in the Skagerrak region during the last 200 years at a decadal resolution from a single sediment core. The temperature estimates closely resemble regional instrumental temperature records, from annual SST for TEX_{86} and summer air

temperatures for MAT, providing further support for the use of GDGT proxies in marine and continental paleoreconstruction studies.

3.6 References

Global Runoff Data Centre (GRDC) (http://grdc.bafg.de)

Gyllencreutz R (2005) Holocene and Latest Glacial Paleoceanography in the North-Eastern Skagerrak. Thesis for the degree of Doctor of Philosophy in General and Historical Geology, Department of Geology and Geochemistry, Stockholm University, Stockholm (Sweden).

Gyllencreutz R, Jakobsson M and Backman J (2005). Holocene sedimentation in the Skagerrak interpreted from chirp sonar and core data. Journal of Quaternary Science 20, 21-32.

Gyllencreutz R and Kissel C (2006) Lateglacial and Holocene sediment sources and transport patterns in the Skagerrak interpreted from high-resolution magnetic properties and grain size data. Quaternary Science Reviews 25, 1247-1263.

Herfort L, Schouten S, Boon JP and Sinninghe Damsté JS (2006a) Application of the TEX_{86} temperature proxy to the southern North Sea. Organic Geochemistry 37, 1715-1726.

Herfort L, Schouten S, Boon JP, Woltering M, Baas M, Weijers JWH, and Sinninghe Damsté JS (2006b) Characterization of transport and deposition of terrestrial organic matter in the southern North Sea using the BIT index. Limnology and oceanography 51, 2196-2205.

Hopmans EC, Weijers JWH, Schefuss E, Herfort L, Sinninghe Damsté JS and Schouten S (2004) A novel proxy for terrestrial organic matter in sediments based on branched and isoprenoid tetraether lipids. Earth and Planetary Science Letters 224, 107-116.

Huguet C, Smittenberg RH, Boer W, Damsté JSS and Schouten S (2007) Twentieth century proxy records of temperature and soil organic matter input in the Drammensfjord, southern Norway. Organic geochemistry 38, 1838-1849.

International Comprehensive Ocean-Atmosphere Data Set (ICOADS) (http://icoads.noaa.gov/).

Kim J, Schouten S, Hopmans EC, Donner B and Sinninghe Damsté JS (2008) Global sediment core-top calibration of the TEX_{86} paleothermometer in the ocean. Geochimica et Cosmochimica Acta 72, 1154-1173.

Kornilova O and Rosell-Melé A (2003) Application of microwave-assisted extraction to the analysis of biomarker climate proxies in marine sediments. Organic Geochemistry 34, 1517-1523.

Ménot G, Bard E, Rostek F, Weijers JWH, Hopmans EC, Schouten S and Sinninghe Damsté JS (2006) Early reactivation of European rivers during the last deglaciation. Science 313, 1623-1625.

Moen SH and Hansen JE (2008) Rimfrost (www.rimfrost.no).

Schlitzer R (2008) Ocean Data View, http://odv.awi.de

Schouten S, Hopmans EC, Pancost RD, Sinninghe Damsté JS (2000) Widespread occurrence of structurally diverse tetraether membrane lipids: evidence for the ubiquitous presence of low-temperature relatives of hyperthermophiles. Proceedings of the Natural Academy of Sciences 97 (26), 14421– 14426.

Schouten S, Hopmans EC, Schefuss E, Sinninghe Damsté JS (2002) Distributional variations in marine crenarchaeotal membrane lipids: a new tool for reconstructing ancient sea water temperatures? Earth and Planetary Science Letters 204, 265-274.

Senneset L (2002) A record of high resolution ocean variability from Skagerrak over the past 900 years. Master thesis, University of Bergen (Bergen).

Sinninghe Damsté JS, Ossebaar J, Schouten S, Verschuren D (2008) Altitudinal shifts in the branched tetraether lipid distribution in soil from Mt. Kilimanjaro (Tanzania): Implications for the MBT/CBT continental palaeothermometer. Organic geochemistry, 2008.

van Dongen BE, Rijpstra WIC, Philippart JM, de Leeuw JW and Sinninghe Damsté, JS (2000) Biomarkers in upper Holocene Eastern North Sea and Wadden Sea sediments. Organic Geochemistry 31, 1533-1543.

Weijers JWH, Schefuss E, Schouten S, Damsté JSS (2007a) Coupled thermal and hydrological evolution of tropical Africa over the last deglaciation. Science 315, 1701.

Weijers JWH, Schouten S, Hopmans EC, Geenevasen JAJ, David ORP, Coleman JM, Pancost RD and Sinninghe Damsté JS (2006a) Membrane lipids of mesophilic anaerobic bacteria thriving in peats have typical archaeal traits. Environmental Microbiology 8, 648-657.

Weijers JWH, Schouten S, Spaargaren OC and Sinninghe Damsté JS (2006b) Occurrence and distribution of tetraether membrane lipids in soils: Implications for the use of the TEX_{86} proxy and the BIT index. Organic geochemistry 37, 1680-1693.

Weijers JWH, Schouten S, van den Donker JC, Hopmans EC, Sinninghe Damsté JS (2007b) Environmental controls on bacterial tetraether membrane lipid distribution in soils. Geochimica et cosmochimica acta 71, 703-713.

Wuchter C, Schouten S, Coolen MJL, Sinninghe Damste JS (2004) Temperature–dependent variation in the distribution of tetraether membrane lipids of marine Crenarchaeota: Implications for TEX_{86} paleothermometry. Paleoceanography 19, PA4028.

Wuchter C, Schouten S, Wakeham SG Sinninghe Damsté JS (2005) Temporal and spatial variation in tetraether membrane lipids of marine Crenarchaeota in particulate organic matter: Implications for TEX86 paleothermometry. Paleoceanography 20, PA3013.

Wuchter C, Schouten S, Wakeham SG and Sinninghe Damsté JS (2006) Archaeal tetraether membrane lipid fluxes in the northeastern Pacific and the Arabian Sea: Implications for TEX_{86} paleothermometry. Paleoceanography 21, PA4208.

CHAPTER 4

Exploring seasonal variability in MBT′/CBT air temperature estimates

4.1. Abstract

The MBT'/CBT index has been recently proposed as a proxy for reconstructing past mean annual air temperatures (MAT). It is based on the relative distribution of branched glycerol dialkyl glycerol tetraethers (brGDGTs). A previous study in the Skagerrak suggested a possible seasonal bias of the proxy towards summer temperatures, and that the brGDGTs may reach the marine environment with the highest discharge period of the Glomma River. With the aim to assess these issues we sampled soils from Øsaker (Norway) and Ulldeter (Pyrenees) monthly for one year. In addition, we collected monthly samples of suspended matter from the Glomma River for one year, and from a stream of water in Ulldeter during spring and summer. We analyzed core brGDGT (C-brGDGT) and intact brGDGT (I-brGDGT) distributions in all samples, and calculated past MAT estimates based on both core (C-MAT_{est}) and intact brGDGTs (I-MAT_{est}). C-MAT_{est} and I-MAT_{est} in soil samples from both locations did not display any seasonal variability. Similarly, C-MAT_{est} for the recently eroded soil particulate matter in Ulldeter and for the suspended matter transported with the Glomma River were close to MAT. However, I-MAT_{est} in these recently eroded soil particulates showed some changes in spring and summer in Ulldeter, and from October to December in the Glomma River. The transport of brGDGTs to the Skagerrak did not co-vary with the Glomma River discharge cycle. The C-MAT_{est} from deposited sediment in Ulldeter were close to MAT but in the Skagerrak the reconstructed values were closer to summer temperatures. In conclusion, a different source for brGDGTs in the Skagerrak or *in situ* production might explain the comparatively high C-MAT_{est} observed in recent sediments from the Skagerrak.

Keywords branched GDGTs; MBT/CBT; temperature; intact polar lipids; core lipids.

4.2. Introduction

The MBT/CBT index was recently proposed as a proxy to estimate past mean annual air temperatures (MAT) from marine and lacustrine sediments (Weijers et al., 2007a). It is based on the relative abundance of branched glycerol dialkyl glycerol tetraethers (brGDGTs) that are cell membrane lipids presumably synthesized by a group of bacteria (Weijers et al., 2009). The specific organisms that synthesize brGDGTs are still unknown, but based on brGDGT distributions they are hypothesised to be anoxic acidophiles (Peterse et al., 2010). As only one molecular structure of a brGDGT

(m/z 1022) was identified in two species of the phylum *Acidobacteria* (Sinninghe Damsté et al., 2011) the brGDGTs remain orphan lipids.

BrGDGTs have been found in soils and peat bogs worldwide (e.g. Sinninghe Damsté et al., 2000; Weijers et al., 2006). They have also been detected in marine sedimentary cores, and it has been assumed they were mainly transported by river runoff (Hopmans et al., 2004) and in lower amounts by winds (Fietz et al., 2011). After analysis of brGDGTs in 134 globally distributed soil samples, Weijers et al. (2007a) found that the relative amount of methyl branches of the brGDGTs (MBT) correlated with MAT ($R^2 = 0.62$) and with the pH of the soil ($R^2 = 0.37$). The relative amount of cyclopentyl moieties from brGDGTs (CBT) correlated with the pH of the soil ($R^2 = 0.70$) (Weijers et al., 2007a). The correlation between MAT and the MBT/CBT was defined as $MBT = 0.122 + 0.187 \cdot CBT + 0.020 \cdot MAT$ ($R^2 = 0.77$) and the calibration error is ~5 ^oC. Recently a new study expanded the calibration with the analysis of 278 globally distributed soils and modified the index to MBT'/CBT (Peterse et al., 2012). A new transfer function for calculating MAT was defined as $MAT = 0.81 - 5.67 \cdot CBT + 31.0 \cdot MBT'$ ($R^2 = 0.59$). The new equation has lower correlation coefficient than the original from Weijers et al (2007a), the calibration error is the same as in the original, but it gives absolute values that are usually closer to instrumental temperatures (Peterse et al., 2012).

The MBT/CBT proxies for reconstructing past temperatures are based on core brGDGTs (Figure 1.9; Chapter 1; p. 18). However, in living cells, the lipid bilayer that forms the cell membrane is composed of GDGTs that have polar head groups attached to the glycerol moieties. These are usually referred to as intact polar lipids (hereafter I-brGDGTs) (Figure 1.10; Chapter 1; p. 19). The polar head groups are enzimatically cleaved in a few days or weeks after the cell dies (Harvey et al., 1986; White et al., 1979). The remaining structures are referred to as core GDGTs (hereafter C-brGDGTs). Intact polar lipids are considered to be biomarkers for living biomass (Huguet et al., 2010; Lipp et al., 2008; Pitcher et al., 2009), but they may also be partly fossil (Schouten et al., 2010).

The MBT/CBT proxy has been used to reconstruct past changes in MAT at different temporal scales and in a wide range of geographical settings, such as the Congo deep sea fan (Weijers et al., 2007b), North America (Fawcett et al., 2011), East Greenland (Schouten et al., 2008), and the Arctic (Weijers et al., 2007c). However, a reconstruction of MAT (estimated with MBT/CBT) conducted in a marine sedimentary core from the Skagerrak Strait, off southern Norway and Sweden, yielded reconstructed temperature estimates (hereafter MAT_{est}) closer to regional summer temperatures than to MAT for the last 200 years (Rueda et al., 2009; Chapter 3). It was

suggested that the agreement with summer temperatures could be explained by three factors. First, the brGDGTs might be transported from the southern North Sea and thus reflect higher temperatures than expected MAT, given the lower latitude origin. Second, increased amounts of brGDGTs could be transported to the marine environment in the summer season when the highest river discharge of the Glomma River to the Skagerrak occurs. Alternatively, the organisms synthesizing brGDGTs could be more active during summer months, as Scandinavian soils are snow covered and frozen for several months of the year (Rueda et al., 2009).

We recalculated the MAT_{est} with the new calibration from Peterse et al. (2012) to test if the discrepancy between regional MAT in southern Norway and MAT_{est} was due to calibration constraints. The recalculated MAT_{est} gave lower absolute temperature values (ca. 3 ^{o}C in average) but these values are still closer to summer temperatures than to MAT. An additional possibility is that part of the brGDGTs in the marine Skagerrak is produced *in situ*. It has been recently suggested that brGDGTs could be produced *in situ* in some marine environments (Fietz et al., 2012; Peterse et al., 2009; Zhu et al., 2011). However, this has not been empirically demonstrated to date.

This chapter seeks to address two of the questions raised in the Rueda et al. (2009) study on the seasonality of the brGDGTs abundances (Chapter 3): (I) Are the organisms synthesizing brGDGTs more active during summer months in sites where soil is frozen during most of the year? (II) Does the transport of brGDGTs with the Glomma River increase coinciding with the highest river discharge in summer? In addition, we studied if the brGDGTs MAT_{est} signal is preserved from the erosion and transport of the sediment to its deposition

To achieve these goals we sampled soils monthly during a year in Øsaker (Norway) and Ulldeter (the Pyrenees), two sites with similar climatic conditions but different locations and latitudes (separated by 17 latitudinal degrees; Figure 4.1). We also collected water from the Glomma River each month during an annual cycle at a site close to the river mouth into the Skagerrak, southern Norway. In the Ulldeter area, we deployed sediment traps to catch the soil suspended particulate matter eroded and transported with water in a stream and also the sediment deposited in the river bed. We analyzed both C-brGDGTs and I-brGDGTs to examine if there were differences in MAT_{est} or brGDGT concentration between both fossil and presumably living lipid pools.

4.3. Study area and sampling description

The two sites selected (Figure 4.1) display a large seasonal amplitude of temperatures and a similar mean annual precipitation. The temperature and precipitation data from Øsaker (Bioforsk AgroMetBase, 2011) and Ulldeter (Servei Meteorològic de Catalunya, 2011) during the studied periods are shown in Figure 4.2.

Øsaker is a research farm located in the municipality of Sarpsborg in southern Norway (meteorological station at 59°19'09" N, 11°02'33"E, 45 m a.s.l.). It is situated 300 m from Lake Vestvannet which drains into the Glomma River. The MAT in Øsaker during the sample year (December 2010 – November 2011) was 6 ºC (Figure 4.2A). The temperature difference between the warmest month (July; 17.1 ºC) and the coldest month (December; -10.9 ºC) was 28 ºC. The soil temperature at 10 cm depth shows a similar variability to air temperature in Øsaker, but the soil average annual temperature is 7.7 ºC (1.7 ºC higher than air temperature). In the soil, the difference between the warmest month (July; 18.2 ºC) and the coldest month (December; -0.4 ºC) was 18.6 ºC. Total annual precipitation was 1033 mm, with maximum accumulation in September (236 mm) and minimum in December (20 mm).

Each month soils were sampled in a forested area 70 m away from the meteorological station (59°19'11.31" N, 11°02'32.10"E, 47 m a.s.l.). The first 5 cm corresponding to the soil horizon O were removed using a pick and a shovel. The first 2 cm of soil horizon A were sampled from a 100 cm^2 surface. Samples were stored in plastic bags and frozen at – 20 ºC until analysis. Water samples were collected from the Glomma River at Sandesund (Sarpsborg; 59º16'16.16'' N, 11º05'36.73'' E, 2.5 m asl) each month from February 2011 until January 2012. The site is located 8 km downstream from the meteorological station and 25 km upstream from the Glomma River mouth to the Skagerrak. Every month 10 L of water were collected from the river. Water samples were sequentially filtered through Millipore glass fibre filters of 2.7 μm and 0.7 μm pore diameter (47 mm filter diameter). Only the 0.7 μm filters were used for GDGT analysis.

Ulldeter is a glacial cirque in the Catalan Eastern Pyrenees (meteorological station at 42º25'19.37''N, 2º15'08.53''E, 2364 m asl). During the study period (June 2010 – May 2011) MAT in Ulldeter was 3.3 ºC and the temperature difference between the warmest month (July; 12.7 ºC) and the coldest month (January; -2.8 ºC) was 15.5 ºC (Figure 4.2B). Soil temperature is not available at the Ulldeter meteorological station. The total annual precipitation was 1264 mm. The months with maximum and minimum rainfall accumulation were October (228 mm) and February (44 mm).

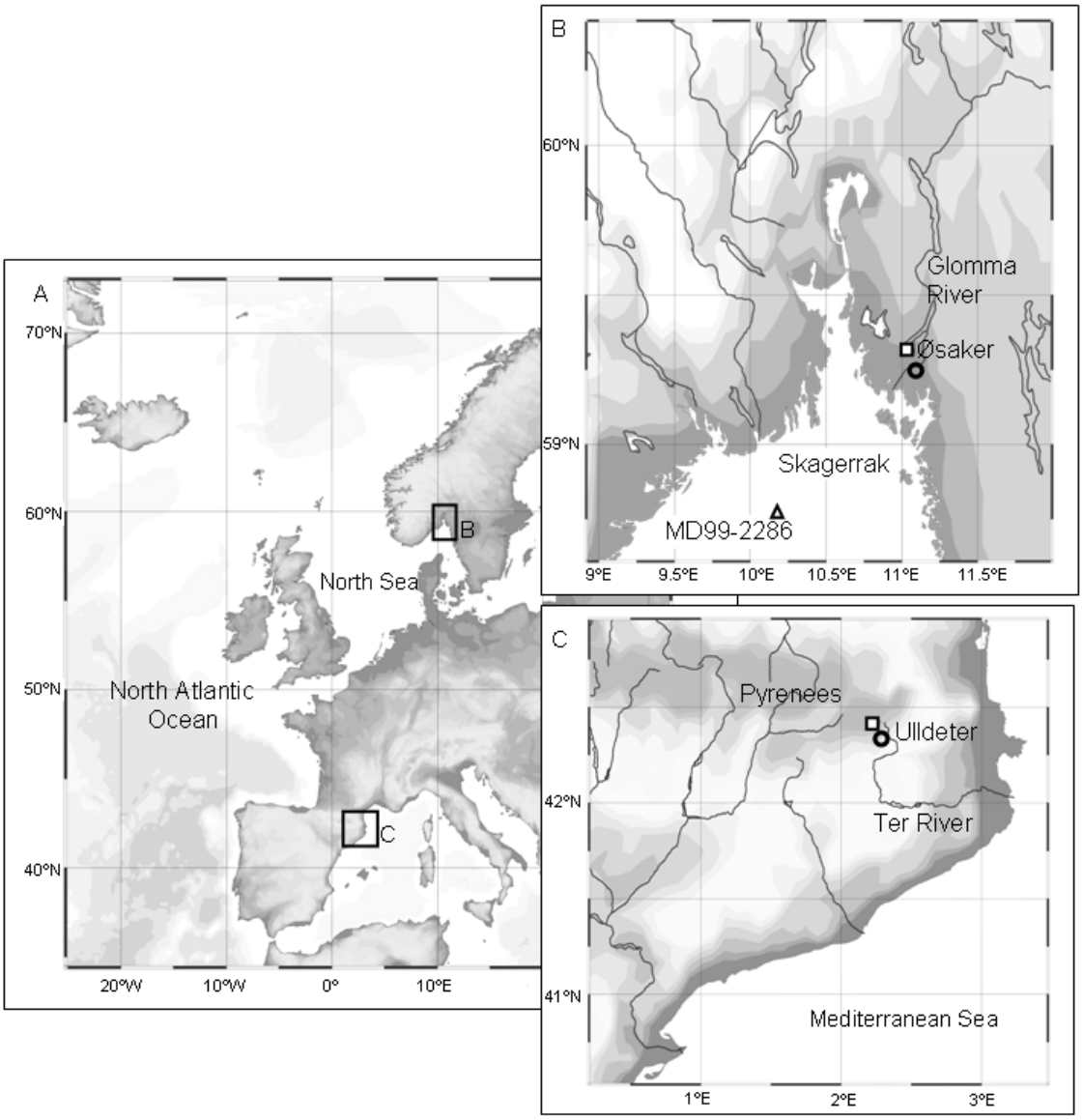

Figure 4.1. (A) General location of the two studied sites. (B) Øsaker, southern Norway. (C) Ulldeter, Catalan Eastern Pyrenees. The black square indicates the location of the meteorological stations and the soil sampling sites. The sites where river water was collected and where sediment traps were deployed are shown with a circle. The location of core MD99-2286 (Rueda et al., 2009) is shown with a triangle in B. Map base from Ocean Data View (Schlitzer, 2010).

Samples were collected in a flat terrain 100 m northwards from the meteorological station (42º25'21.73''N, 2º15'04.60''E, 2392 m asl) each month from June 2010 to May 2011. Using a pick and a shovel the first 3 cm corresponding to soil horizon O were removed. Afterwards, 2 cm of soil horizon A were sampled from a surface of 100 cm^2. Samples were stored in plastic bags and frozen at – 20 ºC until analysis. The source of Ter River is close to the sampling site. In spring and summer 2011, two sediment traps were installed in streams in the Ulldeter area. The aim was to

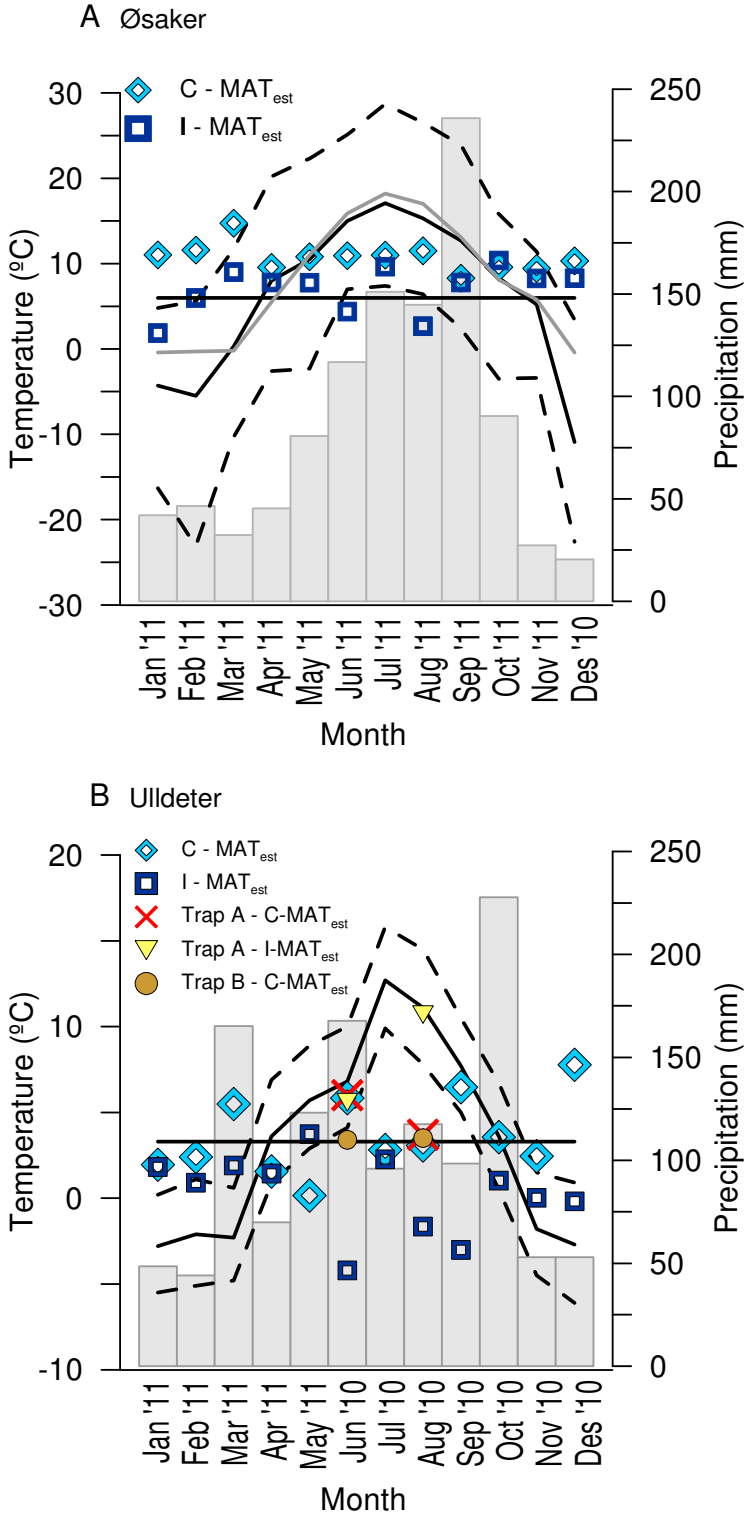

Figure 4.2. Meteorological data and GDGT based temperature estimates for Øsaker (A) and Ulldeter (B) (Bioforsk AgroMetBase, 2011; Servei Meteorològic de Catalunya, 2011). Instrumental temperature is given as an average for the study period (black continuous line) and averaged maximum and minimum values (black discontinuous lines). The instrumental annual mean is indicated with a horizontal black line. Monthly precipitation is shown with grey bars. The results for the GDGT based estimates (MBT′/CBT) based on core GDGTs (C-MAT_{est}, pale blue diamond) and intact GDGTs (I-MAT_{est}, dark blue square) are shown for the monthly sampled soils. The results for the river stream sediment trap (trap A) are shown with inverted yellow triangles (I-MAT_{est}) and a red cross (C-MAT_{est}). C-MAT_{est} for the sediment trap located at the river bed is marked with golden circles.

catch the sediments eroded, transported and afterwards deposited in the Ter River to analyze the brGDGTs distribution in the transported and eventually deposited material. One sediment trap was installed in a mountain slope where a small stream of water drained down to feed the Ter River (Trap A, 42º25'14.92''N, 2º15'10.76''E, 2300 m asl). The other sediment trap was deployed in a small meander in Ter River (Trap B, 42º25'15.68''N, 2º15'13.97''E, 2274 m asl). Samples were stored frozen at -20 ºC until analysis.

4.4. Results and discussion

4.4.1 Abundance of core and intact brGDGTs

4.4.1.1 Soils

The average soil organic carbon composition is higher in Øsaker (85% LOI) than in Ulldeter (35% LOI). The average pH of the collected soil samples was lower in Øsaker (pH = 4) than in Ulldeter (pH = 5.5). The abundance of brGDGTs in soils was normalized per gram organic carbon to reduce the effect of the possible variability in organic biomass productivity between samples (Figure 4.3). The average concentration of C-brGDGTs in Øsaker is 27 μg g_{TOC}^{-1} and in Ulldeter is 11 μg g_{TOC}^{-1}. Average concentrations of I-brGDGTs are lower than those of C-brGDGTs at both sites, but they are also higher in Øsaker (20 μg g_{TOC}^{-1}) than in Ulldeter (5 μg g_{TOC}^{-1}).

The pH difference between the soils from Øsaker and Ulldeter is probably one factor accounting for the difference in average abundances found at the two study sites as brGDGTs are usually found in higher amounts in acidic soils than in basic soils (Weijers et al., 2007c, Peterse et al., 2010). In addition, Øsaker soils contain higher abundances of organic matter than Ulldeter soils and probably more nutrients would be available in these soils for the growth of bacteria synthesizing brGDGTs, which have been suggested to be heterotrophic (Weijers et al., 2010). Indeed high abundances of brGDGTs are usually found in peat bogs where high amounts of organic carbon are present (Weijers et al., 2006).

The concentration of both core and intact brGDGTs is more variable in Øsaker than in Ulldeter. In Øsaker the concentration ranges between 3 and 73 μg g_{TOC}^{-1} for C-brGDGTs and from 0.6 to 56 μg g_{TOC}^{-1} for I-brGDGTs. Here the variability in C- and I-brGDGTs is coupled with the exception of February, October and November. In Ulldeter the abundance of C-brGDGTs ranges between 2 and 20 μg g_{TOC}^{-1} while the concentration of I-brGDGTs is much lower. From January to November it ranges from 0.2 and 10 μg g_{TOC}^{-1} and in December it increases sharply to 24 μg g_{TOC}^{-1}(Figure 4.3). In

Ulldeter the variability of I-brGDGTs and C-brGDGTs is not coupled as it occurs in Øsaker.

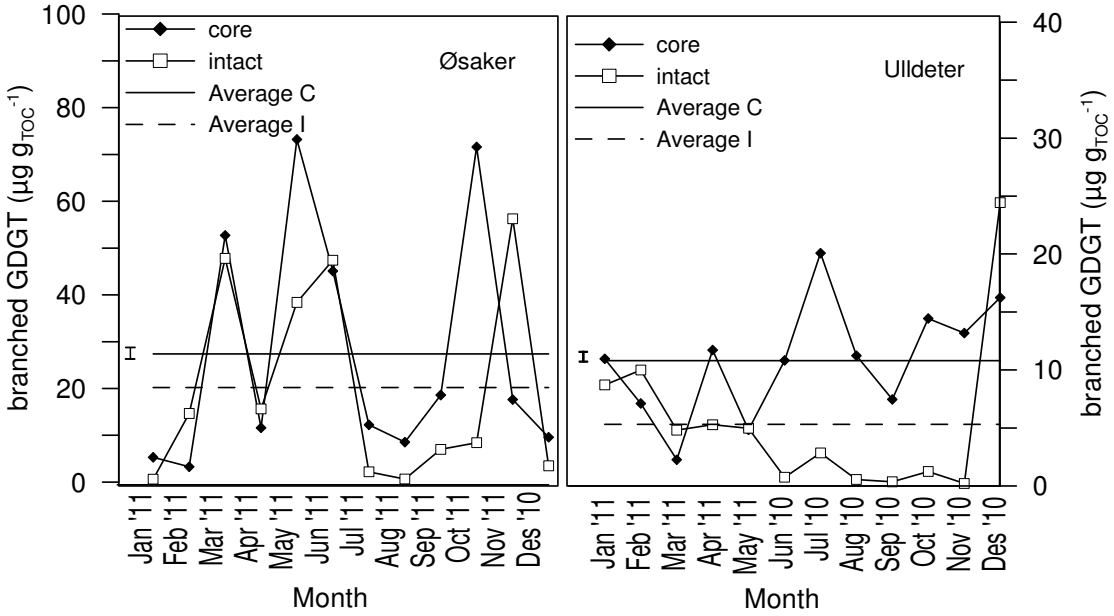

Figure 4.3. Concentration of core and intact brGDGTs (µg g_{TOC}^{-1}) in soil samples from Øsaker (left) and Ulldeter (right). Single concentrations of core brGDGTs (black diamond), intact brGDGTs (white square), average concentrations of core brGDGTs in all the samples (continuous horizontal line) and average concentration of intact brGDGTs (discontinuous horizontal line) are shown. The floating error bar at the left side of the y-axis shows the reproducibility of the measurement.

The intra-annual variability in C-brGDGTs concentration is not likely affected by environmental parameters if we take into account that C-brGDGTs are likely reflecting the fossil lipid pool, which might have a turnover time of 18 years (Weijers et al., 2010). Instead C-brGDGT variability is most likely driven by the spatial heterogeneity of soils (Weijers et al., 2011). The I-brGDGTs are hypothesised to reflect the living biomass Therefore the variability in I-brGDGTs abundance between samples could be due to various environmental parameters affecting the lipid production in living cells. However, the abundance of both C- and I-brGDGTs is not linearly related to temperature, precipitation, humidity, evapotranspiration or aridity index through the year (Figure 4.4). It is likely that both of the C- and I-brGDGT lipid pools are the result of brGDGT accumulation over time (Weijers et al., 2011). Therefore the soil samples taken each month during one year might likely be replicates of the same bacterial community adapted to mean annual environmental conditions at the site where they where collected. As the samples were taken each month from the same area but not

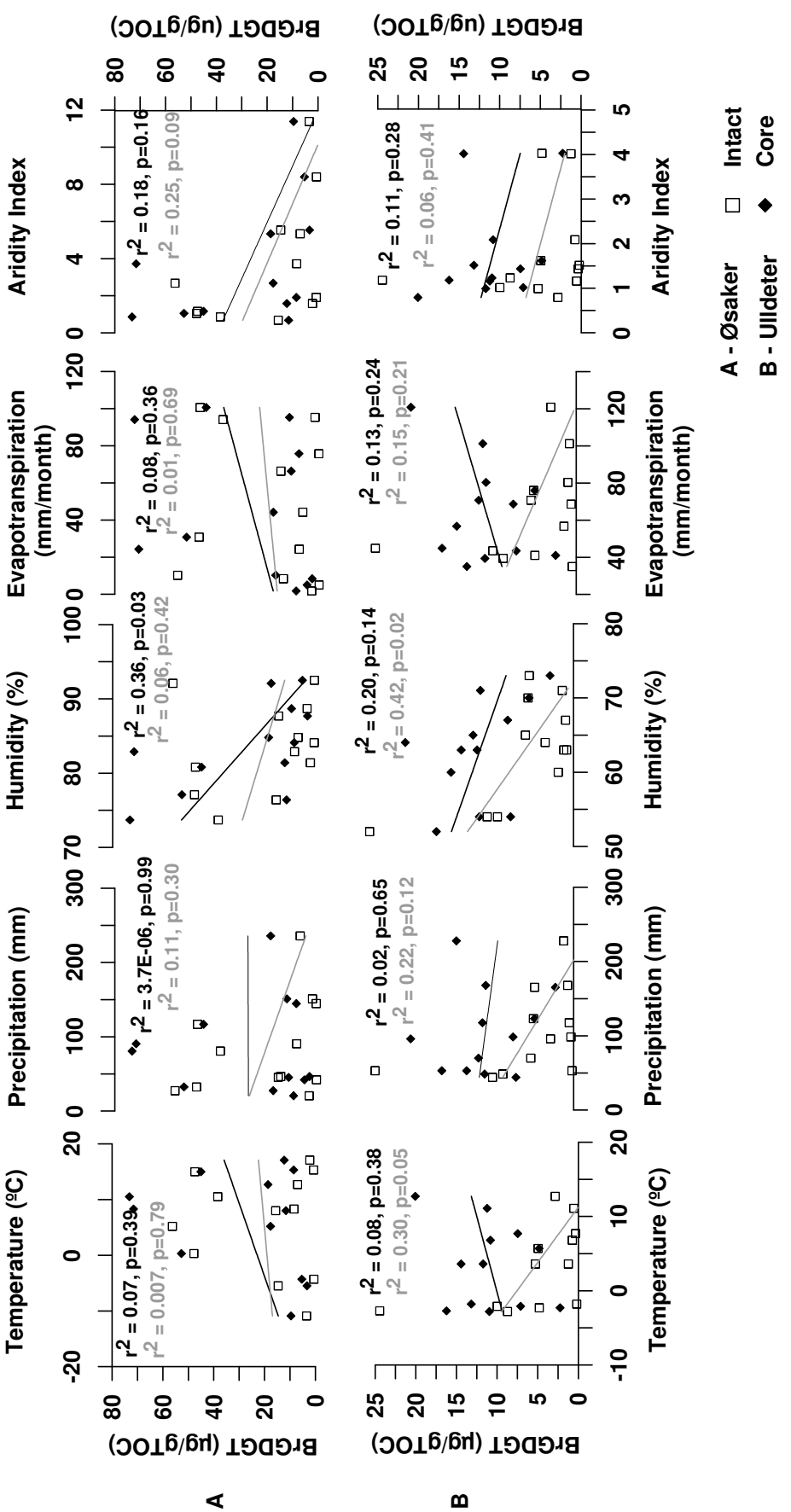

Figure 4.4. Concentration of intact (white square) and core (black diamond) branched GDGTs (µg g_{TOC}^{-1}) in Ørsaker (A) and in Ulldeter (B) plotted against environmental parameters (temperature, precipitation, humidity, evapotranspiration and the aridity index). Linear correlations between concentration of brGDGTs and environmental parameters are shown for core brGDGTs (black line) and intact brGDGTs (grey line) and the correspondent regression coefficient (r^2) and p values.

from the same exact site, the spatial heterogeneity of soils is also reflected in the brGDGTs measurements.

On the other hand, a combination of multiple parameters such as temperature, pH, ionic strength and community composition could together control the GDGT lipid composition (Boyd et al., 2011). If multiple factors were to control the abundance of I-brGDGTs and C-brGDGTs in soils, we might not have all the necessary information to find an accurate relationship between the combination of environmental parameters and the lipid distribution. This becomes specially challenging since we still do not know which exact species synthesize brGDGT. Microbial communities are highly diverse and they might respond differently to the same environmental factors. Further research is needed to understand the response of (Acido)bacteria to change in various environmental factors and to explore the behaviour of the different populations at the subgroup level in terrestrial environments (Naether et al., 2012; Rasche et al., 2011).

4.4.1.2 Transport of brGDGTs

Glomma River

The mean river discharge for the Glomma River at Solbergfoss (50 km north from Sandesund, where the samples were collected) for the period 1901 – 2007 as well as the maximum and minimum monthly discharges for this period are shown in Figure 4.5 (Global Runoff Data Centre, 2011). The highest river discharge occurs during May, June and July. In Chapter 3 we hypothesized that the highest flux of GDGTs to the Skagerrak study site might occur during summer, when the highest river discharge occurs (Rueda et al., 2009). To test this hypothesis, soil particulate matter was analyzed in water that was collected from the Glomma River at Sandesund each month during one year.

The water samples contained both C- and I-brGDGTs (Figure 4.5) during the study period and showed average abundances of 16.1 ng L^{-1} for C- brGDGTs and 5.2 ng L^{-1} for I – brGDGTs. Maximum and minimum values of C-brGDGTs were found in April (54.3 ng L^{-1}) and in February (1.5 ng L^{-1}). Abundances of I-brGDGTs were low in 9 out of the 12 samples, ranging between 0.2 – 3.0 ng L^{-1}. The highest I-brGDGTs concentrations were found in March, June and December (9.3 – 22.9 ng L^{-1}; Figure 4.5). The concentrations of both C- and I-brGDGTs are decoupled from the Glomma River discharge cycle. For example, the concentration of C-brGDGTs is not higher during summer when the highest river discharge occurs and the peak in C-brGDGTs concentration is in April, one month before the beginning of the increased discharge

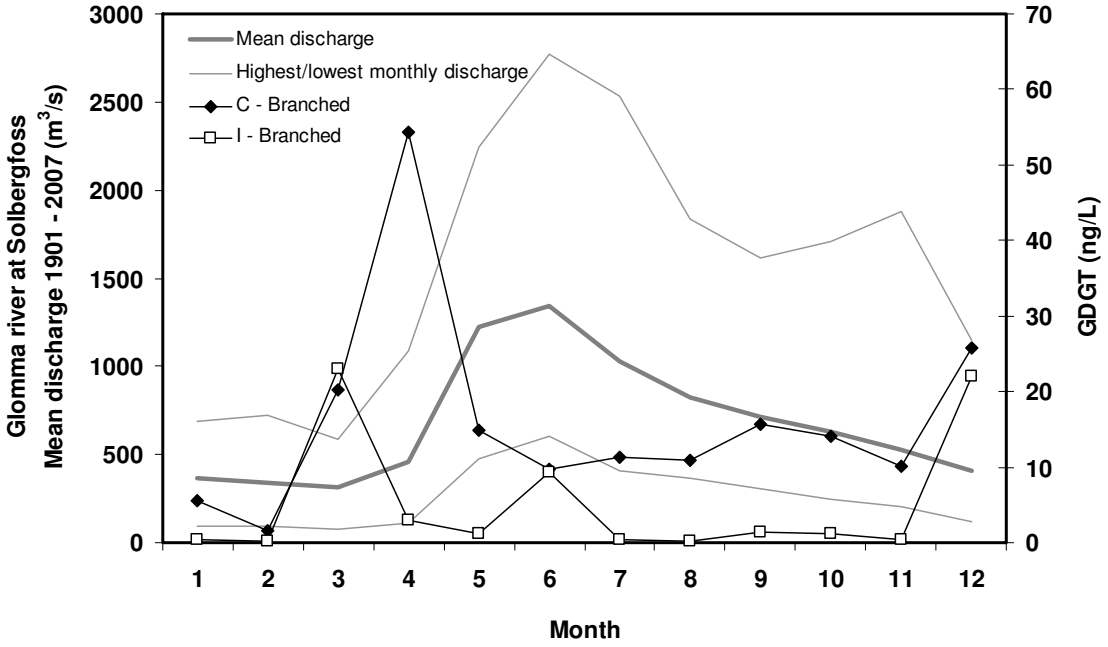

Figure 4.5. Concentration of brGDGTs (ng L^{-1}) in water samples from the Glomma River. Concentration of core brGDGTs (black diamonds) and intact brGDGTs (white squares) are compared to mean discharge (m^3 s^{-1}, thick grey line) of Glomma River at Solbergfoss for the period 1901-2007 (Global Runoff Data Centre, 2011). The highest and the lowest monthly discharges for the entire data period are shown with thin grey lines.

period. The highest abundance of I-brGDGTs occurs in March, thus also decoupled from the discharge cycle. During the rest of the year, concentrations of C-brGDGTs and I-brGDGTs are close to the average values. Therefore brGDGTs are not preferentially transported to the Skagerrak during summer.

Ulldeter

In Ulldeter the abundances of C-brGDGTs were also higher than those of I-brGDGTs for the two seasons studied and generally higher in spring than in summer. The accumulated abundance of C-brGDGTs in spring (0.60 μg g^{-1}) was higher than in summer (0.26 μg g^{-1}) and the accumulated amount of I-brGDGTs was also higher in spring (0.34 μg g^{-1}) than in summer (0.15 μg g^{-1}). The sediment traps collected the material eroded mainly by run-off after precipitation. As the accumulated precipitation in Ulldeter was higher in spring (361 mm) than in summer (312 mm), the difference in concentration of brGDGTs between the two seasons could be due to an increased amount of soil particulate matter transported during spring rather than during summer seasons. Another factor to consider is that the differences in concentration could be among the range of natural variability for these kinds of samples. However

this can not be contrasted because at this point there are no other published studies that have followed the same approach.

4.4.2 MBT'/CBT estimates

4.4.2.1 Soils

The MAT_{est} (using the MBT'/CBT) calculated with C-brGDGTs (hereafter C-MAT_{est}) do not follow temperature seasonality in Øsaker or Ulldeter (Figure 4.2). In Øsaker the C-MAT_{est} for the whole study period ranges between 8.3 and 14.7 ^{o}C with no clear variability trend (Figure 4.2A). The average C-MAT_{est} is 10.7 ^{o}C which is 4.7 ^{o}C above the instrumental measurements of MAT in Øsaker and 3 ^{o}C above average soil temperature measurements. In Ulldeter, the C-MAT_{est} range between 0.1 and 7.8 ^{o}C with no clear trend of variability. The average C-MAT_{est} for the 12 samples is 3.6 ^{o}C which is only 0.3 ^{o}C above instrumental MAT (Figure 4.2B). In both study sites C-MAT_{est} values do not show a clear trend of variability but rather oscillate around the MAT. The absolute average C-MAT_{est} only differ 0.3 ^{o}C from annual MAT in Ulldeter whereas in Øsaker they differ in 4.9 ^{o}C from MAT and 3 ^{o}C from soil temperatures.

Similarly, the MAT_{est} (using the MBT'/CBT) calculated with I-brGDGTs (hereafter I-MAT_{est}) does not follow the annual temperature variability in either of the two sites (Figure 4.2). Regarding the absolute values, in Øsaker I-MAT_{est} range between 1.9 and 10.4 ^{o}C and has an average of 7.0 ^{o}C, which is 1.0 ^{o}C warmer than instrumental MAT and only 0.7 ^{o}C warmer than average soil temperatures (Figure 4.2A). In Ulldeter I-MAT_{est} average is 0.3 ^{o}C which is 3 ^{o}C lower than MAT (Figure 4.2B). The I-MAT_{est} did not follow the seasonal temperature variability at either of the two sites. The absolute temperature average I-MAT_{est} was very close to MAT and soil temperature in Øsaker while in Ulldeter they differed in 3 ^{o}C. The opposite was observed for C-MAT values which were closer to MAT in Ulldeter rather than in Øsaker.

The findings of the current study are similar to those observed in soils from the United States of America, the Netherlands and the United Kingdom (Weijers et al., 2011). They did not find a clear change in the distribution of C- or I-brGDGT lipids with seasonal temperature change. The authors also found similar MAT_{est} year round and their absolute values were similar to MAT (Weijers et al., 2011). They related this finding to the turnover time of the brGDGTs in soils which is estimated to be of 18 years for C-brGDGTs in arable soils (Weijers et al., 2010) and longer than one year for I-brGDGTs (Weijers et al, 2011). Moreover they suggested that the standing stock of brGDGTs already existing in the soil matrix might be larger than the newly produced

during a seasonal cycle (Weijers et al., 2011).We agree with the factors pointed by Weijers et al. (2011), but these may not be the only causes for the lack of seasonal variability in C- and I-MAT_{est}.

As the turnover time of GDGTs has been suggested to be 18 years (Weijers et al., 2010), the C-MAT_{est} in monthly sampled soils will combine temperature signals for at least this entire period. This could theoretically be circumvented by using I-brGDGTs, however, intact polar lipids may also be partly fossil, thus masking real living biomass production (Schouten et al., 2010). Thus, I-MAT_{est} is representative of an average temperature that corresponds to several years of production and accumulation of I-brGDGTs.

Another possible reason for the lack of seasonal trends in C-MAT and I-MAT parameters could be found in the biological behaviour of the still unknown presumed bacterial organisms synthesize brGDGTs. For instance, bacteria can adapt to changes in environmental conditions such as temperature, soil moisture, available carbon and nitrogen via a change in the microbial community (Cruz-Martínez et al., 2012). In fact, distinct microbial populations are found in a single soil depending on its temperature. For instance, a specific microbial community with a lipid pool adapted to low temperatures was found in a soil that was perennially frozen, whereas in the soil horizon characterized with less extreme temperatures another microbial community was described, adapted to variable temperatures (Mangelsdorf et al., 2009). Additionally, it has been found that in cold regions soil microorganisms adapt to extreme seasonal environmental change between winter and spring adapting the microbial biomass and the community composition (Wu et al., 2011). Alternatively, the organisms synthesising brGDGT could have a strong and rapid response to soil temperature change by changing their respiration as it has been seen before for microbial populations (Hartley et al., 2008). If the organisms that synhesize brGDGTs behaved in a similar way, as the above mentioned microbes, it could be the case that they would not need to change the relative distribution of lipids in their cell membrane to adapt to short term (seasonal) temperature changes.

4.4.2.2 Transport

Ulldeter

We analyzed recently eroded soil particulate matter to compare their brGDGT distributions with those from their source soils. For the sediment traps deployed in Ulldeter the C-MAT_{est} was 6.0 ^{o}C in spring and 3.7 ^{o}C in summer (Trap A, Figure 4.2B).

These values are closer to MAT (3.3 ºC) than to spring (2.3 ºC) or summer (10.2 ºC) temperatures. Interestingly, the I-MAT_{est} values show seasonal variability at the same trap in Ulldeter (Trap A, Figure 4.2B). Spring I-MAT_{est} is 5.6 ºC and increases to 10.6 ºC in summer. The spring I-MAT_{est} value is between annual and spring temperatures. It is 2.3 ºC higher than annual (3.3 ºC) and 3.3 ºC higher than spring (2.3 ºC) temperatures respectively. The summer sample I-MAT_{est} is only 0.4 ºC above the instrumental temperature for summer in Ulldeter (10.2 ºC). Even though we only have two samples accounting for the two seasons, we observe a temperature change in the distribution of I-brGDGTs in the recently eroded and transported sediment in Ulldeter. A possible explanation is that the recently eroded sediment might be fresher than the analysed soil samples, containing recent I-brGDGTs and has a negligible contribution of fossil I-GDGTs. Future studies with a more exhaustive sampling would be needed to test this.

Glomma River

In contrast, at the Glomma River site the average C-MAT_{est} is 5 ºC and only differs in 1 ºC with the instrumental MAT in Øsaker which is 6 ºC (Figure 4.6). The C-MAT_{est} values are generally close to MAT which fits in with the soil results from the area except in the December sample where it increases up to 14.4 ºC (Figure 4.6). I-brGDGTs were very low in some samples and some lipids were below detection limit. The average I-MAT_{est} is 5.3 ºC and has a wide range of variability between samples. They did not generally follow seasonal changes in temperature with the exception of October, November and December when I-MAT_{est} decreased together with MAT at Øsaker (Figure 4.6).

While in Ulldeter the area where the analyzed soil suspended particulate matter was eroded is well delimited, the origin of brGDGTs from the Glomma River samples is not so well constrained. This might explain the differences observed between the two data sets.

4.4.2.3 Deposition

Ulldeter

The C-MAT_{est} for the sediments deposited in Ter River during spring and summer seasons are 3.4 ºC and 3.5 ºC respectively (Trap B, Figure 4.2B), thus they are closer to Ulldeter MAT (3.3 ºC) than to specific seasons. In fact C-MAT_{est} values in Ulldeter do not show seasonality in either soil origin or transport or deposition. I-

brGDGTs were under limit of quantification in Ter River samples, thus I-MAT$_{est}$ could not be calculated.

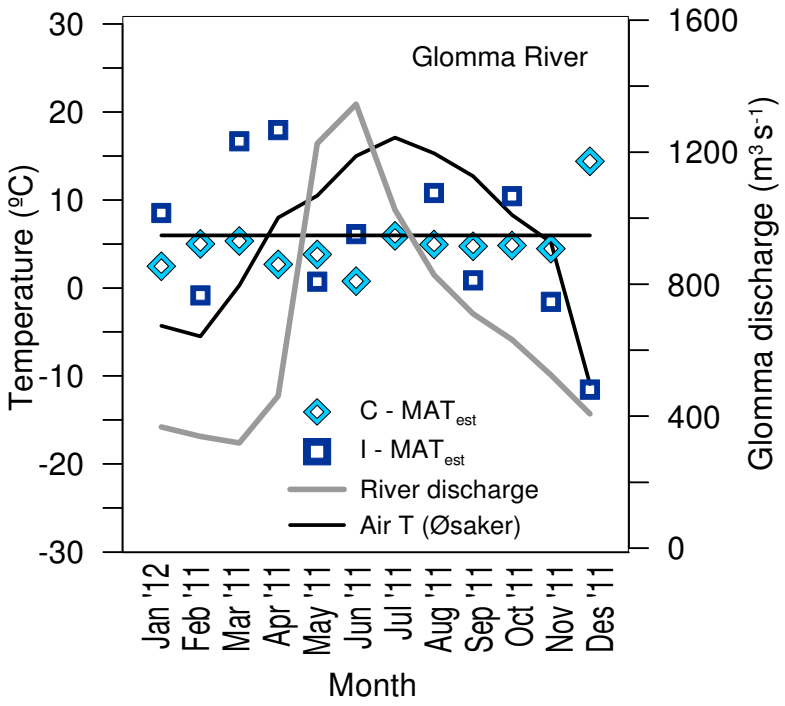

Figure 4.6. Glomma River water samples C-MAT$_{est}$ (light blue diamond) and I-MAT$_{est}$ (dark blue square) estimates plotted with Glomma River discharge (grey), Øsaker monthly air temperature (black curve) and annual mean (black horizontal line).

The Skagerrak

The surface sediment from the north-eastern Skagerrak core studied in chapter 3 showed values closer to summer temperatures (Rueda et al., 2009). The surface sediment from core MD99-2286 has a C-MAT$_{est}$ value of 16 ºC calculated with the calibration from Weijers et al. (2007a) or 13 ºC when calculated with the calibration from Peterse et al. (2012). For comparison with the data generated here, we use the C-MAT$_{est}$ obtained with the calibration from Peterse et al. (2012). MAT at Øsaker are 6 ºC and in the integrated area from seven meteorological stations in the Skagerrak zone is 8 ºC (Rueda et al., 2009).

The average C-MAT$_{est}$ in the Glomma River (5 ºC) are close to annual means in Øsaker (6 ºC). But the sediment deposited in the Skagerrak has C-MAT$_{est}$ temperatures that are 7 ºC higher than Øsaker MAT and 5 ºC higher than regional MAT in the Skagerrak. This may be explained by at least three hypotheses. First, the brGDGTs might come from a mixture of different sources in the Skagerrak. For instance from a large drainage area from the Glomma River, not only constrained to southern Norway. Second, it was suggested that the brGDGTs could originate in the southern North Sea

and sediment into the Skagerrak transported by the North Atlantic Current (Rueda et al., 2009). In this case the sediments would come from a region located southwards and this could contribute to explain the high MAT estimates. Third, there could be a mixture of *in situ* production and transported brGDGTs as it has been suggested before that there could be *in situ* production of brGDGTs in some marine environments (Fietz et al., 2012; Peterse et al., 2009; Zhu et al., 2011). However this remains to be demonstrated.

4.5. Conclusions

The temperatures estimated from the analysis of both C- or I-brGDGTs in soil samples from southern Norway and the southeastern Pyrenees do not follow the air or soil temperature seasonality. The MAT_{est} values are closer to MAT rather than any specific season at both locations whether they were measured using C- or I-GDGTs. Values of C-MAT_{est} in either of the two sites derived from C-brGDGTs in suspended particles are also close to the annual means, but the I-MAT_{est} showed a seasonal bias in Ulldeter for spring and summer, and in the Glomma River only from October to December. The transport of brGDGTs to the Skagerrak is not enhanced during the summer months when Glomma River runoff is increased as the concentrations of C- and I-brGDGTs are decoupled from the river discharge cycle. When looking at the deposition sites, C-MAT_{est} values were very close to instrumental MAT in Ulldeter but closer to summer values in the Skagerrak. We conclude that the brGDGTs found in north-eastern Skagerrak might be a result of a mixture between lipids transported from a southernmost location and *in situ* production.

4.6. References

Bioforsk AgroMetBase (2011). Available at http://lmt-cloud.bioforsk.no/agrometbase/getweatherdata.php.

Boyd ES, Pearson A, Pi Y, Li W-J, Zhang YG, He L, Zhang CL, Geesey GG. (2011) Temperature and pH controls on glycerol dibiphytanyl glycerol tetraether lipid composition in the hyperthermophilic crenarchaeon Acidilobus sulfurireducens. Extremophiles: life under extreme conditions 15(1): 59–65: doi:10.1007/s00792-010-0339-y.

Cruz-Martínez K, Rosling A, Zhang Y, Song M, Andersen GL and Banfield JF (2012) Effect of rainfall-induced soil geochemistry dynamics on grassland soil microbial communities. Applied and environmental microbiology 78(21): 7587–7595: doi:10.1128/AEM.00203-12.

Fawcett PJ, Werne JP, Anderson RS, Heikoop JM, Brown ET, Berke MA, Smith SJ, Goff F, Donohoo-Hurley L, Cisneros-Dozal LM, Schouten S, Sinninghe Damsté JS, Huang Y, Toney J, Fessenden J, WoldeGabriel G, Atudorei V, Geissman JW and Allen CD (2011)

Extended megadroughts in the southwestern United States during Pleistocene interglacials. Nature 470(7335): 518–521: doi:10.1038/nature09839.

Fietz S, Huguet C, Bendle J, Escala M, Gallacher C, Herfort L, Jamieson R, Martínez-Garcia A, McClymont EL, Peck VL, Prahl FG, Rossi S, Rueda G, Sanson-Barrera A and Rosell-Melé A (2012) Co-variation of crenarchaeol and branched GDGTs in globally-distributed marine and freshwater sedimentary archives. Global and Planetary Change 92–93: 275–285: doi:10.1016/j.gloplacha.2012.05.020.

Fietz S, Martínez-Garcia A, Hambach B, Ho SL, Lamy F, Geibert W, Gersonde R and Rosell-Melé A (2011) Organic aerosol transport and deposition over the Southern Ocean. 25th International Meeting on Organic Geochemistry (IMOG 2011) O-20.

Global Runoff Data Centre (2011) Long-Term Mean Monthly Discharges and Annual Characteristics of GRDC Station / Global Runoff Data Centre. Koblenz, Germany: Federal Institute of Hydrology (BfG).

Hartley IP, Hopkins DW, Garnett MH, Sommerkorn M and Wookey PA (2008) Soil microbial respiration in arctic soil does not acclimate to temperature. Ecology letters 11(10): 1092–1100: doi:10.1111/j.1461-0248.2008.01223.x.

Harvey HR, Fallon RD and Patton JS (1986) The effect of organic matter and oxygen on the degradation of bacterial membrane lipids in marine sediments. Geochimica et Cosmochimica Acta 50(5): 795–804: doi:10.1016/0016-7037(86)90355-8.

Hopmans EC, Weijers JW., Schefuß E, Herfort L, Sinninghe Damsté JS and Schouten S (2004) A novel proxy for terrestrial organic matter in sediments based on branched and isoprenoid tetraether lipids. Earth and Planetary Science Letters 224(1-2): 107–116: doi:10.1016/j.epsl.2004.05.012.

Huguet C, Urakawa H, Martens-Habbena W, Truxal L, Stahl DA and Ingalls AE (2010) Changes in intact membrane lipid content of archaeal cells as an indication of metabolic status. Organic Geochemistry 41(9): 930–934: doi:10.1016/j.orggeochem.2010.04.012.

Lipp JS, Morono Y, Inagaki F and Hinrichs K-U (2008) Significant contribution of Archaea to extant biomass in marine subsurface sediments. Nature 454(7207): 991–994: doi:10.1038/nature07174.

Mangelsdorf K, Finsel E, Liebner S and Wagner D (2009) Temperature adaptation of microbial communities in different horizons of Siberian permafrost-affected soils from the Lena Delta. Chemie der Erde - Geochemistry 69(2): 169–182: doi:10.1016/j.chemer.2009.02.001.

Naether A, Foesel BU, Naegele V, Wüst PK, Weinert J, Bonkowski M, Alt F, Oelmann Y, Polle A, Lohaus G, Gockel S, Hemp A, Kalko EKV, Linsenmair KE, Pfeiffer S, Renner S, Schöning I, Weisser WW, Wells K, Fischer M, Overmann J and Friedrich MW (2012) Environmental factors affect Acidobacterial communities below the subgroup level in grassland and forest soils. Applied and environmental microbiology 78(20): 7398–7406: doi:10.1128/AEM.01325-12.

Peterse F, Kim J-H, Schouten S, Kristensen DK, Koç N and Sinninghe Damsté JS (2009) Constraints on the application of the MBT/CBT palaeothermometer at high latitude environments (Svalbard, Norway). Organic Geochemistry 40(6): 692–699: doi:10.1016/j.orggeochem.2009.03.004.

Peterse F, Van der Meer J, Schouten S, Weijers JWH, Fierer N, Jackson RB, Kim J-H and Sinninghe Damsté JS (2012) Revised calibration of the MBT–CBT paleotemperature proxy based on branched tetraether membrane lipids in surface soils. Geochimica et Cosmochimica Acta 96: 215–229: doi:10.1016/j.gca.2012.08.011.

Peterse F, Nicol GW, Schouten S and Sinninghe Damsté JS (2010) Influence of soil pH on the abundance and distribution of core and intact polar lipid-derived branched GDGTs in soil. Organic Geochemistry 41(10): 1171–1175: doi:10.1016/j.orggeochem.2010.07.004.

Pitcher A, Hopmans EC, Schouten S and Sinninghe Damsté JS (2009) Separation of core and intact polar archaeal tetraether lipids using silica columns: Insights into living and fossil biomass contributions. Organic Geochemistry 40(1): 12–19: doi:10.1016/j.orggeochem.2008.09.008.

Rasche F, Knapp D, Kaiser C, Koranda M, Kitzler B, Zechmeister-Boltenstern S, Richter A, Sessitsch A (2011) Seasonality and resource availability control bacterial and archaeal communities in soils of a temperate beech forest. Isme Journal 5(3): 389–402: doi:10.1038/ismej.2010.138.

Rueda G, Rosell-Melé A, Escala M, Gyllencreutz R and Backman J (2009) Comparison of instrumental and GDGT-based estimates of sea surface and air temperatures from the Skagerrak. Organic Geochemistry 40(2): 287–291: doi:10.1016/j.orggeochem.2008.10.012.

Schlitzer R (2010) Ocean Data View. Available at http://odv.awi.de.

Schouten S, Eldrett J, Greenwood DR, Harding I, Baas M and Damste JSS (2008) Onset of long-term cooling of Greenland near the Eocene-Oligocene boundary as revealed by branched tetraether lipids. Geology 36(2): 147–150: doi:10.1130/G24332A.1.

Schouten S, Middelburg JJ, Hopmans EC and Sinninghe Damsté JS (2010) Fossilization and degradation of intact polar lipids in deep subsurface sediments: A theoretical approach. Geochimica et Cosmochimica Acta 74(13): 3806–3814: doi:10.1016/j.gca.2010.03.029.

Servei Meteorològic de Catalunya (2011). Available at www.meteo.cat.

Sinninghe Damsté J, Hopmans EC, Pancost RD, Schouten S and Geenevasen JAJ (2000) Newly discovered non-isoprenoid glycerol dialkylglycerol tetraether lipids in sediments. Chemical Communications (17): 1683–1684: doi:10.1039/B004517I.

Sinninghe Damsté JS, Rijpstra WIC, Hopmans EC, Weijers JWH, Foesel BU, Overmann J and Dedysh SN (2011) 13,16-Dimethyl Octacosanedioic Acid (iso-Diabolic Acid), a Common Membrane-Spanning Lipid of Acidobacteria Subdivisions 1 and 3. Applied and Environmental Microbiology 77(12): 4147–4154: doi:10.1128/AEM.00466-11.

Weijers JWH, Panoto E, Van Bleijswijk J, Schouten S, Rijpstra WIC, Balk M, Stams AJM and Sinninghe Damsté JS (2009) Constraints on the Biological Source(s) of the Orphan Branched Tetraether Membrane Lipids. Geomicrobiology Journal 26(6): 402–414: doi:10.1080/01490450902937293.

Weijers JWH, Bernhardt B, Peterse F, Werne JP, Dungait JAJ, Schouten S and Sinninghe Damsté JS (2011) Absence of seasonal patterns in MBT–CBT indices in mid-latitude soils. Geochimica et Cosmochimica Acta 75(11): 3179–3190: doi:10.1016/j.gca.2011.03.015.

Weijers JWH, Schefuß E, Schouten S and Damsté JSS (2007b) Coupled Thermal and Hydrological Evolution of Tropical Africa over the Last Deglaciation. Science 315(5819): 1701 –1704: doi:10.1126/science.1138131.

Weijers JWH, Schouten S, Sluijs A, Brinkhuis H and Sinninghe Damsté JS (2007c) Warm arctic continents during the Palaeocene-Eocene thermal maximum. Earth and Planetary Science Letters 261(1-2): 230–238: doi:10.1016/j.epsl.2007.06.033.

Weijers JWH, Schouten S, Spaargaren OC and Sinninghe Damsté JS (2006) Occurrence and distribution of tetraether membrane lipids in soils: Implications for the use of the TEX86 proxy and the BIT index. Organic Geochemistry 37(12): 1680–1693: doi:10.1016/j.orggeochem.2006.07.018.

Weijers JWH, Schouten S, Van den Donker JC, Hopmans EC and Sinninghe Damsté JS (2007a) Environmental controls on bacterial tetraether membrane lipid distribution in soils. Geochimica et Cosmochimica Acta 71(3): 703–713: doi:10.1016/j.gca.2006.10.003.

Weijers JWH, Wiesenberg GLB, Bol R, Hopmans EC and Pancost RD (2010) Carbon isotopic composition of branched tetraether membrane lipids in soils suggest a rapid turnover and a heterotrophic life style of their source organism(s). Biogeosciences Discuss. 7(3): 3691–3734: doi:10.5194/bgd-7-3691-2010.

White DC, Davis WM, Nickels JS, King JD and Bobbie RJ (1979) Determination of the sedimentary microbial biomass by extractable lipid phosphate. Oecologia (40): 51–62.

Wu F, Yang W, Zhang J, Liu L and Wang A (2011) Changes in soil microbial biomass and bacterial diversity during the transition from winter to growing season in the subalpine/alpine forests. African Journal of Microbiology Research 5(31): 5575–5583: doi:10.5897/AJMR11.288.

Zhu C, Weijers JWH, Wagner T, Pan JM, Chen JF and Pancost RD (2011) Sources and distributions of tetraether lipids in surface sediments across a large river-dominated continental margin. Organic Geochemistry 42(4): 376–386: doi:16/j.orggeochem.2011.02.002.

CHAPTER 5

Coupling of air and sea surface temperatures in the eastern Fram Strait during the last 2000 years

This chapter is a modified version of an article published in:

Rueda G, Fietz S, Rosell-Melé A, (2013) Coupling of air and sea surface temperatures in the eastern Fram Strait during the last 2000 years. *The Holocene* doi: 10.1177/0959683612470177.

5.1. Abstract

The Arctic has undergone significant changes in the last 20-30 years. The understanding of these changes is limited by the time span or resolution of existing climate records. The main gateway of heat to the Arctic Ocean is the Fram Strait, between Greenland and Svalbard. We have reconstructed past air and sea surface temperatures and relative variations in freshwater extent in a marine core from eastern Fram Strait which spans the last 2000 years. The results show a progressive increase in air temperature and a decrease in the upper mixed water layer temperature, together with an increase in freshwater content during the last 1000 years. Considering the oceanographic features of the eastern Fram Strait, these results suggest that there might have been a progressive increase in the inflow of Atlantic water during the last 1000 years, accompanied by an increase in atmospheric heat transport, causing a progressive sea ice melting and subsequent cooling and freshening of the upper mixed water layer in this area. We suggest that our data show long scale average changes in the modes of positive and negative Arctic multidecadal variability over the last 2000 years.

Keywords Fram Strait; sea surface temperature (SST); air temperature; Atlantic water; alkenones; GDGTs.

5.2. Introduction

Average air temperatures have increased faster in the Arctic than in the rest of the world during the last 100 years (Chylek et al., 2009), which makes the region one of the world's most sensitive areas to climate change. This has been partly attributed to the ice/snow albedo temperature feedback (IPCC, 2007). The Arctic sea ice cover and extent has been thinning and retreating pronouncedly in the last three decades, coinciding with the average warming (Polyak et al., 2010). Most of the heat and mass exchanges between the North Atlantic and the Arctic Ocean occur through the Fram Strait (Aagaard and Greisman, 1975). Warm, salty Atlantic water enters the strait heading north carried by the West Spitsbergen Current, while a large part of Arctic low salinity upper ocean water and sea ice drain southwards with the East Greenland Current (Figure 5.1). This export of freshwater is important because it influences the stratification of the water column in sensitive deep water formation regions and the strength of the Atlantic meridional overturning circulation (Holland et al., 2001). From direct observations and modelling it has become apparent that the mean balance of freshwater in the polar and subpolar oceans and the inflow of Atlantic water to the

Arctic are highly variable in seasonal, decadal and interdecadal scales (Dukhovskoy et al., 2004; Polyakov et al., 2004). This variability may be partly attributed to large amplitude multidecadal fluctuations as the variable impacts of the North Atlantic Oscillation (NAO; Hurrell, 1995), the Arctic Oscillation (AO; Thompson and Wallace, 1998) or the Arctic Ocean Oscillation (AOO; Proshutinksy and Johnson, 1997). An increase in freshwater export from the Arctic (Blindheim et al., 2000; Jahn et al., 2010) and decrease in salinity and sea ice extent in the subpolar North Atlantic and the Arctic (Curry et al., 2003) have been observed over the past decades. Those trends seem to be related to the NAO amplification since the 1960s. Enhanced trade winds, higher net precipitation and continental ice melting for example result in enhanced export of ice and freshwater from the Arctic (Curry et al., 2003). This freshwater export can spread eastwards over the Norwegian Sea causing a freshening and cooling of the upper water layer (Björk et al., 2001).

In order to improve our understanding of the ice-ocean-atmosphere interactions in the eastern Fram Strait, we show how atmospheric and upper ocean temperature changes have been coupled over the last 2000 years and relate it to previously published data over the same time span and region.

5.3. Study area

The Fram Strait has contrasting spatial and seasonal oceanographic conditions. The study region is located in the eastern Fram Strait (Figure 5.1), and it is influenced by the West Spitsbergen Current. This becomes colder and fresher towards high latitudes (Hansen and Østerhus, 2000; Walczowski et al., 2005) and injects relatively warm and saline Atlantic water below the ice covered, cold and fresh Polar water cap of the Arctic Ocean (Aagaard et al., 1985). Parts of the West Spitsbergen Current separate from the main current in the central Fram Strait and flow south as the subsurface return Atlantic current (Gascard et al., 1988). The East Spitsbergen Current joins the West Spitsbergen Current and supplies cold water and sea ice from the northwestern Barents Sea to the eastern Fram Strait as it moves northward as a coastal current (Johannessen, 1986). In the western Fram Strait the cold and low salinity waters from the Arctic flow southward along the Greenland margin and form the East Greenland Current (Figure 5.1). This circulation pattern results in a variable sea ice cover in the Fram Strait with permanent ice covered areas in the west, permanent ice free areas in the southeast and seasonally variable sea ice conditions in the central and eastern parts of the Fram Strait (Vinje and Finnekåsa, 1986). In the eastern Fram Strait, the warm and saline Atlantic water flows in the subsurface, between 50 and 600 m

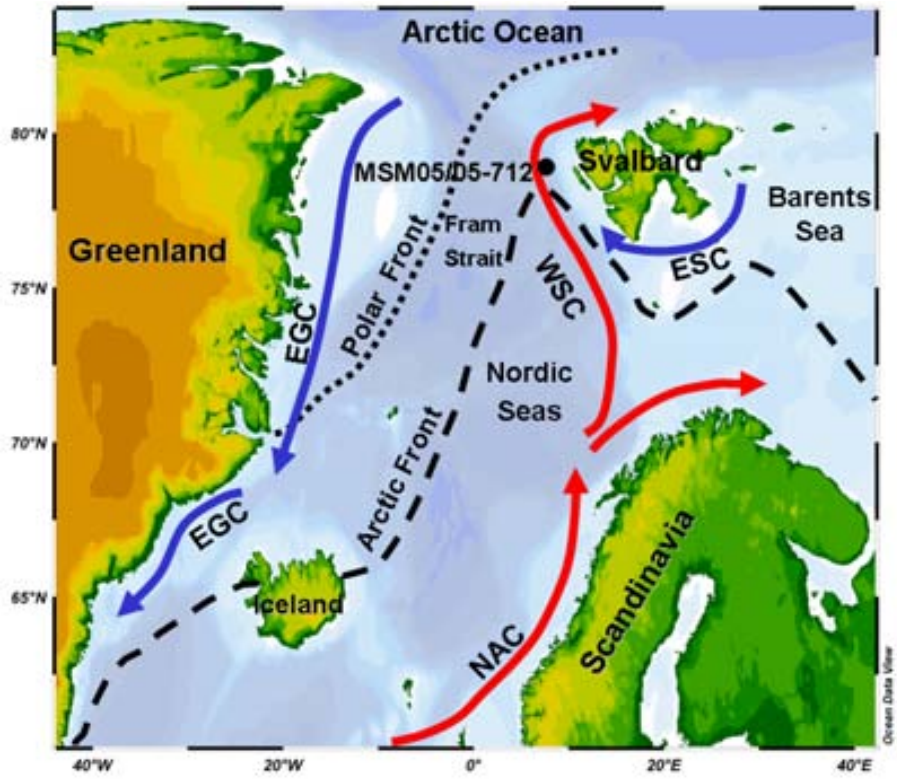

Figure 5.1. Locations of core MSM05/05-712-1 (black dot; 78°54.94' N, 6°46.04' E, 1490 m depth) and principal ocean surface currents. Red arrows indicate warm surface currents whereas blue arrows depict cold currents. The modern average position of the Arctic front and the Polar front are represented with dashed lines. WSC: West Spitsbergen Current, ESC: East Spitsbergen Current, NAC: North Atlantic Current, EGC: East Greenland Current. Map drawn with Ocean Data View (Schlitzer, 2010).

water depth. It cools and freshens as it flows north into the Arctic Ocean, releasing heat into the atmosphere and developing a colder and less saline superficial mixed water layer (0 – 50 m water depth) as it melts the Arctic sea ice (Rudels et al., 2005). This surface mixed layer is characterized by seasonally variable temperatures and salinities.

At the coring site, the water temperatures at the sea surface (2 m depth) varied between 4 ^{o}C (October) and 8 ^{o}C (August; Spielhagen et al., 2011) in October 2006 and August 2007. At the limit between the buoyant mixed layer and the Atlantic water (50 m), and also at the bottom of the Atlantic water layer (600 m), the difference between both seasons was just 1 ^{o}C at both depths (for more details in modern sea water conditions see Spielhagen et al., 2011). The coring site location is close to the Arctic Front (Figure 5.1), which separates the Atlantic and fresh Arctic waters of the Greenland gyre (Aken et al., 1995), and corresponds to the maximum limit of sea ice in winter. The sea ice seasonal coverage at the coring site has a large interannual variability, ranging between 0 and 6 months yr^{-1} (Bonnet et al., 2010).

5.4. Description of samples and proxies used

Both air and sea surface temperature records were obtained from the same marine sediment core, MSM05/05-712-1, retrieved from the slope of the Svalbard western continental margin (78°54.94' N, 6°46.04' E, 1490 m depth, Figure 5.1) and sub-sampled at 1 cm intervals. The record spans the last 2000 years approximately. The age model is based on 5 accelerator mass spectrometry ^{14}C age measurements on planktonic foraminifera (Table 5.1; Spielhagen et al., 2011). The sampling resolution is in average ca. 45 years per data point.

Table 5.1. Age model for core MSM05/05-712-1 based on AMS ^{14}C ages. A correction of 402 year was applied to account for the air-sea reservoir difference (Spielhagen et al., 2011)

Laboratory reference	Core depth (cm)	Dated species	^{14}C age BP	Year AD
KIA39656	0.25	*Neogloboquadrina pachyderma (sin.)* and mixed planktonic foraminifera	Bomb age	2007
KIA39262	14.75	*Neogloboquadrina pachyderma (sin.)*	820±25	1486
KIA39041	21.50	*Neogloboquadrina pachyderma (sin.)*	1290±30	1112
KIA39263	30.75	*Neogloboquadrina pachyderma (sin.)*	1760±25	647
KIA38079	42.00	*Neogloboquadrina pachyderma (sin.)*	2270±25	72

In July 2009, during ARK-XXIV/1 expedition, water samples from the western Spitsbergen continental margin were collected at different water depths close to the coring site (78°50.30'N, 6°42.22'E). An inline filtration system was used to collect 8 L of water from 6 m depth, and a CTD rosette device was used to retrieve 28 L at 30 m, 53.5 L at 250 m and 57.5 L at 1604 m. All samples were filtered on board through GF/F filters (0.7 μm pore size) and stored frozen.

To estimate sea surface temperature (SST) we used the U^K_{37} index (Brassell et al., 1986) calculated from the relative concentration in sediments of the di-, tri- and tetraunsaturated C_{37} alkenones through the equation $U^K_{37} = (C_{37:2}-C_{37:4})/(C_{37:2}+C_{37:3}+C_{37:4})$. The U^K_{37} was then converted to temperature using the regression SST (°C) = $(U^K_{37} - 0.162)/0.029$ from a core top calibration (using annual means for SST) in the northeastern Atlantic (Rosell-Melé et al., 1995). The error of the regression is 0.5 °C (calculated from the deviations for the intercept and slope at 95% significance level given in Rosell-Melé et al. (1995)). The percentage of the $C_{37:4}$ alkenone to the total abundance of C_{37} alkenones ($\%C_{37:4} = (C_{37:4}/(C_{37:2}+C_{37:3}+C_{37:4}))\cdot 100$) in the record is used as an additional tracer to infer variations in the meridional extent of polar and subpolar conditions through time (Bendle et al., 2005). The alkenone pattern in samples from core MSM05/05-712-1 (Figure 5.2) indicates influence of Atlantic water mass (Bendle and Rosell-Melé, 2004). This indicates that even though

the site is located at high latitude in a polar marginal environment, alkenones can be used for estimating past SST in this core.

To estimate air temperature we used a novel biomarker proxy derived from bacteria in soils, the MBT'/CBT index (Peterse et al., 2012; modified after the original MBT/CBT index from Weijers et al., 2007a). The MBT'/CBT index is obtained from quantifying relative abundances of branched glycerol dialkyl glycerol tetraethers (GDGTs) using the equations CBT = -log([1020 + 1034] / [1022 + 1036]) and MBT' = [1022 + 1020 + 1018] / [1022 + 1020 + 1018 + 1036 + 1034 + 1032 + 1050] where the numbers refer to the protonated masses of branched GDGTs (Figure 1.9; Chapter 1; p. 18). The resulting values of the CBT and MBT' indices were converted to mean air temperature (MAT) using the equation MAT = 0.81 – 5.67×CBT + 31.0×MBT' (Peterse et al., 2012). The MBT'/CBT calibration to MAT has an error of 5 ^{o}C. For this reason, here we focus on the qualitative interpretation of relative variations of temperature estimated throughout the core. This proxy has been used to describe past changes in air temperature at different temporal scales and in a wide range of geographical settings, such as the Congo deep sea fan (Weijers et al., 2007b), North America (Fawcett et al., 2011), East Greenland (Schouten et al., 2008), and the Arctic (Weijers et al., 2007c).

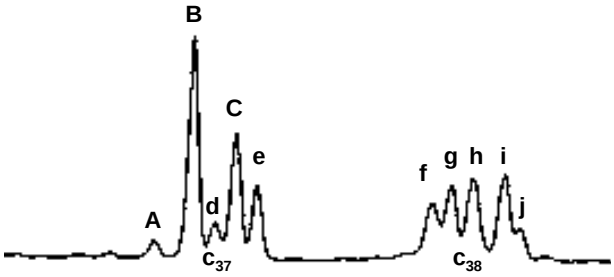

Figure 5.2. Representative GC-FID trace of alkenone patterns in core MSM05/05-712-1. Alkenones used in this study are: (A) $C_{37:4}$ Me; (B) $C_{37:3}$ Me; (C) $C_{37:2}$ Me. The other compounds were identified to determine the alkenone water mass *fingerprint* as described by Bendle and Rosell-Melé (2004): (d) $C_{36:3}$OMe, (e) $C_{36:2}$OMe, (f) $C_{38:4}$Me, (g) $C_{38:3}$Et, (h) $C_{38:3}$Me, (i) $C_{38:2}$Et, (j) $C_{38:2}$Me.

5.5. Results and discussion

5.5.1. Origin of the branched GDGT signal

A key issue in the application of the air temperature proxy from soil GDGTs in a marine record is to establish their origin. Initially the synthesis of branched GDGTs was postulated to occur exclusively in continental environments (Weijers et al., 2007a). Soils were shown to be a major source of branched GDGTs (Weijers et al., 2009) and

their biosynthesis was ascribed to anoxic bacteria (Weijers et al., 2007a), although the only source organisms proven to produce branched GDGTs so far are terrestrial acidobacteria (Sinninghe Damste et al., 2011). At the moment there is no reported evidence that branched GDGTs are biosynthesized in the open ocean and deep sea sediments, such as the coring site studied here. Branched GDGTs were found to decrease seawards from the continent (Hopmans et al., 2004; Kim et al., 2006), and fluvial transport of branched GDGTs from peats and soils to the oceans could be inferred from the detection of substantial amounts of branched GDGTs in river water, and a high branched GDGT concentration in the water of a Swiss peat bog (Herfort et al., 2006). To explain the discrepancy in MAT estimates between soils and fjord sediments from Svalbard, Peterse et al. (2009) hypothesized that part of the branched GDGTs found in the fjords may be produced *in situ*. However, we note that the distributions of branched GDGTs in those soil and fjord samples from NW Svalbard (Peterse et al., 2009) are not comparable to the average distributions of branched GDGTs found in our core MSM05/05-712-1 for the last 2000 years (Figure 5.3). We consider thus that the branched GDGTs in our core might have a wider source, as the eastern Fram Strait is exposed to the arrival of terrigeneous detritus transported to the site with drifting sea ice, which can be melted by the inflowing warm Atlantic water.

The source of high amounts of ice rafted material (IRD) released during the summer melting of the ice margin over our study region has been attributed to the Svalbard archipelago and the northern Barents sea (Hebbeln and Wefer, 1991; Hebbeln, 2000). Hebbeln (2000) reported high particle flux events in winter, due to the input of IRD derived from the Svalbard archipelago even in situations when the Svalbard ice margin did only reach the vicinity of the site. The material from the Barents Sea may reach the coring site transported with the East Spitsbergen Current. Drifting ice transport of branched GDGTs was indeed suggested by Yamamoto et al. (2008) in the central Arctic. In addition, Kim et al. (2011) studied the origin of the organic matter in a wide set of samples from Svalbard and found a significant IRD input in front of glaciers that due to the slow melting of icebergs could influence the whole fjord system and beyond. Furthermore, the analysis of water column samples obtained in July 2009 close to the coring site shows that 85% of the relative abundance of detected branched GDGTs are found near the water surface, at 6 m water depth, whereas only 7% were found at 30 m and 4% at 250 m and 1604 m (Figure 5.3). This would suggest that the branched GDGTs entered the marine system at the sea surface, and are not produced at depth, or at least that the input at the sea surface via IRD would be higher than a hypothetical *in situ* production deeper down in the water column. Incidentally, the MAT estimates from the MBT'/CBT indices for these samples in the surface waters are

10 ºC (at 6 m water depth) and 8.5 ºC in the surface sediment. Interestingly, even considering the MAT calibration error of 5 ºC, these values are closer to July average (5.3 to 6.4 ºC) air temperatures rather than to annual mean air temperatures (from -8.5 to -1.6 ºC) in western Spitsbergen (Norwegian Meteorological Institute, 2010). In summary, we argue that branched GDGTs in our study site are likely associated to IRD originating from a wide area that includes the Svalbard archipelago and the northern Barents Sea, while a contribution from Svalbard continental run off seems also feasible.

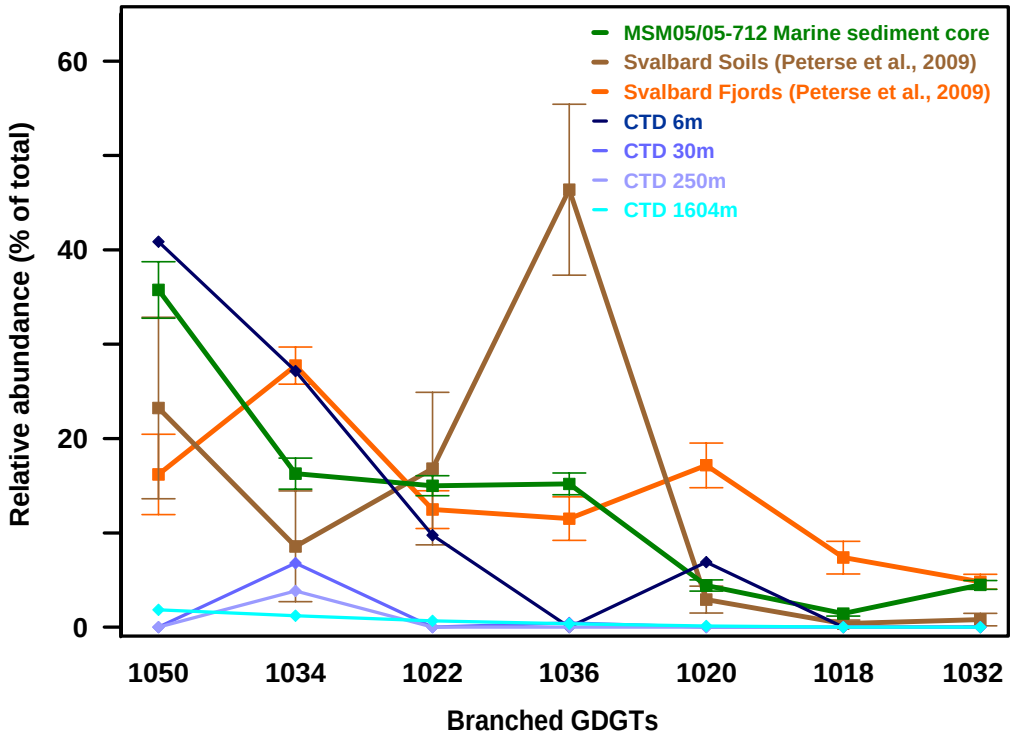

Figure 5.3. Average distribution and standard deviation of branched GDGTs measured in core MSM05/05-712-1 (78°54.94' N, 6°46.04'E) (green line; n=43), in a previous study (Peterse et al., 2009) from soils in three locations in NW Svalbard (brown line; n=9), surface sediments from a NW Svalbard fjord system (orange line, n=29) and at 6m, 30m, 250m, 1604m water column depth (blue lines) (78º50.30'N, 6º42.22'E).

5.5.2. Air and Sea Surface temperatures variability

During the last 2000 years the reconstructed climatic parameters show several short time fluctuations as well as centennial scale trends (Figure 5.4). The SST from the upper mixed layer estimated from $U^{K}_{37'}$ and the MAT attributed to the region of the Svalbard archipelago, estimated from MBT'/CBT both indicate the past occurrence of various cooling-warming episodes (Figure 5.4A). Specifically, in the period between ~AD 72 and AD 330, SST increased by 2 ºC and MAT decreased by ca. 1 ºC, followed by a SST cooling of ~2.5 ºC from ~AD 330 to AD 685 SST and a MAT warming of ~1.5 ºC from ~AD 330 to AD 840. From AD 685 to 1000 SST increased ~2 ºC while MAT

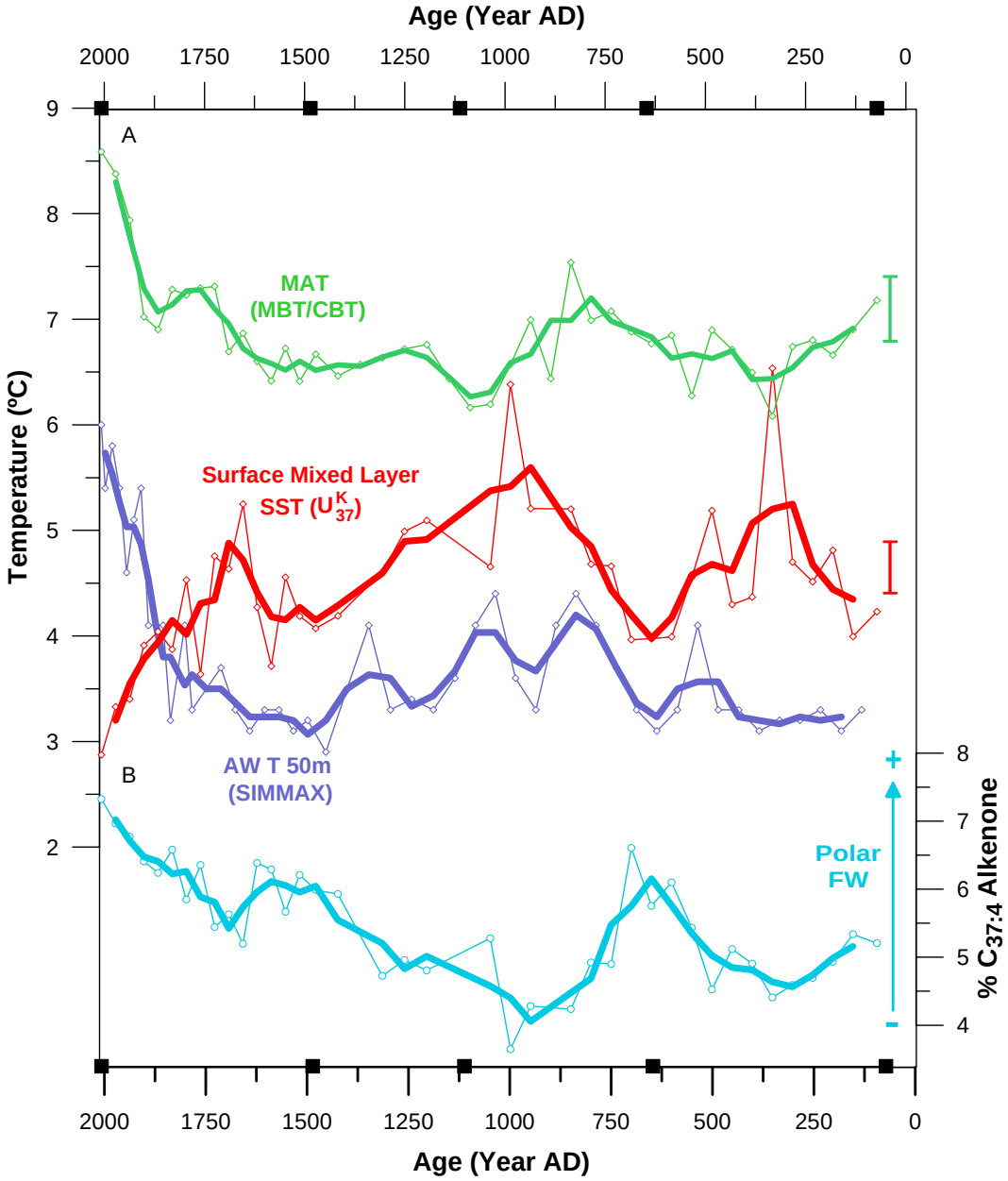

Figure 5.4. Paleoclimatic reconstruction in core MSM05/05-712-1 for the last 2000 years. (A) U^{K}_{37} SST (ºC) (red) depicting surface mixed water layer temperature, Atlantic water temperature at 50 m depth (purple) from Spielhagen et al. (2011) and MBT'/CBT regional air temperature (ºC) estimates (green). (B) Percentage of $C_{37:4}$ to C_{37} alkenones as indicator of polar/freshwater extent (blue). A three point running average is shown with a thick line for all the datasets. Black squares in the age axis indicate dating points resulting from ^{14}C AMS measurements (Spielhagen et al., 2011). Floating error bars at the right side of the figure show the analytical error (reproducibility).

decreased ~1.5 ºC from AD 840 to 1000. After these successive warming and cooling periods, since AD 1000 there was a time interval with a sustained increase of ~2.5 ºC in MAT, and a decrease in SST of about ~3.5 ºC until present. These trends were more

accentuated during the last 500 years. There is a continuous increase in $\%C_{37:4}$ (Figure 5.4B) since AD 1000, that suggests increasingly colder and fresher surface waters at the coring site.

In Figure 5.4A we also plot the results of the SIMMAX modern analog technique applied on planktic foraminifer species, which reflect mid-summer conditions in the uppermost part of the Atlantic water layer averaged over a few decades in the same marine sedimentary core (Spielhagen et al., 2011). The Atlantic water temperature shows similar trends as the MAT, specially during the last 500 years when both increase.

Previous studies determined an increase in the inflow of Atlantic water in the north of Svalbard during the last 1000 years (Slubowska et al., 2005), coinciding with colder and more unstable conditions than in preceding time intervals and with increased ice rafting in western Svalbard (Slubowska-Woldengen et al., 2007). Quantitative SST reconstructions based on dinocyst assemblages from a sediment core located close to our site (JM-06-WP-04-MCB; 78°54.9′N, 6°46.0′ E) registered a cooling of 4 ^{o}C for the last 300 years (Bonnet et al., 2010). For the same time period, our results are coherent with the cooling registered by the dinocysts, showing a SST decrease of ca. 2 ^{o}C. In contrast, during the last 1000 years regional MAT increased ~1 ^{o}C until AD 1860, and by 1.5 ^{o}C in the last 150 years, reaching a value of 8.5 ^{o}C, which is the highest value for the whole record. This coincides with a strengthened subsurface Atlantic water inflow to the eastern Fram Strait after ~1860 described by Werner et al. (2011), based on the amount of subpolar planktic foraminifera *Turborotalia quinqueloba* in the same marine sedimentary core.

Considering the oceanographic characteristics of the coring site, we suggest that during the last 1000 years there was an increase in the northward flow of warm Atlantic water, as also suggested by Slubowska et al. (2005) for the last 1000 years and by Spielhagen et al. (2011) for the last 160 years. We postulate that this took place together with an enhancement of the atmospheric circulation that brought northwards warmer air to the Svalbard area, as interpreted from the air temperature estimates. These phenomena could have enhanced the melting of the sea ice, releasing colder and less saline upper layer water in the eastern Fram Strait (Figure 5.5). Warmer air temperatures leading to increased river runoff (Peterson et al., 2002) and negative mass balance of circum-Arctic glaciers (Dowdeswell et al., 1997), specially those from Svalbard, could be additional sources of freshwater to the area.

5.5.3. Mechanism of long term climate variability

The Arctic responds to low frequency intrusions of Atlantic warm/cold air mass anomalies with alternating regimes of weakened/strengthened anticyclonic Beaufort Gyre circulation, and intensified/suppressed cyclonic circulation in the eastern Arctic (Polyakov and Johnson, 2000). At decadal time scales, the atmospheric and oceanic variability in the Arctic is driven by changes in the AO (Thompson and Wallace, 1998) and the NAO (Hurrell, 1995); high AO/NAO is associated with a cyclonic circulation regime and low AO/NAO is related to an anticyclonic circulation regime (Dukhovskoy et al., 2004; Proshutinsky and Johnson, 1997). From modern observations and statistical analysis, ~50-80 year low frequency oscillations have been identified in Northern Hemisphere surface air temperatures for the North Atlantic Ocean (Schlesinger and Ramankutty, 1994). Depending on the atmospheric pressure system at sea level and the cyclonic circulation over the Arctic two phases of such multidecadal variability (MDV) can prevail at these longer time scales. During the positive phase of Arctic MDV there

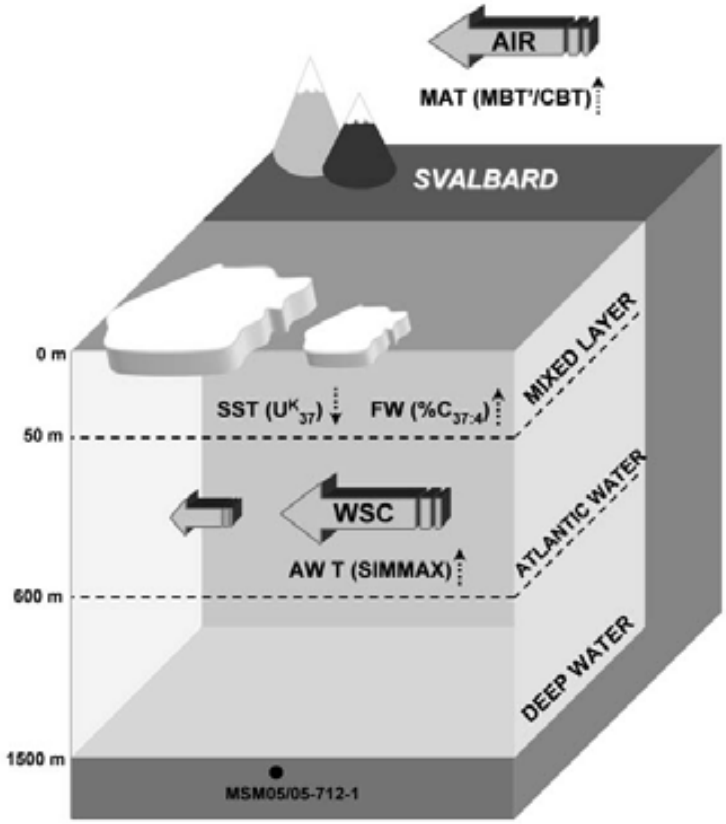

Figure 5.5. Water column structure in western Svalbard and air - ocean interactions during a positive phase of Arctic MDV. The northward transport of warm air and Atlantic water (AW) via the West Spitsbergen Current (WSC) are enhanced (MAT MBT'/CBT and AW T SIMMAX increase). Sea ice melts releasing colder and fresher water (FW) to the surface mixed layer (SST U^K_{37} decreases and %$C_{37:4}$ increases). During negative phase of MDV these interactions are weakened.

is an enhancement in the warm air and Atlantic water inflow from the North Atlantic to the Arctic, and an excess of sea ice and freshwater transport from the Arctic through the Fram Strait, whereas in the negative phase these interactions are weakened (Figure 5.5; Polyakov et al., 2004; 2010). Our data suggest that during the last ~1000 years, a relative dominance of the positive phase of Arctic MDV prevailed. This trend started ~1000 years ago and prevailed until ~AD 1860, when there was an intensification in the increase of Svalbard air temperatures: in the past 150 years air temperature increase doubled on average between ~AD 1000 and 1860, accompanied by an enhancement of Atlantic water inflow to the Fram Strait as described by Spielhagen et al. (2011). Given that for the same time period the rate of change in air temperature is not mirrored by a change in the rate of SST decrease, we suggest that the rise in Svalbard air temperatures since AD 1860 could be driven by the impact of human activity on climate superimposed on the longer term natural warming and the mean relative dominance in the positive phase of MDV that began around AD 1000.

Recently, through an empirical orthogonal function analysis of deep ocean and near surface instrumental observations of the North Atlantic, it was demonstrated that the recent warming over the North Atlantic is linked to both long term climate change (including anthropogenic and natural) and MDV over the last 80 years of the twentieth century (Polyakov et al., 2010). Considering that the mechanisms of MDV observed in instrumental records can be projected onto longer time scales, our results indicate long term changes in the phases of Arctic MDV during the last 2000 years.

5.6. Conclusions

We have reconstructed past air and sea surface temperatures and variations in freshwater extent in the eastern Fram Strait for the last 2000 years. During the last 1000 years, air temperature increased continuously while the upper mixed water layer temperature decreased and the amount of polar freshwater present in the area increased. Considering the oceanographic conditions of the area, there might have been an increase in the inflow of Atlantic water during the last 1000 years together with an increase in atmospheric heat transport which caused a progressive sea ice melting and cooling of the upper mixed surface layer in the eastern Fram Strait. Assuming that the mechanisms of MDV derived from relatively short instrumental records can be projected onto longer time scales, our results may indicate the occurrence of a mean relative dominance in the positive phase of the Arctic MDV for the last 1000 years. We suggest therefore that the data presented here show long scale average changes in the mean modes of positive and negative Arctic MDV over the last 2000 years.

5.7. References

Aagaard K and Greisman P (1975) Toward new mass and heat budgets for the Arctic Ocean. Journal of Geophysical Research 80(27): 3821–3827, DOI:10.1029/JC080i027p03821.

Aagaard K, Swift JH and Carmack EC (1985) Thermohaline circulation in the Arctic Mediterranean seas. Journal of Geophysical Research 90(C3): 4833–4846, DOI:198510.1029/JC090iC03p04833.

Aken van, HM Budéus G and Hähnel M (1995) The anatomy of the Arctic frontal zone in the Greenland Sea. Journal of Geophysical Research 100(C8): 15,999–16,014, DOI:199510.1029/95JC01176.

Bendle J and Rosell-Melé A (2004) Distributions of UK37 and UK37' in the surface waters and sediments of the Nordic Seas: Implications for paleoceanography. Geochemistry Geophysics Geosystems 5: Q11013, DOI: 200410.1029/2004GC000741.

Bendle J, Rosell-Melé A and Ziveri P (2005) Variability of unusual distributions of alkenones in the surface waters of the Nordic seas. Paleoceanography 20: PA2001, DOI: 200510.1029/2004PA001025.

Björk G, Gustafsson BG and Stigebrandt A (2001) Upper layer circulation of the Nordic seas as inferred from the spatial distribution of heat and fresh water content and potential energy. Polar Research 20(2): 161–168, DOI: 10.1111/j.1751–8369.2001.tb00052.x.

Blindheim J, Borovkov V, Hansen B, Malmberg SA, Turrell WR and Østerhus S. (2000) Upper layer cooling and freshening in the Norwegian Sea in relation to atmospheric forcing. Deep Sea Research Part I: Oceanographic Research Papers 47(4): 655–680, DOI: 10.1016/S0967–0637(99)00070–9.

Bonnet S, de Vernal A, Hillaire-Marcel C, Radi T and Husum K (2010) Variability of sea-surface temperature and sea ice cover in the Fram Strait over the last two millennia. Marine Micropaleontology 74(3–4): 59–74, DOI: 10.1016/j.marmicro.2009.12.001.

Brassell SC, Eglinton G, Marlowe IT, Pflaumann U and Sarnthein M (1986) Molecular stratigraphy: A new tool for climatic assessment. Nature 320(6058): 129–133, DOI: 10.1038/320129a0.

Curry R, Dickson B and Yashayaev I (2003) A change in the freshwater balance of the Atlantic Ocean over the past four decades. Nature 426(6968): 826–829, DOI: 10.1038/nature02206.

Chylek P, Folland CK, Lesins G, Dubey MK and Wang M (2009) Arctic air temperature change amplification and the Atlantic multidecadal oscillation. Geophysical Research Letters 36(L14801): 5, DOI: 200910.1029/2009GL038777.

Dowdeswell JA, Hagen JO, Björnsson H Glazovsky AF, Harrison WD, Holmlund P, Jania J, Koerner RM, Lefauconnier B, Ommanney CSL, Thomas RH (1997) The mass balance of circum-Arctic glaciers and recent climate change. Quaternary Research 48(1): 1–14, DOI: 10.1006/qres.1997.1900.

Dukhovskoy DS, Johnson MA and Proshutinsky A (2004) Arctic decadal variability: An auto-oscillatory system of heat and fresh water exchange. Geophysical Research Letters 31, DOI: 200410.1029/2003GL019023.

Escala M, Fietz S, Rueda G and Rosell-Melé A (2009) Analytical considerations for the use of the paleothermometer tetraether index 86 and the branched vs isoprenoid tetraether index regarding the choice of cleanup and instrumental conditions. Analytical Chemistry 81(7): 2701–2707, DOI: 10.1021/ac8027678.

Fawcett PJ, Werne JP, Anderson RS, Heikoop JM, Brown ET, Berke MA, Smith SJ, Goff F, Donohoo-Hurley L, Cisneros-Dozal LM, Schouten S, Sinninghe Damsté JS, Huang Y, Toney J, Fessenden J, WoldeGabriel G, Atudorei V, Geissman JW and Allen CD (2011) Extended megadroughts in the southwestern United States during Pleistocene interglacials. Nature 470(7335): 518–521, DOI: 10.1038/nature09839.

Fietz S, Martínez-Garcia A, Rueda G, Peck VL, Huguet C, Escala M, Rosell-Melé A (2011) Crenarchaea and phytoplankton coupling in sedimentary archives: Common trigger or metabolic dependence? Limnology and Oceanography 56: 1907–1916, DOI: 10.4319/lo.2011.56.5.1907.

Gascard JC, Kergomard C, Jeannin PF and Fily M (1988) Journal of Geophysical Research 93(C4): 3613–3641, DOI: 10.1029/JC093iC04p03613.

Hansen B and Østerhus S (2000) North Atlantic-Nordic seas exchanges. Progress In Oceanography 45(2): 109–208, DOI: 10.1016/S0079–6611(99)00052-X.

Hebbeln D (2000) Flux of ice-rafted detritus from sea ice in the Fram Strait. Deep Sea Research Part II: Topical Studies in Oceanography 47(9–11): 1773–1790, DOI: 10.1016/S0967–0645(00)00006–0.

Hebbeln D and Wefer G (1991) Effects of ice coverage and ice-rafted material on sedimentation in the Fram Strait. Nature 350(6317): 409–411, DOI: 10.1038/350409a0.

Herfort L, Schouten S, Boon JP, Woltering M, Baas M, Weijers JWH, Sinninghe Damsté JS (2006) Characterization of transport and deposition of terrestrial organic matter in the southern North Sea using the BIT index. Limnology and Oceanography 51(5): 2196–2205, DOI: 10.4319/lo.2006.51.5.2196.

Holland MM, Bitz CM, Eby M and Weaver AJ (2001) The role of ice–ocean interactions in the variability of the north Atlantic thermohaline circulation. Journal of Climate 14(5): 656–675, DOI: 10.1175/1520–0442(2001)014<0656:TROIOI>2.0.CO;2.

Hopmans EC, Weijers JW, Schefuß E, Herfort L, Sinninghe-Damste JS and Schouten S (2004) A novel proxy for terrestrial organic matter in sediments based on branched and isoprenoid tetraether lipids. Earth and Planetary Science Letters 224(1–2): 107–116, DOI: 10.1016/j.epsl.2004.05.012.

Hurrell JW (1995) Decadal trends in the north Atlantic oscillation: Regional temperatures and precipitation. Science 269(5224): 676–679, DOI: 10.1126/science.269.5224.676.

IPCC (2007) Climate change 2007: The physical science basis. In: Solomon S, Qin D, Manning M Chen Z, Marquis M, Averyt KB, Tignor M and Miller HL (ed.) Contribution of Working Group I to the Fourth Assessment Report of the Intergovernmental Panel on Climate Change. Cambridge: Cambridge University Press, pp. 459–483.

Jahn A, Tremblay B, Mysak LA and Newton R (2010) Effect of the large-scale atmospheric circulation on the variability of the Arctic Ocean freshwater export. Climate Dynamics 34(2–3): 201–222, DOI: 10.1007/s00382–009–0558-z.

Johannessen OM (1986) Brief overview of the physical oceanography. In: Hurdle BG (ed.) The Nordic Seas. New York: Springer, pp. 103–127.

Kim JH, Peterse F, Willmott V, Kristensen DK, Baas M, Schouten S, Sinninghe Damsté JS (2011) Large ancient organic matter contributions to Arctic marine sediments (Svalbard). Limnology and Oceanography 56: 1463–1474, DOI: 10.4319/lo.2011.56.4.1463.

Kim JH, Schouten S, Buscail R, Ludwig W, Bonnin J, Sinninghe Damsté JS, Bourrin F (2006) Origin and distribution of terrestrial organic matter in the NW Mediterranean (Gulf of Lions): Exploring the newly developed BIT index. Geochemistry Geophysics Geosystems 7: Q11017, DOI: 2006 10.1029/2006GC001306.

Kornilova O and Rosell-Melé A (2003) Application of microwave-assisted extraction to the analysis of biomarker climate proxies in marine sediments. Organic Geochemistry 34(11): 1517–1523, DOI: 10.1016/S0146–6380(03)00155–4.

Martínez-Garcia A, Rosell-Melé A, Geibert W, Gersonde R, Masqué P, Gaspari V, Barbante C. (2009) Links between iron supply, marine productivity, sea surface temperature, and CO_2 over the last 1.1 Ma. Paleoceanography 24(PA1207): 14, DOI: 10.1029/2008PA001657.

Norwegian Meteorological Institute (2010) Available at: http://met.no/. Accessed: 6 September 2010.

Peterse F, Kim J-H, Schouten S, Kristensen DK, Koç N, Sinninghe Damsté JS (2009) Constraints on the application of the MBT/CBT palaeothermometer at high latitude environments (Svalbard, Norway). Organic Geochemistry 40(6): 692–699, DOI: 10.1016/j.orggeochem.2009.03.004.

Peterse F, Meer J van der, Schouten S, Weijers JWH, Fierer N, Jackson RB, Kim J-H, Sinninghe Damsté JS (2012) Revised calibration of the MBT-CBT paleotemperature proxy based on branched tetraether membrane lipids in surface soils. Geochimica et Cosmochimica Acta, DOI: 10.1016/j.gca.2012.08.011.

Peterson BJ, Holmes RM, McClelland JW, Vorosmarty CJ, Lammers RB, Shiklomanov AI, Shiklomanov IA, Rahmstorf S (2002) Increasing river discharge to the Arctic Ocean. Science 298(5601): 2171–2173, DOI: 10.1126/science.1077445.

Polyak L, Alley RB, Andrews JT, Brigham-Grette J, Cronin TM, Darby DA, Dyke AS, Fitzpatrick JJ, Funder S, Holland M, Jennings AE, Miller GH, O'Regan M, Savelle J, Serreze M, St. John K, White JWC, Wolff E (2010) History of sea ice in the Arctic. Quaternary Science Reviews 29(15–16): 1757–1778, DOI: 10.1016/j.quascirev.2010.02.010.

Polyakov IV, Alexeev, VA, Bhatt US, Polyakova EI, Zhang X (2010) North Atlantic warming: Patterns of long-term trend and multidecadal variability. Climate Dynamics 34(2): 439–457, DOI: 10.1007/s00382–008–0522–3.

Polyakov AGV, Timokhov LA, Bhatt US, Colony RL, Simmons HL, Walsh D, Walsh JE, Zakharov VF. (2004) Variability of the intermediate Atlantic water of the Arctic Ocean over the last 100 years. Journal of Climate 17(23): 4485–4497, DOI: 10.1175/JCLI-3224.1.

Polyakov IV and Johnson MA (2000) Arctic decadal and interdecadal variability. Geophysical Research Letters 27(24): 4097–4100, DOI: 10.1029/2000GL011909.

Proshutinsky AY and Johnson MA (1997) Two circulation regimes of the wind-driven Arctic Ocean. Journal of Geophysical Research 102(C6): 12493–12514, DOI: 199710.1029/97JC00738.

Rosell-Mele A., Eglinton G., Pflaumann U. and Sarnthein M. (1995) Atlantic core-top calibration of the UK37 index as a sea-surface palaeotemperature indicator. Geochimica et Cosmochimica Acta 59(15): 3099–3107: doi:10.1016/0016-7037(95)00199-A.

Rudels B, Björk G, Nilsson J, Winsor P, Lake I, Nohr C (2005) The interaction between waters from the Arctic Ocean and the Nordic Seas north of Fram Strait and along the East Greenland Current: Results from the Arctic Ocean-02 Oden expedition. Journal of Marine Systems 55(1–2): 1–30, DOI: 10.1016/j.jmarsys.2004.06.008.

Schlesinger ME and Ramankutty N (1994) An oscillation in the global climate system of period 65–70 years. Nature 367(6465): 723–726, DOI: 10.1038/367723a0.

Schlitzer R (2010) Ocean Data View. Available at: http://odv.awi.de. Accessed: 6 September 2010.

Schouten S, Eldrett J, Greenwood DR, Harding I, Baas M, Sinninghe Damsté JS (2008) Onset of long-term cooling of Greenland near the Eocene-Oligocene boundary as revealed by branched tetraether lipids. Geology 36(2): 147–150, DOI: 10.1130/G24332A.1.

Sinninghe Damste JS, Rijpstra WIC, Hopmans EC, Weijers JWH, Foesel BU, Overmann J, Dedysh SN (2011) 13,16-dimethyl octacosanedioic acid (iso-diabolic acid), a common membrane-spanning lipid of acidobacteria subdivisions 1 and 3. Applied and Environmental Microbiology 77(12): 4147–4154, DOI: 10.1128/AEM.00466–11.

Slubowska MA, Koç N, Rasmussen TL, Klitgaard Kristensen D (2005) Changes in the flow of Atlantic water into the Arctic Ocean since the last deglaciation: Evidence from the northern Svalbard continental margin, 80°N. Paleoceanography 20(PA4014), DOI: 10.1029/2005PA001141.

Slubowska-Woldengen M, Rasmussen TL, Koç N, Klitgaard Kristensen D, Nilsen F, Solheim A, (2007) Advection of Atlantic water to the western and northern Svalbard shelf since 17,500 cal yr BP. Quaternary Science Reviews 26(3–4): 463–478, DOI: 10.1016/j.quascirev.2006.09.009.

Spielhagen RF, Werner K, Sørensen SA, Zamelczyk K, Kandiano E, Budeus G, Husum K, Marchitto TM, Hald M. (2011) Enhanced modern heat transfer to the Arctic by warm Atlantic water. Science 331(6016): 450–453, DOI: 10.1126/science.1197397.

Thompson DWJ and Wallace JM (1998) The Arctic oscillation signature in the wintertime geopotential height and temperature fields. Geophysical Research Letters 25(9): 1297–1300, DOI: 199810.1029/98GL00950.

Vinje T and Finnekåsa Ø (1986) The ice transport through the Fram Strait. Norsk Polarinstitutt Skrifter 186.

Walczowski W, Piechura J, Osinski R Wieckzorek P (2005) The West Spitsbergen Current volume and heat transport from synoptic observations in summer. DeepSea Research Part I: Oceanographic Research Papers 52(8): 1374–1391, DOI: 10.1016/j.dsr.2005.03.009.

Weijers J, Panoto E, van Bleijswijk J, Schouten S, Rijpstra WIC, Balk M, Stams A, Sinninghe Damste JS (2009) Constraints on the biological source(s) of the orphan branched tetraether membrane lipids. Geomicrobiology Journal 26(6): 402–414, DOI: 10.1080/01490450902937293.

Weijers JWH, Schouten S, Van den Donker JC, Hopmans EC and Sinninghe Damsté JS (2007a) Environmental controls on bacterial tetraether membrane lipid distribution in soils. Geochimica et Cosmochimica Acta 71(3): 703–713, DOI: 10.1016/j.gca.2006.10.003.

Weijers JWH, Schefuß E, Schouten S and Sinninghe Damsté J (2007b) Coupled thermal and hydrological evolution of tropical Africa over the last deglaciation. Science 315(5819): 1701–1704, DOI: 10.1126/science.1138131.

Weijers JWH, Schouten S, Sluijs A, Brinkhuis H and Sinninghe Damsté JS (2007c) Warm arctic continents during the Palaeocene-Eocene thermal maximum. Earth and Planetary Science Letters 261(1–2): 230–238, DOI: 10.1016/j.epsl.2007.06.033.

Werner K, Spielhagen RF, Bauch D, Hass HC, Kandiano E, Zamelczyk K (2011) Atlantic water advection to the eastern Fram Strait – Multiproxy evidence for late Holocene variability. Palaeogeography, Palaeoclimatology, Palaeoecology 308(3–4): 264–276, DOI: 10.1016/j.palaeo.2011.05.030.

Yamamoto M, Okino T, Sugisaki S, Sakamoto T (2008) Late Pleistocene changes in terrestrial biomarkers in sediments from the central Arctic Ocean. Organic Geochemistry 39(6): 754–763, DOI: 10.1016/j.orggeochem.2008.04.009.

CHAPTER 6

Sea ice cover and water mass variability in the Barents Sea during the last 4400 years

6.1. Abstract

The Arctic sea ice cover is an important component of the climate system as it regulates the heat exchange between the atmosphere and the ocean. The northward flowing Atlantic current brings warm and salty water to the Barents Sea and it is an important factor for regulating sea ice extent variability at multidecadal to centennial time scales. We analyzed the recently proposed IP25 proxy as well as alkenones to reconstruct past variations in sea ice cover and water mass for the last 4400 years in a marine record located in the eastern Barents Sea. A progressive decrease in $\%C_{37:4}$ from 4400 to 1700 BP together with stable and low concentrations of IP25 and alkenones indicate that during this period cold climate conditions and polar water masses influenced the eastern Barents Sea. The permanent sea ice cover edge was close to the coring site. From 1700 to 500 BP lower values of $\%C_{37:4}$, increasing values of total alkenone abundance and stable IP25 concentrations indicate a progressive transition towards an increased inflow of Atlantic water and warmer climate conditions. We propose that during this interval the sea ice cover maximum extent began to retreat. During the last 500 years we observe a pronounced increase in the IP25 abundance, $\%C_{37:4}$ values characteristic of an area partly influenced by Atlantic water mass and high alkenone concentrations. During this period there was a progressive warming and/or an increase in the transport of Atlantic Water to the Arctic probably triggering a north easterly retreat in the sea ice cover minimum extent, suggesting that the study site has probably been in the seasonal sea ice area from 1500 AD to present.

Keywords Barents Sea; Holocene; sea ice; Atlantic water; IP25; alkenones.

6.2. Introduction

During the last five decades, sea ice extent and thickness of summer circumpolar Arctic sea ice has declined abruptly (Kinnard et al., 2011), and model simulations display a late summer ice free Arctic Ocean by the end of the 21st century (Arzel et al., 2006). Arctic sea ice cover influences global climate through its role in regulating heat exchange between the ocean and the atmosphere (Divine and Dick, 2006; Polyak et al., 2010). The extent and seasonality in sea ice cover is controlled by variability in ocean and atmospheric currents, sea surface temperature (SST), and surface air temperature. The relative importance of these factors varies by location throughout the Arctic (Dyck et al., 2010).

The region of the Nordic Seas, comprising the Iceland, Greenland, Norwegian and the Barents seas is particularly important for global climate. In this region, warm and salty Atlantic water enters the Arctic Ocean mainly via the Fram Strait and the Barents Sea (Figure 6.1). The northward flowing Norwegian Atlantic Current splits into the West Spitsbergen Current and the North Cape Current. The former heads north to Svalbard and the latter heads east to the Barents Sea before entering the Arctic Ocean (Figure 6.1) (Helland-Hansen and Nansen, 1909; Rudels et al., 1999). In Chapter 5 we discussed the influence of the water inflow through the Fram Strait on Arctic and Nordic Seas oceanography and climate. In this chapter the discussion is focussed on the Barents Sea.

The Barents Sea has a seasonal ice cover with a minimum extent in September and a maximum ice extent in March/April (Arthun et al., 2012). At multidecadal time scales the sea ice variability in the Barents Sea is mainly affected by the Atlantic Water inflow (Vinje, 2001). In turn, the Atlantic inflow depends on the decadal pattern of variability of the North Atlantic Oscillation (NAO), that affects the intensity of the northward flowing Norwegian Current, and the multidecadal changes in sea surface temperature of this current which is defined as the Atlantic Multidecadal Oscillation (AMO) mode of variability (Venegas and Mysak, 2000). In the Barents Sea, changes in atmospheric circulation have a secondary role in the control of sea ice concentration and thickness (Dyck et al., 2010).

To contextualize the recent changes in sea ice we need long term, preferentially decadal resolved records, that provide a framework for a better understanding of the mechanisms regulating sea ice cover variability. As the instrumental observations are limited to the last century or even the last decades, we need to rely on proxy based estimates to obtain information on longer time scales. Here, we discuss a reconstruction of past conditions in sea ice cover and water mass variability in the eastern Barents Sea during the last 4400 years at multidecadal resolution. The aim is to contribute to decipher the natural mechanisms or modes of climate variability that triggered climatic changes in this region during the late Holocene.

6.3. Study area

The Barents Sea is a marginal sea of the Arctic Ocean. It is located north of Norway and Russia, southeast of Svalbard and west of Novaya Zemlya (Figure 6.1). The eastern Barents sea is one of the main gateways of Atlantic Waters and heat to the Arctic Ocean, where it mixes with polar waters losing most of its heat to the Arctic atmosphere (Helland-Hansen and Nansen, 1909; Rudels et al., 1999; Arthun and

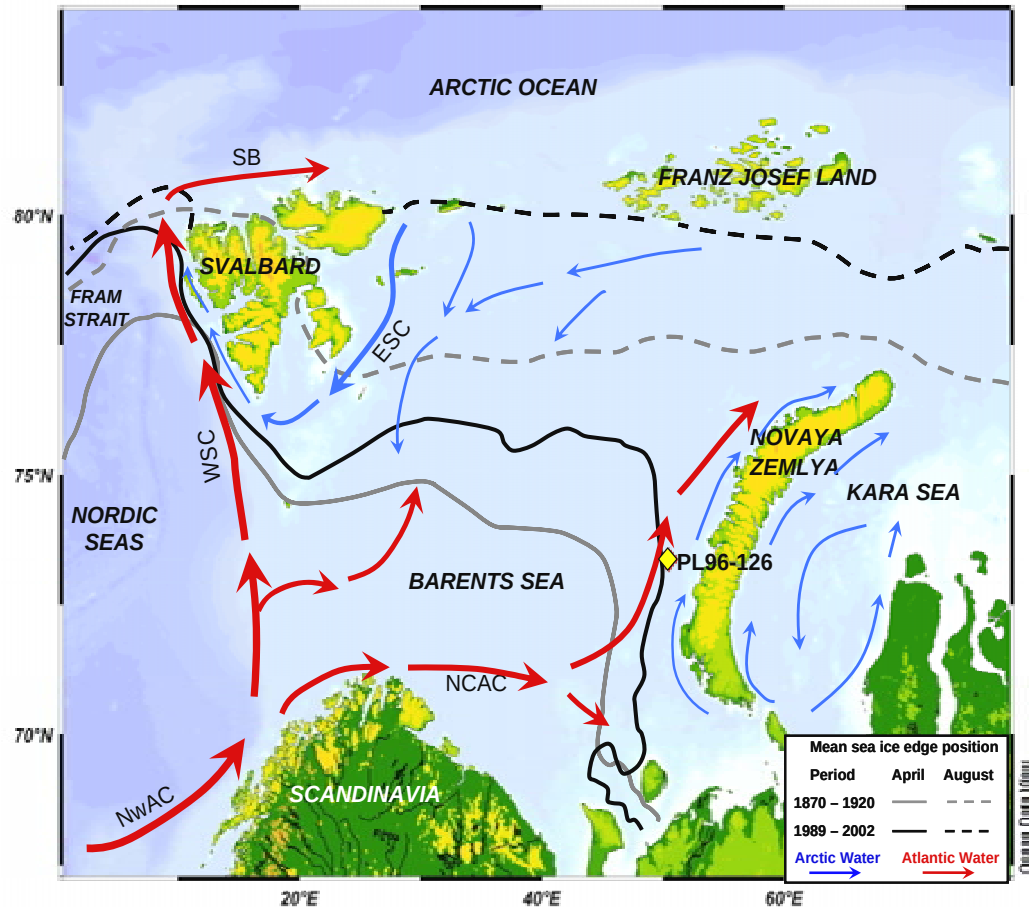

Figure 6.1. Map of the Barents Sea with present day circulation patterns, mean sea ice edge positions and core location. The pathways of Atlantic water (red) and Arctic water (blue) are shown with arrows. The main currents are labelled with abbreviations: Norwegian Atlantic Current (NwAC); North Cape current (NCaC); West Spitsbergen Current (WSC); Svalbard Branch (SB) and East Spitsbergen Current (ESC). The mean sea ice edge position for the period 1870 – 1920 (grey) and for the period 1989 – 2002 (black) are shown for April maximum sea ice extent (continuous line) and August minimum extent (dashed line). Sea ice edge position data were retrieved from the National Snow and Ice Data Center (Divine & Dick 2007). Core PL96-126 position denoted with a yellow diamond.

Schrun, 2010). The Barents Sea has seasonally variable sea ice cover conditions, with maximum sea ice extent at the end of winter, and minimum sea ice extent in summer (Divine and Dick, 2006; Polyak et al., 2010). The maximum sea ice extent (mean sea ice edge position at mid April) and the minimum sea ice extent (average position at mid August) corresponding to historic sea ice edge positions for the periods 1870-1920 and 1989-2002 are shown in Figure 6.1 (Divine and Dick, 2006).

Interannual variability in Barents Sea ice cover reflects the variability of the Atlantic inflow (Arthun et al., 2012). The site where core PL96-126 was retrieved has been in the seasonal sea ice zone at least since 1870, and it is directly influenced by relatively warm and dense Atlantic waters (Voronina et al., 2001). During the period

1966-1988, the probability of encountering the mean sea ice edge position at site PL96-126 at the end of April was about 40% (Vinje and Kvambekk, 1991). At least during this time interval, there was a northeastward increasing variability in the ice edge (Vinje and Kvambekk, 1991). These features make it an appropriate setting for investigating past variations in sea ice cover extent and variability in the inflow of Atlantic water to the Barents Sea during the last 4400 years at multidecadal resolution.

6.4. Description of samples and proxies used

Core PL96-126 was retrieved from the eastern Barents Sea with a gravity corer (Figure 6.1; 73º 37.5′ N, 50º 43.0′ E; 270 m water depth; Voronina et al., 2001). Its age model was based on three ^{14}C AMS measurements conducted in samples where there was a sufficient amount of calcareous material from benthic foraminifera to allow the analysis, as the calcium carbonate content in the core is below 2% (Table 1; Voronina et al., 2001). The core has a sedimentation rate of 60 to 120 cm Kyr^{-1} and its basal age is 4375 years BP (Voronina et al., 2001). We analyzed the whole core at 1 cm intervals to obtain a quasi-decadal resolution environmental reconstruction over the last 4400 years. The time resolution of the record is between 10 to 20 years, depending on the core depth.

Table 6.1. Age model for core PL96-126 based on AMS ^{14}C ages. A correction of 460 year was applied to account for the air-sea reservoir difference (Voronina et al., 2001).

Laboratory reference	Core depth (cm)	Material dated	^{14}C age	Corrected ^{14}C age	Calibrated year BP
AA35044	203	*Nuculoma tenuis*	2545±45	2085	2126
AA39574	294	Shell debris	3326±57	2866	3000
AA34310	353	Benthic foraminifers	4315±50	3855	4375

To reconstruct sea ice cover variability we used the recently proposed sea ice proxy IP25, which is based on the measurement of the sedimentary abundance of a single highly branched mono-unsaturated isoprenoid that is specific of sea ice diatoms (Belt et al., 2007). Although IP25 is a very novel proxy, it has already been used in several studies to reconstruct past sea ice cover variations i.e. in North Iceland sea for the last millennium (Massé et al., 2008), the Fram Strait during the Holocene and also the last 30.000 years (Müller et al., 2009, 2012), the Canadian Arctic during the Holocene (Belt et al., 2010; Vare et al., 2009) and the Barents Sea only for the last three centuries (Vare et al., 2010).

Under perennial ice cover conditions the accumulation of diatoms synthesizing IP25 and its subsequent release to the seafloor is significantly reduced, mainly because of limited light conditions (Belt et al., 2007). In 2011, Müller et al. proposed that a way to distinguish between open water and permanent sea ice cover conditions could be to compare the IP25 abundance with that of a phytoplankton productivity marker (Figure 6.2). Under conditions permanently devoid of sea-ice, no IP25 is detected in sediments and high abundances of the phytoplankton marker are observed. When closer to the sea ice edge, high abundances of both the IP25 and the productivity marker are detected, while under a permanent sea ice cover there is a quasi negligible flux of both IP25 and the generic productivity marker (Müller et al., 2011). The reliability of this interpretation scenario depends on the assumption that export and preservation controls on the biomarkers are similar.

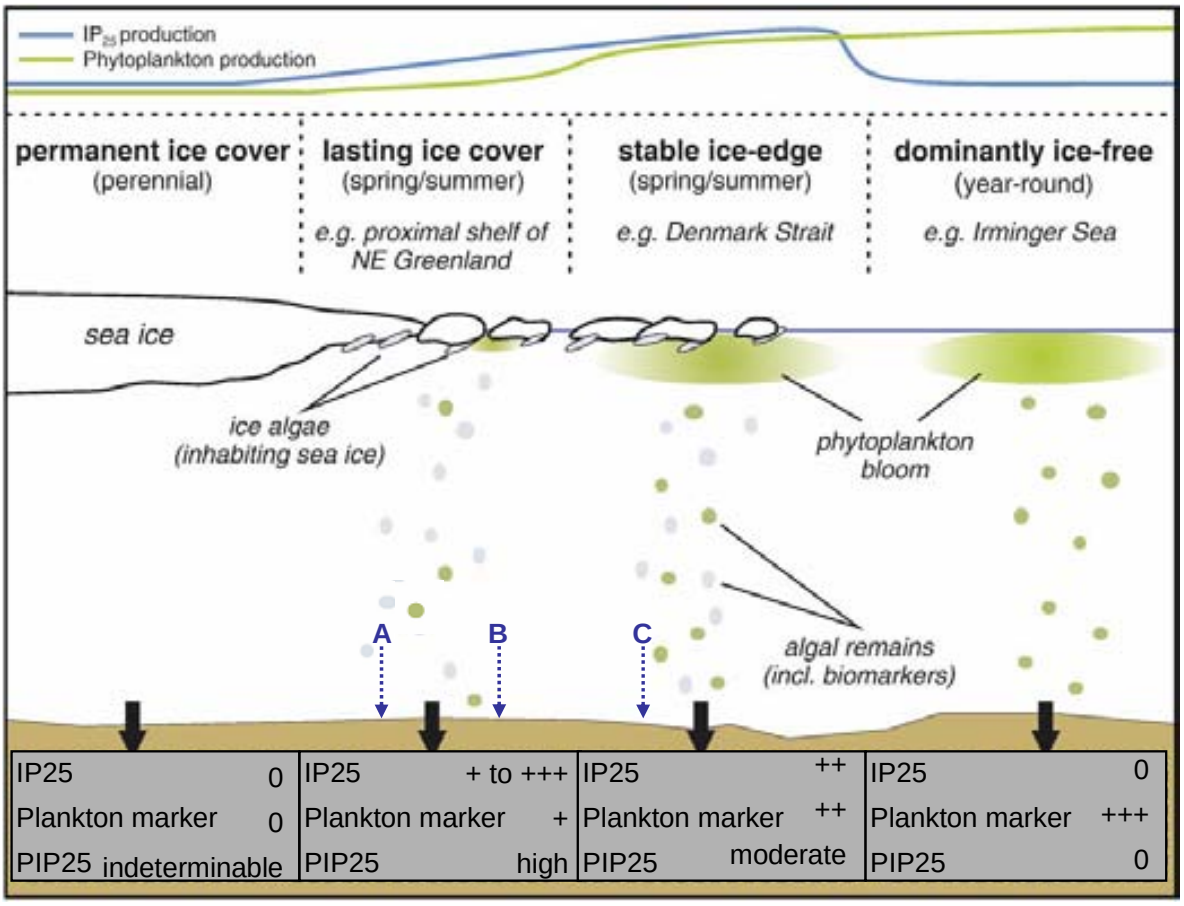

Figure 6.2. Simplified scheme of phytoplankton and ice algae productivity conditions in high latitude Northern Hemisphere seas during an annual cycle. In permanent sea ice cover conditions IP25 and the plankton marker can not be detected in the sediment. In the area with seasonal sea ice cover conditions, the IP25 and the plankton marker have variable abundances. When the area is devoid of sea ice cover year-round, only the phytoplankton marker will be detected in the marine sedimentary core and no IP25 can be detected as it is specific of sea ice diatoms. The scheme is modified after Müller et al. (2011). The blue arrows indicate the different sea ice cover conditions over the coring site discussed in the text.

We analyzed alkenones to estimate past variations in SST, polar water extent as well as export productivity of the algae responsible for their biosynthesis. Alkenones are lipids synthesized by haptophyte algae some of which are coccolithophorids (Volkman et al., 1980). To estimate SST we used the $U^{K'}_{37}$ index (Prahl and Wakeham, 1987) calculated from the relative concentration in sediments of the di- and tri-unsaturated C_{37} alkenones ($C_{37:2}$, $C_{37:3}$) through the equation $U^{K'}_{37} = (C_{37:2})/(C_{37:2}+C_{37:3})$. The $U^{K'}_{37}$ was converted to temperature through the regression SST (^{o}C) = ($U^{K'}_{37}$ – 0.044) /0.033 from a core-top Global Ocean calibration (Müller et al., 1998). The percentage of the $C_{37:4}$ alkenone to the total abundance of C_{37} alkenones ($\%C_{37:4} = (C_{37:4}/(C_{37:2}+C_{37:3}+C_{37:4}))\cdot 100$) in the record is used to infer variations in the extent of polar and subpolar conditions through time (Bendle et al., 2005). In the Barents Sea the highest alkenone fluxes were detected during summer months (Thomsen et al., 1998). The total concentration of alkenones is used to track changes in export paleoproductivity and as a complementary plankton marker for interpreting IP25 abundance variability downcore.

To determine if changes in the input or preservation of organic matter could control biomarker abundances through time, we analyzed the organic carbon content, the C/N ratio and the isotope abundance ratios of carbon (δ^{13}Corg) and of nitrogen (δ^{15}N) at 10 cm intervals in core PL96-126.

6.5. Results and discussion

6.5.1 Sea ice cover and water mass variability

Sea ice cover influenced the coring site during the last 4400 years, as IP25 could be detected throughout the record (Figure 6.3D). Downcore IP25 values range between 0.2 and 2.4 ng gdw^{-1} and have an average value of 0.8 ng gdw^{-1}. The most obvious change in the whole record occurred during the last 500 years when there was a prominent and continued increase in the flux of IP25 to the seafloor reaching the highest levels of the last 4400 years.

The concentration of alkenones is 1.8 μg gdw^{-1} on average through the record (Figure 6.3C). Two major periods can be distinguished; (I) prior to ca. 1700 BP (~300 AD) characterized by lower abundance of alkenones, with most of the data points below the mean value of the whole record; and (II) after 1700 BP (~300 AD) where the concentration of alkenones is higher and most of the data points are above the average concentration value. This indicates an increase in export productivity of haptophyte algae responsible for alkenone synthesis mainly during summer. Alkenones have been

found in suspended matter from the Greenland Sea in conditions of up to 80% sea ice cover. Although in this situation the absolute amounts were very low compared to concentrations in Atlantic water masses (Bendle and Rosell Melé, 2004).

The SST estimated with the $U^{K'}_{37}$ index averages 7 ^{o}C and shows some oscillations through the core (Figure 6.3B). Rosell-Melé (1998) established an approximate threshold value for $\%C_{37:4}$ (5%) to set an indicative boundary from which caution is needed to interpret $U^{K'}_{37}$ absolute SST estimates. In some settings of the Nordic Seas the relationship of $U^{K'}_{37}$ with SST is no longer linear when high values of $\%C_{37:4}$ alkenone are present (Rosell-Melé, 1998). The $\%C_{37:4}$ values in the earliest part of our record are very high (around 50%) and decrease significantly towards the present, reaching average values around 10% (Figure 6.3A). The $\%C_{37:4}$ found in our analyses of alkenones in the Barents Sea record is comparatively high and above the threshold value. Therefore, caution is due at the interpretation of the absolute values of SST in our record.

There is a strong correlation between values of $\%C_{37:4}$ and the water mass type in the Nordic Seas (Bendle et al., 2005). High values of $\%C_{37:4}$ (40-77%) are indicative of polar waters, low values (0-3%) characterize Atlantic waters and low to intermediate values (0-28%) are found in Arctic and Norwegian coastal waters where both water mass types are mixed (Bendle et al., 2005). The absolute concentrations of alkenones are very low in polar waters compared to Arctic and Atlantic water masses where they increase (Bendle et al., 2005). Hence, comparatively high downcore alkenone abundances and low $\%C_{37:4}$ may indicate an increased influence of Atlantic Water, whereas comparatively low alkenone abundances and high $\%C_{37:4}$ would indicate increased influence of polar waters mixed with Atlantic Water. In our record the values of $\%C_{37:4}$ decrease from 50 to 10%, and the average abundance of alkenones increases progressively from 4400 years BP towards present. Based on the downcore variability of $\%C_{37:4}$ and on the concentration of alkenones, we consider that during the last 4400 years there was a progressive transition from an environment influenced by predominantly polar water mass to an environment progressively more influenced by Atlantic water mass.

From 4400 to 1700 BP, steryl alkyl ethers were found to coelute with alkenones in the gas chromatographic analysis. Such compounds have been suggested to be synthesized exclusively by diatoms, however they have yet to be described in diatoms or in any other putative source organism (Brassell, 2009). Another eukaryotic phytoplankton or zooplankton origin seems plausible too (Brassell, 2009). Environmental conditions leading to production of such compounds, have been proposed to be limited to Tertiary/Quaternary sediments deposited in marine

environments, generally characterized by cool waters and/or seasonal upwelling (Brassell, 2009).

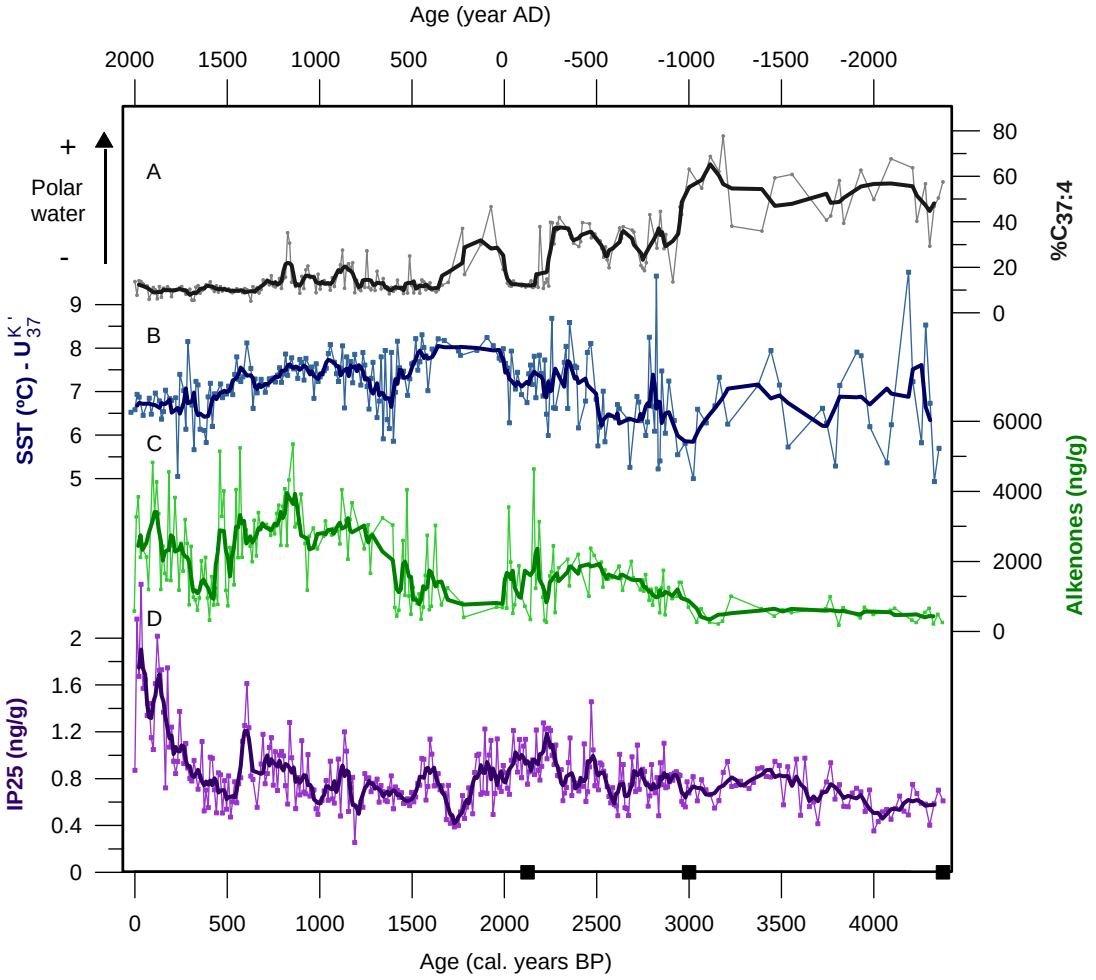

Figure 6.3. Paleoclimatic reconstruction in core PL96-126 for the last 4400 years BP. (A) percentage of alkenone $C_{37:4}$. (B) Sea surface temperature estimated from $U^{K'}_{37}$. (C) Total alkenone concentration. (D) Abundance of IP25. Data are shown as single data points (linked with a thin line) and smoothed with a five-point running mean average (thick line). The black squares in age axis depict the ^{14}C AMS measurements. The x-axis below gives age in years BP as given in the age model by Voronina et al. (2001). The above x-axis gives age in years AD considering year 0 BP the year 1996 AD.

The organic carbon content does not show significant variations downcore as it has an average value of 2.5%, and ranges between 2% and 3% except for one data point with a value of 1.5% (Figure 6.4B). Therefore, the relative variability of the organic biomarker concentrations discussed here (IP25, alkenones) were unlikely influenced by changes in total organic carbon or preservation/degradation of organic matter downcore. The C/N ratio does not show major changes and ranges between 9 and 10 indicating that the organic matter was mainly originated from marine algae (Figure

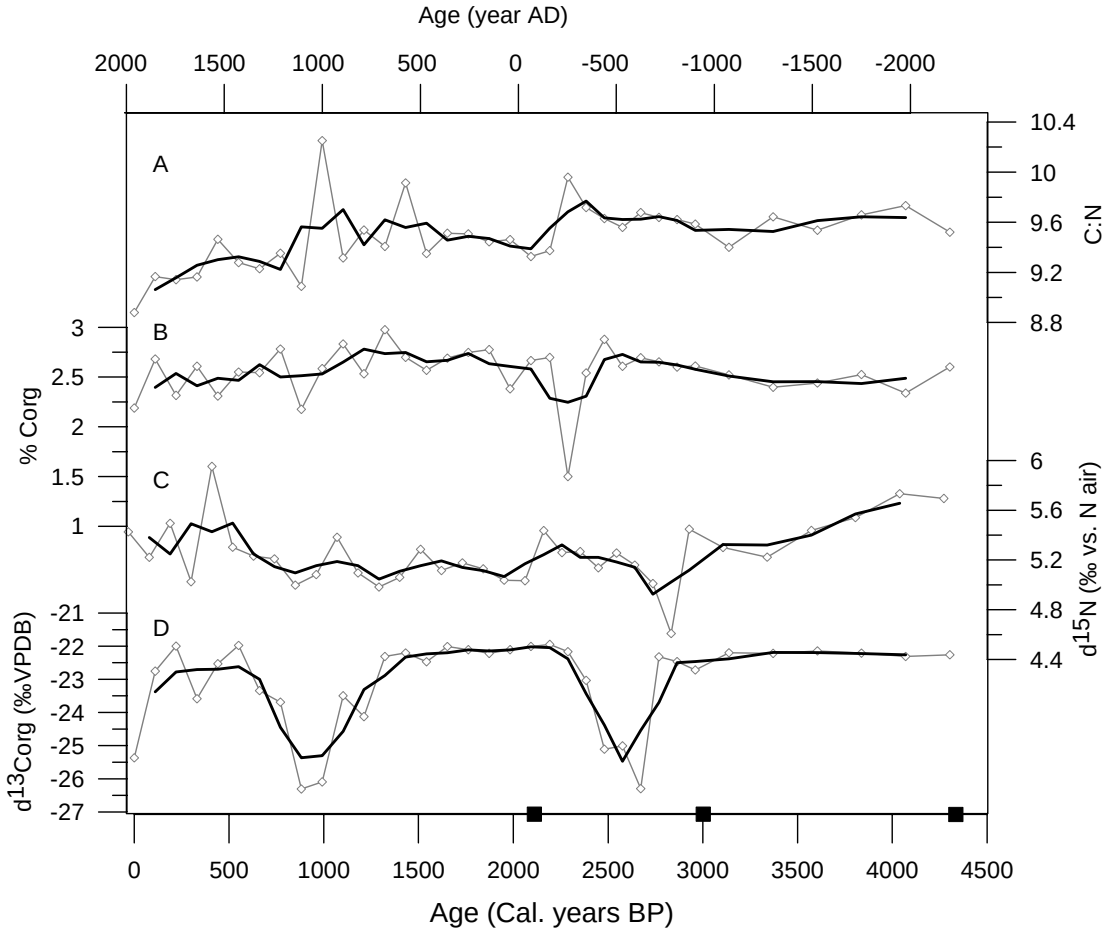

Figure 6.4. Carbon and nitrogen abundances and stable isotopes analyzed in core PL96-126 at low resolution (every 10 cm). (A) Carbon vs nitrogen ratio (C/N) (B) Percentage of organic carbon (%Corg) (C) $\delta^{15}N$ (‰VPDB) (D) $\delta^{13}Corg$ (‰VPDB). The black squares in age axis depict the ^{14}C AMS measurements Voronina et al. (2001).

6.4A; Meyers, 1994). Therefore, marine productivity is high in this area. The $\delta^{13}Corg$ (‰VPDB) data show values around -23‰ through the last 4400 years corroborating that the signal comes from marine phytoplankton (Figure 6.4D; Meyers, 1994). However, there are two short periods at 2700 – 2400 BP and 1000 – 800 BP with values down to -26‰. Terrestrial organic carbon from C3 plants has distinctive $\delta^{13}Corg$ values between -25.5 and -29.3‰ (Winkelmann and Knies, 2005). These two periods likely reflect a mixture of planktonic organic matter and terrestrial organic material with isotopically lighter values as terrestrial organic carbon from C3 plants has $\delta^{13}Corg$ values between -25.5 and -29.3‰ (Schubert and Calvert, 2001). Finally the $\delta^{15}N$ (‰VPDB) show an average value of 5.2 and range between 4.6 and 6 ‰ with no clear trend of variability (Figure 6.4C). These values reflect the inflow of warm and relatively nitrate rich surface waters from the North Atlantic water current inflow to the eastern

Barents Sea (Schubert and Calvert, 2001). Isotopically similar values between 4.6 and 7.4 ‰ were found in surface sediments from the Svalbard region, reflecting the inflow of Atlantic Water via the West Spitsbergen Current (Schubert and Calvert, 2001).

From our results, we interpret that during the period from ca. 4400 BP to 1700 BP, the eastern Barents Sea was characterized by cold environmental conditions. Polar water masses influenced the area (high $\%C_{37:4}$), there was low summer productivity (low abundance of alkenones), cool waters (production of steryl alkyl ethers) and the limit of the minimum extent of the sea ice cover was probably close to the coring site (nearby sea ice melting indicated by presence of IP25). The sea ice cover conditions over the coring site during this period is illustrated in Figure 6.2 (blue arrow, position A). A transition towards warmer conditions took place from 1700 to 500 BP (300 to 1500 AD) resulting in increased productivity of alkenones and progressively decreased values of $\%C_{37:4}$. We suggest that during this period there was a progressive increase in the Atlantic water inflow. The abundance of IP25 does not show an increase as marked as that of the alkenones. This suggests that warmer oceanic conditions allowed increased alkenone productivity in summer open water conditions and that the sea ice edge minimum extent in summer started to retreat (Figure 6.2, blue arrow, position B). Finally, during the last ~500 years the values of $\%C_{37:4}$ decrease to 10 % indicating an increased influence of Atlantic water mass and we observe a pronounced increase in IP25 and high abundance of alkenones. We suggest that during this period there was a progressive north easterly retreat and enhanced melting of the ice edge minimum extent (Figure 6.2, blue arrow, position C). The study area remained under the seasonal sea ice zone, and the sea ice cover extended progressively during winter and melted over the study area during summer. This situation allowed an increased productivity of alkenones and a progressive increase in the accumulated flux of IP25 in the seafloor.

Shapiro et al. (2003) developed a continuous record for April ice edge position in the Barents Sea for the period 1850 – 2001, based on observational data sets. They concluded that there was a north-eastward retreat in the mean ice edge position from 1850 to present. They found that the largest variability of the sea ice edge position occurred in the area influenced by the warm Atlantic water inflow (Shapiro et al. 2003). Divine & Dick (2006) analyzed the historical variability of the sea ice edge position over the Nordic Seas from April through August for the period 1750 – 2002. They found oscillations in ice cover with periods of about 60 to 80 years – more prominent in the Greenland Sea - and 20 to 30 years – dominant in the Barents Sea – both superimposed on a general negative trend (Divine and Dick, 2006). They associated such multidecadal oscillations with the low frequency oscillation in the Arctic and also with the North Atlantic thermohaline circulation variability (Divine and Dick, 2006).

Taking into account the findings by Shapiro et al. (2003) and Divine and Dick et al. (2006) we interpret from our results that there was a progressive north-eastward retreat of the sea ice cover in the eastern Barents Sea mainly triggered by an enhancement in the heat transport carried with the North Atlantic Current, which may have started before than observed in the instrumental record, about 500 years ago. Based on these findings we suggest that the coring site remained in the area of seasonal sea ice cover conditions with increasing seasonal melting from about ~1500 AD to present. The exactitude of this date is limited by the constraints of the age model in core PL96-126.

6.5.2 Applying a quantitative approach for reconstructing sea ice cover conditions

In an attempt to develop a tool for reconstructing sea ice cover conditions quantitatively, Müller et al. (2011) analyzed IP25 and open water phytoplankton derived biomarkers (brassicasterol and dinosterol) in surface sediments from the northern North Atlantic and combined them (Müller et al., 2011). The phytoplankton marker-IP25 index (PIP25) can be useful to avoid over- or underestimating sea ice cover conditions (Müller et al., 2011).

The PIP25 index was proposed by (Müller et al., 2011) as:

PIP25 = IP25 /(IP25 +(phytoplankton marker * C))

Where "IP25" and "phytoplankton marker" are given in their respective concentrations. Accounting for a possible significant concentration difference between IP25 and the phytoplankton marker, a concentration balance factor between the two markers is taken into account as follows:

C = mean IP25 concentration/mean phytoplankton marker concentration

Müller et al. (2011) calibrated the PIP25 index in surface sediments to modern sea ice coverage satellite data in the Atlantic Arctic (Fram Strait) obtaining a good correlation (R^2 = 0.74). The same approach was applied to surface sediments from the Barents Sea obtaining a weaker correlation (R^2 = 0.57; Navarro-Rodriguez et al., 2012). Low values of PIP25 (below 0.2) would stand for ice free conditions; intermediate values (0.2 - 0.5) for variable or less sea ice cover; high values (0.5 - 0.75) would be indicative of a marginal ice zone and finally the highest values (0.75 – 1) would indicate perennial sea ice cover (Müller et al., 2011).

Here we used the concentration of alkenones as a phytoplankton marker for estimating the PIP25 index (Figure 6.5) with the aim to compare the resulting values with the paleoclimate interpretation based on the individual downcore variability of various proxies (section 6.5.1, Figure 6.4). We consider the qualitative variability of the PIP25 index in terms of high, intermediate or low values. The PIP25 index shows high frequency variability at decadal to multidecadal time scales in our core. High average PIP25 values were observed during the period 4400 to 1700 BP which is consistent with our interpretation of a perennial sea ice cover in the eastern Barents Sea and generally colder climate conditions. For the period 1700 – 500 BP intermediate to low average PIP25 values would indicate seasonal sea ice cover conditions. However, from the individual proxy trends of variability (Figure 6.3), we suggest that there was a progressive increase in the influence of Atlantic Water and that the summer (August) sea ice edge started to retreat. During the last 500 years there is a return to intermediate to high PIP25 values that could be indicative of both perennial sea ice or a seasonal sea ice zone. However based on the individual proxy variability trends, we suggest that there was a progressive retreat in the August (annual minimum) sea ice cover, an increased Atlantic water mass influence, and that the coring site was in the seasonal sea ice zone.

At this stage, we consider that it is more accurate to interpret the individual downcore variability of IP25 together with the downcore variability of complementary proxies. The PIP25 index alone can give place to ambiguous interpretation, and should be only used in regions where high correlations with satellite derived sea ice concentrations were found. In fact, the application of the PIP25 to a set of cores located east and west of the Fram Strait showed that similar values of PIP25 could be obtained if both the phytoplankton marker and IP25 were high (representing sea ice edge conditions), or when they were low (indicating an extended ice cover) (Müller et al., 2012). For this reason they recommended comparing such estimates with individual IP25 and phytoplankton marker changes downcore and use the PIP25 only for complementary information (Müller et al., 2011; 2012). The same conclusions were reached for the Barents Sea regarding PIP25 as the agreement between this proxy and the satellite derived mean spring sea ice concentrations was found to be quite variable (Navarro-Rodriguez et al., 2012).

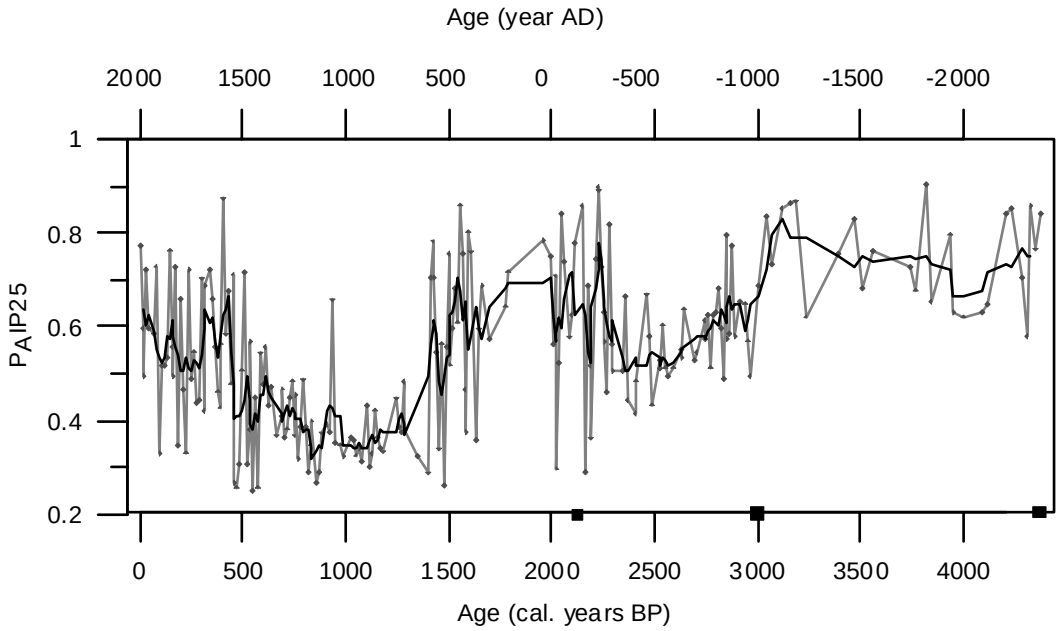

Figure 6.5. Application of the phytoplankton IP25 index, calculated with the abundance of alkenones in core PL96-126 (P_AIP25). Data is shown as individual data points (thin grey line) and smoothed 5-point running mean average (thick black line). The black squares in age axis depict the ^{14}C AMS measurements (Voronina et al., 2001).

6.5.3 Comparison with previous studies

6.5.3.1 Barents Sea

Core PL96-126 was previously studied by Voronina et al. (2001). They determined past variations in sea surface conditions through the analysis of dinocyst assemblages at an interval of one sample every 10 cm, obtaining a century scale resolution. In our study we analyzed the whole core at 1 cm interval, obtaining a multidecadal scale resolution. Voronina and co-workers also analyzed a core located further south spanning 8.8 Kyr. They found high variability in the duration of the ice cover through the time, suggesting that ice cover developed in average for 2 – 3 months year^{-1}, with periods of more extensive sea ice cover up to 6 months year^{-1} and lower temperature and salinity (Voronina et al., 2001). In general, in the two cores studied they found a colder climate starting about 4 – 5 Kyr ago, characterized by generally lower temperatures together with some cooling pulses at 1.5 – 1 Kyr intervals, possibly linked to a decrease in Atlantic water inflow to the area. They suggested that the colder climate could have been accompanied by a reduced atmospheric transport from the North Atlantic to Eurasia. The Atlantic water drift would have been reduced, allowing winter sea ice cover to expand southwards (Voronina et al. 2001 and references therein). This is partly in agreement with our

dataset where we suggest colder conditions influenced the region from 4.4 to 1.7 Kyr ago.

The IP25 biomarker was previously applied in the Barents Sea in three box cores located in the north, southeast and southwest of the area, spanning the last 300-500 years (Vare et al., 2010). From these records it was argued that ice free conditions in the southwest Barents Sea prevailed during the last 300 years, in contrast with variable spring sea ice cover in the north and southeast region (Vare et al., 2010). They found their results consistent with previous studies derived from observational records of the position of the sea ice edge (Divine and Dick, 2006; Shapiro et al., 2003). One of the three cores that they analyzed is located in the southeast Barents Sea (BASICC 43, 72º 32.31N, 45º 44.27E) relatively close to core PL96-126 (73º37.5'N, 50º43.0'E). The normalized IP25 flux from BASICC 43 core (Vare et al., 2010) increases from 1700-1900AD, and during the subsequent 100 years, decreases towards present. In core PL96-126, IP25 abundance also increases towards present, consistent with the results from Vare et al., 2010. They also analyzed the %Corg and the C/N ratios in order to see if the changes in IP25 were influenced by organic matter changes. In all the three cores, they found C/N ratios around 7-9, indicative of marine source for organic matter and consistent with previous analysis of surface sediment in this region (Vare et al. 2010 and references therein). The organic carbon content values were below 3% in all cores and did not show major changes downcore, also comparable to previous studies (Vare et al. 2010 and references therein). These results are also comparable with our results in the most modern part of PL96-126.

A study conducted in the southwestern Barents Sea covering the entire Holocene at high resolution with a multiproxy approach (Risebrobakken et al., 2010) revealed warm early Holocene summer temperatures with a maximum 8.600 years BP that continued with a progressive cooling with minimum temperatures occurring between 2.400 – 1.100 years BP. They reported highly variable conditions during the late Holocene, with temperature variability of larger amplitude than those obtained from modern instrumental measurements (Risebrobakken et al., 2010).

Ślubowska-Woldengen et al. (2008) reconstructed ocean circulation changes during the last 16.000 – 2.000 years BP, from compiling 12 previously published records of the distribution of benthic foraminifera fauna and ice rafted debris. The records were located in the Nordic and Barents Seas, and in sites that at present are influenced by the inflow of Atlantic water (Ślubowska-Woldengen et al., 2008). For the period 4.000 – 2.000 years BP, in the cores around the Svalbard margin and in the Barents Sea, they found that this period was characterized by a return of polar conditions with colder and fresher bottom water masses, a reduction in the inflow of Atlantic water and

increased sea ice cover extent in comparison to the early Holocene (Ślubowska-Woldengen et al., 2008).

For the most recent time span, we can compare our results with those from ilson et al. (2011). They reconstructed climatic changes analyzing benthic foraminifera in a record located in the western Barents Sea spanning the last 1.400 years. They found an overall warming trend of about 2.6 ^{o}C in the bottom waters, of which 1 ^{o}C occurred only during the last 100 years. Such warming is accompanied by an increase in the foraminifera flux, a progressive depletion of δ^{13}C and changes in benthic foraminifera species, overall indicating a progressive increase in productivity which was more pronounced in the last 200 years. These results are coherent with our results from PL96-126 as there is an increase in productivity and a progressive warming towards present.

Past variability in the temperature and inflow of the western branch of the Atlantic Water inflow to the Arctic (the West Spitsbergen Current) shows warming trends comparable to our findings in the eastern Barents Sea. For instance, a multiproxy study from a marine sedimentary core located at the northern Svalbard continental margin and directly influenced by the Svalbard Branch of the West Spitsbergen Current, revealed that Atlantic water inflow weakened progressively during the mid-Holocene. From 4500 to 1100 years BP the inflow was particularly weak (Slubowska et al., 2005). After this period of cool conditions, Atlantic inflow increased during the last 1000 years (Slubowska et al., 2005). The air and sea surface temperature records reconstructed from a marine sedimentary core located in the western Svalbard continental margin and directly affected by the West Spitsbergen current also show an increase in the inflow of Atlantic Water starting 1000 years ago that was intensified during the last 500 years (Chapter 5, Rueda et al, 2013). In the same marine sedimentary core, a progressive warming of the subsurface Atlantic Water started 500 years ago and was intensified during the last 120 years (Spielhagen et al., 2011). In addition, an air temperature record obtained from lacustrine sequences from Western Svalbard showed a gradual air temperature increase over West Spitsbergen from AD 1600 to 1900 (D'Andrea et al., 2012). The conclusions from these studies fit well with our interpretation from core PL96-126 in the Barents Sea, located in the eastern branch of the northward flowing Atlantic Water to the Arctic. Therefore during the last 500 years there was an enhancement of or a warming in the Atlantic Water current, and it is reflected in both of its current branches that flow to the Arctic: the West Spitsbergen Current keeping its track further north to Svalbard and the Norwegian Current entering the Barents Sea.

6.5.3.2 Pan-arctic sea ice reconstructions

Arctic wide compilations of reconstructed past climatic and sea ice conditions show that the major changes occurred during the last decades of the 20th century (Figure 6.6A;B) (Kaufman et al., 2009; Kinnard et al., 2011). Specifically, a synthesis of decadal resolved proxy temperature records from terrestrial sites (trees, lakes, ice) in the Arctic (poleward 60°N) shows a cooling during the last 2000 years, reversed during the 20th century with the warmest decades of the whole reconstruction occurring in the period 1950-2000 AD (Figure 6.6A; Kaufman et al., 2009). A circum-Arctic compilation of high-resolution terrestrial proxies for past extent of summer sea ice indicates that the duration and magnitude of last decades reduction in sea ice cover is unprecedented during the last 1.450 years (Figure 6.6B; Kinnard et al., 2011). It seems that in the eastern Barents Sea the sea ice retreat and the environmental warming started some centuries before - around 500 years BP - compared to the global Arctic past climatic estimations. But a progressive warming was also observed in the West Spitsbergen current during the last 500 years as discussed above. Probably the Arctic wide compilations generated until now hide such important regional variability in Arctic climate change (Blackford et al., 2012) or the temperature response to the reconstructed increase in heat transfer to the Arctic did not start until 1900 AD (D'Andrea et al., 2012).

6.5.4 Mechanisms of multidecadal to multicentennial variability in Atlantic water inflow and sea ice cover conditions

At decadal to multidecadal time scales, sea ice variability in the Barents Sea is mainly dependent on the variability of the Atlantic Water inflow and temperature, with changes in the relative mean predominant patterns of the NAO and the AMO modes of variability playing a significant role (Venegas and Mysak, 2000). During the positive signature of the NAO, the North Atlantic storm track penetrates deeper in the eastern Arctic, weakening the Arctic High. The Icelandic low deepens, enhancing the southerly and the northerly winds near Scandinavia and along Greenland's east coast respectively (Deser et al., 2000; Dyck et al., 2010). Such conditions profoundly influence local winter sea ice conditions in the Barents Sea. Therefore during a positive mode of the NAO there is less winter sea ice in the Barents Sea, due to an enhanced exchange between the northward flowing relatively warm and saline Atlantic water with the cold and fresh Arctic water taking place in the Barents Sea (Venegas and Mysak, 2000). On the other hand, in the negative phase of the NAO the central Arctic is characterised by a strong and persistent Arctic High, the Atlantic water does not extend so far north

and the formation of sea ice during winter is enhanced in the Barents Sea (Deser et al., 2000; Dyck et al., 2010).

At multidecadal to multicentennial time scales, sea ice variability in the Barents Sea is generally controlled by changes in the thermohaline circulation or meridional overturning circulation (Jungclaus et al., 2005). The AMO mode of variability dominated subsurface water temperature changes from 1900 to 2006 AD in the Barents Sea (Levitus et al., 2009). Sea ice decrease in the Barents Sea may be due to heating from the subsurface of the water column, therefore an enhanced inflow in the Atlantic Water current can contribute to sea ice cover declining (Levitus et al., 2009). The climatic variation in the Barents Sea region is affected by the large scale climatic fluctuations covering the entire North Atlantic Ocean (Levitus et al., 2009; Skagseth et al., 2008). Such link between climate processes and sea ice based on instrumental observations can be extended further back in time. Macias Fauria et al. (2009) reconstructed maximum sea ice extent for the Western Nordic Seas during the period 1200-1997 AD, combining a northern Finland regional tree-ring chronology with an ice core in Svalbard. Variability in decadal to centennial sea ice extent was dominated by oscillations associated with decadal variations in the NAO and also multidecadal low frequency oscillations at a 50-120 year timescale that could be related to the AMO mode of variability.

Climatic features related to the ocean – ice – atmosphere system such as the thermohaline circulation, the inflow of Atlantic water to the Arctic and the NAO or the AMO modes of climate variability are intimately linked to sea ice variability in the Barents Sea. Therefore the biomarker analysis from core PL96-126 can provide information on past variations in the long term mechanisms of climate variability in the Barents Sea for the last 4400 years. The variability in the abundance of IP25 was related to changes in the phases of the NAO in a study conducted in the Fram Strait (Müller et al., 2012). Elevated IP25 and phytoplankton concentrations were associated to a relative predominance of a positive NAO index, whereas periods with decreased amounts of both IP25 and phytoplankton markers were associated with relative dominance of a negative NAO index (Müller et al., 2012).

From our record we interpret that a relative dominance of the negative phases of the NAO or the AMO modes of climate variability might have prevailed from 4400 to 1700 years BP at multidecadal to multicentennial time scales. The inflow or the temperature of the North Atlantic Current was reduced and cold, predominantly polar water masses dominated in the eastern Barents Sea. The maximum sea ice edge was extended to the south. This interpretation fits with a gradual transition towards a

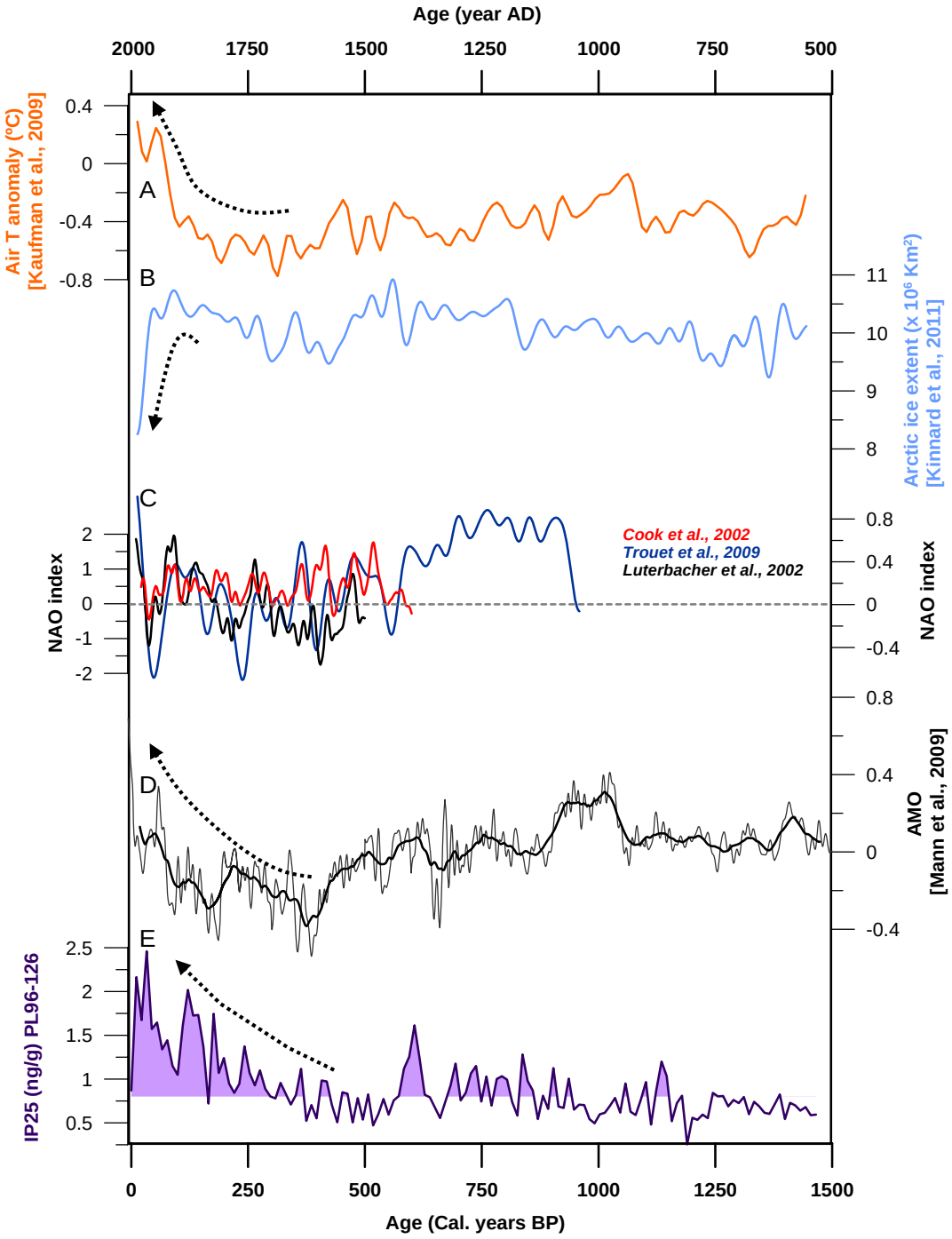

Figure 6.6. Comparison between IP25 concentration in core PL96-126 and other reconstructions. (A) Arctic surface air temperature anomaly (orange; Kaufman et al., 2009). (B) Arctic sea ice cover extent for late summer, forty-year smoothed (blue; Kinnard et al., 2011). (C) Various NAO index reconstructions. Right y-axis; Cook et al., 2002 (red) and Luterbacher et al. 2002 (black). The data is standardized relative to 1961-1990, smoothed with 30 year Gaussian filter (both data taken from Jones et al., 2001). Left y-axis; NAO index from Trouet et al., 2009 (black) smoothed with 30-year spline and normalized to 1500-1983 period. (D) Atlantic Multidecadal Oscillation (AMO) as variability in SST over the North Atlantic region and 51 year running mean average (thick black line; Mann et al., 2009) (E) IP25 in core PL96-126 from the Barents Sea. The filled area indicates the values exceeding the average value for the whole reconstruction.

relative dominance of the negative phase of the NAO as suggested to occur in the Nordic Seas after 4000 years BP (Andersen et al., 2004).

Between 1700 and 500 BP a transition towards a less cold environment started. Probably the inflow of warm Atlantic water reached further north because the pressure differences characterizing the NAO mode of climate variability were variable. Alternating modes of positive and negative phases of the NAO or the AMO may have been frequent from 1700 to 500 BP. For this period, we can compare our results with a NAO index reconstruction spanning the last 1000 years (Figure 6.6C; blue; Trouet et al., 2009). A mean relative positive phase of the NAO index prevailed from 1000 to 600 BP, which the authors attributed to the Medieval Climate Anomaly, a period characterized by warmer than average conditions in some regions (Trouet et al., 2009). A reconstruction of the AMO spanning the last 1500 years described as SST averaged over the North Atlantic Ocean is shown in Figure 6.6D (Mann et al., 2009). During the period 1500 – 500 BP alternating modes of positive and negative SST anomalies at multidecadal time scales are observed. A long term decrease in SST is observed at multicentennial time scales.

During the last 500 years there was an increase in the transport and/or temperature of the Atlantic water current as indicated by progressively increased influence of Atlantic water mass in the study area. This was probably triggered by more frequent periods with positive NAO phases, and/or a relative dominance of a positive AMO mode of climate variability that led to a reduced winter sea ice cover and to an increase in seasonality of sea ice cover over the study area. During this period, the winter maximum sea ice edge position would have retreated north-eastwards due to the influence of the high pressure system enhancing the winds and the transport of the North Atlantic water current further north and/or by increasing temperatures of the North Atlantic current. In summer, seasonal sea ice cover melting would facilitate the delivery of IP25 to the seafloor and in open water conditions high abundances of alkenones were synthesized. In fact the available NAO reconstructions covering the last ~600 years (Cook et al., 2002) and the last ~400 years (Luterbacher et al., 2001) show several periods with positive NAO conditions (Figure 6.6C, threshold limit for positive index denoted with grey dashed line). The observed 20th century trend towards more positive NAO conditions may have occurred several times since 1500 AD (Jones et al., 2001). At multidecadal to multicentennial time the reconstruction of the AMO mode of variability shows a progressive increase in the SST anomaly during the last 400 years that was more accentuated during the last 200 years (Mann et al. 2009; Figure 6.6D). The relative predominance of more frequent positive states of the AMO and the NAO modes of climate variability are important factors to account for

the northwards retreat of the minimum extent of the sea ice cover in the eastern Barents Sea during the last 500 years.

6.6. Conclusions

Past variations in sea ice cover extent, water mass variability and export productivity were reconstructed in the eastern Barents Sea for the last 4400 years. During the last 4400 years there was a progressive transition from predominantly cold polar water mass conditions towards relatively warm Atlantic water mass influence. From 4400 to 1700 BP a high amount of polar water mass and a southwards extended limit of the minimum extent of the sea ice cover characterized the region. Probably a predominant negative state of the NAO and/or the AMO modes of climate variability prevailed during this period. Between 1700 and 500 BP (300 and 1500 AD) there was a transition period towards warmer environmental conditions. There was a progressive increase in the Atlantic water mass influence and the minimum extent of the sea ice cover began to retreat to the northeast. During this period alternating phases of the NAO and the AMO modes of climate variability were frequent. During the last 500 years there was an increase in the temperature and/or in the inflow of Atlantic water to the Arctic. In the Barents Sea the minimum extent of the sea ice cover retreated progressively towards the north-east and the study area remained in the seasonal sea ice zone for the last 500 years. We suggest that during the last 500 years, more periods with positive NAO and AMO conditions prevailed.

6.7. References

Andersen C, Koç N, Jennings A and Andrews JT (2004) Nonuniform response of the major surface currents in the Nordic Seas to insolation forcing: Implications for the Holocene climate variability. Paleoceanography 19(2): PA2003: doi:10.1029/2002PA000873.

Årthun M and Schrum C (2010) Ocean surface heat flux variability in the Barents Sea. Journal of Marine Systems, 83, 88–98.

Årthun M, Eldevik T,Smedsrud L, Skagseth Ø and Ingvaldsen R (2012) Quantifying the influence of Atlantic heat on Barents Sea ice variability and retreat. Journal of Climate 25, 4736-4743 doi:10.1175/JCLI-D-11-00466.1.

Arzel O, Fichefet T and Goosse H (2006) Sea ice evolution over the 20th and 21st centuries as simulated by current AOGCMs. Ocean Modelling 12(3–4): 401–415: doi:10.1016/j.ocemod.2005.08.002.

Belt ST, Massé G, Rowland SJ, Poulin M, Michel C and LeBlanc B (2007) A novel chemical fossil of palaeo sea ice: IP25. Organic Geochemistry 38(1): 16–27: doi:10.1016/j.orggeochem.2006.09.013.

Belt ST, Vare LL, Massé G, Manners HR, Price JC, MacLachlan SE, Andrews JT and Schmidt S (2010) Striking similarities in temporal changes to spring sea ice occurrence across the central Canadian Arctic Archipelago over the last 7000 years. Quaternary Science Reviews 29(25-26): 3489–3504: doi:10.1016/j.quascirev.2010.06.041.

Bendle J and Rosell-Melé A (2004) Distributions of UK37 and UK37′ in the surface waters and sediments of the Nordic Seas: Implications for paleoceanography. Geochemistry, Geophysics, Geosystems 5(11): doi:10.1029/2004GC000741.

Bendle J, Rosell-Melé A and Ziveri P (2005) Variability of unusual distributions of alkenones in the surface waters of the Nordic seas. Paleoceanography 20: PA2001: doi:200510.1029/2004PA001025.

Blackford JJ, Ryan PA, Akinyemiju B and Hughes PD (2012) Arctic climate change in recent centuries: a review. Geophysical Research Abstracts 14, EGU2012-6737.

Brassell SC (2009) Steryl ethers in a Valanginian claystone: Molecular evidence for cooler waters in the central Pacific during the Early Cretaceous? Palaeogeography, Palaeoclimatology, Palaeoecology 282(1–4): 45–57: doi:10.1016/j.palaeo.2009.08.009.

Brown T, Belt S, Philippe B, Mundy C, Massé G, Poulin M and Gosselin M (2011) Temporal and vertical variations of lipid biomarkers during a bottom ice diatom bloom in the Canadian Beaufort Sea: further evidence for the use of the IP25 biomarker as a proxy for spring Arctic sea ice. Polar Biology 34(12): 1857–1868: doi:10.1007/s00300-010-0942-5.

Cook ER, D'Arrigo RD and Mann ME (2002) A Well-Verified, Multiproxy Reconstruction of the Winter North Atlantic Oscillation Index since A.D. 1400. Journal of Climate 15(13): 1754–1764.

D'Andrea WJ, Vaillencourt DA, Balascio NL, Werner A, Roof SR, Retelle M and Bradley RS (2012) Mild Little Ice Age and unprecedented recent warmth in an 1800 year lake sediment record from Svalbard. Geology: doi:10.1130/G33365.1.

Deser C, Walsh JE and Timlin MS (2000) Arctic sea ice variability in the context of recent atmospheric circulation trends. Journal of climate 13(3): 617–633.

Divine DV and Dick C (2006) Historical variability of sea ice edge position in the Nordic Seas. Journal of Geophysical Research 111: 14 PP.: doi:200610.1029/2004JC002851.

Dyck S, Tremblay LB and de Vernal A (2010) Arctic sea-ice cover from the early Holocene: the role of atmospheric circulation patterns. Quaternary Science Reviews 29(25–26): 3457–3467: doi:10.1016/j.quascirev.2010.05.008.

Esper J, Frank D, Büntgen U, Verstege A, Luterbacher J and Xoplaki E (2007) Long-term drought severity variations in Morocco. Geophysical Research Letters 34(17): L17702: doi:10.1029/2007GL030844.

Gerdes R and Schauer U (1997) Large-scale circulation and water mass distribution in the Arctic Ocean from model results and observations. Journal of Geophysical Research 102(C4): 8467–8483: doi:10.1029/97JC00102.

Helland-Hansen B and Nansen F (1909) The Norwegian Sea; its physical oceanography based upon the Norwegian researches 1900-1904. Kristiania: Det Mallingske bogtrykkeri.

Jones PD, Osborn TJ and Briffa KR (2001) The Evolution of Climate Over the Last Millennium. Science 292(5517): 662–667: doi:10.1126/science.1059126.

Jungclaus JH, Haak H, Latif M and Mikolajewicz U (2005) Arctic–North Atlantic Interactions and Multidecadal Variability of the Meridional Overturning Circulation. Journal of Climate 18(19): 4013–4031: doi:10.1175/JCLI3462.1.

Kaufman DS, Schneider DP, McKay NP, Ammann CM, Bradley RS, Briffa KR, Miller GH, Otto-Bliesner BL, Overpeck JT, Vinther BM and Arctic Lakes 2k Project Members (2009) Recent Warming Reverses Long-Term Arctic Cooling. Science 325(5945): 1236–1239: doi:10.1126/science.1173983.

Kinnard C, Zdanowicz CM, Fisher DA, Isaksson E, Vernal A de and Thompson LG (2011) Reconstructed changes in Arctic sea ice over the past 1,450 years. Nature 479(7374): 509–512: doi:10.1038/nature10581.

Levitus S, Matishov G, Seidov D and Smolyar I (2009) Barents Sea multidecadal variability. Geophysical Research Letters 36(19): L19604: doi:10.1029/2009GL039847.

Luterbacher J, Xoplaki E, Dietrich D, Jones P, Davies T, Portis D, Gonzalez-Rouco J, Von Storch H, Gyalistras D, Casty C and Wanner H (2001) Extending North Atlantic oscillation reconstructions back to 1500. Atmosph. Sci. Lett. 2(1-4): 114–124.

Macias Fauria M, Grinsted A, Helama S, Moore J, Timonen M, Martma T, Isaksson E and Eronen M (2009) Unprecedented low twentieth century winter sea ice extent in the Western Nordic Seas since A.D. 1200. Climate Dynamics 34(6): 781–795: doi:10.1007/s00382-009-0610-z.

Mann ME, Zhang Z, Rutherford S, Bradley RS, Hughes MK, Shindell D, Ammann C, Faluvegi G and Ni F (2009) Global Signatures and Dynamical Origins of the Little Ice Age and Medieval Climate Anomaly. Science 326(5957): 1256–1260: doi:10.1126/science.1177303.

Massé G, Rowland SJ, Sicre M-A, Jacob J, Jansen E and Belt ST (2008) Abrupt climate changes for Iceland during the last millennium: Evidence from high resolution sea ice reconstructions. Earth and Planetary Science Letters 269(3-4): 565–569: doi:10.1016/j.epsl.2008.03.017.

Meyers PA (1994) Preservation of elemental and isotopic source identification of sedimentary organic matter. Chemical Geology 114, 289-302

Müller J, Masse G, Stein R and Belt ST (2009) Variability of sea-ice conditions in the Fram Strait over the past 30,000 years. Nature Geosci 2(11): 772–776: doi:10.1038/ngeo665.

Müller J, Wagner A, Fahl K, Stein R, Prange M and Lohmann G (2011) Towards quantitative sea ice reconstructions in the northern North Atlantic: A combined biomarker and numerical modelling approach. Earth and Planetary Science Letters 306(3-4): 137–148: doi:10.1016/j.epsl.2011.04.011.

Müller J, Werner K, Stein R, Fahl K, Moros M and Jansen E (2012) Holocene cooling culminates in sea ice oscillations in Fram Strait. Quaternary Science Reviews 47: 1–14: doi:10.1016/j.quascirev.2012.04.024.

Müller PJ, Kirst G, Ruhland G, von Storch I and Rosell-Melé A (1998) Calibration of the alkenone paleotemperature index U37K′ based on core-tops from the eastern South Atlantic and the global ocean (60°N-60°S). Geochimica et Cosmochimica Acta 62(10): 1757–1772: doi:10.1016/S0016-7037(98)00097-0.

Navarro-Rodriguez A, Belt ST, Knies J and Brown TA (2013) Mapping recent sea ice conditions in the Barents Sea using the proxy biomarker IP25: implications for palaeo sea ice reconstructions. Quaternary Science Reviews: doi:10.1016/j.quascirev.2012.11.025.

Polyak L, Alley RB, Andrews JT, Brigham-Grette J, Cronin TM, Darby DA, Dyke AS, Fitzpatrick JJ, Funder S, Holland M, Jennings AE, Miller GH, O'Regan M, Savelle J, Serreze M, John K, White JWC and Wolff E (2010) History of sea ice in the Arctic. Quaternary Science Reviews 29(15-16): 1757–1778: doi:10.1016/j.quascirev.2010.02.010.

Prahl FG and Wakeham SG (1987) Calibration of unsaturation patterns in long-chain ketone compositions for palaeotemperature assessment. Nature 330(6146): 367–369: doi:10.1038/330367a0.

Proctor, Baker and Barnes (2002) A three thousand year record of North Atlantic climate. Climate Dynamics 19(5): 449–454: doi:10.1007/s00382-002-0236-x.

Risebrobakken B, Moros M, Ivanova EV, Chistyakova N and Rosenberg R (2010) Climate and oceanographic variability in the SW Barents Sea during the Holocene. The Holocene 20(4): 609–621: doi:10.1177/0959683609356586.

Rosell-Melé A (1998) Interhemispheric Appraisal of the Value of Alkenone Indices as Temperature and Salinity Proxies in High-Latitude Locations. Paleoceanography 13(6): PAGES 694–703.

Rudels B, J. Friedrich H and Quadfasel D (1999) The Arctic Circumpolar Boundary Current. Deep Sea Research Part II: Topical Studies in Oceanography 46(6-7): 1023–1062: doi:10.1016/S0967-0645(99)00015-6.

Rueda G, Fietz S, Rosell-Melé A, (2013) Coupling of air and sea surface temperatures in the eastern Fram Strait during the last 2000 years. The Holocene doi: 10.1177/0959683612470177.

Schubert CJ and Calvert SE (2001) Nitrogen and carbon isotopic composition of marine and terrestrial organic matter in Arctic Ocean sediments : implications for nutrient utilization and organic matter composition. Deep-sea research. Part 1. Oceanographic research papers 48(3): 789–810.

Serreze MC, Barrett AP, Slater AG, Steele M, Zhang J and Trenberth KE (2007) The large-scale energy budget of the Arctic. Journal of Geophysical Research 112(D11): D11122: doi:10.1029/2006JD008230.

Shapiro I, Colony R and Vinje T (2003) April sea ice extent in the Barents Sea, 1850–2001. Polar Research 22(1): 5–10: doi:10.1111/j.1751-8369.2003.tb00089.x.

Skagseth O, Furevik T, Ingvaldsen R, Loeng G, Mork KA, Orvik KA and Ozhigin V (2008) Volume and heat transports to the Arctic Ocean via the Norwegian and Barents seas, in Arctic-Subarctic Ocean Fluxes, edited by R. R. Dickson, J. Meincke, and P. Rhines, pp. 45– 64, Springer, Dordrecht, Netherlands.

Slubowska MA, Koç N, Rasmussen TL and Klitgaard-Kristensen D (2005) Changes in the flow of Atlantic water into the Arctic Ocean since the last deglaciation: Evidence from the northern Svalbard continental margin, 80°N. Paleoceanography 20(PA4014): doi:10.1029/2005PA001141.

Ślubowska-Woldengen M, Koç N, Rasmussen TL, Klitgaard-Kristensen D, Hald M and Jennings AE (2008) Time-slice reconstructions of ocean circulation changes on the continental shelf in the Nordic and Barents Seas during the last 16,000 cal yr B.P. Quaternary Science Reviews 27(15–16): 1476–1492: doi:10.1016/j.quascirev.2008.04.015.

Spielhagen RF, Werner K, Sørensen SA, Zamelczyk K, Kandiano E, Budeus G, Husum K, Marchitto TM, Hald M. (2011) Enhanced modern heat transfer to the Arctic by warm Atlantic water. Science 331(6016): 450–453, DOI: 10.1126/science.1197397.

Strong C and Magnusdottir G (2011) Dependence of NAO variability on coupling with sea ice. Climate Dynamics 36(9): 1681–1689: doi:10.1007/s00382-010-0752-z.

Thomsen C, Schulz-Bull DE, Petrick G and Duinker JC (1998) Seasonal variability of the long-chain alkenone flux and the effect on the U37k'-index in the Norwegian Sea. Organic Geochemistry 28(5): 311–323: doi:10.1016/S0146-6380(98)00003-5.

Trouet V, Esper J, Graham NE, Baker A, Scourse JD and Frank DC (2009) Persistent Positive North Atlantic Oscillation Mode Dominated the Medieval Climate Anomaly. Science 324(5923): 78–80: doi:10.1126/science.1166349.

Vare LL, Massé G and Belt ST (2010) A biomarker-based reconstruction of sea ice conditions for the Barents Sea in recent centuries. The Holocene 20(4): 637 –643: doi:10.1177/0959683609355179.

Vare LL, Massé G, Gregory TR, Smart CW and Belt ST (2009) Sea ice variations in the central Canadian Arctic Archipelago during the Holocene. Quaternary Science Reviews 28(13-14): 1354–1366: doi:10.1016/j.quascirev.2009.01.013.

Venegas SA and Mysak LA (2000) Is There a Dominant Timescale of Natural Climate Variability in the Arctic? Journal of Climate 13(19): 3412–3434: doi:10.1175/1520-0442(2000)013<3412:ITADTO>2.0.CO;2.

Vinje T (2001) nomalies and trends of sea-ice extent and atmospheric circulation in the Nordic Seas during the period 1864-1998. Journal of Climate 14 (3), 255–267.

Vinje T and Kvambekk ÅS (1991) Barents Sea drift ice characteristics. Polar Research 10(1): 59–68: doi:10.3402/polar.v10i1.6728.

Volkman JK, Eglinton G, Corner EDS and Forsberg TEV (1980) Long-chain alkenes and alkenones in the marine coccolithophorid Emiliania huxleyi. Phytochemistry 19(12): 2619–2622: doi:10.1016/S0031-9422(00)83930-8.

Voronina E, Polyak L, Vernal AD and Peyron O (2001) Holocene variations of sea-surface conditions in the southeastern Barents Sea, reconstructed from dinoflagellate cyst assemblages. Journal of Quaternary Science 16(7): 717–726: doi:10.1002/jqs.650.

Wilson LJ, Hald M and Godtliebsen F (2011) Foraminiferal faunal evidence of twentieth-century Barents Sea warming. The Holocene 21(4): 527–537: doi:10.1177/0959683610385718.

Winkelmann D and Knies J (2005) Recent distribution and accumulation of organic carbon on the continental margin west off Spitsbergen. Geochemistry, Geophysics, Geosystems 6(9): doi:10.1029/2005GC000916.

CHAPTER 7

Late Holocene North Atlantic Sea Surface Temperature Cooling Reversed by Progressive Warming since AD 1600 in the Skagerrak.

7.1. Abstract

Variability in the North Atlantic Oscillation (NAO) and in the Atlantic Multidecadal oscillation (AMO) have great influence on northern Europe's climate. We reconstructed sea surface temperatures (SST) at decadal resolution in a marine sedimentary core (MD99-2286) located in the Skagerrak, which receives more than 90% of its water from the North Atlantic Current. Our reconstruction shows an overall decrease in SST since AD 0 to AD 1300, in common with reconstructions elsewhere in the North Atlantic region, which is probably related to a decrease in summer insolation at high latitudes during the late Holocene. However from AD 1600 until AD 2000 we observe a reversal in long term cooling despite the continuous decrease in summer insolation. We argue that warming in SST during the last 400 years was caused by changes in the North Atlantic Current starting ca. AD 1600, which was forced by a progressive predominance of positive modes of the NAO and the AMO. The results further confirm the important role of the North Atlantic Ocean and the variability in the inflow of North Atlantic water to the North Sea and the Skagerrak, as an important factor regulating continental northern - central Europe climate at multidecadal to multicentennial scales.

Keywords Skagerrak; North Atlantic; alkenones; sea surface temperature; late Holocene; multidecadal variability.

7.2. Introduction

Sea surface temperature (SST) variability in the North Atlantic Ocean basin influences European climate at yearly to multidecadal timescales (Sutton and Hodson, 2005). Various parameters affect long term variability in SST over this region such as internal variability in the Atlantic Meridional Overturning Circulation, variation in the inflow of the North Atlantic Current (NAC) which is controlled by subpolar gyre dynamics and changes in the pressure gradient at sea level over the North Atlantic zone. The North Atlantic Oscillation (NAO; Hurrell, 1995) and the Atlantic Multidecadal Oscillation (AMO; Kerr, 2000) are climate indices used for defining features of natural modes of climate variability in the North Atlantic region.

The NAO is a mode of climate variability relevant at decadal time scales. It is defined as the variation of the pressure gradient between the Iceland Low and the

Azores High pressures at sea level from daily to multidecadal time scales (Hurrell, 1995). Variability in this pressure gradient has an effect on the strength and direction of westerly winds and storm tracks over the North Atlantic, and influences European climate with a positive correlation with temperature and precipitation over the continent (Hurrell, 1995). When there are strong westerly winds carrying heat and moisture over Northern Europe resulting in relatively warm and stormy climate over central Europe and Scandinavia, and colder and drier conditions in southern Europe, the NAO index is in a positive mode. Instead, when the westerlies are weaker and their track is directed southwards bringing warmer and wetter conditions over middle and southern Europe, while northern Europe is colder and drier, the NAO is in a negative mode (Hurrell, 1995). The correlation between SST and the changing phases of the NAO mode of climate variability is not stationary. Based on instrumental data, higher correlations were found when the NAO index was characterized by strong decadal variability and mainly positive values, whereas lower correlations were identified when the NAO index showed weak decadal variability (Walter and Graf, 2002).

The AMO has been identified as a pattern of multidecadal variability in SST in the North Atlantic Ocean with a periodicity of ~60-90 years (Schlesinger and Ramankutty, 1994; Kerr, 2000). The AMO index is calculated as the difference between SST over the North Atlantic Ocean and SST in the rest of Worlds' Oceans. It has been observed that the AMO has shifted between positive and negative SST anomalies lasting several decades. This oscillatory mode in North Atlantic Ocean SST is driven by changes in the strength of the thermohaline circulation and it is linked to internal variability in the ocean-atmosphere system (Delworth and Mann, 2000; Knight et al., 2005). A quasi persistent 55 to 70 year oscillation affected SST in the North Atlantic region, suggesting that the AMO influenced Holocene climate variability (Knudsen et al., 2011).

Studies at decadal resolution are fundamental for studying both long term leading modes of climate variability and short term changes in climate in the North Atlantic region. The Skagerrak, located between the North Sea and the Baltic Sea and bordered by the coasts of Scandinavia (Figure 7.1) is a potential site for studying the interaction between the open marine and the continental environments at decadal resolution. In the Skagerrak–Baltic area various environmental parameters have been reported to be correlated with the changing phases of the NAO mode of climate variability (Koslowski and Glaser, 1999; Drinkwater et al., 2003; Nordberg et al., 2000; Hagberg and Tunberg, 2000; Brutckner and Mackensen, 2006). Here we reconstructed SST variability in the Skagerrak during the last 2000 years at decadal resolution. The aim was to investigate SST variability in the Skagerrak and its relationship with North

Atlantic modes of climate variability and central Europe continental climate during the last 2000 years.

7.3. Study area

Circulation and sedimentation patterns in the Skagerrak are driven by the inflow of Atlantic water carried with the NAC related to large scale atmospheric and oceanic circulation patterns (Figure 7,1; Stigebrandt, 1983; Otto et al., 1990). During the last 8500 years sediments in north-eastern Skagerrak consisted of mixed material from the Atlantic Ocean and southern North Sea, Scandinavia and the Baltic Sea (Gyllencreutz, 2005). The sediment contribution from Scandinavia and the Baltic Sea has been estimated to be about 15% of all deposited sediments in the Skagerrak (Gyllencreutz and Kissel, 2006; Longva and Thorsnes, 1997). During the last 900 years until present sedimentation has been clearly dominated by southern North Sea and Atlantic Ocean sources, as shown by mineral magnetic properties measured in the same core, MD99-2286 (Gyllencreutz and Kissel, 2006).

The NAC enters the North Sea stimulating a counterclockwise circulation (Hass, 1996). This water circulation forms the Jutland Current that continues up into the Skagerrak and enters the Kattegat as well (Conradsen and Heier-Nielsen, 1995). There it mixes with the Baltic Current, a relatively fresh and cold surface outflowing current from the Baltic. The mixture of these two water masses forms the Norwegian Coastal Current, which makes a counter-clockwise turn in the northeastern end of the Skagerrak, outflowing and exiting the Skagerrak along the Norwegian coast (Gyllencreutz and Kissel, 2006). During the cyclonic turn in the northeastern Skagerrak there is an increase in water depth, and the velocity of the current is reduced beyond the limit where turbulence can sustain a stable concentration of suspended matter. For this reason high sedimentation rates (up to 1 $cm \cdot year^{-1}$) are found in the northeastern and central parts of the Skagerrak (Rodhe and Holt, 1996; Bøe et al., 1996)

Core MD99-2286 (58°43.77'N, 10°12.31'E; 225 m water depth, 32.4 m length) was retrieved from north-eastern Skagerrak (Figure 7.1) by R/V *Marion Dufresne* using a CALYPSO corer, a giant piston corer. The age model was established using 27 AMS ^{14}C dates for the entire core which covers the entire Holocene and latest Glacial sediments. Here, we focus on the last 2000 years period where 7 AMS ^{14}C define the age model (Table 1; Gyllencreutz et al., 2005). The upper part of the core was in addition dated with 4 indirect ^{210}Pb dates via correlation with the ^{210}Pb-dated gravity core Sk000209-2 (58°43'50.4''N, 10°11'46.8''E 226 m water depth, 622 m from core MD99-2286) (Gyllencreutz, 2005; Senneset, 2002).

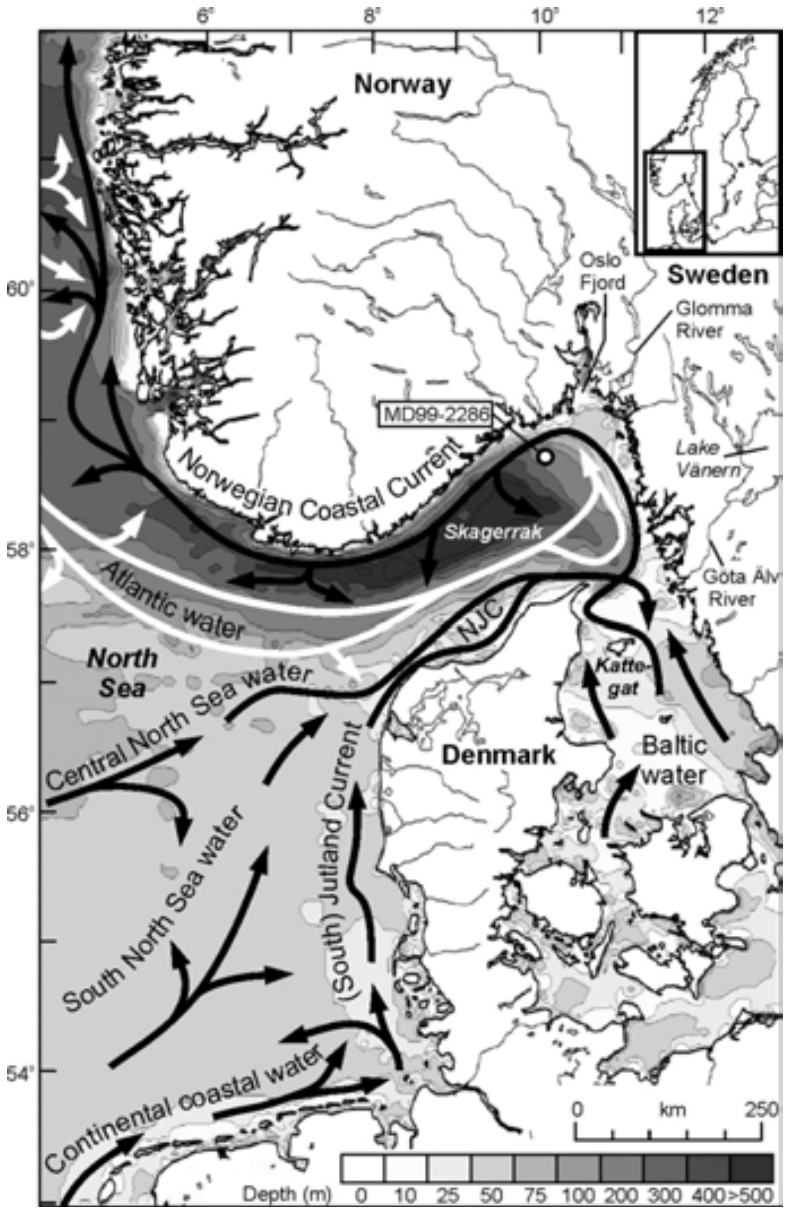

Figure 7.1.Bathymetry and general ocean circulation in the Skagerrak. Bathymetry is indicated with a grey color scale. The white arrows indicate the Atlantic Water path flowing directly into the Skagerrak. NJC stands for North Jutland Current. Core MD99-2286 location is marked with a white circle. The map is from Gyllencreutz (2005).

7.4. Proxies and time series analysis

To estimate SST we used the $U^{K'}_{37}$ index (Prahl and Wakeham, 1987) calculated from the relative concentration in sediments of the di- and tri- unsaturated C_{37} alkenones ($C_{37:2}$, $C_{37:3}$) through the equation $U^{K'}_{37} = (C_{37:2})/(C_{37:2}+C_{37:3})$. The $U^{K'}_{37}$ was converted to temperature through the regression SST (^{o}C) = ($U^{K'}_{37}$ – 0.044) /0.033 from a core-top Global Ocean calibration (Müller et al., 1998). To estimate water mass variability we used the percentage of the $C_{37:4}$ alkenone to the total abundance of C_{37}

Table 7.1. Age model for core MD99-2286 based on AMS ^{14}C ages analysed in shells from gastropod, mollusc and benthic foraminifera species. A correction of 400 year was applied to account for the air-sea reservoir difference (Gyllencreutz, 2005).

Laboratory reference	Core depth (cm)	Dated species	^{14}C age BP	Age range (cal. yr BP)		
				Max (1σ)	Median	Min (1σ)
ETH-24001	268	*Ennucula tenuis*	535±50	252	166	113
ETH-24397	319.5	*Thyasira equalis*	730±45	417	372	320
ETH-25547	370.5	*Nucula tumidula*	900±60	548	513	467
ETH-26938	481.5	Foraminifera (mixed fauna)	1225±55	824	768	699
ETH-26940	640.5	Foraminifera (mixed fauna)	1530±50	1146	1080	1024
ETH-25956	801	Foraminifera (mixed fauna)	1915±55	1518	1458	1398
ETH-26390	1001	Foraminifera (mixed fauna)	2175±50	1819	1766	1705
ETH-26941	1070.5	Foraminifera (mixed fauna)	2440±55	2138	2076	1997

alkenones ($\%C_{37:4} = (C_{37:4}/(C_{37:2}+C_{37:3}+C_{37:4}))\cdot 100$; Bendle et al., 2005). The export productivity was estimated with the analysis of total abundances of alkenones and chlorins. The source origin of the sediments was characterized with the analysis of n-alkanes and the measure of the carbon preference index (CPI). For detailed information on the biomarkers and the analytical methods see chapters 1 and 2.

Predominant periodicities throughout the SST record were analyzed with the REDFIT technique (Schulz and Mudelsee, 2002) using the PAST software (Hammer et al., 2001). This procedure can work directly with unevenly spaced data, previously detrended. REDFIT estimates a spectrum using a Lomb-Scargle periodogram and Monte Carlo simulations for bias correction. The approach performs a test of the red noise level (AR(1)) and denotes which periodicities are present in the record and significant above the red noise and a specific significance level (i.e. 90%, 95%).

Change in the periodicities through time at different time scales was analyzed using a wavelet coherence analysis (Torrence and Compo, 1998). In this procedure, the time series is decomposed into several wavelets, which map the temporal changes in the periodicities. The variability of the periodicities is then highlighted through the record at different timescales. The previously detrended data was also converted to an evenly spaced data set prior to using this methodology. The Morlet wavelet was used as a basis function. MATLAB software was used to perform this analysis.

Significance of Zero Crossings of the Derivative (SiZer) was used to investigate if the visually inspected trends in the alkenone data at different time scales were statistically significant features (Chaudhuri and Marron, 1999). The SiZer plot consists of a map with x axis as time (age AD) and y axis as the logarithmic function of the family of smooths for a wide range of bandwidths (h). The SiZer analysis shows whether at a specific point (time, h) the first derivative of a curve is statistically

different from zero. If it is above zero, there is a significant increase in the curve (shown in blue in the SiZer map). If the derivative is below zero, there is a significant decrease in the curve (shown with red area) and if the value is around zero there is an insignificant change (indicated with purple colour). The open software R was used to perform this analysis (Sonderegger, 2012).

7.5. Results and discussion

7.5.1. Water mass and SST variability in the Skagerrak during the last 2000 years

During the last 2000 years, sediments in the Skagerrak had Atlantic and southern North Sea sources, with minor contributions from Scandinavian runoff and Baltic Sea outflow (Gyllencreutz and Kissel, 2006). Therefore, the environmental parameters reconstructed from core MD99-2286 provide information on past changes in the southern North Sea and Skagerrak region in addition to the NAC. We analyzed n-alkanes to qualitatively assess the origin of organic matter in the study area. For the last 2000 years the CPI values for n-alkanes with chain lengths between 25 and 34 averaged 3.3, and ranged between 1.8 and 4.4 (Figure 7.2B). CPI values of this range are found in marine environments with contributions from higher plants, suggesting a terrestrial contribution to the marine environment. In the Skagerrak, these terrestrial sources were derived from Scandinavia river run off and dust transported with the westerly winds. River run-off in the Skagerrak accounts for ~10% of the total freshwater input in the area (Gustafsson and Stigebrandt, 1996).

The percent of total organic carbon (TOC%), was quite stable for the last 2000 years in the northeastern Skagerrak (Figure 7.2A). The TOC% ranged between 1 and 2%, and increased progressively towards present. The highest values were detected from AD1850 to 2000 (Figure 7.2A; Erbs-Hansen et al., 2011). The alkenone and chlorin concentrations were normalized to the percentage of total organic carbon (TOC%) to account for possible change in preservation of the biomarkers (Figure 7.2C;D). The concentration of chlorins can be used as an indicator for total primary exported production (Harris et al., 1996). During the last 2000 years we observe two periods of increased total export productivity: the first during AD 750 – 950 and the second during AD 1800 – 2000. These two periods coincided with higher than average TOC values (Figure 7.2A;C). Erbs-Hansen et al. (2011) linked periods of increased TOC content to increased low quality nutrients, enhanced turbidity and warming in bottom

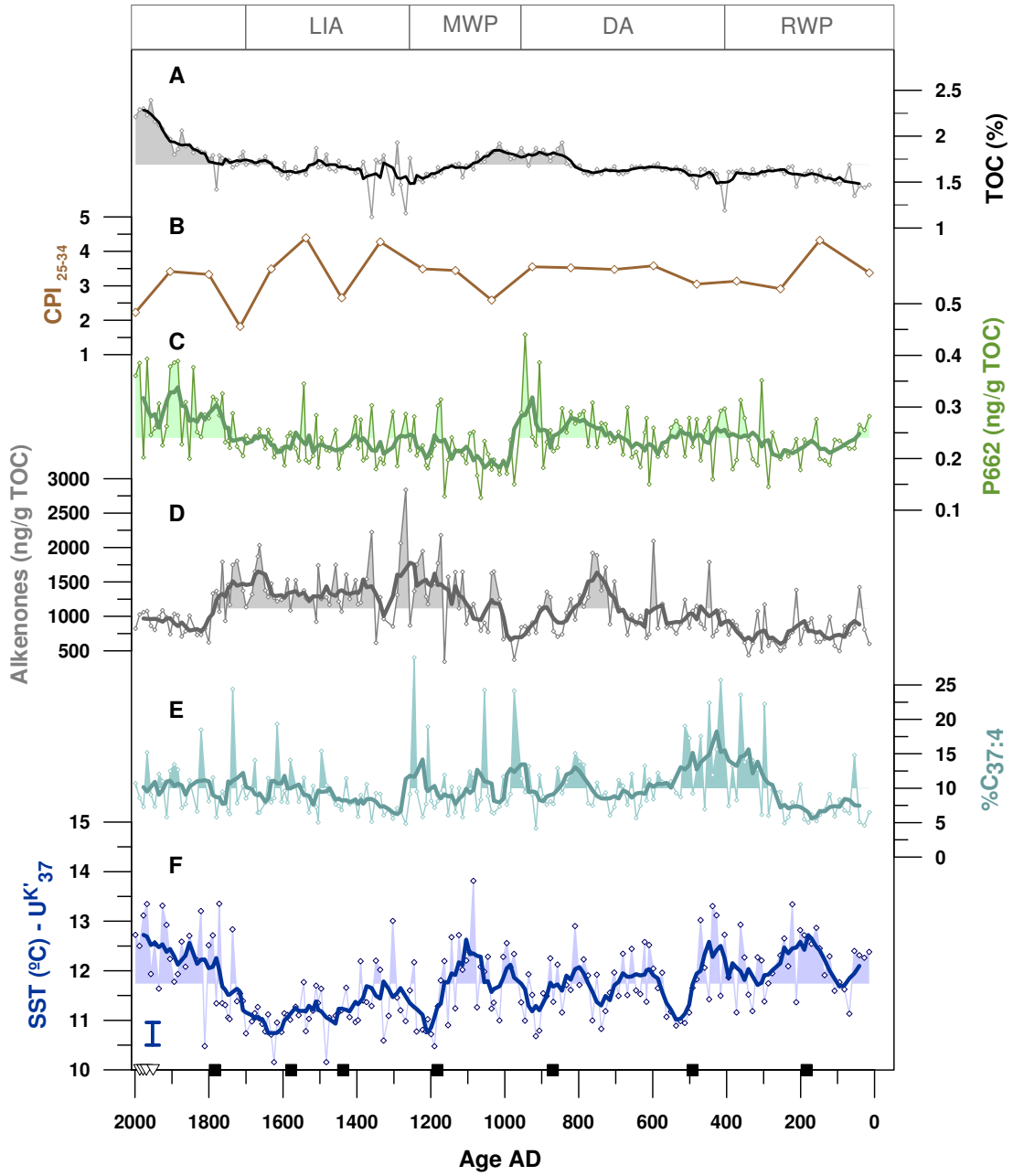

Figure 7.2. Core MD99-2286 environmental reconstruction for the last 2000 years AD. The thick lines indicate 5-point running mean averages. The values above the mean for the whole period are marked as filled areas. The labels on top of the figure indicate the European climate periods: Roman Warm Period (RWP), Dark Ages (DA), Mediaeval Warm Period (MWP), Little Ice Age (LIA) (e.g. Mayewski et al., 2004, Bianchi et al., 1999, Mann et al., 2009) (A) Total organic carbon (TOC%) (Erbs-Hansen et al., 2011). (B) CPI ratio of n-alkanes (25-34 carbon chain length). (C) Abundance of chlorins normalized per TOC (ng g_{TOC}^{-1}) at 662 bandwidth (green). (D) Total abundance of alkenones normalized per TOC (ng g_{TOC}^{-1}) (grey). (E) Relative presence of alkenone $C_{37:4}$ over the rest of its counterparts (%$C_{37:4}$) (light blue). (F) SST reconstruction from the $U^{K'}_{37}$ index (dark blue). The floating error bar at the SST Y-axis indicates the laboratory analytical error (reproducibility) for the SST (ºC) measurements. The black squares in the x-axis indicate the ^{14}C AMS measurements in which the age model is based (Gyllencreutz et al., 2005). The white inversed triangles indicate the complementary ^{210}Pb dates for the upper part of the core (Senneset, 2002; Gyllencreutz, 2005).

water temperature estimated from benthic foraminifera in core MD99-2286. In our study we found SST values estimated from $U^{K'}_{37}$ to be higher than average during these two periods as well (Figure 7.2F).

We interpret the concentration of alkenones as an indicator of exported productivity from haptophyceae algae, their source organisms. During the last 2000 years the total concentration of alkenones averaged 1100 ng g_{TOC}^{-1} and ranged between 340 and 2800 ng g_{TOC}^{-1}. Non normalized per TOC values are between 550 and 3550 ng g^{-1} which are comparable to the alkenone abundances in surface sediments from the Skagerrak reported by Blanz et al. (2005). Total alkenone concentrations were found in major abundances in surface sediments retrieved from the Skagerrak center (up to 12200 ng g^{-1}). Alkenone abundances decreased to 6000 ng g^{-1} in the eastern Skagerrak, down to 1500 ng g^{-1} in the northern Kattegat and the lowest values were found in the inner Baltic Sea (1000 ng g^{-1}) surface sediments (Blanz et al., 2005). Alkenone concentrations decline progressively from the Skagerrak towards the inner Baltic Sea (Blanz et al., 2005). Variability in the $\%C_{37:4}$ signal downcore indicates a water mass change, with high $\%C_{37:4}$ values indicative of a strengthening of the Baltic Sea outflow to the Skagerrak (Blanz et al., 2005). Therefore combining the abundances of alkenones and the $\%C_{37:4}$ index we can qualitatively estimate the variability in water mass change in the Skagerrak sector.

Our record shows comparatively low alkenone abundances between 0 and 700 AD, around AD 900 - 1000 and AD 1800 – 2000. During the period AD 1000 – 1800 the alkenone abundance values are generally above the average for the whole period recorded, in contrast to AD 0 – 1000 which showed generally low concentrations. The $\%C_{37:4}$ values are higher during 300 - 500 AD and around AD 800 and 900 (Figure 7.2E). The period AD 1100 until 2000 is characterized by more stable $\%C_{37:4}$ values, generally lower than 10% but with abrupt short term peaks reaching values up to 15-20% (Figure 7.2E). Low alkenone concentrations and high $\%C_{37:4}$ indicate that from AD 0 to 600 there were periods with increased Baltic outflow (Figure 7.2D;E). This finding is in line with results concerning the magnetic properties of core MD99-2286, which indicate periods of enhanced Baltic water influence until AD 750 (Erbs-Hansen et al., 2011; Gyllencreutz and Kissel, 2006). During the last 1000 years, comparatively high alkenone abundance and low $\%C_{37:4}$ would indicate more Atlantic-like water mass conditions in the Skagerrak. Changes in foraminifera species suggest enhanced Atlantic water inflow after AD 850 in the same core (Erbs-Hansen et al., 2011). Besides the general trends, some spikes with high $\%C_{37:4}$ indicate short pulses of Baltic water outflow over the last 2000 years, which were more frequent in the first millennia of our record (AD 0 - 1000).

When $\%C_{37:4}$ values are higher than 10%, the $U^{K'}_{37}$ is no longer linearly related to SST in the Skagerrak-Kattegat region (Blanz et al., 2005). Nevertheless accurate past sea surface temperatures can be obtained in the Skagerrak sector using the $U^{K'}_{37}$ index, because $U^{K'}_{37}$ SST estimates from surface sediment samples plot within 1ºC of the global calibration by Müller et al. (1998) (Blanz et al., 2005). Furthermore, comparison between the modern instrumental SST from the Skagerrak during the last 200 years (Chapter 3) with SST – $U^{K'}_{37}$ estimates for the same period show that the SST calculated with $U^{K'}_{37}$ values (using the calibration from Müller et al., 1998) fall between annual and summer SST instrumental measurements. In addition the alkenone pattern in samples from core MD99-2286 (Figure 7.3) is indicative of the presence of Atlantic water mass in the study site (Bendle and Rosell-Melé, 2004), giving further support to the use of this proxy in this area. Inclusion of the $C_{37:4}$ in the calibration did not improve the relationship to SST in this area (Blanz et al., 2005), therefore we used $U^{K'}_{37}$ instead of U^{K}_{37}.

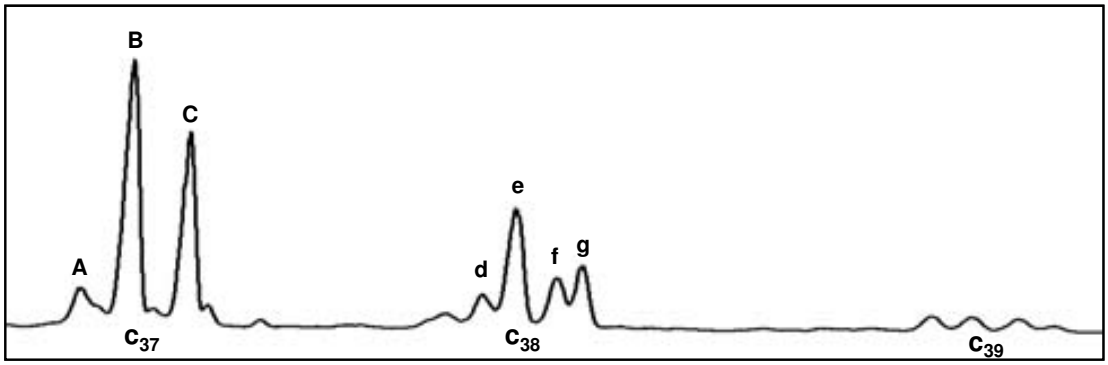

Figure 7.3. Representative GC-FID trace of alkenone patterns in core MD99-2286. Alkenones used in this study are: (A) $C_{37:4}$ Me; (B) $C_{37:3}$ Me; (C) $C_{37:2}$ Me. The other compounds were identified to determine the alkenone water mass *fingerprint* as described by (Bendle and Rosell-Melé, 2004): (d) $C_{38:3}$Et, (e) $C_{38:3}$Me, (f) $C_{38:2}$Et, (g) $C_{38:2}$Me.

During the last 2000 years, SST estimates ($U^{K'}_{37}$ calibration from Müller et al. (1998)) average 11.7 ºC. The SST record shows apparent cycles of warm and cold values (Figure 7.2F), Three periods of warmer conditions, with temperatures ~1ºC above the record mean can also be seen. These periods are located in the earliest part of the record, until AD 470, the middle part AD 980 – 1180 and the recent part from AD 1770 until AD 2000. Cold periods with temperatures ~1ºC below the record mean were also detected, as two periods characterized by short term pulses of lower temperatures, at AD 480 - 575 and AD 1175 – 1240, and a more extended period of colder SST conditions spanning from AD 1360 to 1700. The period between AD 580 and 980 shows two repeated warm – cool cycles. Major climatic changes, concerning

generally warmer or cooler conditions have been described to affect Europe during the last 2000 years. These periods are known as the Roman Climatic Optimum (BP 300 until AD 400) when mild climate conditions prevailed; the Dark Ages (AD 400-950), the Medieval Warm Period (AD 950 - 1250), the Little Ice Age (AD 1250 – 1700) and the recent warming since AD 1850 (Bianchi and McCave, 1999; Hass, 1996; Mann et al., 2009; Mayewski et al., 2004). However the timing, extent and magnitude of these periods are not homogeneous and change according to the region (Hughes and Diaz, 1994). In our record, climatic periods comparable to those previously defined can be identified between the periods AD 0 – 470 (warm), AD 1175-1240 (warm) and AD 1360-1700 (cold) (Figure 7.2F). After the cooling ending around AD 1700, SSTs increased towards present.

7.5.1.1. Significant trends and natural variability in SST

To assess if the visually inspected SST trends were statistically significant we generated a SiZer plot with the SST raw data (Figure 7.4A; Chaudhuri and Marron, 1999). The SiZer plot consists of a map with x axis indicating time (age AD) and y axis the logarithmic function of the family of smooths for a wide range of bandwidths (h). It shows whether the visually inspected increasing or decreasing trends in the data are statistically significant, or just random data variability from multidecadal to multicentennial time scales. The information is given at different points through the record (x-axis), and at different time scales of variability (y-axis). Significant decreasing trends are shown in red, increasing curvatures are marked in blue, and natural variability of the data (no significant changes in the curvatures) is shown in purple (Figure 7.4A).

At multicentennial time scales (Figure 7.4A; upper part of the SiZer map) red predominates during the period AD 0 – 1300, indicating there was significant long term cooling. Between AD 1300 and 1600 purple dominates the map, indicating that the changes in the data are part of its natural variability. From AD 1600 to AD 2000, the extended blue area in the left (x-axis) middle (y-axis) part of the SiZer map (Figure 7.4A) indicate that there was a significant warming taking place at multidecadal to centennial time scales. At multidecadal scale there are four short term, abrupt, significant changes in temperature. Two significant abrupt coolings are found between AD ~ 440 - 510 and 1080 - 1190. Two significant short term temperature increase periods are found between AD ~ 70 – 160 and 520 – 600. The significant cooling from AD 0 to 1300 at multicentennial frequency might have to do with summer solar insolation decrease during the last 2000 years (Figure 7.4B). Visual comparison of

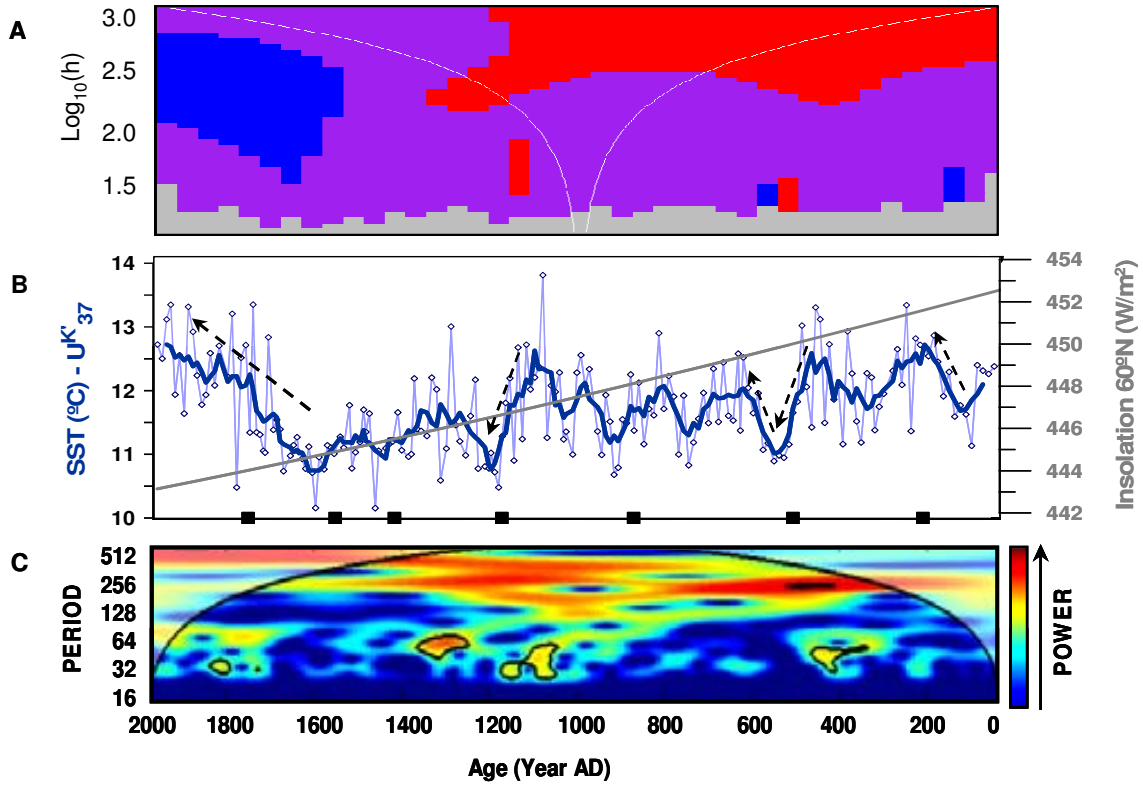

Figure 7.4. (A) SiZer map of SST in core MD99-2286. The plot is a function of location (time, x-axis) and scale (multidecadal to multicentennial variability; h, y-axis). An increase in the derivative (a significant warming trend) is shown in blue, a decrease in the derivative (cooling trend) is noted in red and no change in the derivative (natural variability of the data) is shown in purple. The distance between the two curved white lines indicate the scale at each level of resolution (Chaudhuri and Marron, 1999). (B) SST ($U^{K'}_{37}$) from core MD99-2286 with a 5-point running mean average (thick blue line). Summer insolation at 60ºN for the last 2000 years (grey line; Laskar, 2004). The arrows indicate the significant changes from the SiZer map. (C) Morlet wavelet transform coherence analysis of SST in core MD99-2286 (Torrence and Compo, 1998). The color scale at the right Y-axis indicates the power (increasing from blue to red) and the shadowed area corresponds to the cone of influence (non significant data because of edge effects). The periodicities with significance above 95% are circled with a black line.

insolation at 60ºN (Laskar et al., 2004) with SST (Figure 7.4B) denotes that they both decreased visually until AD 1600. The significant decrease in SST during AD 0 – 1300 could have been a response to change in insolation. From AD 1600 to AD 2000 insolation continued decreasing but the cooling trend in SST changed to a progressive and statistically significant warming, at multidecadal to multicentennial scale. This warming could have been triggered by changes in internal variability of the ocean – atmosphere system, such as an increase in the advection of the NAC bringing relatively warm waters to northern Europe. Air temperature, SST and westerly winds are highly and significantly correlated to NAO variability along the Norwegian Skagerrak coast. High SST, air temperature and westerly winds were observed in years of positive NAO index and vice versa (Fromentin et al., 1998). A reconstruction of the NAO spanning

the last 500 years showed that since AD 1500 there were several periods with positive NAO values (Luterbacher et al., 2001). The observed increase in SST from AD 1600 until 2000 in our Skagerrak record could be related to a mean predominance of the positive phase of the NAO and/or AMO affecting this region since approximately AD 1600.

7.5.1.2. Climatic cycles in SST record

In order to find significant periodicities in the SST record resolved on a decade scale, we performed time series analysis using the software REDFIT (Schulz and Mudelsee, 2002) on the raw SST data from core MD99-2286 after detrending the data (Figure 7.5). The lower grey line in Figure 7.5 shows the theoretical significance level for red noise at different periodicities. The upper grey lines show the periodicities which are significantly different from the red noise at 90 and 95% confidence interval levels (CI). At multicentennial time scales, there is a prominent 220 year period with a CI above 95% and a 397 year period with a CI above 90%. At multidecadal scale, there are two periods of 27 and 31 years above a 90% CI.

In order to study the evolution through time of any significant periodicities, we used (Morlet) Wavelet analysis (Torrence and Compo, 1998) on the detrended and evenly spaced SST data. The local wavelet power spectrum shows the presence of the different periodicities at different time scales during the last 2000 years (Figure 7.4C).

At multicentennial time scales, the 397 year period (according to REDFIT analysis, CI above 90%) is present from AD 600 to 1400. The 220 year period is relevant during the time interval from 0 to 1600 AD. This period is continuously present during this time interval, with increased strength during AD 200-500. At multidecadal scales periods of ~ 30 years are significant above 95% (circled with a black line). Those periods are present at distinct parts of the record in an intermittent pattern (between AD ~350-450, ~1000-1200, ~1250-1400 and ~1800-1850). The 220 year period has been reported in the literature to be related to total solar irradiance variability. Specifically, this periodicity has been linked to the Suess (or De Vries) cycle which has a periodicity of 225 years and a solar origin (Wagner et al., 2001). Previously, cycles of ~260 years were also found in the region, i.e. in glaciolacustrine sediments from northern Norway (Matthews et al., 2000) and marine sediments from the Baltic Sea (Kunzendorf and Larsen, 2002) and also cycles of ~200 years in the Baltic Sea (Yu, 2003).

At multidecadal scale, the periods of ~30 years present in our SST record, could be linked to internal variability of the ocean – atmosphere system. The AMO has

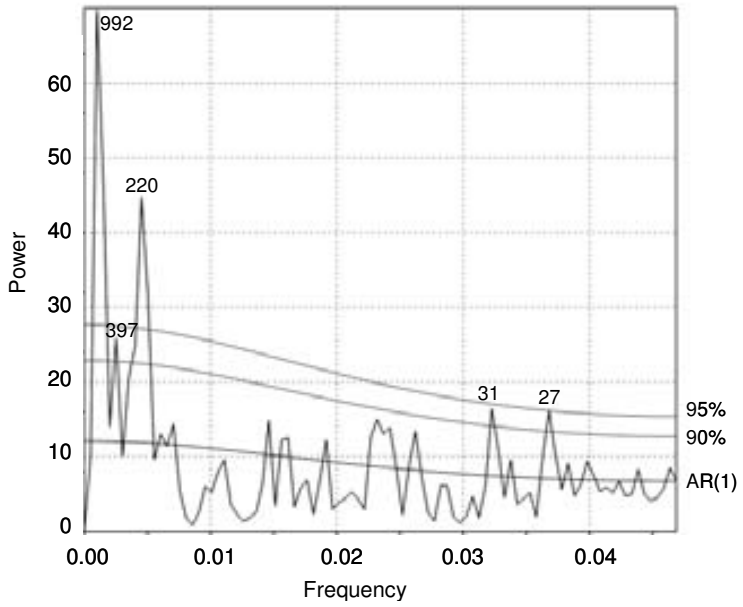

Figure 7.5. Red noise and frequencies in SST data from core MD99-2286. The red noise level is shown with a grey line (AR(1)). The frequencies statistically significant above 90 and 95% confidence interval (grey lines) are labeled with the corresponding period (years). The analysis was done with REDFIT (Schulz and Mudelsee, 2002).

usually been described as having a periodicity of 60 – 90 years (Kerr, 2000; Schlesinger and Ramankutty, 1994), but recent proxy and model results show a more complex picture with variable periodicities ranging from 30 to 100 years (Delworth and Mann, 2000; Hubeny et al., 2006; Knight et al., 2005). The statistically significant cycles of ~30 years found in our record might be linked to the AMO signal. Figure 7.6E shows the AMO reconstruction covering the last 1500 years from Mann et al. (2009), described as SST averaged over the North Atlantic ocean as defined by Kerr (2000). The AMO is marked by substantial multidecadal variability. To compare decadally resolved SST - $U^{K'}_{37}$ records with the AMO variability at long time scales, it is recommended to filter the data in order to decrease the noise contribution (Heslop and Paul, 2011). After filtering the data we can visually compare the AMO reconstruction (Mann et al., 2009) to our SST record from the Skagerrak at multicentennial scales. We must take into account that the absolute temperature change is 3-fold higher in the Skagerrak SST record reconstructed from alkenones than in the AMO reconstruction. The 51 year filtered AMO record (thick black line in figure 7.6E) shows that at multicentennial time scales, there was a long term cooling from AD 500 to AD 1600, followed by a progressive warming period. This warming took place at two steps; a first period from AD 1600 to around 1750 that ended with a short cooling and a second period from AD 1800 that was characterized by a progressive warming until present (discontinuous vertical lines in Figure 7.6). Both records show higher than average SST during the time

interval AD 900 – 1100 that corresponds to the MWP. The similarities between the AMO record and the Skagerrak SST reconstruction show the close links between North Atlantic Ocean heat transport variability and northern Europe climate at multicentennial time scales.

7.5.2. Regional climate during the last 2000 years

The significant cooling observed in our record at multicentennial time scales from AD 0 to 1300 is related to a general decrease in SST observed in several records from the North Atlantic region (Marchal et al., 2002). In some records a warming is also observed during the last centuries usually starting later than the warming observed in our SST record from AD 1600 to present (Figure 7.6). The majority of the records cited here show multidecadal and multicentennial variability. Here we focus on the long term multicentennial variability.

A decrease in bottom water temperature of ca 1 ^{o}C was found for the period BC 49 to AD 1350 in a northern Norway fjord reconstruction from ^{18}O in benthic foraminifera, which the authors associated to the decreasing insolation (Figure 7.6A) (Hald et al., 2011). The authors found an unprecedented warming from AD 1800 until 2000 in northern Norway bottom water temperature, which they associated to polar amplification of global warming. In our record a significant warming started at AD 1600, which is 200 years earlier than in the northern Norway record. Using the same technique, bottom water temperatures were reconstructed in the Skagerrak for the last 1200 years (Figure 7.6B; Brückner and Mackensen, 2006). The authors found a close relationship between long term bottom temperature variability and the NAO during the last 1200 years, and a progressive increase in temperature starting at AD 1800. A regional climate model from the Baltic area for the last thousand years, simulated a gradual cooling until AD 1700 that continued with an increase in temperature during the last centuries (Schimanke et al., 2012). In central Europe, air temperatures reconstructed from documentary data for the last millennium (Figure 7.6C), also show multidecadal variability, a warming around AD 1200 followed by a gradual cooling at multicentennial scales with its minima at AD 1700 (Glaser and Riemann, 2009). A warming trend was observed from AD 1800 to present with a magnitude of 1 ^{o}C (Figure 7.6C; Glaser and Riemann, 2009).

The available NAO reconstructions spanning the last 500 years (Lutherbacher et al., 2002; Cook et al., 2002) or the last 950 years (Trouet et al., 2009) show sustained periods with predominantly positive NAO that lasted several decades, which was alternated with periods of negative NAO (Figure 7.6G). During the last 200 years the three NAO

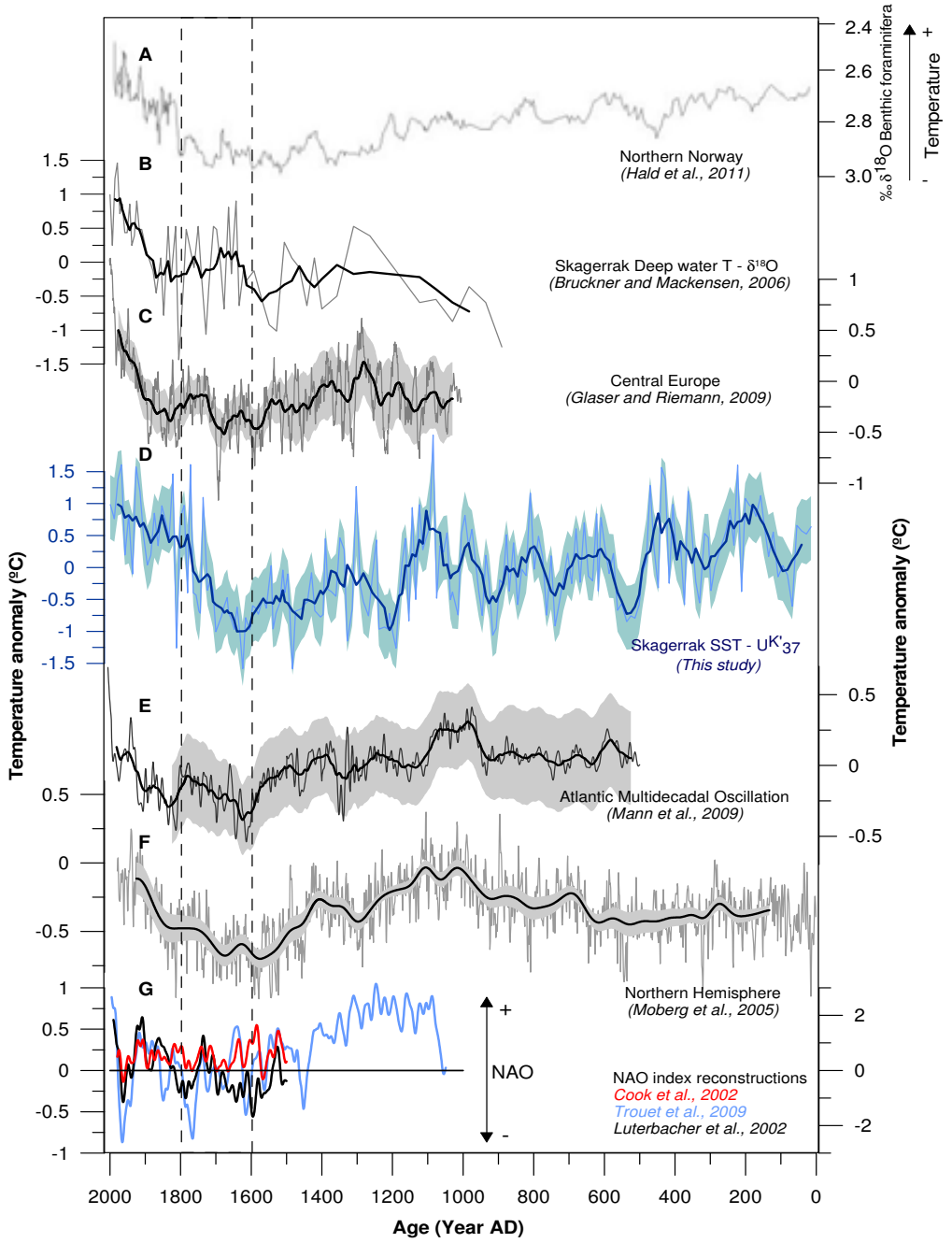

Figure 7.6. Comparison between the SST record (blue) generated in this study and previously published records (black and grey). The discontinuous lines indicate the period AD 1600 – 1800 and 1800 – 2000. Bottom water temperature variability estimated from the analysis of benthic foraminifera in (A) Malangen Fjord, Northern Norway (Hald et al., 2011) and (B) the Skagerrak (Brückner and Mackensen, 2006). The thick black line is a 5 point running mean average. (C) Reconstruction of central Europe air temperature from documentary data (Glaser and Riemann, 2009); 11 year moving average temperature anomaly over period 1761-1970 (grey) and 51 year running mean average (thick black line). The grey area is the estimated error for the 11 year moving average (1σ). (D) SST from core MD99-2286 (this study); raw data (pale blue) and 5 year running mean average (thick dark blue line). The blue area shows the upper and lower 1σ estimates taking into account the 0.5ºC of analytical error. (E) Atlantic Multidecadal Oscillation (AMO) (Mann et al., 2009) as variability in SST over the North Atlantic region; 1850-2006 principal component-filtered instrumental observations (grey) and 51 year running mean average (thick black line). The grey area shows the 95% uncertainty interval. (F) Multiproxy reconstruction of Northern Hemisphere temperature (Moberg et al., 2005) given as temperature anomalies for 1961-90 average (grey) and lower and upper bounds of uncertainty (thin black lines) of the 80-yr component AD 133–1925 (thick black line). (G) Reconstructions of the North Atlantic Oscillation (left axis, red, Cook et al., 2002; left axis, black, Lutherbacher et al., 2002; right axis, blue, Trouet et al., 2009).

reconstructions show long periods with the NAO in a positive phase that are more frequent than periods with the NAO in a negative phase. At multidecadal to multicentennial time scales, the variability in the AMO is visually comparable to the SST variability throughout our Skagerrak record (Figure 7.6D;E). This reinforces the fact that changes in the thermohaline circulation and the inflow of Atlantic water shape climate variability in this region at multidecadal to multicentennial time scales.

The similarities between temperature trends found in these paleoclimatic records, located in southern and northern Norway, in the Baltic and in central Europe further corroborate the links between the variability in internal factors like the AMO, the NAO the NAC heat transport, and external forcing factors such as the solar irradiance, in shaping both oceanic and continental climate in the Skagerrak region and northern Europe during the late Holocene at multicentennial time scales.

Considering wider geographical scales more similarities between our record and previous reconstructions can be observed at multicentennial time scales. For instance, in the northeastern Atlantic, records of planktonic foraminiferal Mg/Ca ratios and oxygen isotopic compositions reveal a general long term cooling at multicentennial scales during the late Holocene (Richter et al., 2009). These authors related the cooling trend to variability in solar forcing and reduced heat transport from the ocean associated with predominant periods of negative NAO during the last 2400 years. A compilation of alkenone-derived SST measurements from seven cores located in the northeastern Atlantic and the Mediterranean, also documented a general long term cooling during the Holocene (Marchal et al., 2002). A multiproxy study compilation of marine records along the western European margin found lower temperatures during the period AD 1300 and 1900 and progressively warmer SSTs during the last 200 years (Eiríksson et al., 2006). Global temperature estimates from low and high resolution proxy data in the Northern Hemisphere also report a warming during the last 400 years (Figure 7.6F; Moberg et al., 2005). Estimates of Northern Hemisphere ground surface temperature measurements in 700 boreholes (Pollack and Smerdon, 2004) show a warming of 1^{o}C during the last 500 years, half of which fall in the twentieth century only. These reconstructions from an area covering the North Atlantic are consistent with the trends observed in our SST record further indicating the connections between the northern North Atlantic SST variability, the AMO, and the climate trends in northern Europe. In addition, in Chapters 5 and 6 of this thesis we found a continuous change in the proxy records that started ca. 500 years ago, which we attributed to a progressive increase in the inflow or in the temperature of the NAC from AD 1500 to present.

7.6. Conclusions

During the last 2000 years, SST in the Skagerrak varied at both multidecadal and multicentennial scales. A cyclicity with a period of 220 years, significant at 95% confidence level, dominates during most of the record, whereas periods of ~30 years are present intermittently. These periodicities are linked to solar variability and to variability of the AMO. At multidecadal time scales there were two significant warming events at ~ AD 70 – 160 and 520 – 600 and two significant cooling events at AD ~ 440 - 510 and 1080 - 1190. At multicentennial time scales, there is a statistically significant cooling from AD 0 until AD 1300 followed by a transition period with natural climatic variability and a statistically significant warming from AD 1600 until AD 2000. The general cooling trend is probably linked to a decrease in summer insolation at high latitudes during the late Holocene. The cooling was progressively reversed by a long term warming trend in spite of continued decreasing insolation. This warming could be linked to a different climate forcing, related to internal variability of the ocean – atmosphere system.

Comparing our SST record from the Skagerrak with a terrestrial air temperature record from central Europe, a reconstruction of SST in northern Norway and a model output of SST in the Baltic we found similarities regarding the long term general trends at multicentennial scales. Particularly, a cooling in the earlier part of the record continued with an increase in temperatures from AD 1600, 1700 or 1800 depending on the reconstruction. Comparing the Skagerrak reconstruction with a general North Atlantic Ocean reconstruction for the AMO, we see visually comparable trends at multicentennial scales. The results further confirm the important role of the North Atlantic Ocean, and specifically the inflow of North Atlantic water to the North Sea and the Skagerrak, as an important factor regulating continental central Europe climate at multicentennial scales. The temperature increase in the last centuries could be caused by an enhancement of the NAC transport starting ca. AD 1600 as also observed from high latitude records in Chapters 5 and 6 of this thesis. The mechanisms triggering such enhanced inflow could be linked to the internal variability of the ocean – atmosphere system, such as a progressive predominance of positive modes of the North Atlantic Oscillation. During the late Holocene, changes in SST at multidecadal to multicentennial time scales found in our record and in several studies from the North Atlantic region can be attributed to both variability in solar forcing and also changes in heat transport via the NAC, promoted by shifts in the predominant state of the NAO and AMO variability.

7.7. References

Bendle J and Rosell-Melé A (2004) Distributions of UK37 and UK37′ in the surface waters and sediments of the Nordic Seas: Implications for paleoceanography. Geochemistry Geophysics Geosystems 5: 19 PP.: doi:200410.1029/2004GC000741.

Bianchi GG and McCave IN (1999) Holocene periodicity in North Atlantic climate and deep-ocean flow south of Iceland. Nature 397(6719): 515–517: doi:10.1038/17362.

Blanz T, Emeis K-C and Siegel H (2005) Controls on alkenone unsaturation ratios along the salinity gradient between the open ocean and the Baltic Sea. Geochimica et Cosmochimica Acta 69(14): 3589–3600: doi:10.1016/j.gca.2005.02.026.

Bøe R, Rise L, Thorsnes T, De Haas H, Sæter OM, Kunzendorf H (1996) Sea bed sediments and sediment accumulation rates in the Norwegian part of the Skagerrak. Geological Survey of Norway Bulletin 430, 75-84.

Brutckner S and Mackensen A (2006) Deep-water renewal in the Skagerrak during the last 1200 years triggered by the North Atlantic Oscillation: evidence from benthic foraminiferal δ8O. The Holocene 16(3): 331–340: doi:10.1191/0959683605hl931rp.

Chaudhuri P and Marron JS (1999) SiZer for Exploration of Structures in Curves. Journal of the American Statistical Association 94(447): 807: doi:10.2307/2669996.

Conradsen K and Heier-Nielsen S (1995) Holocene paleoceanography and paleoenvironments of the Skagerrak-Kattegat, Scandinavia. Paleoceanography 10(4): 801–813: doi:10.1029/95PA01142.

Delworth TL and Mann ME (2000) Observed and simulated multidecadal variability in the Northern Hemisphere. Climate Dynamics 16(9): 661–676: doi:10.1007/s003820000075.

Drinkwater KF, Belgrano A, Borja A, Conversi A, Edwards M, Greene CH, Ottersen G, Pershing AJ and Walker H (2003) The response of marine ecosystems to climate variability associated with the North Atlantic Oscillation. Geophysical Monograph 134, 211 -34.

Eiríksson J, Bartels-Jónsdóttir HB, Cage AG, Gudmundsdóttir ER, Klitgaard-Kristensen D, Marret F, Rodrigues T, Abrantes F, Austin WEN, Jiang H, Knudsen K-L and Sejrup H-P (2006) Variability of the North Atlantic Current during the last 2000 years based on shelf bottom water and sea surface temperatures along an open ocean/shallow marine transect in western Europe. The Holocene 16(7): 1017–1029: doi:10.1177/0959683606hl991rp.

Erbs-Hansen DR, Knudsen KL, Gary AC, Gyllencreutz R and Jansen E (2011) Holocene climatic development in Skagerrak, eastern North Atlantic: Foraminiferal and stable isotopic evidence. The Holocene: doi:10.1177/0959683611423689.

Fromentin J, Stenseth NC, Gjster J, Johannessen T and Planque B (1998) Long-term fluctuations in cod and pollack along the Norwegian Skagerrak coast. Marine Ecology Progress Series 162: 265–278: doi:10.3354/meps162265.

Glaser R and Riemann D (2009) A thousand-year record of temperature variations for Germany and Central Europe based on documentary data. Journal of Quaternary Science 24(5): 437–449: doi:10.1002/jqs.1302.

Gustafsson B and Stigebrandt A (1996) Dynamics of the freshwater-influenced surface layers in the Skagerrak. Journal of Sea Research 35(1–3): 39–53: doi:10.1016/S1385-1101(96)90733-9.

Gyllencreutz R (2005) Late Glacial and Holocene paleoceanography in the Skagerrak from high-resolution grain size records. Palaeogeography, Palaeoclimatology, Palaeoecology 222(3–4): 344–369: doi:10.1016/j.palaeo.2005.03.025.

Gyllencreutz R and Kissel C (2006) Lateglacial and Holocene sediment sources and transport patterns in the Skagerrak interpreted from high-resolution magnetic properties and grain size data. Quaternary Science Reviews 25(11–12): 1247–1263: doi:10.1016/j.quascirev.2005.11.002.

Gyllencreutz R, Jakobsson M and Backman J (2005) Holocene sedimentation in the Skagerrak interpreted from chirp sonar and core data. Journal of Quaternary Science 20(1): 21–32: doi:10.1002/jqs.892.

Hagberg J and Tunberg BG (2000) Studies on the covariation between physical factors and the long-term variation of the marine soft bottom macrofauna in western Sweden. Estuarine, Coastal and Shelf Science 50, 373 -85.

Hald M, Salomonsen GR, Husum K and Wilson LJ (2011) A 2000 year record of Atlantic Water temperature variability from the Malangen Fjord, northeastern North Atlantic. The Holocene: doi:10.1177/0959683611400457.

Hammer Ø, Harper DAT and Ryan PD (2001) PAST: Paleontological statistics software package for education and data analysis. Palaeontologia Electronica 4(1): 9pp

Harris PG, Zhao M, Rosell-Melé A, Tiedemann R, Sarnthein M and Maxwell JR (1996) Chlorin accumulation rate as a proxy for Quaternary marine primary productivity. Nature 383(6595): 63–65: doi:10.1038/383063a0.

Hass HC (1996) Northern Europe climate variations during late Holocene: evidence from marine Skagerrak. Palaeogeography, Palaeoclimatology, Palaeoecology 123(1–4): 121–145: doi:10.1016/0031-0182(95)00114-X.

Heslop D and Paul A (2011) Can oceanic paleothermometers reconstruct the Atlantic Multidecadal Oscillation? Climate of the Past 7(1): 151–159: doi:10.5194/cp-7-151-2011.

Hubeny JB, King JW and Santos A (2006) Subdecadal to multidecadal cycles of Late Holocene North Atlantic climate variability preserved by estuarine fossil pigments. Geology 34(7): 569–572: doi:10.1130/G22671.1.

Hughes MK and Diaz HF (1994) Was there a "medieval warm period", and if so, where and when? Climatic Change 26(2-3): 109 – 142: doi:10.1007/BF01092410.

Hurrell JW (1995) Decadal Trends in the North Atlantic Oscillation: Regional Temperatures and Precipitation. Science 269(5224): 676–679.

Kerr RA (2000) A North Atlantic Climate Pacemaker for the Centuries. Science 288(5473): 1984–1985: doi:10.1126/science.288.5473.1984.

Knight JR, Allan RJ, Folland CK, Vellinga M and Mann ME (2005) A signature of persistent natural thermohaline circulation cycles in observed climate. Geophysical Research Letters 32(20): L20708: doi:10.1029/2005GL024233.

Knudsen MF, Seidenkrantz M-S, Jacobsen BH and Kuijpers A (2011) Tracking the Atlantic Multidecadal Oscillation through the last 8,000 years. Nature Communications 2: 178: doi:10.1038/ncomms1186.

Koslowski G and Glaser R (1999) Variations in reconstructed ice winter severity in the western Baltic from 1501 to 1995, and their implications for the North Atlantic Oscillation. Climatic Change 41, 175-91.

Kunzendorf H and Larsen B (2002) A 200–300 year cyclicity in sediment deposition in the Gotland Basin, Baltic Sea, as deduced from geochemical evidence. Applied Geochemistry 17(1): 29–38: doi:10.1016/S0883-2927(01)00088-9.

Laskar J, Robutel P, Joutel F, Gastineau M, Correia ACM and Levrard B (2004) A long-term numerical solution for the insolation quantities of the Earth. Astronomy and Astrophysics 428(1): 261–285: doi:10.1051/0004-6361:20041335.

Longva O and Thorsnes T (1997) Skagerrak in the past and at the present: an integrated study of geology, chemistry, hydrography and microfossil ecology. Norges Geologiske Undersøkelse (NGU) Special Publication 8, 1-100.

Luterbacher J, Xoplaki E, Dietrich D, Jones P, Davies T, Portis D, Gonzalez-Rouco J, Von Storch H, Gyalistras D, Casty C and Wanner H (2001) Extending North Atlantic oscillation reconstructions back to 1500. Atmospheric Science Letters 2(1-4): 114–124.

Mann ME, Zhang Z, Rutherford S, Bradley RS, Hughes MK, Shindell D, Ammann C, Faluvegi G and Ni F (2009) Global Signatures and Dynamical Origins of the Little Ice Age and Medieval Climate Anomaly. Science 326(5957): 1256–1260: doi:10.1126/science.1177303.

Marchal O, Cacho I, Stocker TF, Grimalt JO, Calvo E, Martrat B, Shackleton N, Vautravers M, Cortijo E, Van Kreveld S, Andersson C, Koç N, Chapman M, Sbaffi L, Duplessy J-C, Sarnthein M, Turon J-L, Duprat J and Jansen E (2002) Apparent long-term cooling of the sea surface in the northeast Atlantic and Mediterranean during the Holocene. Quaternary Science Reviews 21(4–6): 455–483: doi:10.1016/S0277-3791(01)00105-6.

Matthews JA, Olaf Dahl S, Nesje A, Berrisford MS and Andersson C (2000) Holocene glacier variations in central Jotunheimen, southern Norway based on distal glaciolacustrine sediment cores. Quaternary Science Reviews 19(16): 1625–1647: doi:10.1016/S0277-3791(00)00008-1.

Mayewski PA, Rohling EE, Curt Stager J, Karlén W, Maasch KA, David Meeker L, Meyerson EA, Gasse F, Van Kreveld S, Holmgren K, Lee-Thorp J, Rosqvist G, Rack F, Staubwasser M, Schneider RR and Steig EJ (2004) Holocene climate variability. Quaternary Research 62(3): 243–255: doi:10.1016/j.yqres.2004.07.001.

Moberg A, Sonechkin DM, Holmgren K, Datsenko NM and Karlén W (2005) Highly variable Northern Hemisphere temperatures reconstructed from low- and high-resolution proxy data. Nature 433(7026): 613–617: doi:10.1038/nature03265.

Müller PJ, Kirst G, Ruhland G, Von Storch I and Rosell-Melé A (1998) Calibration of the alkenone paleotemperature index U37K′ based on core-tops from the eastern South Atlantic and the global ocean (60°N-60°S). Geochimica et Cosmochimica Acta 62(10): 1757–1772: doi:10.1016/S0016-7037(98)00097-0.

Nordberg K, Gustafsson BG and Krantz AL (2000) Decreasing oxygen concentrations in the Gullmar Fjord, Sweden, as confirmed by benthic foraminifera, and the possible association with NAO. Journal of Marine Systems 23, 303-16.

Otto L, Zimmerman JTF, Furnes GK, Mork M, Saetre R and Becker G (1990) Review of the physical oceanography of the North Sea. Netherlands Journal of Sea Research 26(2–4): 161–238: doi:10.1016/0077-7579(90)90091-T.

Pollack HN and Smerdon JE (2004) Borehole climate reconstructions: Spatial structure and hemispheric averages. Journal of Geophysical Research 109(D11): D11106: doi:10.1029/2003JD004163.

Richter TO, Peeters FJC and Van Weering TCE (2009) Late Holocene (0–2.4 ka BP) surface water temperature and salinity variability, Feni Drift, NE Atlantic Ocean. Quaternary Science Reviews 28(19–20): 1941–1955: doi:10.1016/j.quascirev.2009.04.008.

Rodhe J and Holt N (1996) Observations of the transport of suspended matter into the Skagerrak along the western and northern coast of Jutland. Journal of Sea Research 35(1–3): 91–98: doi:10.1016/S1385-1101(96)90738-8.

Schimanke S, Meier HEM, Kjellström E, Strandberg G and Hordoir R (2012) The climate in the Baltic Sea region during the last millennium simulated with a regional climate model. Clim. Past 8(5): 1419–1433: doi:10.5194/cp-8-1419-2012.

Schlesinger ME and Ramankutty N (1994) An oscillation in the global climate system of period 65-70 years. Nature 367(6465): 723–726: doi:10.1038/367723a0.

Schulz M and Mudelsee M (2002) REDFIT: estimating red-noise spectra directly from unevenly spaced paleoclimatic time series. Computers & Geosciences 28(3): 421–426: doi:10.1016/S0098-3004(01)00044-9.

Senneset L (2002) A Record of High Resolution Ocean Variability from Skagerrak Over the Past 900 Years. Masters thesis, Department of Geology, University of Bergen, Norway. 1-58.

Sonderegger D 2012. SiZer: Significant Zero Crossings (R package), available at http://cran.r-project.org/web/packages/SiZer/index.html (26 September 2012)

Stigebrandt A (1983) A Model for the Exchange of Water and Salt Between the Baltic and the Skagerrak. Journal of Physical Oceanography 13(3): 411–427: doi:10.1175/1520-0485(1983)013<0411:AMFTEO>2.0.CO;2.

Sutton RT and Hodson DLR (2005) Atlantic Ocean Forcing of North American and European Summer Climate. Science 309(5731): 115–118: doi:10.1126/science.1109496.

Torrence C and Compo G (1998) A Practical Guide to Wavelet Analysis. Bulletin of the American Meteorological Society 79(1): 61–78: doi:10.1175/1520-0477(1998)079<0061:APGTWA>2.0.CO;2.

Van Loon H and Rogers JC (1978) The Seesaw in Winter Temperatures between Greenland and Northern Europe. Part I: General Description. Monthly Weather Review 106(3): 296–310: doi:10.1175/1520-0493(1978)106<0296:TSIWTB>2.0.CO;2.

Wagner G, Beer J, Masarik J, Muscheler R, Kubik PW, Mende W, Laj C, Raisbeck GM and Yiou F (2001) Presence of the Solar de Vries Cycle (205 years) during the Last Ice Age. Geophysical Research Letters 28(2): 303–306: doi:10.1029/2000GL006116.

Walter K and Graf HF (2002) On the changing nature of the regional connection between the North Atlantic Oscillation and sea surface temperature. Journal of Geophysical Research, 107, D17. doi: 10.1029/2001JD000850

Yu S-Y (2003) Centennial-scale cycles in middle Holocene sea level along the southeastern Swedish Baltic coast. Geological Society of America Bulletin 115(11): 1404–1409: doi:10.1130/B25217.1.

CHAPTER 8

Summary, conclusions and future work

The purpose of this dissertation was to contribute new data to gain a better understanding on past climate variability in the North Atlantic during the late Holocene. The study area is particularly important for modulating European climate, and it is sensitive to changes in the internal modes of climate variability. The aim was also to place the present warming of climate into a wider temporal context. The climate reconstructions were undertaken using well established biomarker proxies as well as recently developed ones. In Chapters 3 and 4 we tested the applicability of the relatively new TEX_{86} and MBT/CBT indices in a marine coastal environment as well as in soils. In Chapters 5, 6 and 7 we described new climate reconstructions for the eastern Fram Strait, the Barents Sea and the Skagerrak covering the last 2000 or 4400 years at decadal or multidecadal resolution.

In Chapter 3 we used a GDGT based approach to reconstruct sea surface temperatures (SST) and air temperatures in the Skagerrak region at decadal resolution. We compared the temperature estimates to instrumental SST and air temperature records from the region covering the last 200 years. We found that for this time period the GDGT derived estimates resembled annual SST for TEX_{86}, but those temperatures derived using the combined MBT/CBT indices were closer to summer air temperatures rather than mean annual temperatures (MAT). We discussed possible explanations for the MBT/CBT bias towards summer temperatures in the Skagerrak, such as enhanced productivity of GDGT lipids in soils during summer months, or preferential transport of GDGT from the continent to the marine environment in summer months when Glomma River runoff is increased, or an allochthonous origin of the GDGT signal in the Skagerrak.

To test these hypotheses, we conducted a year round field study in southern Norway and the Pyrenees (Chapter 4). We examined core and intact branched GDGTs distributions in soils that were collected each month, as well as in samples of transported and deposited suspended organic matter (Chapter 4). We found that temperatures calculated using the concentrations of both core and intact GDGTs did not follow seasonal temperature change in soil samples at either of the study sites. The absolute temperature values were closer to annual temperatures rather than to any specific season. The transport of core branched GDGTs did not change the temperature estimates either, but temperatures estimated with intact GDGTs concentrations analyzed in recently eroded suspended particulate organic matter showed seasonal temperature variability in some samples. In addition, the transport of branched GDGTs was decoupled from the Glomma River discharge cycle therefore they are not preferentially transported to the Skagerrak during summer months as suggested in Chapter 3. Regarding the samples of deposited organic matter, temperatures estimated

with core GDGTs were close to annual means in the Pyrenees, but closer to summer temperatures in the Skagerrak. *In situ* GDGT production in the Skagerrak can not be discarded as a source for these lipids, which are usually associated to terrigenous inputs. The branched GDGTs found in the Skagerrak might be a result of a mixture between lipids transported from southernmost locations and *in situ* production.

In Chapter 5 we used alkenone and GDGT based proxies to reconstruct past air, SST and polar freshwater extent variability in the eastern Fram Strait for the last 2000 years. Temperature fluctuations were detected at multicentennial scales, and we found a progressive increase in air temperature during the last 1000 years, which was simultaneous with a temperature decrease in the upper mixed water layer. Polar freshwater in the area seemed to increase during this period. Taking into account the oceanographic features of the eastern Fram Strait, we suggested that there was an enhancement of heat transport via the North Atlantic Current to this area, starting at ~1000 AD, that was more accentuated during the last 500 years. Simultaneously, there was a progressive sea ice melting and a cooling of the upper mixed surface layer in the eastern Fram Strait. Our climate reconstruction may indicate long term average changes in the positive and negative modes of Arctic multidecadal variability in this region over the last 2000 years. During the last 1000 years, a mean relative dominance in the positive phase of this mode of variability may have prevailed at multicentennial time scales.

In Chapter 6, past variations in sea ice cover, marine export productivity and variability in the extension of Polar and Atlantic water masses were reconstructed in the eastern Barents Sea using alkenones and IP25 biomarkers. We proposed that during the last 4400 years there was a progressive change from more polar, cold, water mass conditions towards more Atlantic-like, warmer, environmental conditions as indicated by a progressive decrease in $\%C_{37:4}$ from 4400 BP towards present. Considering the concentration of alkenones as a marker of phytoplankton summer export productivity, combined with the abundance of IP25, we suggested that there was a progressive cooling from 4400 BP towards 1700 BP, with important polar water mass influence and extended sea ice cover, probably due to a lower influence of Atlantic water mass reaching the Barents Sea. A progressive transition towards greater inflow of Atlantic water took place after 1700 BP (~300 AD), with an increase in summer export productivity and less extended sea ice cover. From 500 BP (~1500 AD) towards present, there was a progressive increase in Atlantic Water inflow, and a northeastern retreat of the minimum extent of the sea ice edge. We suggested that during the last 500 years, more periods with positive NAO conditions prevailed.

In Chapter 7 we reconstructed SST variability in the Skagerrak at decadal resolution, finding high variability in SST from multidecadal to multicentennial time scales. We performed a SiZer analysis to check which of the visually inspected SST trends were statistically significant. We found that, at a multicentennial scale, there was a long term SST cooling trend in the Skagerrak from AD 0 until AD 1300 that could be related to a decrease in summer insolation at high latitudes during the late Holocene, which is coherent with previous findings from records of SST in the North Atlantic. This trend was reversed by a progressive warming taking place from AD 1600 until AD 2000 in spite of continued decreased insolation. We suggested that this warming trend was linked to an enhancement in the heat transport carried by the North Atlantic Current starting ca. AD 1600. The mechanisms triggering such enhanced inflow could be linked to internal variability of the ocean – atmosphere system, such as a progressive predominance of positive modes of the NAO and the AMO. The SST reconstruction is visually comparable to a reconstruction of the AMO at multicentennial time scales but with different temperature anomaly magnitudes, suggesting a strong link between SST variability over the North Atlantic region and in the Skagerrak region. The SST record from the Skagerrak is also comparable to an air temperature reconstruction for central Europe, suggesting a close link between ocean and continental temperature variability in this region.

A relevant finding to emerge from this study is the connection between the three new climate reconstructions on multidecadal to multicentennial time scales. From the records located in the eastern Fram Strait and the Barents Sea, positioned in the two main paths where the northward flowing North Atlantic Current meet the Arctic, we interpret there was a progressive temperature increase probably due to an enhancement in the heat transport carried by the North Atlantic Current. This trend started at ~1000 – 1300 AD but was accentuated from ~1500-1600 AD until the most recent part of the records. In the Skagerrak, an area influenced by 90% North Atlantic water, a long term cooling that lasted until AD 1300 was reversed by a progressive warming since AD 1600 even though insolation continued to decrease. We suggest that the warming trends observed in the three records during the last ~400 years were caused by changes in internal modes of climate variability such as predominantly positive phases of the Arctic MDV, the NAO or the AMO. The discussed trends found in our records, are statistically significant at multidecadal to multicentennial time scales according to a SiZer analysis conducted in our biomarker reconstructions (Figure 8.1).

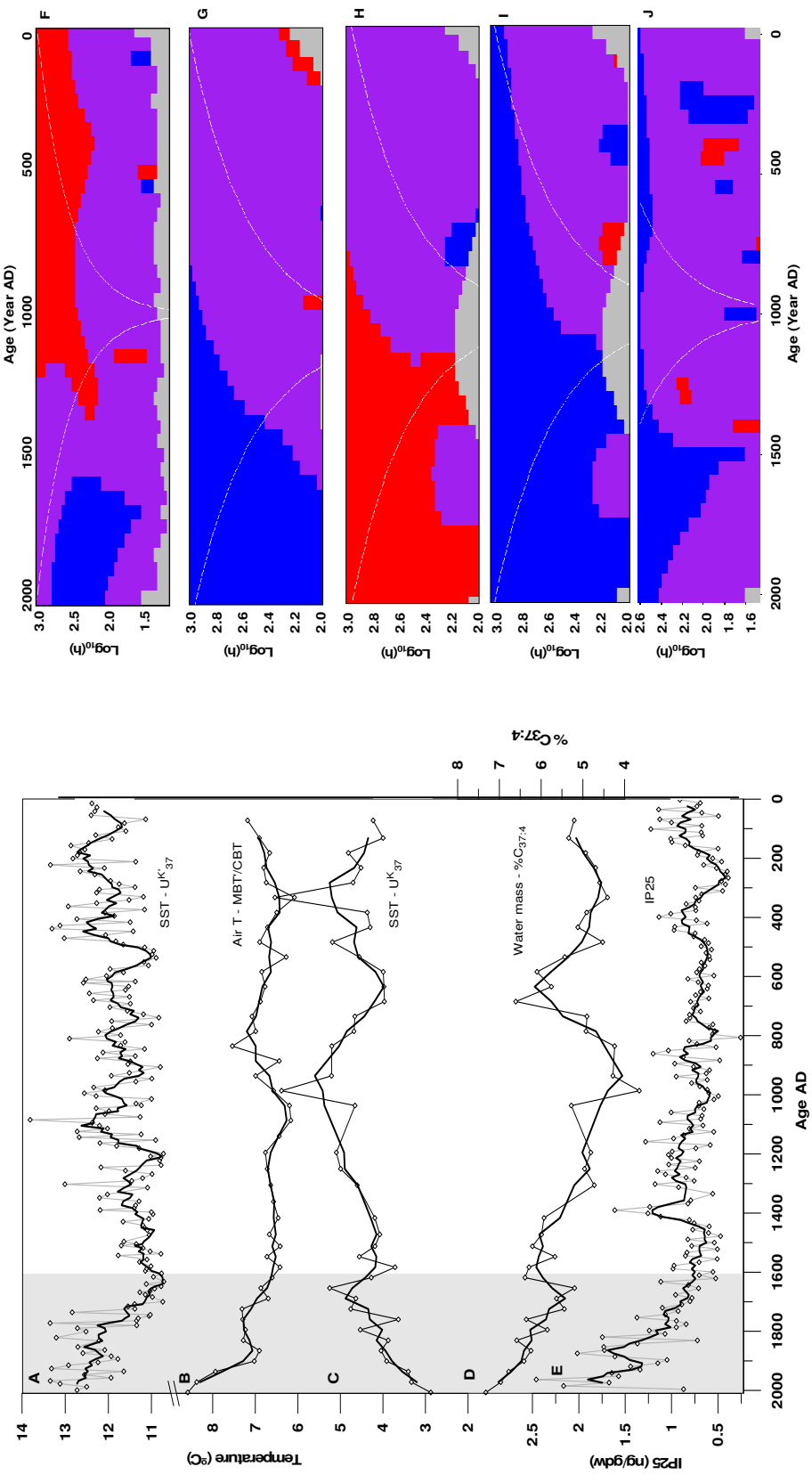

Figure 8.1. Compilation of various biomarker based reconstructions generated in this thesis. On the left, graphs A-E show the raw data (grey) and a five point running average (black thick line). On the right (F-J), plots resulting from the SiZer analysis of the raw data shown in the left, which were done to test if the trends are statistically significant. (A, F) SST ($U^{K'}_{37}$) for core MD99-2286 (Skagerrak). (B, G) Air temperature (MBT'/CBT); (C, H) Surface mixed water layer temperature ($U^{K'}_{37}$); (D, I) Variability in water mass type ($\%C_{37:4}$) for core MSM05/05-712-1 (Eastern Fram Strait). (E, J) IP25 abundance indicative for variability in sea ice cover when combined with a plankton marker (see chapter 6) for core PL96-126 (eastern Barents Sea). The SiZer plot is a function of location (time, x-axis) and scale (h, y-axis). An increase in the derivative (a significant warming trend) is shown in blue, a decrease in the derivative (cooling trend) is noted in red and no change in the derivative (natural variability of the data) is shown in purple. See chapter 7 for details and references about SiZer analysis.

Previously published reconstructions of Northern Hemisphere temperatures show great low frequency variability at centennial time scales, as mentioned in Chapter 1. But these reconstructions usually agree with the original *hockey stick* dataset in that the 20th century temperatures are the warmest of the last 1300 years. The new climate reconstructions generated here, show high variability at multidecadal scales and long term trends at multicentennial scales. Regarding the 20th century temperatures, only the air temperature reconstruction from the eastern Fram Strait shows a steep temperature increase since AD 1860 until present, reaching the highest temperature values for the whole record. For the Barents Sea record, we could not generate quantitative reliable SST estimates with the biomarkers that we used. In the Skagerrak, there are periods through the entire record with SST values of a magnitude comparable to the most recent part of the record. However, from the existing scientific literature and particularly from the exhaustive studies conducted by the Intergovernmental Panel on Climate change, it is recognized that since the 1970s global average temperatures have increased considerably partly due to anthropogenic activity and the effects of this warming trend are already noticeable. Therefore we conclude that the impact of human activity on climate is superimposed on a longer term warming trend caused by changes in natural modes of climate variability that progressively affected the study areas during the last ~400 years.

The results presented here have thrown up many questions in need of further investigation. Regarding the proxies based on GDGTs, the origin of these lipids in the Skagerrak should be addressed before applying these proxies in this area with reliability. In addition, further research should investigate if branched GDGTs can be synthesized *in situ* in the Skagerrak and in other marine environments. Research efforts should be made to find the source organisms responsible for synthesizing these lipids in soils. The causes for variability in temperature estimates with the transport of intact GDGTs in our study area are not well understood and could be further investigated by expanding the limits of the study period and region. Concerning the paleoclimate reconstructions, further work needs to be done to validate whether the natural climate variability trends found in this study were caused by the internal and external modes of climate variability that we suggested here. Incorporating the newly generated proxy data to climate models that combine different climate forcings could be a way to address this question. Furthermore, in our reconstructions the recent warming trend starts at ~1600 AD which is 100-200 years earlier than observed in other reconstructions that show a warming from the little ice age to the present. Further research is needed to determine if this early starting warming trend is characteristic for this particular region.

List of figures

CHAPTER 1

CHAPTER 2

CHAPTER 3

CHAPTER 4

CHAPTER 5

CHAPTER 6

CHAPTER 7

CHAPTER 8

List of tables

CHAPTER 2

CHAPTER 5

CHAPTER 6

CHAPTER 7

Appendix I: List of publications.

Peer reviewed

(1) Escala M, Fietz S, Rueda G and Rosell-Melé A (2009) Analytical considerations for the use of the paleothermometer tetraether index(86) and the branched vs isoprenoid tetraether index regarding the choice of cleanup and instrumental conditions. *Analytical chemistry* 81(7): 2701–2707: doi:10.1021/ac8027678.

(2) Rueda G, Rosell-Melé A, Escala M, Gyllencreutz R, Backman J, (2009) Comparison of instrumental and GDGT based estimates of sea surface and air temperatures from the Skagerrak. *Organic Geochemistry* 40 287-291, doi: 10.1016/j.orggeochem.2008.10.012.

(3) Fietz S, Martínez-Garcia A, Huguet C, Rueda G and Rosell-Melé A (2011) Constraints in the application of the Branched and Isoprenoid Tetraether index as a terrestrial input proxy. *Journal of Geophysical Research: Oceans* 116(C10): doi:10.1029/2011JC007062.

(4) Fietz S, Martínez-Garcia A, Rueda G, Peck VL, Huguet C, Escala M and Rosell-Melé A (2011) Crenarchaea and phytoplankton coupling in sedimentary archives: Common trigger or metabolic dependence? *Limnology and Oceanography* 56(5): 1907–1916: doi:10.4319/lo.2011.56.5.1907.

(5) Fietz S, Huguet C, Bendle J, Escala M, Gallacher C, Herfort L, Jamieson R, Martínez-Garcia A, McClymont EL, Peck VL, Prahl FG, Rossi S, Rueda G, Sanson-Barrera A and Rosell-Melé A (2012) Co-variation of crenarchaeol and branched GDGTs in globally-distributed marine and freshwater sedimentary archives. *Global and Planetary Change* 92–93: 275–285: doi:10.1016/j.gloplacha.2012.05.020.

(6) Fietz S, Huguet C, Rueda G, Hambach B, Rosell-Melé A, (2013) Hydroxylated isoprenoidal GDGTs in the Nordic Seas. *Marine Chemistry* doi 10.1016/j.marchem.2013.02.007.

(7) Rueda G, Fietz S, Rosell-Melé A, (2013) Coupling of air and sea surface temperatures in the eastern Fram Strait during the last 2000 years. *The Holocene* doi: 10.1177/0959683612470177.

(8) Ho SL Mollenhauer G, Fietz S, Martínez-Garcia A, Lamy F, Rueda G, Schipper K, Méheust M, Rosell-Melé A, Stein R, Tiedemann R, (2013) Appraisal of the TEX86 and TEX86L thermometries in the subpolar and polar regions. *Geochimica et Cosmochimica Acta* (in review, GCA-D-12-00354R1).

Non-peer reviewed

(1) Fietz S, Martinez-García A, Rueda G, Rosell-Melé A Biomarker and dust studies (Chapter 4.4 & Ch. 5) (2011) In: The Expedition of the Research Vessel "Polarstern" to the polar South Pacific in 2009/2010 (ed. R. Gersonde). Reports on Polar and Marine Research.

Gemma Rueda Ferrer
Universitat Autònoma de Barcelona
PhD Thesis, 2013

icta Institut de Ciència i Tecnologia Ambientals • UAB
UAB Universitat Autònoma de Barcelona